TECHNISCHE UNIVERSITÄT MÜNCHEN
Lehrstuhl für Steuerungs- und Regelungstechnik

Transparency- and Performance-Oriented Control of Haptic Teleoperation Systems

Carolina U. Passenberg

Vollständiger Abdruck der von der Fakultät für Elektrotechnik und Informationstechnik der Technischen Universität München zur Erlangung des akademischen Grades eines

Doktor-Ingenieurs (Dr.-Ing.)

genehmigten Dissertation.

Vorsitzender: Univ.-Prof. Dr.-Ing. Klaus Diepold

Prüfer der Dissertation:

1. TUM-IAS Jun.-Fellow Dr.-Ing. Angelika Peer
2. Univ.-Prof. Dr.-Ing. Eckehard Steinbach

Die Dissertation wurde am 15.11.2012 bei der Technischen Universität München eingereicht und durch die Fakultät für Elektrotechnik und Informationstechnik am 19.04.2013 angenommen.

Foreword

This thesis summarizes my research conducted in the past four years at the Institute of Automatic Control Engineering, LSR, of the Technische Universität München, Germany. The time at LSR was very pleasant as I found an open-minded, fruitful, and interdisciplinary working environment.

I thank my thesis advisor Dr. Angelika Peer for her steady support and the numerous fruitful discussions. Her ideas and advice along with the freedom of research are invaluable for me. I also want to express my gratitude to my supervisor Prof. Martin Buss for the great opportunity to work as a research assistant at the LSR including the extraordinary collaboration possibilities, and for the confidence in me.

I am also indebted to all my colleagues at the LSR. I enjoyed my time at LSR very much because of the friendly and always supportive team and the laughs that we shared. My particular thank goes to my colleagues from the haptic group who considerably contributed to my work with their fruitful discussions and immense assistance. I also thank the excellent staff in the mechanical and electrical workshop as well as the always helpful and patient system administrator for their repeated efforts in developing and maintaining the hardware setups. Furthermore, this work significantly benefited from the inputs of my team colleagues Raphaela Groten, Antonia Glaser, and from my collegue Verena Nitsch from the Universität der Bundeswehr München. I also thank my colleagues Benjamin Passenberg, Michelle Karg, Thomas Schauss, Daniela Knapp, Harald Voit, and Daniel Althoff for proofreading my thesis.

The thesis was also supported and influenced by the excellent work of my students Andreas Achhammer, Matthias Axenbeck, Robert Engst, Yao Hao, Andreas Spenninger, and Yan Zaripov. Many thanks for the strong commitment and the contributions to this thesis.

Finally, I want to express my deep gratitude to my parents Claudia and Fredi, my sisters Constanze and Clarissa, and my husband Benjamin for their love and their invaluable encouragement all the way long.

Munich, November 2012 Carolina Passenberg

Abstract

Haptic teleoperation systems enable human operators to act in a remote environment while simultaneously perceiving it. The ideal teleoperation system is stable, transparent, and allows to achieve a high task performance. Transparency or an optimal degree of fidelity implies that the dynamics of the technical media, which connect the local and the remote site, is not presented to the human operator. Technical deficiencies of, e.g., actuators, sensors, or the communication channel limit the realization of an ideal teleoperation system. This thesis presents advanced transparency- and performance-oriented controllers that are based on the idea of incorporating online gained knowledge of remote environment, operator, or task (EOT) in the control law. The developed controllers can veritably improve the fidelity and the performance of haptic teleoperation systems beyond those of classical control concepts that are not adaptive to online gained EOT knowledge. In order to combine the benefits of both, transparency- and performance-oriented controllers, this thesis proposes further a novel multi-criteria control concept. The contributions of this thesis are presented in more detail below.

When closing the control loop over the communication channel, stability and fidelity are influenced by the communication channel and the dynamics of all technical media. Model-mediated teleoperation is a promising control concept to eliminate the influence of the remote robot and the communication channel on the fidelity of the system. The idea of this transparency-oriented control concept is to online estimate a haptic map of the remote environment, and to reconstruct this map locally for the operator. As the control loop between local and remote site is opened whenever the estimation converges, a high degree of fidelity is achieved. This thesis investigates and enlarges the applicability of model-mediated teleoperation: i) improvements in fidelity are shown theoretically and experimentally based on a comparison with a classical controller, ii) a novel fidelity measure is proposed, iii) the known literature is extended by a detailed stability analysis for the time-varying and partly switching dynamics of the system, and iv) a comprehensive comparison and extension of environment modeling, estimation, and reconstruction methods is provided. The model-mediated teleoperation approach is validated in experiments.

The performance-oriented control concept investigated in this thesis continuously combines the operator commands with computer-generated commands from a haptic assistance. One of the main challenges when designing haptic assistances is to select the authority behavior of the assistance. This thesis presents a systematic design tool for the authority module of user- and task-adapted, haptic assistances. According to the introduced design tool, a single- or multi-criteria performance measure, a performance reference, and an assistance policy have to be selected when designing the authority policy of a haptic assistance. Based on the proposed design tool, current implementations are classified, and novel design possibilities are identified and explored. The effects of the novel approaches on objective and subjective performance and usability measures are determined in a user study. The results lead to distinct recommendations for the choice of the authority policy module of a haptic assistance depending on the task at hand.

Finally, it is illustrated how multi-criteria controllers can be designed for teleoperation systems. A proof-of-concept study provides a first indication that a suitable integration of single-objective controllers into one system can improve multiple objectives simultaneously.

Zusammenfassung

Mittels haptischer Teleoperationssysteme können Menschen in entfernten Umgebungen agieren und diese gleichzeitig wahrnehmen. Das ideale Teleoperationssystem ist transparent, immersiv und ermöglicht eine hohe Aufgabenleistung. Transparenz bzw. optimale Realitätstreue sind gegeben, wenn die Dynamiken der technischen Medien, die den lokalen und entfernten Ort verbinden, dem menschlichen Operator nicht dargestellt werden. Technische Unzulänglichkeiten der Aktoren, Sensoren oder des Kommunikationskanals führen dazu, dass ein ideales Teleoperationssystem nicht realisiert werden kann. Diese Arbeit präsentiert fortgeschrittene transparenz- und performanzorientierte Regelungskonzepte, die auf der Idee basieren, online generiertes Wissen über Umgebung, Operator oder Aufgabe (EOT) in das Regelgesetz einzubeziehen. Dadurch kann im Vergleich zu klassischen, nicht EOT-adaptiven Reglern die Realitätstreue und Leistung nachweisbar verbessert werden. Um die Vorteile von transparenz- und performanzorientierten Reglern zu kombinieren, wird in dieser Arbeit zudem ein multi-kriterielles Regelungskonzept vorgestellt. Im Nachfolgenden werden die Neuheiten dieser Arbeit genauer beschrieben.

Wenn die Regelschleife über den Kommunikationskanal geschlossen wird, werden Stabilität und Realitätstreue von den Dynamiken aller technischer Medien beeinflusst. Modellvermittelnde Teleoperation (MVT) ist ein vielversprechendes Regelungskonzept, bei dem die Realitätstreue von der Dynamik des entfernten Roboters und des Kommunikationskanals unabhängig ist. Die Idee dieses transparenzorientierten Reglers basiert darauf, eine haptische Karte der entfernten Umgebung online zu schätzen und diese auf lokaler Seite für den Operator zu rekonstruieren. Da bei konvergierter Schätzung die Regelschleife zwischen lokaler und entfernter Seite geöffnet wird, kann mit MVT ein hoher Grad an Realitätstreue erzielt werden. In dieser Arbeit wird MVT intensiv untersucht und ihre Anwendbarkeit erhöht: i) Verbesserungen der Realitätsnähe werden theoretisch und im Vergleich zu klassischen Reglern experimentell gezeigt, ii) ein neuartiges Maß für die Realitätstreue wird vorgeschlagen, iii) eine detaillierte Stabilitätsanalyse für die zeitvarianten und teils schaltenden Systemdynamiken wird präsentiert und iv) Methoden zur Umgebungsmodellierung, -schätzung und -rekonstruktion werden miteinander verglichen. Der MVT-Ansatz wird experimentell validiert.

Das in dieser Arbeit untersuchte, performanzorientierte Regelungskonzept basiert darauf, die Vorgaben des Operators kontinuierlich mit Computer-generierten Vorgaben eines haptischen Assistenten zu kombinieren. Eine der größten Herausforderungen bei dem Design von haptischen Assistenten ist die Wahl des Autoritätsverhaltens. Diese Arbeit stellt ein systematisches Designwerkzeug für das Autoritätsmodul von benutzer- und aufgabenangepassten, haptischen Assistenten vor. Gemäß dieses Designwerkzeuges müssen für das Autoritätsmodul ein ein- oder multikriterielles Performanzmaß, eine Performanzreferenz sowie ein Autoritätsverhalten gewählt werden. Anhand des eingeführten Designwerkzeuges werden bekannte Implementierungen eingeordnet und neue Designmöglichkeiten identifiziert und erforscht. Die Auswirkungen der neuen Ansätze auf objektive und subjektive Maße bezüglich Performanz und Benutzerfreundlichkeit werden in einer Benutzerstudie bestimmt. Die Ergebnisse führen zu Designempfehlungen für die Wahl des Autoritätsmoduls.

Schließlich wird dargestellt, wie multi-kriterielle Regler für Teleoperationssysteme entworfen werden können. Eine Konzeptstudie liefert einen ersten Nachweis dafür, dass eine geeignete Integration von einkriteriellen Reglern mehrere Ziele gleichzeitig verbessern kann.

Contents

Notations

Abbreviations

AbS	Agreement-based Switching
ANOVA	Analysis of Variance
CT	Convergence Time
DoF	Degree of Freedom
EOT	Environment, Operator, and Task
HC	Hunt-Crossley
HS	Hammerstein
JND	Just Noticeable Difference
KV	Kelvin-Voigt
LAA	Linear-Adapting Assistance
LAN	Local Area Network
LTI	Linear Time Invariant
LTV	Linear Time-Varying
MM	Model-mediated
MSD	Mass-Spring-Damper
NA	No Assistance
OCA	Optimal Constant Assistance
PD	Proportional-Derivative
PI	Proportional-Integral
RLS	Recursive Least Squares
VF	Virtual Fixture

Conventions

Scalars, Vectors, and Matrices

Scalars are denoted by upper and lower case letters in italic type. *Vectors* are denoted by lower case letters in boldface type, as the vector $\boldsymbol{x}$ is composed of elements x_i. *Matrices* are denoted by upper case letters in boldface type, as the matrix $\boldsymbol{X}$ is composed of elements x_{ij} (i^{th} row, j^{th} column).

x or X	scalar
$\boldsymbol{x}$	vector
$\boldsymbol{X}$	matrix

Subscripts and Superscripts

$\boldsymbol{a}^T, \boldsymbol{A}^T$	transpose of vector $\boldsymbol{a}$ and matrix $\boldsymbol{A}$
$\boldsymbol{A}^{-1}$	inverse of matrix $\boldsymbol{A}$
$\dot{a}, \ddot{a}$	first and second time derivative of variable a
$\hat{a}$	estimated value of variable a
$\tilde{a}$	filtered value of variable a
a^d	desired value of variable a
a^*	optimal or desired value a
a_0	initial value of variable a
$\boldsymbol{a}_\parallel, \boldsymbol{a}_\perp$	vector $\boldsymbol{a}$ tangential and perpendicular to a path
a_a	variable a associated with an admittance
a_{assist}	variable a associated with assistance
a_c	variable a associated with system in contact
a_e	variable a associated with the environment
a_f	variable a associated with system in free space
a_h	variable a associated with the human operator
a_m	variable a associated with the master device
$a_{\max}$	maximum value of variable a
$a_{\min}$	minimum value of variable a
a_o	variable a associated with an object
a_s	variable a associated with the slave device
a^{rot}	variable a in rotational direction
a^{trans}	variable a in translational direction

Functions and Operators

$\lvert a \rvert$	absolute value of a scalar a
$\lVert \boldsymbol{a} \rVert$	Euclidean norm of a vector $\boldsymbol{a}$
$\lceil a \rceil$	scalar a rounded up
$\det(\boldsymbol{A})$	determinant of a matrix $\boldsymbol{A}$
$\text{eig}(\boldsymbol{A})$	eigenvalue of a matrix $\boldsymbol{A}$
$\text{fft}(\boldsymbol{a})$	fast Fourier transformation of a vector $\boldsymbol{a}$
$\inf(a)$	infimum of a scalar a
$\underset{k}{\text{mean}}(\boldsymbol{a})$	mean of vector $\boldsymbol{a}$ over k samples
$\text{rank}(\boldsymbol{A})$	rank of a matrix $\boldsymbol{A}$
$\text{Re}(a), \text{Im}(a)$	real and imaginary part of a scalar a
$\text{sing}(\boldsymbol{A})$	singular value of a matrix $\boldsymbol{A}$

Symbols

General

$\boldsymbol{A}$	system matrix

$b, \boldsymbol{B}$	scalar damping and damping matrix
$\boldsymbol{b}$	input vector
$\boldsymbol{f}, F$	force in time and Laplace domain
$G(s)$	transfer function
$f(\cdot), g(\cdot), h(\cdot)$	scalar functions
$\boldsymbol{H}$	hybrid matrix
$k, \boldsymbol{K}$	scalar stiffness and stiffness matrix
K_p, K_d, K_i	gain of proportional, derivative and integral controller part
$m, \boldsymbol{M}$	scalar mass and mass matrix
q	zero of transfer function
$\boldsymbol{r}, \boldsymbol{\rho}$	reference in translational and rotational direction
s	Laplace operator
t	time
T_a, TA	sampling time
T_d	time delay
T_{act}, T_{sensor}	time constant of actuator electronics and sensor
u	input
V	velocity in Laplace domain
$\boldsymbol{x}, X$	position in time and Laplace domain, state
$\dot{x}$	velocity in time domain
$\ddot{x}$	acceleration
y	system output
Y	mechanical admittance
z	z-transformation operator
Z	mechanical impedance
$\boldsymbol{\chi}$	concatenation of position, velocity, and acceleration signal
$\boldsymbol{\varphi}$	Euler angles
μ	mean
ω	frequency
$\boldsymbol{\omega}$	angular velocity
$\boldsymbol{\tau}$	torque
$\xi(\cdot)$	switching operator

Transparency-oriented Control

$\overline{a}$	constant value a
a_{mov}	variable a associated with model-mediated teleoperation for movable objects
a_{static}	variable a associated with model-mediated teleoperation for static objects
A	amplitude
$\mathcal{B}$	set of damping values
c	characteristic polynomial
$\boldsymbol{c}$	coordinates of center of mass
$\boldsymbol{C}$	correlation matrix
$C_1, \ldots, C_6, C_m, C_s$	transfer functions of controllers
${}^{\text{WR}}\boldsymbol{d}_{\text{TT}}$	distance vector from wrist frame to tool-tip frame

$D_{\boldsymbol{q}}$	domain of parameters
$\boldsymbol{E}$	unity matrix
$\boldsymbol{e}$	estimation error: $\boldsymbol{e} = \boldsymbol{a} - \hat{\boldsymbol{a}}$
f	frequency
$\mathcal{F}_{\text{robust}}$	robust fidelity measure
$\boldsymbol{g}$	gravity vector
$\boldsymbol{I}$	inertia matrix
$\mathcal{K}$	set of stiffness values
m	mass
$\mathcal{M}$	set of mass values
n	parameter of Hunt-Crossley and Hammerstein model
$\boldsymbol{O}$	sub-matrix of input regressor for movable objects
p	pole of transfer function
$\boldsymbol{P}$	covariance matrix
$\boldsymbol{q}$	parameter vector
$\boldsymbol{Q}$	positive definite matrix
$\boldsymbol{R}$	positive definite matrix
R	reference sensor coordinate system
$S \in \mathbb{R}^n$	parameter set
V	Lyapunov/cost function
$\boldsymbol{z}$	state
$\boldsymbol{\alpha}$	angular acceleration
$\beta_1, \beta_2, \beta_3$	parameters of recursive least squares with adaptive forgetting factor
$\boldsymbol{\Gamma}$	positive definite matrix
$\delta\boldsymbol{x}, \delta\dot{\boldsymbol{x}}$	penetration depth and velocity
δ	small positive number
$\iota(\boldsymbol{A})$	condition number of matrix $\boldsymbol{A}$
$\boldsymbol{\theta}$	parameter vector
$\boldsymbol{\kappa}, \boldsymbol{K}$	adaptation gain vector or matrix
λ	forgetting factor
$\boldsymbol{\phi}$	input regressor
ρ	parameter of recursive least squares with adaptive forgetting factor
σ	standard deviation

Performance-oriented Control

$\overline{a}$	mean value of a
A	continuous agreement measure
C, C^c, C^s, C^{ca}	general, constant, switching, and continuous assistance control policy
C_E	number of errors
$\boldsymbol{D}$	scaling matrix for passive virtual fixture
D	continuous disagreement measure
d_A, d_D	discrete state corresponding to agreement and disagreement
E	efficiency
ET	error time

f_{ext}, f_{int}	external and interactive force
K	number of samples within a trial
$H(\cdot)$	hysteresis operator
$\boldsymbol{n}$	vector $\boldsymbol{n}$ with norm 1
$N(a)$	normalization of measure a to interval [0;1]
P, P^e, P^i, P^r	general, external, internal, and reference performance
S	smoothness of movements
SC	scenario
T	threshold
TCT	task completion time
$\boldsymbol{U}$	scaling matrix for passive virtual fixture
V	number of participants
w	weight
W	mechanical work
WL	perceived workload
$z(X)$	standard score of X
α	assistance level

Multi-Criteria Control

e	control error
j	weight
J	cost function
W	mechanical work
α	parameter of performance-oriented adaptation law
β	parameter of transparency-oriented adaptation law
ϵ	feedback error of adaptation law
γ	parameter of transparency-oriented adaptation law
η	parameter for varying human arm impedance
μ	parameter of performance-oriented adaptation law

1 Introduction

Until recently, the tasks performed by humans were strictly separated from those performed by autonomous robots. Pre-programmed autonomous robots are used in industry for welding, mating, varnishing or assembling parts. The structured and known environment allows to exploit the superior capabilities of robots: high precision and payload, high speed, and constant performance. This reduces costs without the risk of diminished quality. Manpower is required wherever the environment is dynamic, unstructured, or unknown and consequently requires a high adaptability. By perceiving, planning, reasoning, and learning, humans are able to handle these situations. Many of these tasks are, however, exhausting and even dangerous for humans. One large research area is therefore dedicated to the development of autonomous systems with human-like cognitive capabilities. These systems do, however, not yet exhibit full human cognitive capabilities and cannot handle arbitrary and sophisticated manipulation tasks. Teleoperation systems combine human and machine capabilities and therefore represent a bridge technology towards fully automated systems for a variety of different applications. As depicted in [182], research on teleoperation systems started in 1945.

A teleoperation (*tele* from Greek: distant) system extends human capabilities to a distant place. These systems are used to keep the human in a safe place, to reduce travel costs, and to realize and facilitate tedious operations at the limit and beyond human manipulation capabilities. Safety and cost reduction is the main motivation for performing space or underwater operations via teleoperation [168, 170] or for maintenance work in dangerous environments such as nuclear power plants [154]. Micro- and minimally invasive surgery [15, 28, 108] represents another important application area for teleoperation techniques, and micro-assembly [178, 223] and nano-manipulation of cells [184] would not be realizable for humans without technical means. A teleoperation system can furthermore be used to teach new motor skills to humans [29, 48, 103, 141] or, by employing imitation learning techniques, to robots [179].

The technical realization of a teleoperation system as shown in Fig. 1.1 consists of a human-system interface located at the local site, a remotely located robot or teleoperator, and a communication channel, the interconnection between the devices and sites. The human-system interface registers the desired actions of the human operator and provides sensor information from the remote place. Besides visual feedback, haptic (from Greek verb: "to touch") information was found to be important for manipulation tasks as it increases task performance, see [53, 160, 182]. Haptic was defined by Gibson [64] as "the sensibility of the individual to the world adjacent to his body by use of his body". It comprises tactile perception in the form of vibrations, pressure and shear forces, the perception of temperature and pain, proprioceptive perception of postures, and kinesthetic perception of motions and forces. Acoustic feedback provides further insights into textural and material properties of objects and is especially beneficial if multiple humans are

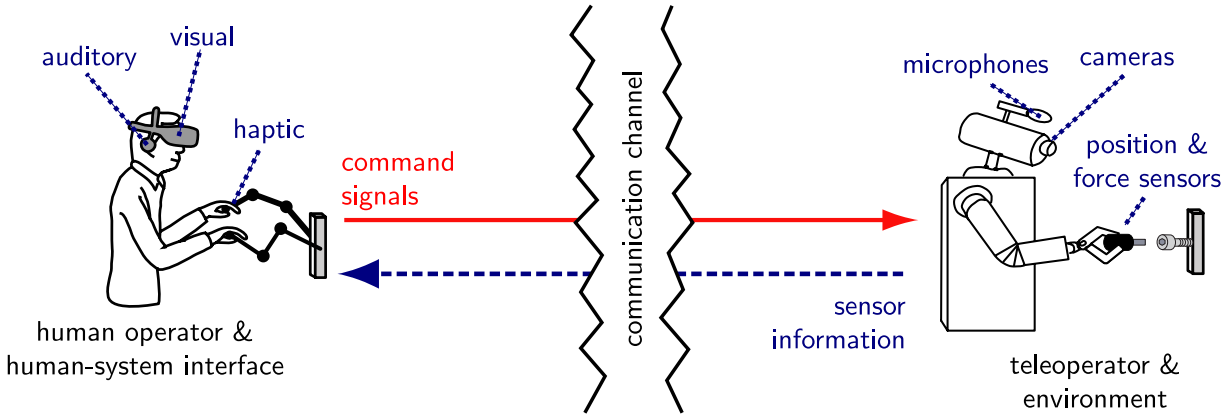

Fig. 1.1: Multi-modal teleoperation system. The human operator interacts with the remote environment by controlling a remotely located teleoperator via a human-system interface. Multi-modal feedback from the remote place is provided.

involved in a teleoperation task like in teaching scenarios. Modern teleoperation systems as e.g. presented in [24] feed multi-modal visual, acoustic and haptic - mainly kinesthetic - information back to the operator, see Fig. 1.1.

Generally, two modes of operations are distinguished for teleoperation systems [182]:
Shared Control realizes a *simultaneous (parallel)* sharing of human and machine capabilities. In other words, the commands and sensor information exchanged between the two sites are first augmented by the machine before being applied to the system. One extremum of shared control is manual control, i.e. the operator is manually performing the desired actions, which are directly sent to the remote environment and reproduced by the remotely located robot or teleoperator in a 1:1 manner. Similarly, sensor information is registered online and is instantaneously sent back to the operator. Thus, haptic information is exchanged bilaterally between both sites, and as the perception of haptic information and manipulating actions is inherently coupled, a control loop is closed between the human operator and the remote environment over the communication channel. The other extremum of shared control is autonomous control. In summary, shared control allows to distribute the payload between human and machine and to achieve performance beyond manual control performance.
Supervisory Control, on the contrary, refers to human and machine actions being performed *sequentially*: the human operator commands, monitors, and controls high-level (sub-)tasks, and the teleoperator autonomously executes them. Time-critical sensor information is only fed to the teleoperator. Thus, the stability-critical control loop is independent of the communication channel, the controlled human-system interface, and the behavior of the human operator.

This work focuses on shared control paradigms for haptic (kinesthetic) teleoperation systems. These systems provide the human operator with haptic feedback by exchanging haptic informations bilaterally between local and remote site. This information enters the controllers on the respective other site. Thus, a control loop is closed over the communication channel, including the human operator and environment. In a bilateral, haptic teleoperation system, the human operator, the environment, and the communication channel

influence the stability of the system together with the dynamics of the devices, actuators, sensors, and controllers. Only a stable system allows to successfully perform manipulation tasks in a remote environment, such that *stability* is a necessary requirement for haptic teleoperation systems. Besides stability, the operator's perception of the remote environment is an important aspect for haptic shared-control teleoperation systems. The ideal teleoperation system provides undisturbed visual, acoustic, and haptic feedback from the remote environment such that the technical media become imperceivable. The teleoperation system is then called *transparent*. Ideally, the operator would also be fully immersed into the remote place, and would *feel present* there. Technical deficiencies limit, however, the practical realization of a stable and transparent teleoperation system and a strong feeling of presence. In other words, there exists a conflict between transparency and stability. The imperfect or missing information can also result in a *performance* degradation such as long-lasting operations, high human effort, or even task failures. The ideal teleoperation is finally comfortable to use for the human operator and its handling is easy to learn. In other words, the *usability* of the system should be as high as possible. In summary, important design objectives for haptic, shared-control teleoperation systems are transparency, high task performance, strong feeling of presence, and high usability.

This thesis is dedicated to the development of adaptive, transparency- and performance-oriented control concepts for haptic teleoperation systems. Control concepts for improving the feeling of presence or usability are not presented in this thesis as quantitative and online evaluable measures for feeling of presence and usability are only partly available so far. The development of presence- and usability-oriented controllers represents, however, an interesting future research direction. The transparency- and performance-oriented control concepts achieve an improvement in one specific objective, transparency or task performance. The idea is to investigate in a first step each single-objective control concept in detail. In a second step, selected transparency- and performance-oriented controllers are integrated into a multi-objective system. Regarding the single-objective controllers, an adaptive, transparency-oriented control concept, that takes online gained knowledge about the environment into account, is investigated. This controller aims at mitigating the conflict between stability and transparency. In a second step, the design of haptic shared-control approaches in the form of haptic assistances is investigated. Haptic assistances are autonomously acting agents that continuously augment the operator commands by haptic, computer-generated commands. The goal is to improve task performance beyond unassisted task execution. In order to fully exploit the capabilities of operator and assistance, an adequate distribution between human and assistance authority over the actions of the system is required. This thesis introduces a design tool for influencing the authority of the assistance. This design tool allows to systematically design flexible, user- and task-adapted assistance sharing policies. In order to approach both objectives, transparency and high task performance, the third part of this thesis is dedicated to multi-objective controllers. The main innovation is the integration of adaptive, transparency- and performance-oriented controllers into one system such that improvements in all objectives are achieved.

1.1 Challenges

The ideal haptic teleoperation system requires answers to research questions from multiple disciplines such as control theory, robotics, human-machine interaction, and psychophysics. The key issues addressed in this thesis are summarized in the following.

Undisturbed Haptic Feedback from the Remote Environment

In a bilateral teleoperation system, motion and force information is exchanged between local and remote site. This closes a control loop including the dynamics of human operator, remote environment, human-system interface or master device, teleoperator or slave device, and communication channel. Consequently, each dynamics influences the stability of the teleoperation system. As additionally the dynamics of operator and environment is often unknown or only approximately known, the controlled teleoperation system has to be robust against parameter variations. The major conflict arises, however, when considering transparency as an additional objective in the design of control concepts for teleoperation systems. Technical characteristics such as the bandwidth of sensors and actuators, measurement noise, the discrete implementation of the controllers as well as time delay and packet loss in the communication change the stability regions and limit the range of undisturbed haptic feedback. Most of the approaches like the 4-channel architecture proposed by Lawrence [116], robust controllers [90, 118, 119, 177, 183, 217], adaptive control approaches [79, 176, 225], the scattering transformation or the wave variable approach [149] are based on the exchange of haptic signals or energy and flow variables. They furthermore do not incorporate online gained knowledge about the environment in the control law. As a consequence, all of these approaches exhibit limitations in presenting an undisturbed haptic feedback to the operator. Only recently, researchers investigated a rather old idea for improving fidelity without risking stability and thereby harming operator, devices, or environment. This control approach is referred to as model-mediated teleoperation. It mediates online gained model parameters of either operator or environment instead of energy/flow variables. The open questions are in terms of a rigorous stability and transparency analysis, generalizability, effectiveness compared to previous approaches and feasibility for teleoperation systems with multiple degrees of freedom and time delay in the communication channel.

User- and Task-Adaptation for High Performance

Besides replicating commands from the operator and feedback from the environment in a 1:1 manner, a variety of different shared control concepts have been proposed in literature to assist the human operator in task execution. Several of these concepts are based on a haptic assistance unit that acts as an independent agent in a teleoperation system and gives additional input to the human commands. The objective is to achieve a performance beyond unassisted performance. Most of the presented approaches provide a fixed amount of assistance, i.e. they do not adapt to the specific user or task. This behavior is unnatural when comparing it with two people physically interacting with each other in order to perform a task. Reed & Peshkin showed in [166] that the roles between two humans

change continuously during task execution. Even though human and machine capabilities are different, it is expected that a suitable adaptation of the amount of assistance requires less effort, avoids failures, and is better accepted by the human operator as the human-machine interaction becomes more cooperative. The open research question is how to realize such a user- and task-adapted assistance.

Integration of Single-Objective Controllers into Multi-Objective System

The ideal augmented teleoperation system finds an optimal trade-off between all objectives: stability, transparency, high performance, high feeling of presence, and high usability. This problem statement can also be described as the minimization of system costs over all stable control parameter sets. The system costs J are often given as a weighted sum of the costs for each optimization criterion, i.e. transparency J_t, (task) performance J_p, feeling of presence J_f and usability J_u

$$\min_{C \in \mathbb{C}} J = w_t J_t + w_p J_p + w_f J_f + w_u J_u \tag{1.1}$$

where $\mathbb{C}$ represents the set of all stabilizing control parameters and w_p, w_t, w_f and w_u represent weights. Most approaches known from literature focus on one of the objectives. It is therefore an open research question how to develop multi-criteria control concepts or integrate control concepts with different objectives into one system. Do the controllers interfere with each other? How can oscillatory and unstable behavior be avoided?

1.2 Main Contributions and Outline of the Thesis

The goal of this thesis is the development of transparency- and performance-oriented controllers for haptic shared-control teleoperation system. Advanced, adaptive control concepts are investigated, that incorporate online gained knowledge about environment, operator, or task in the control law. In a seond step, a multi-objective system, is realized by combining suitable single-objective controllers into one system. The result are improvements with respect to both objectives, transparency and performance.

Before going into detail in the approaches, the terminology and the basic model assumptions are presented in Chapter 2 together with a broad overview of state-of-the-art control approaches. The most prominent classical as well as environment-, operator-, and task-knowledge incorporating control approaches referred to as augmenting or EOT-adapting controllers are presented. A more detailed presentation and analysis of closely related work is provided in each chapter.

Chapter 3 and 4: Transparency-Oriented Control Design

A transparency-oriented control design aims at providing undisturbed haptic feedback from the remote environment to the operator. This can be easily achieved if the remote environment is known. In telerobotics, the remote environment is, however, either completely

unknown or only approximate knowledge about e.g. the type of object is given. The dynamic properties of objects are usually unknown. One approach to overcome this problem was presented by Hannaford in 1989 [75]. It is referred to as impedance-reflecting, VR-based, or *model-mediated teleoperation*. The idea is to online identify a model of the objects in the remote site, to send model information to the operator site and to connect the operator to a local reconstruction of the identified models. Whenever the online identification of the model is finished, the control loop between local and remote site is opened. This leads to significant improvements in fidelity (measure how close the system is from being transparent) without loss of stability. This thesis extends the state-of-the-art in model-mediated teleoperation by a detailed stability and fidelity analysis especially for the transient phase, where the online model identification takes place. As the numerically determined stability regions do often not match with the stability regions of the real system, a novel fidelity measure is introduced that takes this discrepancy to some extent into account. Theoretical, numerical, and experimental evaluations show significant improvements in fidelity compared to a classical control approach based on the bilateral exchange of haptic signals. This thesis provides furthermore a comprehensive summary and comparison of important implementation aspects: modeling, online identification, and reconstruction for static and movable objects. The reconstruction is especially important for systems with time delay in the communication channel. Based on a simulative comparison of different implementation possibilities, a suitable implementation of model-mediated teleoperation is selected and realized. Model-mediated teleoperation is finally extended to allow full 6 degrees-of-freedom manipulation tasks involving static and movable objects. This increases the applicability of the approach considerably. Experimental results show the effectiveness of model-mediated teleoperation compared to a classical two-channel architecture for systems with negligible, medium, and large time delays.

Chapter 5: Performance-Oriented Control Design

As mentioned above, a teleoperation system can also be used to support the operator during task execution by means of a haptic assistance that augments the operator's actions. A variety of assistance concepts are presented in literature. They show that the performance of teleoperated manipulation tasks can be improved beyond purely manual task execution. A systematic way for analyzing and designing especially user- and task-adapted assistances is, however, missing. This thesis introduces a novel design tool for haptic assistances. It can be used to investigate the main components when developing a flexible, user- and task-adapted haptic assistance. It also allows to classify current implementations, to identify unexplored methods, and to compare different assistance concepts. They are characterized by incorporating multiple performance measures and exhibit a constant, switching, or linearly adapting behavior. This thesis also presents new methods for distributing the workload between the haptic assistance and the human operator. These are implemented for a transportation task in a virtual-environment teleoperation system. The task is often encountered in real-environment teleoperation as well. Finally, a user study was conducted to investigate the effects of the different assistance sharing policies on objective and subjective performance measures. This user study allows to compare the different implementations in terms of performance and usability. The tuning effort and

the generalizability of the results is discussed.

Chapter 6: Towards an Integrated Multi-Criteria Control Concept

The design of the ideal teleoperation system requires to optimize several design objectives simultaneously or to find an optimal trade-off between them. Besides approaches based on multi-criteria optimization, it is straightforward to think about combining already tested transparency- and performance-oriented controllers into one multi-objective, haptic teleoperation system. It is, however, not guaranteed that the combination of multiple controllers leads again to a stable system nor that the different criteria are improved. Chapter 6 is dedicated to the integration of single-objective controllers into one system. Compared to approaches based on multi-criteria optimization, the idea of suitably integrating advanced, single-objective controllers has not been addressed in telerobotics literature so far. One integration strategy that is especially suitable for the admittance-type experimental setups considered in this thesis is presented and discussed. As a critical issue besides a suitable integration is to guarantee stability, one strategy for keeping the multi-objective system stable is sketched in this chapter. A first proof-of-concept of an integrated, multi-objective controller for haptic teleoperation is provided. Employing a multi-criteria cost function, the benefit of the integrated system is shown in comparison to a classical control approach. A variety of open questions is identified. These aim at motivating further research in this direction.
Chapter 7 summarizes the contributions and main results of the thesis and highlights future research directions.

2 Design Objectives and Overview of State-of-the-Art Control Concepts

This chapter introduces important design objectives and relevant measures for the design of haptic teleoperation systems. The chapter is further dedicated to the introduction of classical, state-of-the-art controllers and control architectures. Finally, an overview of EOT-adapting controllers is presented, from which the most promising transparency- and performance-oriented control concepts are selected.

From the earliest years of teleoperation on, guaranteeing stability has been investigated. This is one of the most important challenges when designing haptic teleoperation systems. Important control concepts stabilizing teleoperation systems are summarized in a review article by Hokayem & Spong [86]. Besides stability, it became more and more important to also provide an undisturbed haptic feedback to the operator. Yokokohji & Yoshikawa [218] and Lawrence [116] introduced the term transparency. As transparency and stability are conflicting objectives, the challenge is to find an optimal trade-off between them. Besides stability and transparency, a teleoperation system should provide a strong feeling of presence. This requires a human-oriented system and controller design. As the purpose of a teleoperation system is the execution of manipulation tasks in a remote environment, a high task performance is desired. In this context, the possibility of separating the operator's actions from those in the remote site through technical media gave rise to the idea of environment-, operator-, or task-(EOT)-adapting the operator's haptic commands by computer-generated commands and thereby improving task performance. The idea of a haptic assistance sharing the workload with the human came up and resulted in a variety of shared control approaches. Finally, the operator should agree with the actions of the system and should feel comfortable working with the system. In summary, a necessary requirement for the design of haptic teleoperation systems is *stability* and important design objectives are *transparency, strong feeling of presence, high task performance,* and *high usability*. The known telerobotics literature tackles all design objectives. This chapter provides definitions and explanations for each design objective. Furthermore, measures that are relevant for this thesis are presented.

State-of-the-art control approaches for haptic teleoperation systems are categorized in this thesis into two classes: i) *classical control concepts* that do not take online gained knowledge about environment, operator, or task into account, and ii) *EOT-adapting controllers*, see also [238]. As most control approaches concentrate on one design objective only, the class of EOT-adapting controllers can furthermore be categorized according to the design objective a controller focuses on. This chapter provides a detailed overview of state-of-the-art EOT-adapting controllers, while only the most relevant classical controllers are presented.

This chapter starts with a short overview of the different components of a teleoperation system: controlled master and slave device, communication channel as well as human

operator and environment. In Sec. 2.2, an overview of the design objectives is presented together with relevant measures for their evaluation. Sec. 2.3 introduces the classical control concepts that are relevant for this thesis. Finally, a detailed overview of EOT-adapting control concepts is presented for single-user systems and advantages and disadvantages are discussed.

Technical details about the experimental setups with 1 degree of freedom (DoF), 2 DoF and 6 DoF used throughout the thesis for the evaluation of the control concepts can be found in Appendix A.

2.1 System Components

In a bilateral haptic teleoperation system, a human operator performs complex manipulation tasks in a remote environment while receiving haptic feedback. Through the interaction with a haptic interface or master device, the human commands are measured. The remotely located teleoperator or slave device executes the transmitted commands, and registers haptic information about its surroundings. This information is fed back to the local site, where it is displayed to the operator. As haptic data from the local site enters the control on the remote site and vice versa, a control loop is closed over the communication channel and the architecture is called bilateral. The components of a haptic teleoperation system are shown in Fig. 2.1. The concatenation of the controlled master and slave device and the communication channel are represented as a two-port.

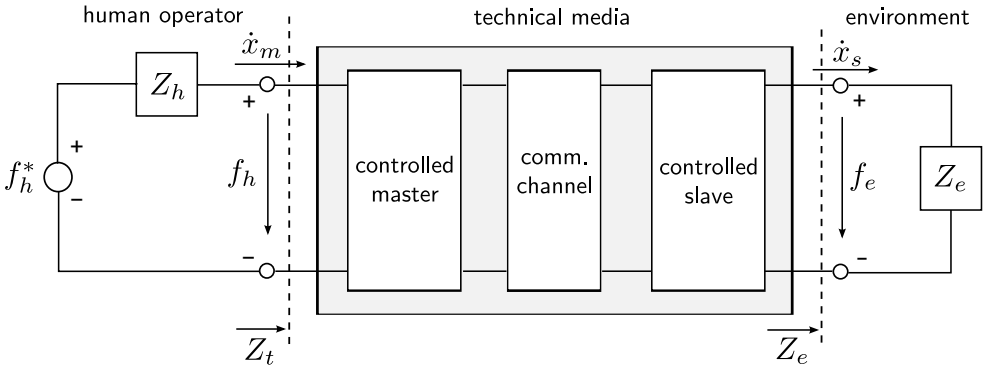

Fig. 2.1: Components of a haptic teleoperation system: human operator represented as a force source and human arm impedance, controlled master and slave device, communication channel, and remote environment represented as an impedance.

All components except for the communication channel exhibit either an *admittance* or an *impedance* characteristic. An admittance represents a dynamic mapping from forces to positions or velocities, while an impedance performs the inverse mapping from positions or velocities to forces. If the impedance and admittance mappings are assumed to be linear and time-invariant, corresponding transfer functions can be derived using the Laplace transformation. Admittance mappings $Y(s)$ and impedance mappings $Z(s)$ are defined as

$$Y(s) = \frac{V(s)}{F(s)} \qquad \text{and} \qquad Z(s) = \frac{F(s)}{V(s)}. \tag{2.1}$$

where s represents the Laplace operator and Laplace transformed variables are written in capital letters. The dependency of variables in Laplace domain on s is often omitted for a shorter presentation. There exists the inverse relationship

$$Y(s) = Z^{-1}(s) \tag{2.2}$$

between admittance and impedance.

The **human operator** commands desired actions of the teleoperator, and reacts to the feedback from the remote environment in order to perform a specific task. He/she is able to (re-)plan actions and modify physiological components like e.g. the grip force and/or arm impedance during task execution. The human operator can be represented as a mechanical one-port with the force-velocity pair of terminals f_h and $\dot{x}_m$. In order to capture the intentional as well as the physiological aspects of the human behavior, the operator dynamics is often modeled as a combination of an exogenous force $f_h^\star$ and an arm impedance $Z_h(s)$.

The **master device** or haptic interface and the **slave device** or teleoperator are robots that execute the received commands. The master is used to display the remote environment to the human, the slave performs the commanded actions in the remote environment. Local controllers have to be designed for both devices, such that they follow the desired inputs.

The operator is connected with the remote environment by exchanging haptic signals via a **communication channel.** The important characteristics for control are the latency or time delay between sending and receiving as well as packet losses (rate, dynamics, bandwidth limitations), as they can easily destabilize the closed-loop system. The characteristics depend on the distance, the time of day as well as the type of communication, e.g. local area networks (LAN) or Internet connections mainly via the UDP protocol. As such, the communication channel properties are also dependent on the application. In a minimally invasive surgery scenario, where the surgeon is in the same hospital as the patient, a local communication technology such as LAN will be chosen. The characteristics are an almost latency-free communication with negligible packet losses. On the contrary, in applications, where a robotic arm at a large distance, e.g. on a different continent, is to be teleoperated, an Internet connection is currently the most suitable communication technology. Consequently, non-negligible, probably time-varying delay and packet losses will occur. Many elegant approaches were developed to handle time delay and packet loss in teleoperation systems, see [86] for an overview.

Remote Environment. The remote environment is the place distant from the operator where the teleoperation takes place. It comprises free space and objects the operator wants to manipulate. The remote environment can be represented as a mechanical one-port with the force-velocity pair of terminals f_e and $\dot{x}_s$.

2.2 Design Objectives

The human-in-the-loop character of a teleoperation system leads to a controller design which is supposed to be human-centered. Thus, besides closed-loop stability as a prerequisite for any control system, *transparency*, *task performance*, and *feeling of presence*

are considered as important aspects. Moreover, a high degree of *usability* is desired such that the operator agrees with the actions of the system, feels comfortable, and gets easily used to it. The definitions of these design objectives and relevant measures for their evaluation are presented in this section.

2.2.1 Transparency

Transparency is a quantifiable objective. It means that the technical medium between operator and environment is not felt, i.e. that the dynamics of master, slave, and communication channel is canceled out. Transparency was independently defined by Yokokohji & Yoshikawa [218] and Lawrence [116]. In the most general way, transparency is defined in [218] as the equality of forces and velocities on master and slave site:

$$f_h(t) = f_e(t) \quad \wedge \quad \dot{x}_m(t) = \dot{x}_s(t) \tag{2.3}$$

where $f_h(t)$ is the force applied by the human operator, $f_e(t)$ the force from the remote environment, $\dot{x}_m(t)$ the master velocity, and $\dot{x}_s(t)$ the slave velocity. The impedance transmitted to the operator, $Z_t(V_m,\, s)$, and the impedance of the real environment, $Z_e(V_s,\, s)$, are defined in the Laplace domain as

$$F_h(s) \;=\; Z_t(V_m(s),\, s) \qquad F_e(s) = Z_e(V_s(s),\, s) \tag{2.4}$$

If the impedance mappings (2.4) are known, the above transparency definition can be transformed into the equality of transmitted and environment impedance and equality of master and slave velocities [116],

$$Z_t(V_s(s),\, s) = Z_e(V_s(s),\, s) \quad \wedge \quad V_m = V_s{}^1. \tag{2.5}$$

According to this definition, a teleoperation system is transparent, if no external dynamics is felt in free space and the impedance of remote objects is exactly represented at the master site during contact. This requires to cancel the dynamics of the devices and to compensate the deficiencies in the communication channel. The resulting transparent system was found to be marginally stable. Consequently, transparency and robustness are conflicting objectives [78] such that a trade-off between them has to be found.

2.2.1.1 Transparency Measures

A measure for transparency is *fidelity*. It describes the capability of a teleoperation system to accurately display the remote environment to the operator. Assuming a fixed experimental setup, the question arises which controller leads to the highest degree of fidelity. In order to answer this question, different measures for assessing the degree of fidelity have been proposed, see [35]. The most popular ones are tracking errors (difference between master and slave position/velocity or force) [218], the Z-width, a measure based on the dynamic range, and the Z-error. Further fidelity measures are e.g. proposed in [238].

[1] In the remainder of this work, the dependence of variables on time and frequency is often omitted for a shorter representation.

The *transparency error* is used as fidelity measure throughout this thesis. It was introduced by Lawrence [116] and is based on the idea that transparency is achieved if the magnitudes of Z_t and Z_e are equal, i.e.

$$\begin{aligned} |Z_t(j\omega)| &= |Z_e(j\omega)| \\ \Leftrightarrow \quad \underbrace{\log|Z_e(j\omega)| - \log|Z_t(j\omega)|_{Z_e}|}_{Z_{e,\mathrm{diff}}(j\omega)} &= 0. \end{aligned} \tag{2.6}$$

The definition of transparency can also be written as

$$\begin{aligned} |Z_t(j\omega)| &= |Z_e(j\omega)| \\ \Rightarrow \quad |Z_t(j\omega)|^2 &= |Z_e(j\omega)|^2 \\ \Leftrightarrow \quad \underbrace{\frac{|Z_t(j\omega)|^2}{|Z_e(j\omega)|^2} - 1}_{Z^{\mathrm{abs}}_{e,\mathrm{diff}}(j\omega)} &= 0. \end{aligned} \tag{2.7}$$

The area between the absolute values of a specific environment impedance curve $|Z_e(j\omega)|$ and the transmitted impedance $Z_t(j\omega)$ over a certain frequency range is consequently a measure for the degree of fidelity and referred to as transparency error. It is defined as

$$Z_{\mathrm{error}}(Z_{e,\mathrm{diff}}) = \frac{1}{\omega_{\max} - \omega_{\min}} \int_{\omega_{\min}}^{\omega_{\max}} |Z_{e,\mathrm{diff}}(j\omega)|^2 d\omega \tag{2.8}$$

As shown in (2.6) it can also be formulated as

$$Z^{\mathrm{abs}}_{\mathrm{error}}(Z_{e,\mathrm{diff}}) = \frac{1}{\omega_{\max} - \omega_{\min}} \int_{\omega_{\min}}^{\omega_{\max}} |Z^{\mathrm{abs}}_{e,\mathrm{diff}}(j\omega)|^2 d\omega \tag{2.9}$$

The lower the transparency error, the higher is the degree of fidelity.

2.2.1.2 Perceived Transparency

Transparency/fidelity definitions and measures can be further relaxed by taking the human perception capabilities and limitations into account. An important measure from psychophysics is the *just noticeable difference (*JND_s*)* which is the smallest difference in a sensor input s that is discriminable for the human operator. The ratio between the change in the perceivable amplitude of the stimulus and the amplitude of the stimulus itself can be assumed to be roughly constant. As a consequence, the JND is often given as the percental change of the amplitude of a stimulus below which the operator does not perceive a difference. The JND for human movement discrimination capabilities in the arm/forearm is e.g. around 8% according to [99]. This implies that an arm movement of 0.3 m cannot be distinguished from any arm movement in the range of $[0.276; 0.324]$ m. An overview of JNDs for physical quantities related to haptic teleoperation such as force, motion, stiffness, inertia, etc. are summarized in [80].

The implication of the just noticeable difference is that the impression of the remote environment is realistic as long as the differences between the transmitted and the real environment do not become perceivable to the human operator. This reduces the required accuracy for haptic feedback to be transparent. This is considered in the recently proposed definition of *perceived transparency* [81]. As long as the transmitted impedance lies in the imperceptible range around the true environment impedances

$$Z_t(j\omega) \in [Z_e(j\omega) - \mathrm{JND}_{Z_e}(j\omega),\ Z_e(j\omega) + \mathrm{JND}_{Z_e}(j\omega)] \tag{2.10}$$

the system is called perceived transparent. It is important to note that the $\mathrm{JND}(j\omega)$ is dependent on the phase difference. As discussed in [81], new findings show that JNDs independent of the phase difference are not suitable here. In this work, the concept of perceived transparency is applied to the equality of forces and velocities, i.e. to the transparency definition by Yokokohji [218]. If the velocities can be assumed to be roughly equal, i.e. $\dot{x}_m \cong \dot{x}_s$, the difference in transmitted and real environment force, $f_{e,t}$ and f_e, is required to be imperceptible:

$$f_{e,t} \ \in [f_e - \mathrm{JND}_f;\ f_e + \mathrm{JND}_f]. \tag{2.11}$$

Vice versa, under the assumption that a stiff force tracking is realized such that $f_h \cong f_e$, a teleoperation system is perceived transparent if the difference in transmitted and real velocity, $\dot{x}_{s,t}$ and $\dot{x}_s$, is not perceivable:

$$\dot{x}_{s,t} \ \in [\dot{x}_s - \mathrm{JND}_{\dot{x}};\ \dot{x}_s + \mathrm{JND}_{\dot{x}}]. \tag{2.12}$$

As the JND*s* were only shown to be phase-dependent for impedances, the JNDs for force, JND_f, and velocity, $\mathrm{JND}_{\dot{x}}$, are still assumed to be static.

2.2.2 Performance

The main purpose of a teleoperation system is to provide technical means to successfully perform a desired task in a remote environment. Consequently, these systems should be designed to achieve high task performance. The minimum required task performance for a specific experimental setup and application area is the realizability of a task. This implies to overcome barriers like distance, scale, time delay, or hazardousness. Moreover, teleoperation systems are not only capable of overcoming limitations in the environment but also those inherent to the operator. For example, by reducing the surgeon's hand tremor in a microsurgical application, the task can be performed even better than if directly performed by the surgeon. Similarly, a micro-assembly task is considerably facilitated for the operator, if the movements can be performed on human scale at the local site and be scaled down at the remote place.

For evaluation, physically accessible quantities have to be found for the considered task. The most common quantities are task completion time, error measures, applied forces, or induced or dissipated energies. A broad overview of performance measures is given in [147] for virtual environments. Recently, Groten [73] presented an overview of performance measures, that were evaluated for different haptic human-human and human-

robot interaction tasks. Table 2.1 summarizes the performance measures that are relevant for this thesis.

Regarding force-related measures, applied forces can be decomposed into external forces, $\boldsymbol{f}_{\text{ext}}$, and interactive forces, $\boldsymbol{f}_{\text{int}}$: $\boldsymbol{f} = \boldsymbol{f}_{\text{ext}} + \boldsymbol{f}_{\text{int}}$. Interactive forces represent tension, compression, shear or tension forces, see also Sec. 2.2.4.3 and occur in bimanual, multi-fingered manipulation of objects [70, 220], in cooperative robotics, see e.g. [18, 31, 107, 180], in haptic human-machine interaction where the machine behaves in a (pro)-active manner, see e.g. [236] and in human-human interaction [72, 164, 190]. Only external forces lead to a motion of the interaction point. Thus, in most cases, only the external forces are important for performance evaluation.

Tab. 2.1: Summary of relevant task performance measures. The measures are assumed to be calculated offline and over a whole trial with a total number of K samples and sampling time T_a. A force vector at sample $k \in \{1, \dots, K\}$ is denoted by $\boldsymbol{f}_k$, and a velocity vector by $\dot{\boldsymbol{x}}_k$. An average value is denoted by an overline.

Temporal	Task completion time	TCT [s]	$\text{TCT} = K \cdot T_a$
Error-related	Number of errors	C_E [samples]	$C_E = \sum c_E$
	Error time	ET [s]	$\text{ET} = C_E \cdot T_a$
Force-related	Mean applied forces	$\overline{f}$ [N]	$\overline{f} = \frac{1}{K} \sum_{k=1}^{K} \lVert \boldsymbol{f}_k \rVert$
	Mean applied external forces	$\overline{f}_{\text{ext}}$ [N]	$\overline{f}_{\text{ext}} = \frac{1}{K} \sum_{k=1}^{K} (\lVert \boldsymbol{f}_{k,\text{ext}} \rVert)$
Energy-related	Mean mechanical work	$\overline{W}$ [Nm/s]	$\overline{W} = \frac{1}{K} \sum_{k=1}^{K} (\lVert \boldsymbol{f}_k^T \dot{\boldsymbol{x}}_k \rVert)$

Besides objective performance measures, the subjectively perceived task performance can be evaluated using questionnaires. The extent to which objective and subjective performance match is important for deriving general guidelines and improving the design. Thus, user studies including questionnaires were conducted throughout the thesis, additionally to obtain objective performance measures.

2.2.3 Feeling of Presence

Feeling of presence is a qualitative objective. It refers to the operator's *feeling of being there*, the feeling of being present in the remote environment [147, 182, 215]. Ideally, the operator cannot distinguish between the feeling of being present in a remote place and the real world. Technical limitations, however, make it difficult to reach this state. But even under the assumption of reaching this state the question arises, why it is important to make the operator feel present at the remote site. The preliminary reason arises from the belief, that presence is correlated with task performance in a positive, causal way [127, 212]. This means that by improving the feeling of presence, task performance is improved as well. Some studies support this statement, see e.g. [100]. Yet, contradictory statements are also found in literature, see [37, 161]. In the study by Clarke [37], it is found, for example, that the prediction of positions on teleoperator site clearly improves task performance, while

participants do not report an improved feeling of presence. Pongrac et al. [161] cannot show a correlation between presence and performance measured over task execution time or covered distance. However, they found a positive effect between feeling of presence and applied forces and torques. Due to these contradictory statements the question of a positive influence of feeling of presence on task performance remains open.

One feasible conclusion whether feeling of presence and task performance are positively correlated is drawn by Welch [212] and Ma et al. [127]. They state that it may depend on the scenario and task, if a correlation between task performance and increased feeling of presence can be expected or not. For everyday tasks, a human may not need a strong feeling of being present in the remote environment, as those tasks are done almost automatically. For unknown tasks or in unstructured, unknown and changing environments, however, a strong feeling of presence will help the operator to better perform the task, such that feeling of presence could have a positive effect on task performance in these kind of scenarios. Besides that, it may also depend on the choice of the task performance measure whether such a correlation exists or not.

Beside the reasoning about a possible correlation between feeling of presence and performance, providing a strong feeling of presence also gives the operator the possibility to perform actions in teleoperation mode similar to actions in the real world [185]. Without a strong feeling of presence, the system cannot be used intuitively and the operator would have to train intensively to control the system in a desired and successful way.

For evaluating feeling of presence, mostly subjective presence measures like questionnaires, see e.g. [215], or ratings are used. The individual and subjective nature of the feeling of presence makes it difficult to derive quantitative measures, based on which control concepts could be developed. Thus, a control approach that directly improves the feeling of presence is not presented in this thesis. It is rather assumed, that a strong feeling of presence can be achieved by providing the operator with feedback from as many different modalities as possible and as realistic as possible.

2.2.4 Usability

Finally, the designed system should be accepted by the users. In ISO 9241-11, usability is defined as "the extent to which a product can be used by specified users to achieve specified goals with effectiveness, *efficiency* and *satisfaction* in a specified context of use." An efficient task execution also implies that the operator has free cognitive resources to e.g. solve unexpected events. This again implies that the *required mental workload* should be small. Otherwise, also the subjective pleasure could be deteriorated. In a shared-control context the commands of a haptic assistance are combined with the operator input. Thus, it is furthermore important that human and machine *agree* in their actions. This thesis addresses the highlighted aspects of usability: efficiency, subjective pleasure, mental workload, and agreement.

2.2.4.1 Efficiency

Efficiency is an evaluation tool often used in engineering or physics to determine the ratio between input and useful output in terms of e.g. electric power, mechanical work, or heat.

It is also determined in economics [47] and in the field of human-computer interaction [16, 151] as outlined by [73]. For the evaluation of human-machine systems, it was first introduced by Hart & Wickens [77]. Groten [73] proposed an efficiency measure for two humans collaborating in a kinesthetic task. This measure is also adopted in this work. A high efficiency is achieved, if the effort is low and the performance is high, see [25]. Efficiency E between task performance P and workload measure W is defined according to [72] as

$$E(P,W) = \frac{z(P) - z(W)}{\sqrt{2}} \tag{2.13}$$

where $z(X) = \frac{X - \text{mean}(X)}{\text{std}(X)}$ is the standard score of X. This efficiency measure is a relative measure, such that only comparisons between different conditions are interpretable.

2.2.4.2 Mental Workload

Questionnaires are so far the main evaluation tool for addressing the perceived workload of users. The NASA TLX questionnaire [93] was designed to determine the mental workload of a user. According to this questionnaire, perceived workload is composed of mental, physical, and temporal demand of the task, subjective effort and performance, and the frustration level in different weighting depending on the users' individual prioritization. The procedure for determining the weights and calculating the overall mental workload is described in [93].

2.2.4.3 Agreement

Agreement in human-machine interaction is identified in this thesis as one important aspect for designing performance-oriented controllers. In [206], a disagreement measure was proposed in the area of powered wheelchairs. It is based on the angle between the desired operator and haptic assistance command. This thesis provides the first objective and quantifiable, force-based agreement measure. The usefulness of the proposed criterion for measuring agreement/disagreement has been evaluated in an experiment presented in Chap. 5 and previously published in [236]. In [239], the agreement measure is used to detect and correct wrongly identified tasks. The agreement measure is based on mean interactive forces $\overline{f_{\text{int}}}$ between human and machine as introduced in Table 2.1. It was already hypothesized in [165] that difference forces between two haptically interacting humans are a "measure of disagreement between the partners". As shown in [72], difference forces can, however, contribute to the motion of the object. Thus, interactive forces as proposed by [72] are used in this study, as they do not lead to motion of the object. Interactive forces occur when two partners push or pull in different directions, i.e. they represent compressive or tension forces, see Fig. 2.2. Under the assumption that the coordinate systems of the applied forces are the same, interactive forces are defined for one direction as follows, see [72] and Fig. 2.2:

$$f_{\text{int}} = \begin{cases} f_1 & \text{if } \text{sign}(f_1) \neq \text{sign}(f_2) \wedge |f_1| \leq |f_2| \\ -f_2 & \text{if } \text{sign}(f_1) \neq \text{sign}(f_2) \wedge |f_1| > |f_2| \\ 0 & \text{else.} \end{cases} \tag{2.14}$$

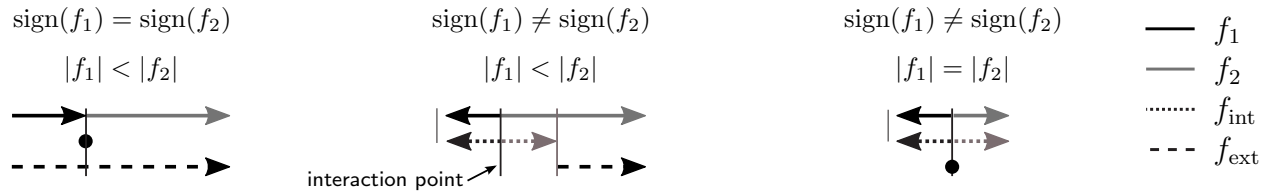

Fig. 2.2: Illustration of interactive forces in one direction. Interactive forces $\boldsymbol{f}_{\text{int}}$ represent tension, compression, or shear forces and do not lead to a motion of the interaction point.

Naming conventions differ from a statistical and engineering point of view. From a statistical point of view, two different scales are used to measure agreement: i) a *nominal* scale only distinguishing agreement and disagreement and ii) a *ratio scale* quantifying the degree of agreement/disagreement. From an engineering point of view, *discrete* refers to nominal scale and *continuous* refers to ratio scale.

The continuous measure is based on mean interactive forces $\overline{f_{\text{int}}}$ of a trial with K samples

$$\overline{f_{\text{int}}} = \underset{K}{\text{mean}}\, |f_{\text{int}}|. \tag{2.15}$$

Continuous disagreement D is measured as the mean interactive forces normalized over a set of R trials $N(\overline{f_{\text{int}}}) = \frac{\overline{f_{\text{int}}}}{\max_R(\overline{f_{\text{int}}})}$. Agreement is the inverse of disagreement leading to

$$A = 1 - N(\overline{f_{\text{int}}}) \qquad D = N(\overline{f_{\text{int}}}). \tag{2.16}$$

As the proposed agreement measure is force-based, the zero point coincides with zero force. The states agreement and disagreement denoted by d_A and d_D are distinguished online based on the measured interactive force f_{int} as

$$d = \begin{cases} d_A & \text{if } |f_{\text{int}}| \leq T_{\text{int}} \\ d_D & \text{else} \end{cases} \tag{2.17}$$

where $T_{\text{int}} > 0$ is a threshold separating agreement from disagreement.

2.3 Classical Control Concepts

In haptic teleoperation, two robotic systems are connected with each other over a communication channel. Thus, the control design comprises the selection of local controllers for each of the devices and the selection of a communication architecture for connecting the two sites. An overview of local controllers as used in many teleoperation systems is provided in Sec. 2.3.1. For the connection of the two robotic systems, a variety of different approaches was developed. In this thesis, two classes of control concepts are distinguished: *classical* and *augmenting* control concepts. A definition and an overview of current classical control concepts that are relevant for this thesis are presented in Sec. 2.3.2, while Sec. 2.4 is dedicated to a detailed overview of augmenting control concepts, the main focus of this thesis.

2.3.1 Local Controllers

The decision on the local controllers is mainly influenced by the type of master and slave devices as well as by the application area and with it the available sensors and actuators. The communication architecture may further restrict the number of suitable local controllers and vice versa.

2.3.1.1 Time-Invariant Controllers

If haptic devices are characterized by a low weight, low inertia, and a high back-drivability and bandwidth such as the Phantom group by Sensable developed at MIT [135], the Novint Falcon [134], or the DLR light-weight arm [82], force sensing capabilities are not necessarily required. Here, especially explicit force or impedance controllers or motion (position/velocity/acceleration) controllers are used. If, on the contrary, haptic devices possess high force output capabilities and a large workspace like the *Haptic*MASTER [42], the DELTA haptic device [68], or the ViSHaRD group [188, 202] together with the anthropomorphic robotic arms, force sensing is provided. Force sensing is required in order to reduce the device dynamics via a controller. The most prominent controllers for these devices are impedance and admittance controller, first introduced by [83]. As shown in Fig. 2.3, the admittance dynamics maps the desired input force f^d to a desired position x^d or position modification δx^d, while the impedance dynamics maps the desired input position to a reference force f^d. Underlying force or position/velocity controllers drive the robot to the desired reference signal. Model-based compensations of device dynamics like frictional or gravitational forces and a force feedforward are often incorporated in the control architecture. As a consequence, neglecting disturbances and controller deficiencies, the closed-loop robotic system behaves according to the dynamics described in the admittance/impedance blocks. The master site admittance/impedance dynamics mostly represents *target dynamics* that is mainly perceivable in free space. The slave site admittance/impedance dynamics often represents a *compliant behavior* which is important for stability during contact. A more detailed description of the different force and motion controllers as well as the different types of impedance/admittance controllers can be found in [201].

2.3.1.2 Adaptive Controllers

Adaptive controllers are used to compensate uncertainties in the master and slave dynamics [176] by estimating a model of the uncertain dynamics and changing the control parameters accordingly. In many cases, adaptive controllers are also designed to compensate for different environments or operator behaviors, see e.g. [79, 225, 226]. In this case, they will be attributed to the class of augmenting controllers.

2.3.2 Control Architectures

Many bilateral controllers do not adapt online to the operator behavior, the encountered remote environment, or the executed task. These control approaches are referred to as *classical control approaches* in this thesis. The tuning of their control parameters can be

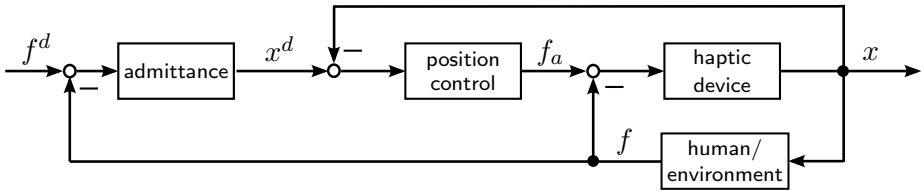

(a) Admittance control

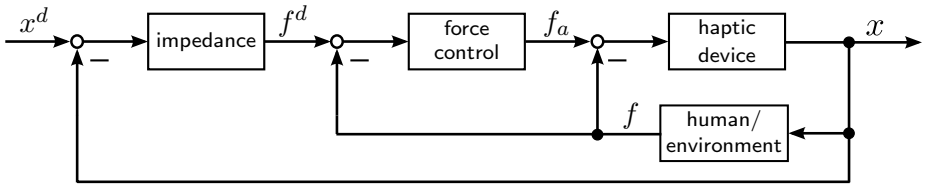

(b) Impedance control

Fig. 2.3: Admittance and impedance controller. A desired force is the input to an admittance controller and a desired position is the input to an impedance controller. The position or force resulting from the admittance/impedance mapping is tracked using position and force controllers, respectively.

based on assumptions like passively behaving operator and environment [149], simplified model assumptions for human and environment, like LTI mass-spring-damper systems with exogenous input force or trajectory [78], or static upper and lower bounds on model parameters or magnitude of transfer functions.

The decision on the communication architecture is based on the characteristics of the communication channel, i.e. whether time delay is present, of which magnitude it is, and whether it is constant or time-varying. Further factors are packet loss and its characteristics and the bandwidth of the communication channel. In the following, the 4- and 2-channel control architectures as proposed by Lawrence [116], adaptive and robust control architectures, and the wave variable approach are presented.

2.3.2.1 4- and 2-Channel Architectures

From a physical point of view, it is intuitive to directly exchange haptic signals between local and remote site.

4-channel Architecture. In this context, Dale A. Lawrence [116] developed the *4-channel architecture* in 1993, see Fig. 2.4. Force and velocity signals are sent from master to slave and vice versa. The controllers are assumed to be linear and time-invariant. The resulting teleoperation system is transparent if the selected controllers compensate perfectly the device dynamics. The controller outputs on master and slave site are the actuator forces f_{am} and f_{as} which are given by

$$f_{am} = C_6 f_h - C_2 f_e - C_m \dot{x}_m - C_4 \dot{x}_s \tag{2.18}$$

$$f_{as} = C_3 f_h - C_5 f_e + C_1 \dot{x}_m - C_s \dot{x}_s, \tag{2.19}$$

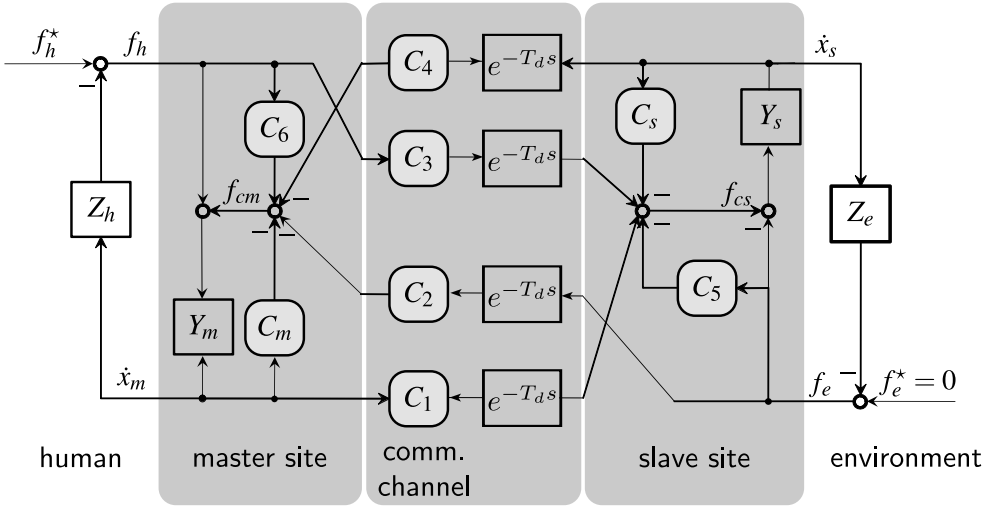

Fig. 2.4: 4-channel architecture introduced by Lawrence [116]. Master force and velocity is sent to the slave site and slave force and velocity is sent to the master site.

where C_m, C_s, C_5, C_6 are referred to as local controllers and C_1, C_2, C_3, C_4 as coordinating controllers. Different types of controllers ranging from explicit force and velocity/position controllers to impedance- and admittance-type controllers can be used. Another representation form originates from network theory. Equivalently to the representation of electrical networks, teleoperation systems can be described as a concatenation of one- and two-ports. In the most compact way, controlled master and slave devices are summarized together

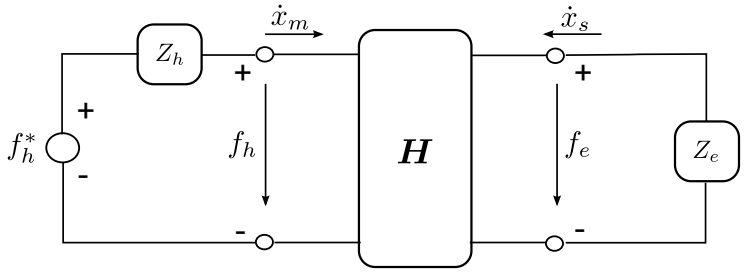

Fig. 2.5: Network representation of a haptic teleoperation system. Operator and environment are represented by one-ports and connected to each other via the two-port consisting of controlled master and slave devices as well as the communication channel.

with the communication channel into one two-port, which is fed from one side by the human operator represented as a generator-type one-port and from the other side by the remote environment represented as a load-type one-port, see Fig. 2.5. This compact representation facilitates the investigation of stability and transparency. The two-port properties are collected in the hybrid network matrix $\boldsymbol{H}$ which maps the signals $[V_m, F_e]$ in the Laplace domain to $[F_h, -V_s]$:

$$\begin{bmatrix} F_h \\ -V_s \end{bmatrix} = \boldsymbol{H} \begin{bmatrix} V_m \\ F_e \end{bmatrix}. \tag{2.20}$$

For the 4-channel architecture, the elements of the $\boldsymbol{H}$ matrix depend on the local and coordinating controllers as well as on the device dynamics Z_m and Z_s

$$\boldsymbol{H} = \begin{bmatrix} h_{11} & h_{12} \\ h_{21} & h_{22} \end{bmatrix} \tag{2.21}$$

$$= \frac{1}{\det \boldsymbol{H}} \begin{bmatrix} (Z_m + C_m)(Z_s + C_s) + C_1 C_4 & C_2(Z_s + C_s) - C_4(1 + C_5) \\ -(C_3(Z_m + C_m) + C_1(1 + C_6)) & (1 + C_5)(1 + C_6) - C_2 C_3 \end{bmatrix} \tag{2.22}$$

where $\det \boldsymbol{H} = (1 + C_6)(Z_s + C_s) - C_3 C_4$. The closed-loop transfer function is found from the $\boldsymbol{H}$ matrix elements as

$$G(s) = \frac{V_m}{F^d} = \frac{h_{22} Z_e + 1}{(h_{22} Z_e + 1) Z_h + \det(\boldsymbol{H}) Z_e + h_{11}}. \tag{2.23}$$

2-channel Architecture. In a 2-channel architecture, only one haptic signal is sent and received on each site. The 2-channel architectures are less complex than the 4-channel architecture and require fewer sensors. The nomenclature in this thesis follows the one proposed in [78]. According to this nomenclature, a 2-channel architecture is denoted by the input signal to the master controller (V: velocity, P: position, F: force) followed by the input signal to the slave controller. In a VF architecture, for example, the slave velocity is received on the master site and the operator force is sent to the slave. Architectures with admittance controllers are marked with an additional 'a' leading to the architectures VaVa or PaPa, FaVa, FaPa, VaFa, PaFa, and FaFa.

The experimental setups used in this thesis are characterized by their admittance-type devices. Especially for the 6 DoF experimental setup, it was found in [155] that the FaFa architecture, shown in Fig. 2.6, is favorable over the other 2-channel architectures as it requires only two parameters to be tuned due to its symmetry. As this architecture is used as

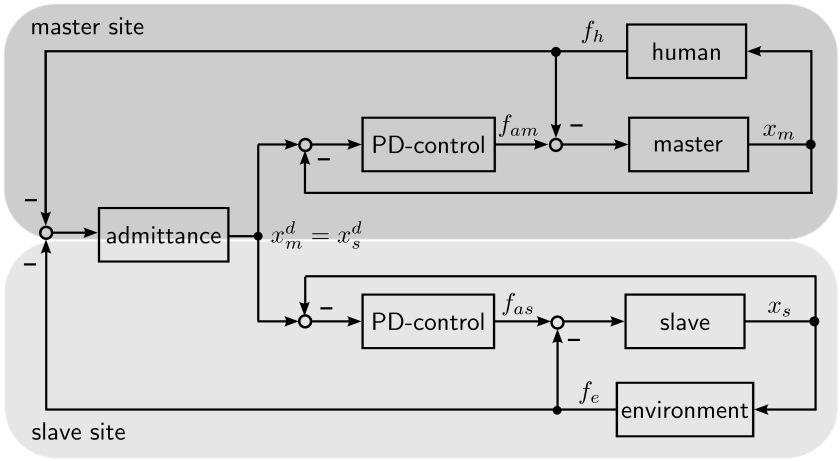

Fig. 2.6: FaFa control architecture. Forces are exchanged between the two sites and enter a cascade control consisting of an admittance and an underlying position (or velocity) controller.

benchmark architecture and as basis for augmenting control concepts, a general description

of the dynamics in state-space notation is introduced next. An arbitrary (linear/nonlinear, time-invariant/time-varying) admittance dynamics is denoted by $g_a(\boldsymbol{\chi}^d, \boldsymbol{p}_a(t))$, where the desired and measured position, x^d and x, measured and desired velocity, $\dot{x}^d$ and $\dot{x}$, and acceleration, $\ddot{x}^d$ and $\ddot{x}$, are summarized in the sets $\boldsymbol{\chi}^d = \{x^d, \dot{x}^d, \ddot{x}^d\}$ and $\boldsymbol{\chi} = \{x, \dot{x}, \ddot{x}\}$, respectively. The models for operator, environment, and haptic devices are introduced in Sec. 2.1. The desired master and slave positions are tracked using proportional-derivative (PD) controllers with gains K_p and K_d, respectively. The possibly time-varying admittance parameters are summarized in the vector $\boldsymbol{p}_a(t)$. Neglecting deficiencies in the communication channel, the 1 DoF dynamics of the FaFa architecture is finally given by

$$\begin{aligned}
\text{(Human)} \quad & 0 = \tilde{f}_h - (m_h\ddot{x}_m + b_h\dot{x}_m + k_h x_m) + f_h^\star && (2.24)\\
\text{(Environment)} \quad & 0 = \tilde{f}_e + g_e(\boldsymbol{\chi}_s) && (2.25)\\
\text{(Master device)} \quad & 0 = \tilde{f}_h - f_m + m_m\ddot{x}_m + b_m\dot{x}_m && (2.26)\\
\text{(Slave device)} \quad & 0 = \tilde{f}_e - f_s + m_s\ddot{x}_s + b_s\dot{x}_s && (2.27)\\
\text{(Master position control)} \quad & 0 = f_m + K_{pm}(x_m^d - x_m) + K_{dm}(\dot{x}_m^d - \dot{x}_m) && (2.28)\\
\text{(Slave position control)} \quad & 0 = f_s + K_{ps}(x_s^d - x_s) + K_{ds}(\dot{x}_s^d - \dot{x}_s) && (2.29)\\
\text{(Master admittance)} \quad & 0 = \tilde{f}_h - \tilde{f}_e + g_{\mathrm{adm}}(\boldsymbol{\chi}_m^d, \boldsymbol{p}_a(t)) && (2.30)\\
\text{(Slave admittance)} \quad & 0 = \tilde{f}_h - \tilde{f}_e + g_{\mathrm{adm}}(\boldsymbol{\chi}_s^d, \boldsymbol{p}_a(t)) && (2.31)
\end{aligned}$$

where $\tilde{f}_h = G_s f_h$ and $\tilde{f}_e = G_s f_e$ are measured and *filtered* human and environment force, see also Sec. 2.1. The unfiltered forces are denoted by f_h and f_e, respectively. The advantage of the FaFa architecture is the small number of parameters. The admittance dynamics on master and slave site has to be the same in order to guarantee position tracking. Thus, apart from the underlying velocity/position controllers, only the parameters of one admittance have to be tuned. Furthermore, the admittance is often characterized by a mass-damper dynamics. This physically motivated model facilitates the parameter tuning further.

2.3.2.2 Robust Controllers

Robust controllers, H_∞ [90, 118, 177, 217] and/or μ-synthesis [119, 183] approaches were mainly developed to deal with time delay in the communication channel. Shadi & Sirouspour [181] combined adaptive controllers and an H_∞ approach to compensate nonlinear master and slave dynamics and to achieve robustness in the presence of constant time delay.

2.3.2.3 Scattering Transformation and Wave Variable Approach

Two of the most prominent approaches for haptic teleoperation systems are the scattering transformation introduced by Anderson & Spong [12] and the wave variable approach proposed by Niemeyer & Slotine [149]. Both methods are especially suitable for systems with deficiencies in the communication channel. A variety of extensions to these methods were proposed in literature. They are summarized in the review article by Hokayem & Spong

[86]. The idea of both approaches consists in passivating[2] the communication channel. This is achieved by exchanging a linear combination of forces and velocities referred to as incident/reflective wave (scattering transformation) or wave variables instead of exchanging haptic signals. The other subsystems of a teleoperation system are assumed to be passive. As all subsystems are concatenated in parallel or feedback connection, it can be shown that the overall system is again passive and, thus, stable.

2.4 EOT-adapting Control Concepts

Besides the classical control approaches, a variety of controllers were developed, which depend explicitly on online gained environment, operator, or task knowledge, see Fig. 2.7. Through the incorporation of this additional knowledge in the controller, quality improvements in terms of an increased degree of fidelity, feeling of presence, or improved task performance can be achieved. As most of the state-of-the-art methods in advanced teleoperation are adaptive to online gained knowledge of either environment, operator, or task, these controllers will be referred to as *EOT-adapting controllers*, see also [238]. The focus on one component (operator, environment, task) is not surprising, as the dynamics and methods for modeling human, environment, or task differ significantly from each other. Considering a transportation task, for example, the important knowledge is the sequence of subtasks to be performed. Subtasks in this case could be path-following, obstacle avoidance, or positioning. For contact with objects in the remote environment, on the contrary, a physically motivated model of the object yields important information.

As this thesis focuses on EOT-adapting controllers for an increased degree of fidelity and performance, the state-of-the-art literature in this area is described in detail in this section and discussed in terms of advantages and disadvantages. The approaches are classified according to the design objective they focus on.

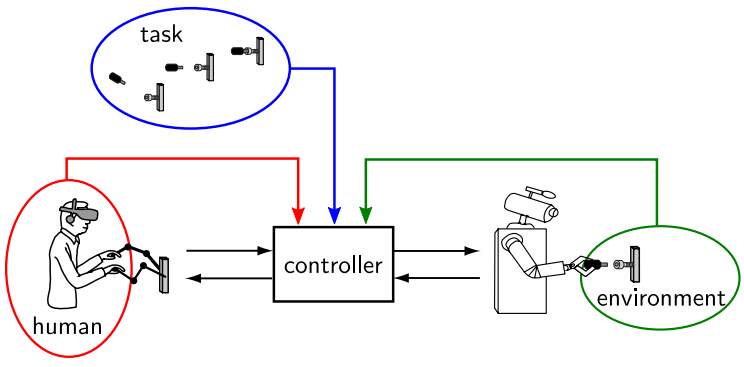

Fig. 2.7: Illustration of an EOT-adapting controller, see also [238]. Online gained knowledge about environment, operator, or task enters the control law.

[2]Passivity is sufficient for stability, see e.g. [104].

2.4.1 Fidelity Augmentation

As mentioned above, EOT-adapting control concepts focus mainly on the incorporation of either environment, operator, or task knowledge. Fidelity augmentation was achieved for environment- and operator-adapting controllers as will be presented in this section. The borders between environment, operator-, and task-adaptation are certainly subject to discussion. According to the classification presented in this thesis, task knowledge was so far not used in order to improve fidelity and may represent a future research direction.

2.4.1.1 Operator-adapting Approaches

Approaches for operator-adapting fidelity augmentation are not limited to telerobotics. Some interesting approaches that can be transferred to telerobotics are also found in the area of human-robot collaborative manipulation (HRCM). The difference between an HRCM system and a shared-control teleoperation system is that the control is distributed between an autonomously acting agent and the operator in teleoperation, while it is shared between a human and an autonomous robot in an HRCM task. When human and robot perform a task together, for example moving an object, one important goal is that the human and robot adapt to each other as humans would do when performing the task together. The adaptation of the robot to the operator can either be realized in a passive or active manner.

Regarding passive approaches for HRCM, one of the first variable impedance controllers was proposed by Ikeura & Inooka [92] and further developed in [163]. A similar approach for the lower extremities was presented by Tanaka et al. [194]. In [92], an offline identification of operator mass and damping was conducted for segmented position and force trajectories of two persons performing a point-to-point movement. In [163], mass, spring and damping coefficients of the human arm impedance were identified offline. As the variance in the mass parameter was low, this parameter was set to a constant value in both cases. The damping parameter [92] or the damping and stiffness parameter [163] of the impedance controller were varied according to the found heuristics to improve human-robot collaboration. This variable impedance controller can equivalently be used as master controller in a teleoperation system. It can be expected that the variable impedance controller facilitates teleoperator motions. This method was further developed by various authors, as presented in the following. The control parameters are made online adjustable and the method exhibits superior performance and becomes suitable for a larger application area. Again, instead of implementing the controller on an autonomous robot, it can be implemented as an autonomously acting agent on the master site of a teleoperation system. The result is a haptic shared-control teleoperation system.

Tsumugiwa et al. [199] adjusted the damping parameter in the robot's admittance controller according to the estimated stiffness of the human arm using an RLS algorithm. As the damping parameter in the controller is chosen as low as possible for a particular arm stiffness, this approach increases the degree of fidelity. Moreover, the precision of a drawing task, collaboratively performed between human and robot, was improved. This concept can also be implemented in a teleoperation system, although attention has to be paid, if contact with remote objects is encountered. If the damping parameter is too small due to

a low arm stiffness the system can become unstable. Consequently, in a teleoperation system, this method would have to be switched off during contact. A user study to show the improvements of this approach compared to non-adaptive approaches was not conducted.

The work of Botturi et al. [19] was inspired from findings in psychophysics. The approach is based on human capabilities of discriminating forces in different directions. In a psychophysical experiment, the authors found a relationship between the just-noticeable difference and force intensity from the environment. This finding was used to derive a scaling function, applied to signals sent from slave to master, in order to improve the haptic feedback. As a result, small force differences should be distinguishable at low force intensities. The approach was therefore found to be most valuable in tasks requiring the distinction of small forces. Although a user study is still missing, preliminary results showed the desired effect.

Another possibility for improving fidelity taking operator knowledge into account was proposed by Kuchenbecker & Niemeyer [112, 113]. The idea was to cancel induced high-frequency motions of the operator. Unexpectedly high force feedback leads to oscillatory operator motions. By canceling the type of motions induced by haptic feedback, the operator's trajectory is considerably smoothened, i.e. less oscillatory. Thus, instead of sending the measured master position, motions based on the model-based estimation of induced dynamics are subtracted from the master position before sending. Results show improved robustness and a more realistic touch of the remote objects. For this approach, it is, however, not clear whether the controllers can be designed such that the system becomes transparent. Also, the approaches presented so far cannot compensate deficiencies in the communication channel and are therefore limited in their applicability to systems with large time delays (≥ 0.5 s).

Summarizing the passive, operator-related approaches [19, 92, 163, 199], an adaptation of the control parameters is limited in the amount of fidelity augmentation, especially compared to active support concepts as presented in the following paragraphs.

An active support of the operator's intended movements is proposed by Jarrasse et al. [97]. The idea is to combine the replay of recorded trajectories either on the position or the actuator torque level with an online force feedback controller such that the operator can alter the replayed trajectory. By predicting human's motion Jarrasse et al. [97] showed an improved fidelity. Interaction forces were considerably reduced, if an equally weighted combination of force feedback and trajectory tracking were used. This implies an improvement in fidelity. As the trajectory tracking seems to be most efficient during the accelerating and decelerating phase, it is proposed at this point to vary the weighting between human and machine input. The experimental results in [97] were obtained for free space motions and can be different for constrained motions. Moreover, a simple replay of trajectories can only be used in a teleoperation system, if the task is repeated several times such that the motion can be recorded. In tasks, where objects in the remote environment are approached, which can be measured using an additional distance sensor, the end-point of the movement can be inferred. A pre-recorded trajectory of the operator can then be scaled to the expected movement and the approach is applicable. The approach is only as good as the movement prediction. Many and sudden changes cannot be tracked well such that this approach has limited applicability to unstructured and non-repetitive tasks.

As one of the main objectives of this thesis is to present a realistic haptic impression of the remote environment, i.e. of objects rather than free space, to the operator, operator-related approaches for fidelity improvement are not further pursued.

2.4.1.2 Environment-adapting Approaches

As known from autonomous robotics, see e.g. [76, 84, 213], the contact with stiff objects can destabilize the system. In autonomous robotic manipulation, compliant motion controllers or a passive mechanical compliance are often used to reduce high interaction forces between robot and environment. Also in haptic teleoperation, one solution to this problem is a highly damped target dynamics on master or a highly compliant controller on slave site. Both types of controllers damp high-frequency force components and avoid large position changes. However, a high damping on master site reduces the degree of fidelity in free space and a highly compliant controller on slave site distorts the haptic impression of an object [76], and the object feels softer than it is. In order to improve the fidelity of these control concepts, the control parameters should be adapted according to the encountered environment.

Love & Book [125] proposed to adapt the damping on master site depending on the estimated environment stiffness. A recursive least-squares (RLS) approach was used for the estimation. Thus, only the minimum damping required for stabilizing the system was applied in free space and the increase of the damping during contact was dependent on the object rigidness. The result is an improvement in fidelity compared to a non-adaptive approach without risking stability.

Taking time delay into account, Cho & Park [32] proposed the adaptation of the slave damping according to the distance between slave and remote objects. The distance was measured using an ultrasonic sensor. The aim of the approach is to obtain both, good tracking performance and robust stability when moving from unconstrained to constrained space. Llewellyn's stability criterion [123] was used for the parameter selection such that stability was guaranteed. The same architecture as in the approach by Love & Book was used. The damping on slave site was smoothly faded between free space and contact damping, starting at a prespecified distance from the object. With this approach, the magnitude of impact forces and the tracking errors were reduced. However, the stability analysis was conducted for a specific object. For different objects, the chosen damping values are consequently not optimal anymore, and a considerable improvement in tracking performance and impact stability cannot be expected.

Al-Jarrah & Zheng [10] proposed a human-inspired approach for choosing the damping in order to minimize the interaction forces. Formulated as an optimization criterion and combined with the finding that the stiffness of a human muscle grows exponentially with the force, an optimal damping is found for the impedance controller. This method was combined in a teleoperation setup by Cheung & Chung [30] with the variable impedance controller by Love & Book [125]. In addition, a Lyapunov-based approach was used to adapt the dynamics of the slave controller. Depending on the measured force from the environment, the adapted slave dynamics were smoothly faded to the biology-inspired impedance controller. The resulting system exhibits desired dynamics using the variable admittance controller on master site and avoids high interaction forces using the human-

inspired impedance controller on slave site.

To improve the fidelity especially for contact with stiff or rough objects, Kuchenbecker & Niemeyer [114] proposed to combine low-frequency position feedback with high-frequency acceleration feedback. The idea is to apply additional forces on the master device such that high-pass filtered accelerations measured at slave site match with the accelerations of the master device. The improvement is a more realistic haptic impression of remote objects, especially in terms of stiffness and roughness. This approach requires to measure the acceleration on slave site and is mainly suited for stiff or rough objects. Its applicability to other types of objects and to systems with deficiencies in the communication channel is an open research question so far.

The fidelity of the approaches presented so far is dependent on the dynamics of the controlled teleoperator and the deficiencies in the communication channel and on the controlled teleoperator. This implies that the control parameters have to be adapted especially to the deficiencies in the communication channel. Thus, an increase in e.g. time delay or packet loss will result in a system with higher damping and/or inertia and fidelity is consequently deteriorated. The approach by Kuchenbecker & Niemeyer [114] is furthermore limited to rough or stiff objects.

Both of these drawbacks can be avoided using "model-mediated teleoperation". By applying this approach, the operator is haptically interacting with a local, estimated, haptic map of the remote environment. After the estimation is converged, the fidelity is independent of the dynamics of the communication channel and controlled slave device, and the operator receives non-delayed feedback. This advantage leads to significant fidelity improvements beyond those of classical and adaptive control approaches, that were presented so far. It is therefore a promising transparency-oriented control approach, that will be further investigated in this thesis. As model-mediated teleoperation is a model-based control approach, its effectiveness is certainly dependent on the accuracy of the model and its estimation. The known literature on model-mediated teleoperation misses i) a stability analysis especially for the phase, where the estimation is active, ii) a detailed fidelity analysis in comparison with classical controllers, and iii) its applicability is limited to translational DoFs and static objects only. This thesis extends model-mediated teleoperation with respect to all these aspects in Chap. 3 and 4. State-of-the-art approaches relating to model-mediated teleoperation are discussed in the corresponding chapter and will not be elaborated further at this point.

2.4.2 Performance Augmentation

The use of technical means such as displays, headsets, and haptic devices for providing multi-modal feedback to the operator of a teleoperation system offers the possibility to augment human actions by computer-generated commands. The augmentations may be presented on different modalities. Augmented reality [106, 117, 124, 138, 197], for example, combines real-word video feedback with virtual, visual cues. For teleoperation, it is shown in [167] that this augmentation can be efficiently used to display warnings such as the entering of forbidden regions or the application of excessive forces. Especially in teleoperation scenarios with time-delays, augmented reality in the form of predictive displays [14, 23, 27, 33, 106] gives the operator an undelayed view of the commanded motions. On

the auditory channel, alarm signals may warn the operator of critical situations or provide additional information [11, 136, 169]. Furthermore, a realistic audio feedback through audio localization and synthesis [102] may facilitate the teleoperation for the human.

Also, a variety of performance-augmenting controllers referred to as haptic assistance has been proposed in order to improve task performance through the haptic channel. As presented in the introduction of this thesis, the resulting system is referred to as shared-control system. Besides teleoperation scenarios [1, 205], applications for shared control systems are also found in micro-surgery [15, 108], vehicle control [2–4, 59, 71, 143, 145], aviation [58, 67, 182], walking support systems [36, 221], or powered wheelchairs [40, 208]. Another important application is learning or rehabilitation of motor skills [48, 109, 110, 120, 131, 207], where the haptic assistance is used to continuously transfer a motor skill to a human. This section presents performance-augmenting controllers that are based on online gained operator- and task-knowledge. Environment-adapting control concepts for performance augmentation were not found in the current state-of-the-art literature and may represent a future research direction.

2.4.2.1 Operator-adapting Approaches

The variable admittance control approach of Duchaine & Gosselin [45] is based on an intuitive relationship between haptic data and human intention. By looking at the time derivative of the applied force and the sign of the velocity, desired accelerating actions of the human can be distinguished from decelerating ones. With this knowledge, the damping parameter in the robot's admittance controller is decreased/increased during accelerating/decelerating motions. Consequently, less effort is required for accelerating motions due to reduced damping, and positioning or stopping motions are facilitated due to increased damping. As shown in a small study [45], the proposed adaptation leads to an improved task performance for a cooperative drawing task and a pick-and-place task. The concept has been extended to three dimensional motions [46]. Furthermore, a stability observer, based on the estimated human arm stiffness, has been introduced to guarantee stability during adaptation of the damping parameter. This method is well applicable in a teleoperation setup, where the damping is chosen to be dependent on the sum of human and environmental force such that contact situations do not destabilize the system. By applying variable impedance control, the reactive behavior of the system, especially during free space motions, can be improved. An active support of the operator's intended movements is, however, not provided. It is consequently questionable whether significant improvements especially in completion times are achievable.

Recent papers in the area of human-robot collaborative manipulation [41, 129] propose motion estimation to improve the performance of the system. Based on an estimated human motion profile according to Flash & Hogan's mimimum-jerk criterion [56], the desired position of an admittance controller x^d is adjusted according to

$$\text{Corteville et al. [41]:} \quad x^d = \int \alpha \hat{\dot{x}} \, \mathrm{d}t \qquad \text{Maeda et al. [129]:} \quad x^d = \hat{x}, \tag{2.32}$$

where $\hat{x}, \hat{\dot{x}}$ represent the estimated motion and velocity, and α determines the level of

assistance. In [129], a nonlinear least-squares method was used to estimate the duration and final position of the movement. With these parameters, the minimum-jerk model is completely determined. In [41], an extended Kalman filter was used to estimate the duration and, thus, the speed of the movement. Comparing an unassisted with an assisted ($\alpha = 0.75$) point-to-point movement, not only the speed profile converges to a bell-shaped profile, but also the applied forces were found to be reduced considerably. In [41], although not representative, the 10 participating operators confirmed an improvement when applying this assistance. Through the active participation of the robot, the task could be performed more easily, and the feeling of cooperating with the machine was found to be improved. In [129], a decrease in unnecessary energy transfer was shown. Only slight adaptations are necessary to make the method applicable in a teleoperation setting. Certainly, if the model of the movement does not fit, the assistance can degrade overall performance. This is observed in [41], where instead of the minimum-jerk model also a triangular speed profile was used.

If time delay is present in the communication channel, one possibility would be to use predictive displays as mentioned at the beginning of this section. However, even in the case of an augmented visual environment, the distinction between contact and non-contact is difficult for the operator due to impaired or insufficient 3D visual feedback. Hence, it is desired to not only predict the motions visually but also haptically. This idea was proposed in [37, 187, 243]. If the prediction works well, the slave tracks the position or velocity of the master without delay. A visual augmentation is consequently not necessary anymore. The approaches [187, 243] are based on an online estimated minimum-jerk trajectory. The operator positions are predicted over the horizon of the one-way time delay. In [187], the prediction of operator trajectories are applied in a teleoperated ball-catching experiment. Experimental results show significant improvements compared to a Smith-predictor approach for time delays of up to 70 ms. In [243], the objective is the minimization of impact forces. Especially in the final phase of the movement, large position overshoots, which can lead to instability when contact is encountered, are reduced and facilitate the positioning of the slave. Although only shown for small round-trip time delays up to 20 ms, this idea is expected to be extensible to larger delays. In [37], a position prediction algorithm based on double exponential smoothing is presented. Compared to Kalman filter-based approaches, double exponential smoothing is faster without degrading performance. The method is applicable in 6 DoF and was successfully applied for time delays of up to 120 ms.

There are, however, two main restrictions of the motion estimation and prediction methods presented above. One restriction is the assumption that the goal position of the movement has to be estimated. In the case of a reaching movement in a teleoperation setup, this implies that positions of objects in the remote environment have to be given. This again raises the need for an additional sensor. Another restriction is that human motions are facilitated through estimation and prediction, but the capabilities of the machine like precision are not fully exploited. With motion estimation and prediction, it can e.g. not be expected that motions in undesired workspace regions are reduced or task completion times are decreased through e.g. faster positioning.

Many tasks especially in minimally-invasive surgery require, however, a high precision.

They become difficult and require a lot of concentration of the operating person due to the physiological tremor that is inherent to all human motions. Due to the spatial decoupling of the human from the environment, teleoperation systems offer the possibility to cancel these involuntary movements on the way from master to slave. A weighted-frequency Fourier linear combiner [171] and an optimal signal processing technique [65] are proposed to cancel tremor. A reduction of tremor motions up to 67% is reported in [171] for physiological tremor without phase lag and up to 97% in [65] for a person with Parkinson's disease. The consequences are improvements in the accuracy of teleoperated tasks. This approach is effective if the tremor of human motions is the main source of performance degradation. The performance-oriented control concept investigated in this thesis should, however, not be restricted to those kind of tasks.

In summary, the presented operator-adapting control concepts for performance augmentation do not fully exploit the capabilities of the machines of a teleoperation system or are restricted to a specific class of tasks and will therefore not be further exploited in this work.

2.4.2.2 Task-adapting Approaches

Potential fields as proposed in [9, 34, 105, 209] provide the operator with haptic cues to avoid certain regions in the workspace of the slave. Either repulsive force fields, potential hills, are created around objects, which should be avoided, or attractive force fields, potential wells, around target regions, where the operator should be directed to. In most cases, these fields are of simple geometric shape, conical, quadratic, or elliptic, but can be superimposed, as shown in [9]. Chong et al. [34] applied this method for collision avoidance in a teleoperation system with multiple operators and robots and time delay in the communication channel. A predictive simulator was introduced, which showed the predicted positions of the other robots, virtually enlarged their thickness and applied a repulsive force field around the other robots, if the distance between two robots became too small. This approach is especially suited to reduce errors and to avoid damage. Significant improvements in task completion times can, however, not be expected as an active support towards the goal is not provided.

Variable position or velocity mappings between master and slave devices as described in [43, 49, 132, 205] represent another group of task-adapting approaches for performance augmentation. Dubey et al. [43] presented a velocity mapping for an improved task execution time in a pointing task as well as in a teleoperated docking task. Manocha et al. [132] applied velocity scaling to pipe cutting such that large unwanted velocities along the pipe axis were avoided. In [49], a variable position mapping is presented with which a desired orientation was maintained more easily and the probability of hard impact was reduced due to slower velocities near walls. In [205], a computer assistance concept for reaching movements is proposed which increases task performance. The presented method corrects the displacement between the teleoperator and a remotely located screw by applying a suitable velocity or force mapping between master and slave device. A position dependent velocity mapping, where only motions perpendicular to the desired path are damped, combined with a final position correction significantly increased positioning accuracy. Furthermore, a high strength of assistance was desired. It is assumed in this

approach that the target is known. In order to analyze the environmental situation and present the correct assistance, the proposed approach was combined in [204] with a scene recognition and intention estimation method. The main unknowns of this approach are i) whether the operator gets used to the different scalings between local and remote site, and ii) whether the capabilities of the machines are fully exploited with this method.

A third, very popular class of task-adapting approaches for performance augmentation are guiding virtual fixtures [15], first proposed by Rosenberg [172]. They are used to improve task performance in terms of execution time, precision and error rates by guiding the human along a predefined path. Typical application areas can be found in training scenarios [109, 110, 120] as well as in teleoperation [1] or in direct haptic human-robot interaction tasks like microsurgery [15, 108]. Rosenberg describes virtual fixtures in [172] as perceptual overlays to improve performance. The way of operation is similar to using a ruler when drawing a straight line, as outlined in his paper. Hereby, speed, accuracy, safety, and easiness are greatly enhanced. Virtual fixtures are applied to either guide the operator's motion along a certain trajectory or path [15] or to prevent penetration into undesired parts of the workspace [6, 153, 172], as shown in Fig. 2.8. Furthermore, VFs can be either of admittance-type, if forces are the input, and velocities or position are the output of the virtual fixtures, or of impedance-type, where input and output are reversed. The advantage of admittance-type VFs lies in their inherent passivity and high precision. To keep the advantage, Pezzementi et al. [158] shows how admittance-type VFs can be applied to impedance-type devices. A stability analysis for forbidden-region virtual fixtures is conducted in [5].

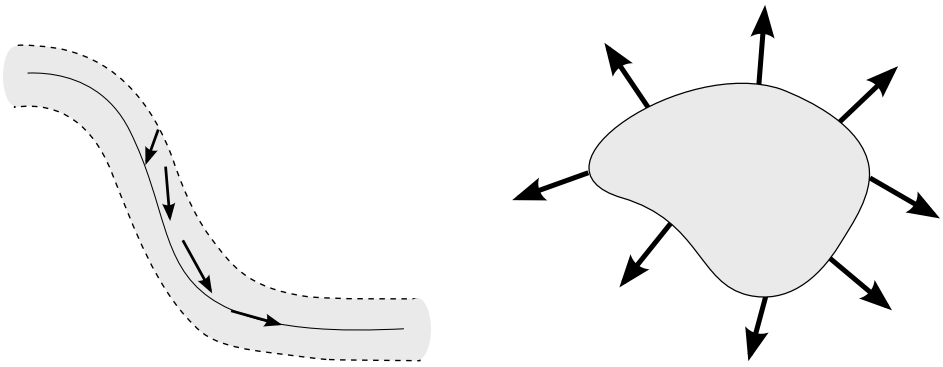

(a) Guiding virtual fixture (b) Forbidden region virtual fixture

Fig. 2.8: Concept of virtual fixtures.

For guiding virtual fixtures, task-relevant motions are supported, while deviations from the desired path are constrained [6], see Fig. 2.8. In a first step, the user's motion is decomposed into a tangential and a perpendicular direction to the desired path. These components are then weighted with different gains, which determine the trade-off between guidance and free motion. In [158], virtual fixtures are proposed, which correct deviations from the desired path and guide the user towards the desired speed profile. For avoiding penetration into critical regions, virtual walls can be implemented. They either attenuate the slave's motion in the undesired direction, or completely suppress it by restricting the slave's position to the uncritical workspace.

For applying the appropriate fixture, the current subtask has to be known. In [1] and [222], a Hidden Markov Model is used to classify the human intended type of task. After training the model, the classifiable tasks can be arbitrarily combined, and a suitable virtual fixture is applied. For guiding VFs, the trajectory that should be followed has to be given. This requires knowledge about the task and the remote environment.

In summary, the main challenges for applying virtual fixtures are the choice of the right fixture, the optimal trade-off between completely human-commanded and purely computer-controlled operation, and the recognition of task primitives. The advantages are i) the applicability to a variety of different tasks, ii) the combination of human- and computer-generated commands, which allows to exploit human and machine capabilities and iii) a large performance augmentation, if the correct assistance is applied with a suitable amount of assistance for a certain task. Due to these advantages, virtual fixtures seem superior to the other performance-oriented control approaches, and are therefore selected as the basic performance-oriented control concept in this thesis.

As presented so far, virtual fixtures operate with a fixed amount of assistance. It was, however, shown in [166] that the workload sharing between two humans is changing during task execution and that they take over different roles. Thus, it can be expected that a haptic assistance with adaptive user- and task-adapting assistance level leads to a similar task performance at reduced effort and failure rates. This again can result in a higher acceptance by the operator. This concept of dynamic role sharing is also investigated for human-robot collaborative manipulation (HRCM), see e.g. [50, 51, 203, 211]. Although these approaches are applied to HRCM tasks, they are directly applicable to teleoperation systems. Role-based shared control over the master device takes hereby place between autonomously acting agent and operator. Dynamic role sharing as e.g. presented in [48, 150, 206, 221], is the main topic of Chapter 5. The state-of-the-art approaches in this field will therefore not be presented at this point.

Concluding the overview of state-of-the-art approaches for fidelity and performance augmentation, model-mediated teleoperation and adaptive, user- and task-adapting virtual fixtures were identified as promising transparency- and performance-oriented control concepts.

2.5 Summary

This chapter introduced the design objectives for haptic teleoperation systems, the system components, and different architectures for connecting these system components via the communication channel. Classical control concepts for haptic teleoperation systems concentrate on finding a trade-off between the degree of fidelity and stability without taking online gained environment, operator, or task (EOT) knowledge into account. Prominent examples are the four-channel architecture proposed by Lawrence and the wave variable approach. EOT-adapting control concepts, the focus of this thesis, incorporate online gained EOT-knowledge in the control law. Current implementations were presented together with a discussion of advantages and disadvantages.

The state-of-the-art approaches achieve improvements in fidelity by using online gained environment knowledge or estimated operator behavior. This knowledge is used to adapt

the controller parameters, to augment the haptic feedback by computer-generated forces or motions, or to control the impact velocity when touching objects. This thesis focuses on a environment-related model-mediated teleoperation approach where the operator interacts with an online estimated virtual copy of the remote environment instead of receiving direct haptic feedback. The advantage of this approach is the undelayed haptic feedback that makes the approach suitable for systems with medium and large time delays in the communication channel. However, the applicability of model-mediated teleoperation is so far limited to translational degrees-of-freedom (DoFs) and tasks with static objects. A rigorous stability and comprehensive fidelity analysis is missing. The following two chapters are devoted to an intensive and detailed analysis of model-mediated teleoperation. This includes stability and fidelity investigations and the extension of the approach to full 6 DoF manipulation tasks involving static and movable objects. Thus, model-mediated teleoperation becomes applicable in a realistic teleoperation setup.

Besides transparency-oriented control concepts, a variety of methods aim at improving task performance. The state-of-the-art shared-control approaches where the commands of an autonomous, haptic assistance are combined with the operator's input lack user- and task-adaptation. Although human and machine capabilities are different, it is expected that such a user- and task-oriented control design makes the human-machine interaction more cooperative. This is expected to result in less required effort, improved usability, and reduced failure rates. A systematic approach for investigating the design possibilities of flexible, user- and task-adapted assistances is, however, missing in the known literature. This thesis provides a first design tool for the assistance level of haptic assistances. The assistance level strongly influences the workload distribution between human and assistance. The introduced design tool allows to systematically explore and extend current implementations towards improved user- and task-adaptation. New performance measures and control policies for selecting the assistance level are proposed. Based on an experimental evaluation and a user study, the different design possibilities are compared.

Although some of the EOT-adapting controllers may improve fidelity and performance, the simultaneous improvement of multiple design objectives has only been presented in the context of robust controller design. Thus, it is interesting to investigate further multi-objective controllers. In this thesis, it will be presented how fidelity- and performance-oriented controllers can be suitably integrated into one system. One implementation possibility will furthermore be evaluated in a proof-of-concept study. It will be shown that improvements in fidelity and task performance can be simultaneously achieved compared to single-objective and classical controllers.

3 Transparency-Oriented Control Concept: Stability and Fidelity Analysis

The ideal teleoperation system allows to achieve a high task performance and is transparent, immersive, comfortable, and easy to use. One possibility to approach the ideal teleoperation system is to design single-objective controllers, that focus on optimizing one objective (transparency, performance, feeling of presence, usability). These controllers can then be combined into a multi-objective system in order to achieve improvements in all design objectives. This thesis starts with the investigation of transparency-oriented controllers. Transparency implies that the controllers cancel all dynamics resulting from the technical components and the operator feels as directly interacting with the remote environment [218]. For free space, transparency implies that the operator has to move his/her arm only and does not have to apply any external force. In contact situations, the dynamics presented to the operator exactly represents the dynamics of the remote objects. Fidelity determines how far the system is from being transparent, i.e. maximum fidelity corresponds to transparency. Technical deficiencies of e.g. the actuators, sensors, controllers, or the communication channel limit the realization of a transparent teleoperation system and require to find a trade-off between fidelity and stability.

The goal of a transparency-oriented controller is to find an optimal trade-off between the two objectives. A variety of control concepts exist in telerobotics literature that tackle this challenge. Classical controllers, as they are referred to in this thesis, do not take knowledge of the environment, operator, or task (EOT), which is gained online, into account in the control law. The 4- and 2-channel architectures as well as robust control methods and partly also adaptive controllers belong to this class, see [86]. The classical control concepts mainly exhibit a high robustness and are consequently applicable to a variety of unstructured and changing environments. The fidelity of classical controllers is, however, limited as actions and reactions are affected by deficiencies in the communication channel and the dynamics of the controlled teleoperator. They are further mainly suitable for small to medium (up to ≈ 0.5 s) time delays. EOT-adapting controllers adapt the control law depending on EOT-information gained online. Using transparency-oriented, EOT-adapting controllers, information about the remote environment is gained online and the control law is adapted such that improvements in fidelity are achieved without risking stability. If, for example, the environment is a soft object, the controller compliance can be reduced, while it has to be increased, if the environment is a stiff, rigid object. As the controller is adapting to each environment specifically, the fidelity can be improved compared to classical controllers.

Based on a state-of-the-art analysis of transparency-oriented, EOT-adapting controllers presented in Sec. 2.4.1, *model-mediated teleoperation* [1], first proposed by Hannaford in 1989

[1] This approach is also referred to as VR-based or impedance-reflecting teleoperation in literature.

[75], was selected as a promising approach to increase the fidelity of a teleoperation system with negligible, medium, and large time delays beyond the fidelity of classical controllers. Model-mediated teleoperation adopts the idea of estimating a haptic map of the operator and/or environment and rendering a virtual copy of this haptic map on the corresponding other site. Thus, instead of exchanging haptic signals, model information is transmitted between the local and the remote site. If the estimation works well, accurate information of the operator and/or the environment is available locally such that the characteristics and dynamics of the controlled master and/or slave and of the communication channel are canceled out. This increases the fidelity without loss of stability.

The current implementations of model-mediated teleoperation focus either on mediating models of the human operator or the remote environment, see also [55]. Thus, knowledge about the type and dynamics of objects and the human behavior are required in order to realize model-mediated teleoperation. The task and approximate knowledge about the type of objects in the remote environment is known a priori in many teleoperation scenarios. Detailed information about the object's dynamics and the human behavior can furthermore be obtained through online exploration and estimation.

As the objective of this work is to present an undisturbed haptic feedback of the remote environment to the human operator, this thesis focuses on environment-related model-mediated teleoperation, i.e. models of the environment are estimated, transmitted, and recreated at the operator site, see Fig. 3.1.

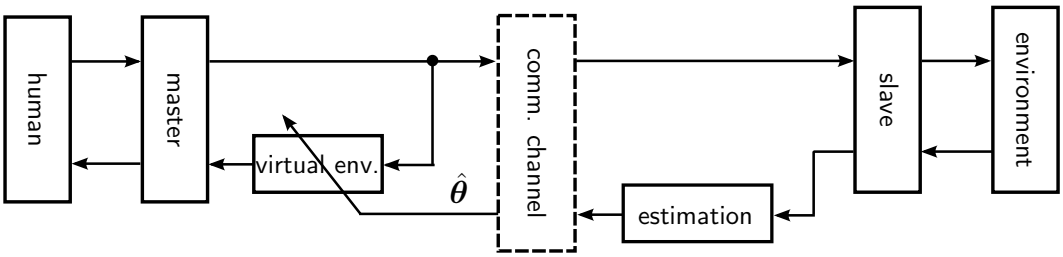

Fig. 3.1: Model-mediated control architecture. The parameters of an environment model, $\boldsymbol{\theta}$, are estimated, $\hat{\boldsymbol{\theta}}$, and transmitted to the operator site, where they are used to reconstruct the remote environment using a local, virtual copy.

The known literature on model-mediated teleoperation misses a stability analysis and a comprehensive fidelity analysis including a comparison with classical control concepts. This chapter extends the state-of-the-art on model-mediated teleoperation with respect to these aspects. It presents i) a detailed stability analysis for the transient phase, where the estimation is active, and for the steady-state phase, where the estimation is converged, and ii) a comprehensive fidelity analysis including the comparison with a classical control concept.

More precisely, stability is investigated in a first step for the transient behavior of model-mediated teleoperation. Static and movable objects are hereby taken into account. The dynamics of the closed-loop system is time-varying and, for static objects, also switching. In this work, the stability analysis is based on advanced analysis tools from adaptive control and the multiple Lyapunov function approach. Using these tools and simplified model assumptions, it will be shown that the transient phase of model-mediated teleoperation is

asymptotically stable for static and movable objects. The theoretical analyses of the transient phase are complemented by a steady-state robust stability analysis. The parameter space approach is used to determine stable and unstable parameter regions. The results of this analysis are the basis for the fidelity analysis.

Regarding the fidelity analysis performed in this chapter, parameters that optimize the Z-error, a fidelity measure known from literature, are determined for the experimental setups used in this thesis. However, some dynamics is always simplified in the stability and fidelity analysis to keep the model complexity and the number of unknown parameters manageable. Also, the discrete nature of the controller is often neglected. This results in stability margins that may not stabilize the real teleoperation system. Consequently, also the parameters optimizing fidelity may destabilize the real system. This is taken into account in a novel fidelity measure, that is introduced in this chapter. It is derived based on the consideration that larger stability regions and stability regions, which exhibit a small Z-error, should result into a higher fidelity than smaller stability regions and stability regions with a high Z-error. Model-mediated teleoperation is finally compared to a classical two-channel teleoperation architecture based on the Z-error as known from literature and based on the new fidelity measure. The results show significant improvements of model-mediated teleoperation compared to the classical control approach.

First, a detailed discussion of state-of-the-art implementations of model-mediated teleoperation is provided in Sec. 3.1. Modeling assumptions for each system component and the closed-loop system are described in Sec. 3.2. Finally, stability and fidelity analyses are provided in Sec. 3.3 and 3.4.

3.1 Overview of Fidelity and Stability Analyses for Model-Mediated Teleoperation

As mentioned in the introduction, either the environment or the operator behavior can be mediated to the respective other site. A classification and overview of model-mediated approaches modelling the operator is provided in [55]. This section is dedicated to a detailed discussion of environment-related model-mediated teleoperation.

If the delay in the communication channel becomes too large, transmitted signals are out of phase compared to local signals. Thereby, the causality between action and reaction gets lost and operators usually change their behavior to a move-and-wait strategy. Similarly, if packet loss is high or transmission rates are low, important haptic information is missing such that the human operator cannot naturally interact with the remote environment. In a model-mediated teleoperation system as described in [37, 91, 139, 140, 200, 219, 243], this limitation is overcome by estimating the geometric shape and the material properties of the objects in the remote environment and rendering a corresponding virtual model on operator site, see Fig. 3.1. Consequently, from the moment on when a first estimate is available on local site, the operator is haptically interacting with a locally rendered, virtual object. The model of the remote environment is essentially predicted over the time delay in the communication channel, such that the operator receives non-delayed feedback. As haptic information of the remote objects is continuously available and without delay, the

approach is robust to deficiencies in the communication channel.

This robust stability property of model-mediated teleoperation was discussed for static objects and time delay in the communication channel in [214]. A rigorous stability proof especially for the switched dynamics that occurs when the system transits from free space to contact is, however, missing. In Sec. 3.3 of this thesis, a first stability proof for model-mediated teleoperation is provided using a simplified dynamic model taking into account the switched and time-varying characteristics.

The application of model-mediated teleoperation leads to a considerable improvement in fidelity as shown in [200] using a quantitative fidelity measure based on the error between ideal and estimated environment model. A comparison with a classical control concept is, however, not provided. Also from a qualitative point of view, a significantly stronger feeling of perceived realism is reported in [243] when applying model-mediated teleoperation. In Sec. 3.4, the so far missing comparison with a classical control concept and the fidelity analysis for different types of objects is provided.

3.2 Modeling Model-Mediated Teleoperation

The stability and fidelity analyses presented in this chapter are performed for the experimental setups used throughout this thesis. These setups are characterized by their admittance-type devices. In the following section, the modeling assumptions for these devices are presented together with models for the human operator, the remote environment, and the communication channel. Further, the dynamics of model-mediated teleoperation is presented for the considered setups.

3.2.1 Modeling Assumptions for System Components

In this section, the modeling assumptions are introduced for each component of a haptic teleoperation system. The model parameters are provided in Appendix A. It is assumed without loss of generality that the Cartesian degrees of freedom (DoF) are decoupled, as this can be achieved using a computed-torque controller. The result are single-DoF models for each direction, which can be analyzed independently.

Human Operator. As mentioned in Sec. 2.1, the operator dynamics is often modeled as a combination of an exogenous force $f_h^\star$ and an arm impedance $Z_h(s)$. According to [85], a mass-spring-damper model can be used for the human arm impedance leading to the operator dynamics

$$f_h = f_h^* - (m_h \ddot{x}_m + b_h \dot{x}_m + k_h x_m) \tag{3.1}$$

$$\Rightarrow Z_h(s) = \frac{F_h^* - F_h}{V_m} = \frac{m_h s^2 + b_h s + k_h}{s}, \tag{3.2}$$

where $m_h \in \mathbb{R}_0^+, b_h \in \mathbb{R}_0^+, k_h \in \mathbb{R}_0^+$ represent the arm mass, damping, and stiffness parameters, respectively. It is assumed that the operator holds on to the master device, such that $x_h = x_m$ holds. A second possibility for modeling the intention of the operator is to

assume a desired trajectory x_m^*, velocity $\dot{x}_m^*$ and acceleration $\ddot{x}_m^*$ profile:

$$-f_h = m_h(\ddot{x}_m - \ddot{x}_m^*) + b_h(\dot{x}_m - \dot{x}_m^*) + k_h(x_m - x_m^*). \tag{3.3}$$

In order to take variations in the rigidness of the operator's grasp into account, the human arm impedance is allowed to vary within a range $Z_h = Z_{h,\min} + \alpha(Z_{h,\max} - Z_{h,\min})$ and $\alpha \in [0;1]$.

Master & Slave. The experimental setups used in this thesis are based on admittance-type devices, but the approaches are also realizable using impedance-type devices. The most important characteristic of admittance-type devices is their high output force capability and a large workspace [38]. Furthermore, the devices allow the manipulation of considerably heavier and stiffer objects than impedance-type devices. As proposed in [218], a simple mechanical model of master and slave device is a mass-damper system with mass $m_{m,s} \in \mathbb{R}^+$ and damping $b_{m,s} \in \mathbb{R}^+$ relating master/slave velocities $\dot{x}_{m,s}$ to actuator forces $f_{am,s}$

$$Y_{m,s}(s) = \frac{V_{m,s}}{F_{am,s}} = \frac{s}{m_{m,s}s^2 + b_{m,s}s}. \tag{3.4}$$

For a more realistic model of the devices, actuator and sensor dynamics is taken into account. The considered admittance-type devices are equipped with DC or brushless DC motors, incremental encoders used as position sensors, and force/torque sensors. The bandwidth of the motors is limited. This bandwidth limitation is modeled as a low-pass with time constant T_{act}. While the processing of the incremental encoder readings is negligible ($T_p < 0.1$ ms, see [155]), the time constant of the force/torque sensor readings T_{sensor} is taken into account in the modeling. Again, a low-pass filter is used to model the sensor dynamics. Thus, the transfer functions from raw forces to filtered actuator/sensor forces $\tilde{f}_{\text{a/s}}$ are given by

$$G_a(s) = \frac{\tilde{F}_a}{F_a} = \frac{1}{1 + s\,T_{\text{act}}} \quad \text{and} \quad G_s(s) = \frac{\tilde{F}_s}{F_s} = \frac{1}{1 + s\,T_{\text{sensor}}}. \tag{3.5}$$

Communication Channel. This thesis focuses on an approach that circumvents network-induced deficiencies and investigates shared-control paradigms for a teleoperation system with latency-free communication and without packet losses. Only constant time delays denoted as T_d are considered such that a signal $x_{\text{rec}}(t)$ received at time t was sent at time $t - T_d$, i.e. $x_{\text{sent}}(t - T_d) = x_{\text{rec}}(t)$.

Remote Environment. The remote environment can be either unstructured, meaning that a priori knowledge about the remote objects is not given, or structured, where some knowledge is assumed. The environment dynamics is assumed to be time invariant and if the teleoperator is in contact with objects, the position of the slave or teleoperator x_s and the object x_e are equal, i.e. $x_s = x_e$ holds. This enables us to express the force f_e resulting from the environment dynamics with teleoperator position x_s, velocity $\dot{x}_s$, and acceleration $\ddot{x}_s$ as:

$$f_e(t) = \begin{cases} 0 & \text{in free space} \\ g_e(x_s, \dot{x}_s, \ddot{x}_s) & \text{in contact.} \end{cases} \tag{3.6}$$

3.2.2 Modeling Assumptions for Closed-Loop System

Based on the models for master and slave device, the control architecture for model-mediated teleoperation is defined next. Please note that the Cartesian degrees of freedom are assumed to be decoupled, such that the models and the subsequent stability analysis is performed for a system with one translational DoF. The master device is controlled using a position- or velocity-based admittance controller, see Fig. 3.2. The virtual admittance

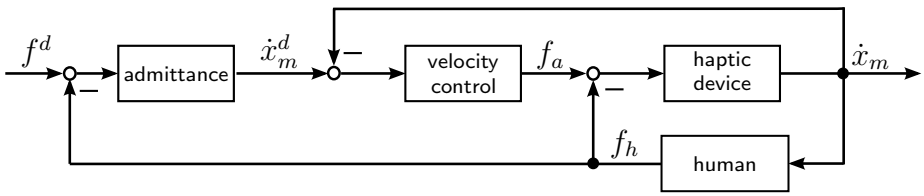

Fig. 3.2: The input to the velocity-based admittance controller on the master site is the difference of desired and operator force. The admittance maps the resulting force to a desired velocity, which is tracked using an underlying velocity controller.

$Y_{am}(s)$ is characterized by a mass-damper system

$$Y_{am}(s) = \frac{V_m^d}{(F_m^d - F_m)} = \frac{1}{m_a\, s + b_a} \tag{3.7}$$

with a virtual mass $m_a \in \mathbb{R}$ and damping $b_a \in \mathbb{R}$. The slave device is controlled using a proportional-derivative (PD) position or proportional-integral (PI) velocity controller. The desired master position is sent to the remote site, and an estimated parameter vector $\hat{\boldsymbol{\theta}}$ is received. An estimated force $\hat{f}_e$ is reconstructed based on the desired master velocity and the received parameters. It is added to the operator force and enters the virtual admittance.

3.2.2.1 System Model A: Full System Dynamics

The full system dynamics is required for the stability analysis of the system in steady-state. In this case, all parameters are time-invariant, such that the dynamics can be described in Laplace domain, see Fig. 3.3. The full system dynamics includes the underlying velocity controller, device, actuator, and sensor dynamics. The discrete nature of the controllers and noisy measurements are, however, not taken into account.

The estimated environment impedance $\hat{Z}_e$ relates the desired master velocity to the reconstructed force in Laplace domain:

$$\hat{Z}_e = \frac{\hat{F}_e}{V_m}. \tag{3.8}$$

As shown in Fig. 3.3, the estimated environment impedance is connected in feedback with the admittance of the master controller where F_h is the input and V_m the output:

$$\frac{V_m}{F_h} = \frac{Y_a}{1 + \hat{Z}_e Y_a} = \frac{1}{\underbrace{Z_a + \hat{Z}_e}_{\hat{Z}_{ae}}} = \hat{Y}_{ae}. \tag{3.9}$$

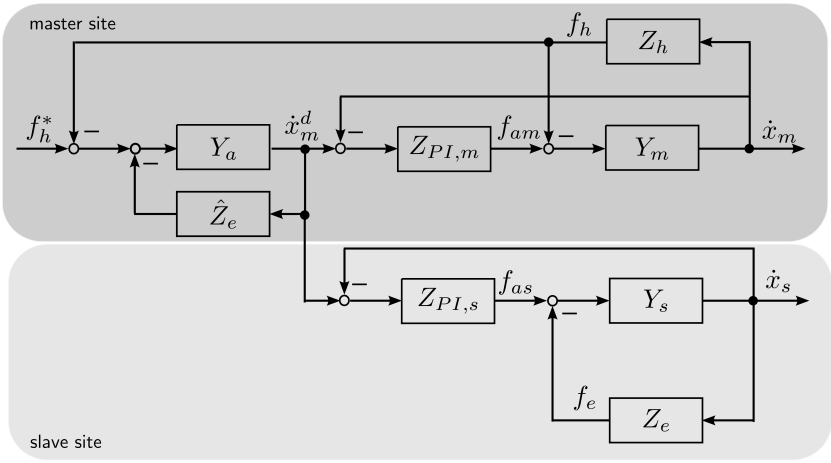

Fig. 3.3: Control architecture of model-mediated teleoperation for the system in steady-state. An admittance controller is used at the master site, a velocity controller at the slave site. The desired velocity is sent from master to slave. The estimated parameters are used at the master site to reconstruct an estimated force.

The control laws can then be written in Laplace domain as:

$$f_{am} = Z_{PI,m}(\dot{x}_m^d - \dot{x}_m) = Z_{PI,m}(\hat{Y}_{ae} f_h - \dot{x}_m) \tag{3.10}$$
$$f_{as} = Z_{PI,s}(\dot{x}_m^d - \dot{x}_s) = Z_{PI,s}(\hat{Y}_{ae} f_h - \dot{x}_s), \tag{3.11}$$

where $Z_{PI} = K_p + \frac{K_i}{s}$ is the transfer function of the underlying velocity controller with proportional gain K_p and integral gain K_i. According to (2.18), the controllers $C_m, C_s, C_1, \ldots, C_6$ are given by

$$C_m = Z_{PI,m}, \quad C_s = Z_{PI,s}, \quad C_3 = C_6 = Z_{PI,m}\hat{Y}_{ae}, \quad C_1 = C_2 = C_4 = C_5 = 0. \tag{3.12}$$

with $Z_m + Z_{PI,m} = Z_{cm}$ and $Z_s + Z_{PI,s} = Z_{cs}$. Using (2.21) the $\boldsymbol{H}$-matrix can be derived:

$$\boldsymbol{H} = \begin{bmatrix} \frac{Z_{cm}Z_{cs}}{(1+Z_{PI,m}\hat{Y}_{ae})Z_{cs}} & 0 \\ -\frac{Z_{PI,m}\hat{Y}_{ae}Z_{cm}}{(1+Z_{PI,m}\hat{Y}_{ae})Z_{cs}} & \frac{1+Z_{PI,m}\hat{Y}_{ae}}{(1+Z_{PI,m}\hat{Y}_{ae})Z_{cs}} \end{bmatrix} = \begin{bmatrix} \frac{\hat{Z}_{ae}Z_{cm}}{\hat{Z}_{ae}+Z_{PI,m}} & 0 \\ -\frac{Z_{PI,m}\hat{Y}_{ae}Z_{cm}}{(1+Z_{PI,m}\hat{Y}_{ae})Z_{cs}} & \frac{1}{Z_{cs}} \end{bmatrix}. \tag{3.13}$$

The master and slave dynamics, $Y_m = \frac{1}{Z_m}$ and $Y_s = \frac{1}{Z_s}$, is described in (3.4). Given the $\boldsymbol{H}$-matrix, the closed-loop transfer function for model-mediated teleoperation is found according to (2.23)

$$\begin{aligned} G_{MM}(s) = \frac{V_m}{F^d} &= \frac{h_{22}Z_e + 1}{(h_{22}Z_e + 1)Z_h + \det(\boldsymbol{H})Z_e + h_{11}} \\ &= \frac{(Z_e + Z_{cs})(\hat{Z}_{ae} + Z_{PI,m})}{(Z_e + Z_{cs})(\hat{Z}_{ae} + Z_{PI,m})Z_h + \hat{Z}_{ae}Z_{cm}(Z_e + Z_{cs})}. \end{aligned} \tag{3.14}$$

3.2.2.2 System Model B: Simplified System Dynamics

The system model B focuses on the dynamics at the master site. In order to allow an analytical stability analysis, the following simplifications are applied:

1. During the transient phase, where the estimated parameters of the remote environment are time-varying, it is assumed that the human arm dynamics is slowly varying and can be neglected compared to the fast changing environment dynamics. This assumption has to be applied, as, to the author's knowledge, there exists no established dynamic models in the current literature, that describe how the human operator changes the parameters of his/her arm impedance in the presence of an external force, that results from a controller with time-varying parameters.

2. The underlying velocity controller on master site is assumed to perfectly cancel the master device dynamics, i.e. $x_m = x_m^d, \dot{x}_m = \dot{x}_m^d$. Thus, the controller is reduced to the admittance dynamics, see also Fig. 3.2.

3. The bandwidth limitation of the force filter and the actuator dynamics is neglected.

4. The operator force acting as an external disturbance on the device is assumed to be compensated.

5. The communication is assumed to be latency-free and lossless. Proving stability for model-mediated teleoperation with time delay in the communication channel remains future work.

The intention of the human operator is modeled as a desired trajectory x_m^*, velocity $\dot{x}_m^*$, and acceleration $\ddot{x}_m^*$ profile. The corresponding operator dynamics is given in (3.3).

The reconstructed environment based on the estimated parameters [2] $\hat{\boldsymbol{\theta}} \in \mathbb{R}^n$ is described as

$$\hat{f}_e = \begin{cases} 0 & \text{in free space} \\ \hat{g}_e(\hat{\boldsymbol{\theta}}(t), x_m, \dot{x}_m, \ddot{x}_m) & \text{in contact.} \end{cases} \tag{3.15}$$

Stability will be analyzed for linear or linearized models of static and movable objects. Proofs for nonlinear models are subject to future research. Linear or linearizable object models can be assumed for most physical objects involved in maintenance scenarios in dangerous environments, space or underwater. They may not be valid for surgery tasks, as the dynamics of human tissue is highly nonlinear.

The resulting dynamic equations of the simplified system are given by

$$f_h - \hat{f}_e = m_a \ddot{x}_m + b_a \dot{x}_m \tag{3.16}$$

which can be simplified with (3.3) and (3.15) to

$$-m_h(\ddot{x}_m - \ddot{x}_m^*) - b_h(\dot{x}_m - \dot{x}_m^*) \tag{3.17}$$

$$-k_h(x_m - x_m^*) - \hat{g}_e(\hat{\boldsymbol{\theta}}, x_m, \dot{x}_m, \ldots) = m_a \ddot{x}_m + b_a \dot{x}_m \tag{3.18}$$

[2] Please note that $\hat{\boldsymbol{\theta}}$ depends on time which is neglected in the following for clarity of presentation.

The state $\boldsymbol{x}$ is defined for model B as

$$\boldsymbol{x} = \begin{bmatrix} x_m - x_m^* \\ \dot{x}_m - \dot{x}_m^* \end{bmatrix}.$$

System Model B_{free}: Simplified System Dynamics for Free Space If the teleoperator is not in contact with any object, i.e. $f_e = 0$, the simplified system dynamics on master site can be given in state-space notation by

$$\dot{\boldsymbol{z}}_{\text{free}} = \boldsymbol{A}_{\text{free}} \boldsymbol{z}_{\text{free}} \tag{3.19}$$

$$= \begin{bmatrix} 0 & 1 \\ -\frac{k_h}{m} & -\frac{b}{m} \end{bmatrix} \boldsymbol{z}_{\text{free}} \tag{3.20}$$

with $m = m_h + m_a$, $b = b_h + b_a$, $\boldsymbol{z}_f = \boldsymbol{x} - \boldsymbol{x}^* = \boldsymbol{x} + A_{\text{free}}^{-1} \boldsymbol{b}_{\text{free}} r_{\text{free}}$, $r_{\text{free}} = m_a \ddot{x}_m^* + b_a \dot{x}_m^*$ and $\boldsymbol{b}_{\text{free}} = [0,\ -\frac{1}{m_h + m_a}]^T$.

System Model B_{mov}: Simplified System Dynamics for Movable Objects Movable objects can be described in terms of the estimated mass $\hat{m}_e \in \mathbb{R}$ as

$$\hat{f}_e = \hat{m}_e \ddot{x}_m \tag{3.21}$$

such that $\hat{\theta} = \hat{m}_e$. The system dynamics is then derived in state-space notation:

$$\dot{\boldsymbol{x}} = \boldsymbol{A}_{\text{mov}}(\hat{\theta}) \boldsymbol{x} + \boldsymbol{b}_{\text{mov}}(\hat{\theta}) r_{\text{mov}} \tag{3.22}$$

$$= \begin{bmatrix} 0 & 1 \\ -\frac{k_h}{m + \hat{m}_e} & -\frac{b}{m + \hat{m}_e} \end{bmatrix} \boldsymbol{x} + \begin{bmatrix} 0 \\ -\frac{1}{m + \hat{m}_e} \end{bmatrix} r_{\text{mov}} \tag{3.23}$$

with the reference r_{mov} given by

$$r_{\text{mov}} = (m_a + \hat{m}_e) \ddot{x}_m^* + b_a \dot{x}_m^*.$$

The system matrix is invertible, i.e. $\operatorname{rank}(\boldsymbol{A}_{\text{mov}}(\hat{\theta})) = 2$, if $\frac{k_h}{m + \hat{m}_e} \neq 0 \ \forall\ t \geq 0$. Hence, the state transformation $\boldsymbol{z}_{\text{mov}} = \boldsymbol{x} - \boldsymbol{x}^\circ = \boldsymbol{x} + A_{\text{mov}}^{-1}(\hat{\theta})\, \boldsymbol{b}_{\text{mov}}(\hat{\theta})\, r_{\text{mov}}$ can be applied to (3.22). With $\dot{\boldsymbol{x}}^\circ = 0$ ($\boldsymbol{x}^\circ$ represents the equilibrium of (3.22)), the system dynamics can finally be written without reference dependency:

$$\dot{\boldsymbol{x}} = \dot{\boldsymbol{z}}_{\text{mov}} + \dot{\boldsymbol{x}}^\circ = \boldsymbol{A}_{\text{mov}}(\hat{\theta})(\boldsymbol{z}_{\text{mov}} + \boldsymbol{x}^*) + \boldsymbol{b}_{\text{mov}}(\hat{\theta}) r_{\text{mov}} \tag{3.24}$$

$$\Rightarrow \dot{\boldsymbol{z}}_{\text{mov}} = A_{\text{mov}}(\hat{\theta}) \boldsymbol{z}_{\text{mov}}. \tag{3.25}$$

System Model $\mathsf{B}_{m,\text{static}}$: Simplified System Dynamics for Static Objects The dynamics of static objects is assumed to be linear and the dynamics will be described in terms of the estimated damping $\hat{b}_e$ and stiffness $\hat{k}_e$ as

$$\hat{f}_e = \hat{b}_e \dot{x}_m + \hat{k}_e (x_m - x_e), \tag{3.26}$$

where x_e is the first point of contact with the object. The reference is

$$r_{\text{static}} = m_a \ddot{x}_m^* + (b_a + \hat{b}_e)\dot{x}_m^* + \hat{k}_e(x_m^* - x_e)$$

leading to the system dynamics in state-space notation:

$$\dot{\boldsymbol{x}} = \boldsymbol{A}_{\text{static}}(\hat{\boldsymbol{\theta}})\boldsymbol{x} + \boldsymbol{b}_{\text{static}} r_{\text{static}} \tag{3.27}$$

$$= \begin{bmatrix} 0 & 1 \\ -\frac{k_h + \hat{k}_e}{m} & -\frac{b + \hat{b}_e}{m} \end{bmatrix} \boldsymbol{x} + \begin{bmatrix} 0 \\ -\frac{1}{m} \end{bmatrix} r_{\text{static}}. \tag{3.28}$$

The parameter vector is defined as $\hat{\boldsymbol{\theta}} = [\hat{b}_e,\ \hat{k}_e]$. The system matrix has again full rank if $\frac{k_h + \hat{k}_e}{m} \neq 0$. This is fulfilled if e.g. the operator holds on to the device or if $m_a > 0$ holds for the virtual admittance mass. Then, the state transformation $\boldsymbol{z}_{\text{static}} = \boldsymbol{x} - \boldsymbol{x}^* = \boldsymbol{x} + A_{\text{static}}^{-1}(\hat{\boldsymbol{\theta}})\boldsymbol{b}_{\text{static}} r_{\text{static}}$ can be applied to the system. This leads to a reference-free system description

$$\dot{\boldsymbol{z}}_{\text{static}} = \boldsymbol{A}_{\text{static}}(\hat{\boldsymbol{\theta}})\boldsymbol{z}_{\text{static}}. \tag{3.29}$$

3.3 Stability Analysis

Model-mediated teleoperation aims at increasing the degree of fidelity compared to classical control concepts without deteriorating the stability of the system. This control concept belongs to the class of adaptive control. Thus, a stability analysis requires to analyze the steady-state as well as the transient behavior of the system. For showing the expected improvement in fidelity, model-mediated teleoperation is compared to a classical two-channel control architecture with force-force exchange. As the control of the classical control architecture is time-invariant, a stability analysis for the transient phase is not required.

Whenever the remote environment changes, the parameters $\hat{\boldsymbol{\theta}}$ of the environment model are adapted. This phase is referred to as the transient phase. After the parameter estimation has converged, the estimated parameters are slowly varying. This will be referred to as the steady-state phase. This section investigates stability for both phases.

3.3.1 Stability Analysis Tools

In a teleoperation system, the operator, the remote environment, the communication channel, and the sensors introduce uncertainties in the system due to their noisy, varying up to switching, unstructured, and potentially unknown behavior. Consequently, the controller is required to be stable with respect to a pre-specified set of uncertainties introduced by the different components.

Suitable stability and robustness analysis tools depend on the class of systems. The dynamics considered in this thesis are linear with partly switching right-hand side, and both, time-invariant and time-varying. The analysis tools for proving stability and investigating robustness that are employed in this thesis are presented for time-invariant systems in the

following subsection, followed by tools for time-varying systems in the subsequent subsection.

3.3.1.1 Linear Time-Invariant Systems

If a system is linear and time-invariant (LTI), stability and robustness can be analyzed in state-space or frequency domain. This section starts with a presentation of a stability and robustness analysis tool for the frequency domain and finishes with a short review of the Lyapunov theory for LTI systems, which requires the system to be represented in state-space notation.

Analysis Tools for Frequency Domain

Theorem 3.3.1 (Input/Output (I/O)-stability [126]) A completely observable and controllable continuous, linear, time-invariant system described by a closed-loop transfer function $G(s)$

$$G(s) = \frac{\sum_{j=1}^{J}(s - q_j)}{\sum_{i=1}^{I}(s - p_i)} \tag{3.30}$$

is I/O-stable, if the poles of $G(s)$, p_i, are shown to have strictly negative real parts [126]:

$$\mathrm{Re}\{p_i\} < 0 \quad \forall\, i = 1, 2, \ldots, I. \tag{3.31}$$

Variables with capital letters are Laplace-transformed and s stands for the Laplace operator. Due to complete controllability and observability properties of the system, I/O-stability corresponds to asymptotic stability. If the system is given in state-space representation (again completely observable and controllable)

$$\dot{\boldsymbol{x}} = \boldsymbol{A}\boldsymbol{x} + \boldsymbol{b}u, \quad \boldsymbol{x}(t_0) = \boldsymbol{x}_0 \tag{3.32}$$

with $\boldsymbol{x} \in \mathbb{R}^n$ the state vector, $u \in \mathbb{R}$ the scalar input, $\boldsymbol{A} \in \mathbb{R}^{n\times n}$ the system matrix and $\boldsymbol{b} \in \mathbb{R}^n$ the input vector, the system is asymptotically stable if the real parts of all eigenvalues $\mathrm{eig}_i(\boldsymbol{A})$ of the matrix $\boldsymbol{A}$ are negative [126]

$$\mathrm{Re}\{\mathrm{eig}_i(\boldsymbol{A})\} < 0 \quad \forall\, i = 1, 2, \ldots, N. \tag{3.33}$$

The closed-loop transfer function for a teleoperation system is given in Sec. 2.3.2.1. The advantage of this stability method is its simplicity, the disadvantage is the required computational effort for taking variations in operator and environment dynamics into account. The above described stability analysis does not guarantee stability for two neighboring parameter sets. Thus, every variation in operator/environment dynamics has to be checked for I/O-stability.

In order to gain information about the acceptable uncertainty, a robustness analysis can be conducted for a specific architecture by testing a set of uncertainties for stability [156]. A graphical tool for investigating I/O-stability for a bounded set of parameter uncertainties is the *parameter space approach* [7]. By solving the conditions for marginal stability denoted in the Laplace domain for the uncertain parameters, boundaries between

stable and unstable regions are obtained in the parameter space. For continuous, linear time-invariant systems, the boundary for I/O-stability in the Laplace domain is the imaginary axis. The poles of a characteristic polynomial c as a function of a parameter vector $\boldsymbol{q} \in D_{\boldsymbol{q}} \subset \mathbb{R}^n$ in an operating domain $D_{\boldsymbol{q}}$

$$c(s, \boldsymbol{q}) = a_0(\boldsymbol{q}) + a_1(\boldsymbol{q})s + \ldots + a_n(\boldsymbol{q})s^n \tag{3.34}$$

can cross the imaginary axis either on the real axis (real root boundary RRB), the imaginary axis (complex root boundary CRB) or at infinity (infinite root boundary IRB) leading to the three conditions for marginal stability as a function of the parameters $\boldsymbol{q}$ and frequency ω

$$\begin{array}{lrcl} \text{RRB:} & a_0(\boldsymbol{q}) = 0 & & \\ \text{CRB:} & \mathrm{Re}\{c(j\omega)\} = 0 & \wedge & \mathrm{Im}\{c(j\omega)\} = 0 \\ \text{IRB:} & a_n(\boldsymbol{q}) = 0. & & \end{array} \tag{3.35}$$

These conditions can be derived from the theorem for robust stability of a single-input single-output system with uncertain parameters $\boldsymbol{q} \in D_{\boldsymbol{q}}$ as proven in Frazer & Duncan [60].

Theorem 3.3.2 (Boundary crossing [7]) The polynomial $c(s, \boldsymbol{q})$ is robustly stable with respect to the uncertain parameter vector $\boldsymbol{q} \in D_{\boldsymbol{q}}$

- if there exists a $\boldsymbol{q} \in D_{\boldsymbol{q}}$ such that $c(s, \boldsymbol{q})$ is stable
- and if none of the boundaries (3.35) intersects the operating domain $D_{\boldsymbol{q}}$.

The advantage of this method is that a closed form of the stability boundaries is found. The disadvantage is that this method is sensitive to the selected frequency range. Furthermore, as the parameter space approach is a graphical analysis tools, uncertainties in more than three variables are difficult to illustrate.
The two stability/robustness methods described so far are not suitable for investigating stability of latency-afflicted teleoperation systems.

Lyapunov Theory

Theorem 3.3.3 (Lyapunov theorem for LTI systems [104]) : The equilibrium $\boldsymbol{x} = \boldsymbol{0}$ of an LTI system represented as

$$\dot{\boldsymbol{x}} = \boldsymbol{A}\boldsymbol{x}, \quad \boldsymbol{x}(t_0) = \boldsymbol{x}_0 \tag{3.36}$$

is globally asymptotically stable iff there exists a positive definite matrix $\boldsymbol{R} = \boldsymbol{R}^T$ for any positive definite matrix $\boldsymbol{Q} = \boldsymbol{Q}^T$ such that

$$\boldsymbol{R}\boldsymbol{A} + \boldsymbol{A}^T\boldsymbol{R} = -\boldsymbol{Q} \tag{3.37}$$

is fulfilled. This equation (3.37) is also referred to as Lyapunov equation. The resulting continuously differentiable, globally positive definite Lyapunov function and globally negative definite time derivative are given by

$$V = \boldsymbol{x}^T\boldsymbol{R}\boldsymbol{x} \qquad \dot{V} = -\boldsymbol{x}^T\boldsymbol{Q}\boldsymbol{x} \tag{3.38}$$

Besides a Lyapunov-based stability analysis [104], further stability analysis tools that are often used for teleoperation systems are the concept of passivity [149] or absolute stability [8]. These methods are also applicable if the communication channel is characterized by non-negligible time delay or packet loss.

3.3.1.2 Linear Time-Varying Systems

As a linear time-varying (LTV) system depends implicitly or explicitly on time, classical frequency domain analysis tools are not applicable. In this thesis, a method from adaptive control as described in [146] is used in order to investigate stability of autonomous LTV systems.

Theorem 3.3.4 (Stability for autonomous LTV system [146]) A time-varying system

$$\dot{\boldsymbol{x}} = \boldsymbol{A}(\boldsymbol{\theta}(t))\boldsymbol{x}, \quad \boldsymbol{x}(t_0) = \boldsymbol{x}_0 \tag{3.39}$$

is asymptotically stable if

$$\lim_{t\to\infty} \boldsymbol{\theta}(t) = \overline{\boldsymbol{\theta}} \tag{3.40}$$

holds and

$$\dot{\boldsymbol{x}} = \boldsymbol{A}(\overline{\boldsymbol{\theta}})\boldsymbol{x} \tag{3.41}$$

is asymptotically stable for every constant parameter vector $\overline{\boldsymbol{\theta}} \in S \subset \mathbb{R}^n$ and S is a compact set.

The disadvantage of this method is that a stability analysis is required for every possible parameter vector $\overline{\boldsymbol{\theta}}$. Hence, a robust stability analysis such as the parameter space approach has to be performed prior to applying the above described theorem for LTV systems.

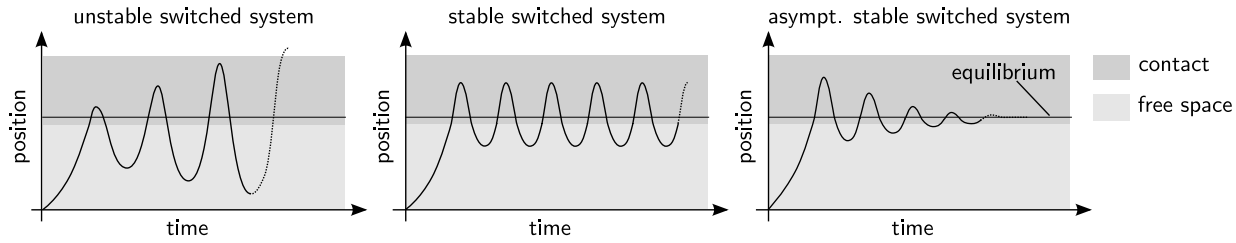

Fig. 3.4: Illustration of unstable, stable, and asymptotically stable behavior of a switched system.

3.3.1.3 Systems with Switched Dynamics

Except for the Lyapunov theory, the classic stability methods presented in the previous section cannot handle switched dynamics, which occurs in a teleoperation system when the teleoperator is driven from free space to contact with an object. Thus, even if the system is shown to be asymptotically stable or passive in free space and contact, the transition between these subsystems is not necessarily stable and/or passive [122, 224].

The finding of instability during transition can also be explained from a physical point of view. At the moment of impact, the teleoperator is suddenly decelerated to almost zero velocity. This means, that the momentum of the teleoperator $p = m_s\dot{x}_s$ decreases. This sudden change in momentum, however, leads to a large change in the interaction force. If the controller of the teleoperator is not adequately damped, the large interaction forces are passed to the controller resulting in a large position change out of the object. If the position change is too large, contact is lost. A switching behavior between free space and contact occurs. If the transition is stable, the interaction forces at the beginning of contact are small enough after a finite number of switchings, such that the system stays in contact with the object. Small interaction forces again imply a small momentum and, thus, a small impact velocity.

One possibility to show stability/passivity of the switched system is to find a global Lyapunov/storage function satisfying the conditions for Lyapunov stability/passivity. As it is often difficult to find such a function, other methods for analyzing stability of switched systems like the multiple Lyapunov/storage function approach have been developed [21, 224].

The stability analysis performed in this chapter is based on the multiple Lyapunov function approach as introduced by Branicky [21].

Theorem 3.3.5 (Multiple Lyapunov Function Approach [21]) Let us denote the end of a phase, where a subsystem was active, as t_i. This time is also referred to as exit time. Branicky showed in his work that a switched system with k different dynamics is asymptotically stable if for each exit time and subsequent switching times $t_{i+2n}, n \in \mathbb{N}^0$ and for all dynamics $p \in \{p_1, p_2, \ldots, p_k\}$

$$-\Delta V_p(t_{i+2}, t_i) > 0 \tag{3.42}$$

holds, where

$$\Delta V_p(t_{i+2}, t_i) = V_p(t_{i+2}) - V_p(t_i). \tag{3.43}$$

This implies, that the Lyapunov energy, i.e. the value of the Lyapunov function, at the end of a phase, where the p-th subsystem is active, has to be smaller than at the end of the previous phase, where the p-th subsystem was active. One example for two different subsystems with Lyapunov functions V_1 and V_2 is illustrated in Fig. 3.5. From phase 1 to 3, there is a non-zero Lyapunov energy decrease, as $V_1(t_1) > V_1(t_2)$, which is not the case between phase 2 and 4, as $V_2(t_2) < V_2(t_4)$. In this case, transition stability cannot be concluded.

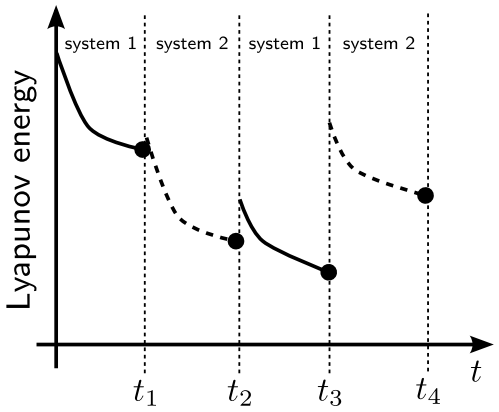

Fig. 3.5: Illustration of multiple Lyapunov function approach as proposed in [22]. Lyapunov energy of subsystem 1 ($V_1(t)$) is represented with solid lines and of subsystem 2 ($V_2(t)$) with dashed lines. Asymptotic stability cannot be shown for this switched system, as $V_2(t_4) > V_2(t_2)$.

The multiple Lyapunov function approach has been applied to teleoperation systems by Ni & Wang [148]. They show that asymptotic stability of a teleoperation system switching between unconstrained and constrained motions depends on the switching strategy between controllers. The multiple storage function approach has been used for investigating passivity of haptic interaction with virtual environments [130]. The problem of applying this approach is that the conditions at the switching points can only be analyzed for simplified model assumptions. Taking a detailed model into account would require a numerical analysis or simulation of the multiple Lyapunov function conditions and the result would guarantee stability only for the considered input signal.

Based on the introduced analyses tools and using the models A and B described in the previous section, stability is analyzed in the following sections for the steady-state and the transient phase.

3.3.2 Stability of the System in Steady-State

In a first step, a robustness analysis based on system model A, see Sec. 3.2.2, is performed for the system in steady-state. Model A is based on the full system dynamics including

the underlying velocity controllers as well as device, actuator, and sensor dynamics. In the steady-state phase, the estimated parameters $\hat{\boldsymbol{\theta}}$ are slowly varying, such that the resulting model-mediated teleoperation system can be considered to be time-invariant.

The parameter space approach as described in Sec. 3.3.1.1 is employed as stability analysis tool. For model-mediated teleopertion, the characteristic polynomial $c_{MM}(s, \boldsymbol{q})$ is determined from the closed-loop transfer function given in (3.14). The characteristic polynomial $c_{MM}(s, \boldsymbol{q}_{MM})$ is the denominator of the transfer function, expressed in terms of impedances. For the following robustness analysis, the underlying velocity controllers are assumed to be tuned. Thus, the only design parameters are the virtual mass and damping, m_a and b_a, of the admittance Y_a. Only non-negative mass and damping values are taken into account in the analysis such that the uncertain parameter vector $\boldsymbol{q}$ is described as:

$$\boldsymbol{q}_{MM} = \{(m_a, b_a) \;\mid\; m_a \in [0; \infty[,\; b_a \in [0; \infty[\}. \tag{3.44}$$

It is furthermore assumed that the estimated parameters are equal to the true parameters of the environment, i.e. $\hat{Z}_e = Z_e$. Robustness is analyzed for the translational degrees of freedom in the horizontal plane of the 6 DoF experimental setup, see Appendix A.6 for a description and a listing of the parameters for master/slave dynamics, velocity controllers, force/actuator filters, and human arm impedance.

Model-mediated teleoperation is compared with a two-channel position-based admittance controller with force-force exchange (FaFa) as described in Sec. 2.3.2.1. The $\boldsymbol{H}$-matrix is listed in Appendix A.2 from which the closed-loop transfer function G_{FaFa} and with it the characteristic polynomial $c_{FaFa}(s, \boldsymbol{q}_{FaFa})$ can be derived. The admissible set of uncertain parameters is the same as for model-mediated teleoperation, $\boldsymbol{q}_{FaFa} = \boldsymbol{q}_{MM}$.

It was shown in [155] for the same admittance-type devices investigated in this thesis, that an increase in the human arm impedance reduces the stability region. The maximum human arm impedance can consequently be regarded as most critical for the stability of the considered admittance-type devices. Thus, the maximum of the human arm dynamics $Z_{h,\max}$ is selected for the robustness analysis. The stability regions in the parameter space $\boldsymbol{q}_{MM}$ and $\boldsymbol{q}_{FaFa}$ are determined for different environment dynamics. The remote environment can be either free space or it is assumed to consist of static objects, movable objects, or objects with a mass-spring-damper (MSD) characteristics. The environment can be represented as on object with MSD characteristics if e.g. a movable object is pushed against a static object like in alignment or insertion tasks. In summary, the robustness analysis is performed for the following environment dynamics:

$$\begin{array}{lll}
\text{Movable:} & Z_e = m_e s, & m_e \in \mathcal{M}_{e,\text{mov}} \\
\text{Static:} & Z_e = b_e + \frac{k_e}{s}, & b_e \in \mathcal{B}_{e,\text{static}},\; k_e \in \mathcal{K}_{e,\text{static}} \\
\text{Mass-Spring-Damper:} & Z_e = m_e s + b_e + \frac{k_e}{s}, & m_e \in \mathcal{M}_{e,\text{MSD}},\; b_e \in \mathcal{B}_{e,\text{MSD}},\; k_e \in \mathcal{K}_{e,\text{MSD}},
\end{array} \tag{3.45}$$

where $\mathcal{M}_e, \mathcal{B}_e$, and $\mathcal{K}_e$ represent discretized parameter sets. The parameter sets were

selected as

$$\begin{aligned}
&\mathcal{M}_{e,\mathrm{mov}}=\{0;4;12;20\}\ \mathrm{kg}\\
&\mathcal{B}_{e,\mathrm{static}}=\{0;50;100;150;200\}\ \mathrm{Ns/m}, \quad \mathcal{K}_{e,\mathrm{static}}=\{5;10;15;20;25\}\ \mathrm{kN/m}\\
&\mathcal{M}_{e,\mathrm{MSD}}=\{0;4;12;20\}\ \mathrm{kg}, \quad \mathcal{B}_{e,\mathrm{MSD}}=\{0;100;200\}\ \mathrm{Ns/m}, \quad \mathcal{K}_{e,\mathrm{MSD}}=\{0;25;50;75;100\}\ \mathrm{kN/m}.
\end{aligned} \tag{3.46}$$

The sets for movable objects and objects with a MSD characteristics also contain the environment dynamics for free space, i.e. $m_e = b_e = k_e = 0$. The frequency is sampled in the interval $\omega \in [10^{-4}; 10^4] \cdot 2\pi$ rad/s. The stable and unstable regions in terms of the admittance parameters m_a and b_a are shown for the considered sets of environment dynamics for both control concepts in Fig. 3.6. By testing one parameter set in either of the regions, it was found that $m_a = 0$ kg and the gray colored areas represent unstable parameter sets, while all white areas represent the stable parameter regions. Please note that plots are not provided if the whole parameter space $m_a > 0,\ b_a > 0$ is stable. This is the case for static objects with $b_e = 200$ Ns/m for the MM architecture.

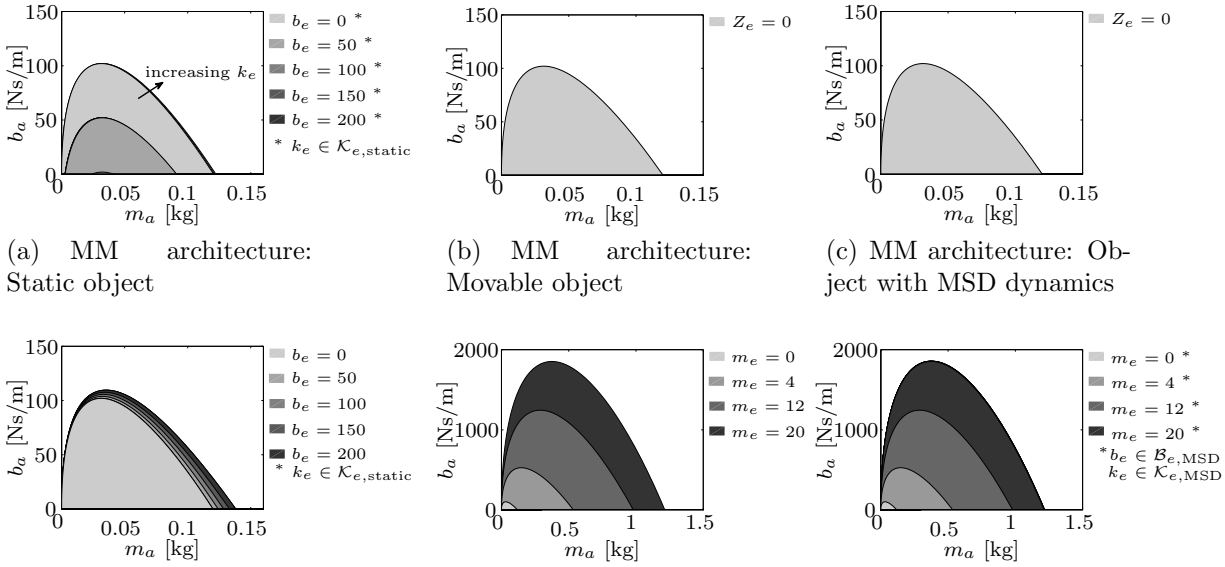

(a) MM architecture: Static object

(b) MM architecture: Movable object

(c) MM architecture: Object with MSD dynamics

(d) FaFa architecture: Static object

(e) FaFa architecture: Movable object

(f) FaFa architecture: Object with MSD dynamics

Fig. 3.6: Stability regions in parameter space (m_a, b_a) for model-mediated teleoperation and the FaFa architecture. All parameters are provided in SI-units. The gray colored areas represent unstable parameter sets.

As the MM and FaFa architecture are equal for the free space condition, $Z_e = 0$, the stability regions are the same. Otherwise, the results reveal significant differences between the two architectures. For all environments and for both architectures, the infinite root boundary (IRB) condition is fulfilled for $m_a = 0$. This axis is consequently unstable reducing the parameter set to $m_a > 0, b_a \geq 0$. For static objects, the instability region of the MM architecture is significantly reduced with an increase in the environment damping b_e, while the instability region of the FaFa architecture increases with increasing damping. For static objects, the instability regions of the FaFa architecture are always larger than those of the MM architecture.

Considering movable objects, the MM architecture contains an unstable region only for $m_e = 0$. For all other tested environment masses, the whole parameter space except for $m_a = 0$ is stable. For the FaFa architecture, on the contrary, the unstable region increases with increasing mass. The results are similar for an environment represented as a mass-spring-damper dynamics. Only for free space, where $m_e = b_e = k_e = 0$, an unstable parameter region is found for the MM architecture. For any other dynamics, the admittance parameters can be arbitrarily selected given that $m_a > 0, b_a \geq 0$ is fulfilled. The instability regions of the FaFa architecture increase for increasing environment masses and damping. In these cases, the parameters for the MM architecture can be selected from a larger range than for the FaFa architecture.

In summary, a robustness analysis was conducted for the system in steady-state. In a next step, stability is analyzed for model-mediated teleoperation system in the transient phase, where the parameters are time-varying.

3.3.3 Stability during the Transient Phase: Movable Objects

During the transient phase, the controller on master site exhibits time-varying behavior. A transient phase occurs when the initial parameters do not correspond to the converged estimated parameters. This is the case, if e.g. one touches an unknown object or if the object changes.

On slave site, a velocity controller with time-invariant control parameters is used to track the desired operator trajectory. Thus, the environment dynamics influences the stability of the closed-loop system on slave site only if the environment force acting as an external disturbance is not compensated. As this force can be measured, it can be compensated and the stability of the system on slave site is consequently independent of the environment dynamics. This implies also that transient stability does not have to be analyzed for the slave site.

The analysis of the system in steady-state was conducted for system model A. In order to determine stability boundaries analytically, which is especially important for the stability analysis based on the multiple Lyapunov theory, the system dynamics has to be reduced. This is achieved by neglecting the underlying velocity controllers as well as device, actuator, and sensor dynamics. The resulting system model is referred to as system model B, see Sec. 3.2.2. As the parameters are time-varying in the transient phase, Theorem 3.3.4 is used for proving stability. It is assumed that all estimation algorithms are stable, such that $\lim_{t\to\infty} \hat{\theta}(t) = \lim_{t\to\infty} \hat{m}_e(t) = \overline{m}_e$ holds. This implies that the parameter $\hat{m}_e$ remains bounded and belongs consequently to a compact set. The stability analysis requires further to prove asymptotic stability for all constant parameters $\overline{m}_e \in S$. The eigenvalues of the system are

$$\mathrm{eig}(A_{\mathrm{mov}}(\overline{\boldsymbol{\theta}})) = -\frac{b \pm \sqrt{b^2 - 4k_h\overline{m}}}{2\overline{m}}. \tag{3.47}$$

The system is asymptotically stable if the real parts of all eigenvalues are negative, see Theorem 3.3.1. Please note that $m_h \geq 0$, $b_h \geq 0$ and $k_h \geq 0$. Restricting further the estimated parameter $\overline{m}_e$ to non-negative values $\overline{m}_e \geq 0$, the real parts of the eigenvalues (3.47) are negative for all $m_a > 0$ and $b_a > 0$. Assuming that the parameter estimation

is stable, the dynamics described by model $\mathrm{B}_{\mathrm{mov}}$ is asymptotically stable according to the stability theorem 3.3.4. Consequently, the manipulation of movable objects using model-mediated teleoperation is asymptotically stable.

It should be noted here that this result holds only for model $\mathrm{B}_{\mathrm{mov}}$. The robustness analysis for system model A and maximum human arm impedance presented in Sec. 3.3.2 revealed that except for free space, all parameters $m_a > 0$ and $b_a > 0$ are stable. For maximum human arm impedance, the real parts of the eigenvalues (3.47) are negative for all $m_a > 0$ and $b_a \geq 0$. Thus, the stability regions for system model A and B are identical for movable objects and maximum human arm dynamics.

In summary, it was shown for system model $\mathrm{B}_{\mathrm{mov}}$ that the system is asymptotically stable when interacting with movable objects using model-mediated teleoperation. Moreover, the simplification of the system dynamics did not lead to different stability regions for maximum human arm dynamics.

3.3.4 Stability during the Transient Phase: Static Objects

Regarding contact with static objects, two situations have to be distinguished: i) the operator establishes and remains in contact with the object or ii) several transitions between contact and free space occur before the teleoperator remains in contact with the object. While stability can be proven with classical stability analysis tools for the first situation, the second situation requires analysis tools for switched systems, a subclass of hybrid systems. Both situations are investigated in this section.

3.3.4.1 Stability during Contact

If the teleoperator remains in contact with a static object, the stability proof can be performed analogously to the one for movable objects, i.e. based on Theorem 3.3.4. Model $\mathrm{B}_{\mathrm{static}}$ is used in order to derive analytical stability boundaries. If the estimation is stable, the parameters remain bounded and belong consequently to a compact set. The eigenvalues of the system are

$$\mathrm{eig}(\boldsymbol{A}_{\mathrm{static}}(\hat{\boldsymbol{\theta}})) = -\frac{\overline{b} \pm \sqrt{\overline{b}^2 - 4\overline{k}m}}{2m}. \tag{3.48}$$

If the estimated parameters $\overline{b}_e$ and $\overline{k}_e$ are constrained to non-negative values $\overline{b}_e \geq 0, \overline{k}_e \geq 0$ and knowing that the parameters of the human arm impedance are non-negative, the real parts of the eigenvalues (3.48) are negative for all $m_a > 0$ and $b_a > 0$. This is essentially the same result as for movable objects. Summarizing, model-mediated teleoperation is asymptotically stable for system model $\mathrm{B}_{\mathrm{static}}$ as long as the teleoperator remains in contact with a static object.

This stability proof holds again only for system model $\mathrm{B}_{\mathrm{static}}$, where significant simplifications were introduced. A comparison with the results from the robust stability analysis reveals that the simplification of the system dynamics does not lead to the same stability regions as for system model A, if the environment damping d_e is small. It is therefore an important future step to extend the stability proofs for the transient phase to system model A. Yet, it seems that numerical simulations will be required. In contrast, an

analytical stability proof is possible for system model B as derived in the following section.

3.3.4.2 Stability when Establishing Contact

As mentioned above, the proof holds only if the teleoperator remains in contact with the object. This is, however, not necessarily given when establishing contact. If contact is lost during the transient phase, the dynamics switches between $\hat{f}_e = 0$ and $\hat{f}_e = \hat{b}_e \dot{x}_m + \hat{k}_e(x_m - x_e)$. In this case, the stability proof as described above is not valid, see also Sec. 3.3.1.3. The analysis for showing stability of the switched dynamics is based on the Lyapunov theory. A global Lyapunov function for the switched dynamics is not found such that the multiple Lyapunov function approach described in Sec. 3.3.1.3 is employed.

Step 1: Stability Proof for Each Phase. The two phases to be distinguished are free space and contact. The first step in the multiple Lyapunov analysis consists in proving stability for free space and contact separately using the Lyapunov theory.

Step 1a: Stability for Free Space. The eigenvalues of the matrix $\boldsymbol{A}_{\text{free}}$, see (3.19), are given by

$$\text{eig}(\boldsymbol{A}_{\text{free}}(\hat{\boldsymbol{\theta}})) = -\frac{b \pm \sqrt{b^2 - 4k_h m}}{2m}. \tag{3.49}$$

Their real parts are negative if $m_a > 0$ and $b_a > 0$. For these admittance parameters, the system is asymptotically stable and there consequently exists a positive definite matrix $\boldsymbol{R}_{\text{free}} = \boldsymbol{R}_{\text{free}}^T$ for some positive definite matrix $\boldsymbol{Q}_{\text{free}} = \boldsymbol{Q}_{\text{free}}^T$, see also [104], such that

$$\boldsymbol{R}_{\text{free}} \boldsymbol{A}_{\text{free}} + \boldsymbol{A}_{\text{free}}^T \boldsymbol{R}_{\text{free}} = -\boldsymbol{Q}_{\text{free}}. \tag{3.50}$$

The corresponding Lyapunov function and its time derivative for free space denoted by V_{free} and $\dot{V}_{\text{free}}$, respectively, is given by

$$V_{\text{free}} = \boldsymbol{z}_{\text{free}}^T \boldsymbol{R}_{\text{free}} \boldsymbol{z}_{\text{free}} = \boldsymbol{z}_{\text{free}}^T \begin{bmatrix} r_{\text{free11}} & r_{\text{free12}} \\ r_{\text{free12}} & r_{\text{free22}} \end{bmatrix} \boldsymbol{z}_{\text{free}} \qquad \dot{V}_{\text{free}} = -\boldsymbol{z}_{\text{free}}^T \boldsymbol{Q}_{\text{free}} \boldsymbol{z}_{\text{free}} < 0. \tag{3.51}$$

Step 1b: Stability for Contact. In order to derive a Lyapunov function for system model B_{static}, a method from adaptive control theory is used. More precisely, the stability proof for contact is performed analogously to the one for an indirect continuous-time model-reference adaptive control (MRAC) problem, see [95]. The system dynamics (3.27) is first rewritten such that the time-varying dynamics of the remote environment is removed from the system matrix $\boldsymbol{A}_{\text{free}}$ and an additional control input $u \in \mathbb{R}$ is added, which includes the removed time-varying parts:

$$\begin{aligned} \dot{\boldsymbol{x}} &= \boldsymbol{A}_{\text{free}} \boldsymbol{x} + \boldsymbol{b}_{\text{free}} r_{\text{free}} + \boldsymbol{b}_{\text{contact}} u \\ &= \begin{bmatrix} 0 & 1 \\ -\frac{k_h}{m} & -\frac{b_h + b_a}{m} \end{bmatrix} \boldsymbol{x} + \begin{bmatrix} 0 \\ -\frac{1}{m} \end{bmatrix} r_{\text{free}} + \boldsymbol{b}_{\text{contact}} u. \end{aligned} \tag{3.52}$$

The objective is to adapt the dynamics (3.52) such that the reference model

$$\begin{aligned}\dot{\boldsymbol{x}}^d &= \boldsymbol{A}^d_{\text{contact}}\boldsymbol{x}^d + \boldsymbol{b}^d_{\text{contact}} r^d_{\text{contact}} \\ &= \begin{bmatrix} 0 & 1 \\ -\frac{k_h+k_e}{m} & -\frac{b_h+b_a+b_e}{m} \end{bmatrix} \boldsymbol{x}^d + \begin{bmatrix} 0 \\ -\frac{1}{m} \end{bmatrix} r^d_{\text{contact}}\end{aligned} \tag{3.53}$$

is tracked, where b_e and k_e are the true environment damping and stiffness and $r^d_{\text{contact}} = m_a\ddot{x}^*_m + (b_a + b_e)\dot{x}^*_m + k_e(x^*_m - x_e)$. It is assumed that the admittance parameters m_a and b_a are selected such that the reference dynamics is asymptotically stable. In a next step, the control law u is selected as

$$u = -\boldsymbol{\theta}^T\boldsymbol{x} + (r^d_{\text{contact}} - r_{\text{free}}). \tag{3.54}$$

As it is known from the analysis for permanent contact, that the estimated parameters appear only in the second row of the system matrix, $\boldsymbol{b}_{\text{contact}}$ is selected as $\boldsymbol{b}_{\text{contact}} = \boldsymbol{b}_{\text{free}}$. This leads to

$$\dot{\boldsymbol{x}} = (\boldsymbol{A}_{\text{free}} - \boldsymbol{b}_{\text{free}}\boldsymbol{\theta}^T)\boldsymbol{x} + \boldsymbol{b}_{\text{free}} r^d_{\text{contact}}. \tag{3.55}$$

It is assumed in the following that $\boldsymbol{\theta}^T$ can be selected such that

$$\boldsymbol{A}^d_{\text{contact}} = \boldsymbol{A}_{\text{free}} - \boldsymbol{b}_{\text{free}}\boldsymbol{\theta}^T \tag{3.56}$$

can be fulfilled. Defining the tracking error $\boldsymbol{e} = \boldsymbol{x} - \boldsymbol{x}^d$ and rewriting the system dynamics as

$$\dot{\boldsymbol{x}} = \underbrace{(\boldsymbol{A}_{\text{free}} - \boldsymbol{b}_{\text{free}}\boldsymbol{\theta}^T)}_{A^d_{\text{contact}}}\boldsymbol{x} + \boldsymbol{b}_{\text{free}} r^d_{\text{contact}} + \boldsymbol{b}_{\text{free}}(u + \boldsymbol{\theta}^T\boldsymbol{x} - (r^d_{\text{contact}} - r_{\text{free}})), \tag{3.57}$$

the error dynamics can be computed using (3.53) and (3.57)

$$\dot{\boldsymbol{e}} = \dot{\boldsymbol{x}} - \dot{\boldsymbol{x}}^d = \boldsymbol{A}^d_{\text{contact}}\boldsymbol{e} + \boldsymbol{b}_{\text{free}}(u + \boldsymbol{\theta}^T\boldsymbol{x} - (r^d_{\text{contact}} - r_{\text{free}})). \tag{3.58}$$

Now, the parameter vector $\boldsymbol{\theta}$ is assumed to be unknown, and has to be substituted by its estimate $\hat{\boldsymbol{\theta}}$. This leads to $u = -\hat{\boldsymbol{\theta}}^T\boldsymbol{x} + (\hat{r}^d_{\text{contact}}(\hat{\boldsymbol{\theta}}) - r_{\text{free}})$ with $\hat{r}^d_{\text{contact}}(\hat{\boldsymbol{\theta}}) = m_a\ddot{x}^*_m + (b_a + \hat{b}_e)\dot{x}^*_m + \hat{k}_e(x^*_m - x_e)$. Inserting it in (3.58) leads to

$$\dot{\boldsymbol{e}} = \boldsymbol{A}^d_{\text{contact}}\boldsymbol{e} + \boldsymbol{b}_{\text{free}}((\boldsymbol{\theta}^T - \hat{\boldsymbol{\theta}}^T)\boldsymbol{x} + (\hat{r}^d_{\text{contact}}(\hat{\boldsymbol{\theta}}) - r^d_{\text{contact}}). \tag{3.59}$$

By further substituting $\tilde{\boldsymbol{\theta}} = \hat{\boldsymbol{\theta}} - \boldsymbol{\theta}$, the error dynamics can be written as:

$$\dot{\boldsymbol{e}} = \boldsymbol{A}^d_{\text{contact}}\boldsymbol{e} - \boldsymbol{b}_{\text{free}}\tilde{\boldsymbol{\theta}}^T(\underbrace{\boldsymbol{x} - \begin{bmatrix} \dot{x}^*_m \\ x^*_m - x_e \end{bmatrix}}_{\overline{\boldsymbol{x}}}). \tag{3.60}$$

The next step consists in determining a Lyapunov function candidate, see also [95]:

$$V_{\text{contact}}(\boldsymbol{e}, \tilde{\boldsymbol{\theta}}) = \boldsymbol{e}^T \boldsymbol{R}_{\text{contact}} \boldsymbol{e} + \tilde{\boldsymbol{\theta}}^T \boldsymbol{\Gamma}_{\text{contact}} \tilde{\boldsymbol{\theta}} \tag{3.61}$$

where $\boldsymbol{\Gamma}_{\text{contact}} = \boldsymbol{\Gamma}_{\text{contact}}^T$ is positive definite. Taking the time derivative of the Lyapunov function candidate and using (3.50) leads to

$$\dot{V}_{\text{contact}}(\boldsymbol{e}, \tilde{\boldsymbol{\theta}}) = -\boldsymbol{e}^T \boldsymbol{Q}_{\text{contact}} \boldsymbol{e} - 2(\boldsymbol{e}^T \boldsymbol{R}_{\text{contact}} \boldsymbol{b}_{\text{free}}) \tilde{\boldsymbol{\theta}}^T \overline{\boldsymbol{x}} + 2\tilde{\boldsymbol{\theta}}^T \boldsymbol{\Gamma}_{\text{contact}} \dot{\tilde{\boldsymbol{\theta}}}. \tag{3.62}$$

In order for $\dot{V}_{\text{contact}}$ to be negative definite, the last two terms should cancel:

$$(\boldsymbol{e}^T \boldsymbol{R}_{\text{contact}} \boldsymbol{b}_{\text{free}}) \tilde{\boldsymbol{\theta}}^T \overline{\boldsymbol{x}} = \tilde{\boldsymbol{\theta}}^T \boldsymbol{\Gamma}_{\text{contact}} \dot{\tilde{\boldsymbol{\theta}}}. \tag{3.63}$$

Equation (3.63) is fulfilled if the control law for the estimation error $\tilde{\boldsymbol{\theta}}$ is selected as

$$\dot{\tilde{\boldsymbol{\theta}}} = (\boldsymbol{e}^T \boldsymbol{R}_{\text{contact}} \boldsymbol{b}_{\text{free}}) \boldsymbol{\Gamma}_{\text{contact}}^{-1} \overline{\boldsymbol{x}}. \tag{3.64}$$

Applying the control law, the time derivative of the Lyapunov function is negative definite:

$$\dot{V}_{\text{contact}}(\boldsymbol{e}, \tilde{\boldsymbol{\theta}}) = -\boldsymbol{e}^T \boldsymbol{Q}_{\text{contact}} \boldsymbol{e} \tag{3.65}$$

with the consequence that $\lim_{t \to \infty} \boldsymbol{e} = 0$. As the reference dynamics is selected such that $\lim_{t \to \infty} \boldsymbol{x}^d = 0$, also the adaptive state $\boldsymbol{x}$ approaches zero asymptotically. This result shows, that for the selected estimation law the system dynamics (3.52) will track the desired dynamics during contact. As the simplified system model B is used for this stability analysis, master and slave position and velocity are assumed to be equal and the estimation law could be based on the master position and velocity. In the final implementation of model-mediated teleoperation, the slave position and velocity are used for the estimation. It therefore remains future work to analyze transition stability for system model A, where the slave dynamics, actuator and sensor dynamics, deficiencies in the communication channel, and possibly time-varying human arm dynamics are considered.

Step 2: Transition Stability. The second step in the multiple Lyapunov function analysis is to prove transition stability. It is assumed that asymptotic stability according to Lyapunov is proven for each subsystem. Here, the two subsystems are free space and contact and asymptotic stability according to Lyapunov was shown for each subsystem separately in the previous section. The transition stability proof performed in the following is based on the multiple Lyapunov function approach proposed by Branicky [22] and on the work by Ni & Wang [148], see Sec. 3.3.1.3.

The proof for transition stability for model-mediated teleoperation and static objects is decomposed into three steps: first, condition (3.42) is shown to be fulfilled for the contact phase. Second, it is assumed that the environment estimation during contact is converged, such that the system tracks the desired system dynamics (3.53). Based on this assumption, condition (3.42) is shown to be fulfilled for the free space phase. In the final third step, transition stability is proven by investigating the convergence phase.

Let us denote switching times where the teleoperator *leaves contact* and enters free space as $t_{i+2n},\ n \in \mathbb{N}^0$. The teleoperator *enters contact* and leaves free space at switching times $t_{i+1+2n},\ n \in \mathbb{N}^0$. For all switching times, the teleoperator position is equal to the position of the wall $x_m = x_e$. It is assumed, that the human intention is to reach the constant position $x_m^* = \text{const.}$ such that $\dot{x}_m^* = \ddot{x}_m^* = 0$ can be assumed. This implies $r_{\text{free}} = 0$ and $z_{\text{free1}} = x_e - x_m^*$, where $\boldsymbol{z}_{\text{free}} = [z_{\text{free1}}, z_{\text{free2}}]^T$, for all switching times.

Step 2a: Transition Stability for Contact. The proof for transition stability starts with the subsystem "contact". The estimation process is stopped in a free space phase, such that $\tilde{\boldsymbol{\theta}}^{i+2n} = \tilde{\boldsymbol{\theta}}^{i+1+2n}$. The state $\boldsymbol{x}$ of the adaptive dynamics

$$\dot{\boldsymbol{x}} = (\boldsymbol{A}_{\text{free}} - \boldsymbol{b}_{\text{free}}\hat{\boldsymbol{\theta}}^T)\boldsymbol{x} + \boldsymbol{b}_{\text{free}} r^d_{\text{contact}}(\hat{\boldsymbol{\theta}}) \tag{3.66}$$

is reset to the state of the real reference system (3.53) whenever the reference system enters the contact phase, i.e.

$$\boldsymbol{x}(t_{i+1+2n}) = \boldsymbol{x}^d(t_{i+1+2n}). \tag{3.67}$$

As a consequence of this reset, $\boldsymbol{e}(t_{i+1+2n}) = \boldsymbol{x}(t_{i+1+2n}) - \boldsymbol{x}^d(t_{i+1+2n}) = \boldsymbol{0}$. A diagonal matrix is selected for $\boldsymbol{\Gamma}_c$ with positive diagonal elements $\gamma_{\text{contact11}} > 0,\ \gamma_{\text{contact22}} > 0$. Evaluating the Lyapunov function for contact (3.61) at switching times t_{i+2n} and t_{i+2+2n} leads to

$$\begin{aligned}
-\Delta V_{\text{contact}}(t_{i+2n}, t_{i+2+2n}) &= V_{\text{contact}}(t_{i+2n}) - V_{\text{contact}}(t_{i+1+2n}) \\
&\quad + V_{\text{contact}}(t_{i+1+2n}) - V_{\text{contact}}(t_{i+2+2n}) \\
&= (\boldsymbol{e}^{i+2n})^T \boldsymbol{R}_{\text{contact}} \boldsymbol{e}^{i+2n} - \underbrace{(\boldsymbol{e}^{i+1+2n})^T \boldsymbol{R}_{\text{contact}} \boldsymbol{e}^{i+1+2n}}_{=0} \\
&\quad + \underbrace{(\tilde{\boldsymbol{\theta}}^{i+2n})^T \boldsymbol{\Gamma}_{\text{contact}} \tilde{\boldsymbol{\theta}}^{i+2n} - (\tilde{\boldsymbol{\theta}}^{i+1+2n})^T \boldsymbol{\Gamma}_{\text{contact}} \tilde{\boldsymbol{\theta}}^{i+1+2n}}_{=0} \\
&\quad + V_{\text{contact}}(t_{i+1+2n}) - V_{\text{contact}}(t_{i+2+2n}) \\
&= \underbrace{(\boldsymbol{e}^{i+2n})^T \boldsymbol{R}_{\text{contact}} \boldsymbol{e}^{i+2n}}_{>0} \\
&\quad + \underbrace{V_{\text{contact}}(t_{i+1+2n}) - V_{\text{contact}}(t_{i+2+2n})}_{>0 \text{ using (3.65)}}.
\end{aligned} \tag{3.68}$$

As (3.68) is positive, the Lyapunov energy decreases from one contact phase to the next one.

Step 2b: Transition Stability for Free Space: Estimation is Converged. Consider again the system during contact. If the estimation is converged during contact, the adaptive system (3.66) tracks the desired system (3.53), i.e. $\boldsymbol{x} \to \boldsymbol{x}^d$. As the reference system (3.53) is asymptotically stable, there exists a positive definite matrix $\boldsymbol{R}_d$ and a positive definite matrix $\boldsymbol{Q}_d = \boldsymbol{Q}_d^T$ such that

$$\boldsymbol{R}_d \boldsymbol{A}_d + \boldsymbol{A}_d^T \boldsymbol{R}_d = -\boldsymbol{Q}_d. \tag{3.69}$$

This leads to the following positive definite Lyapunov function and its negative definite time derivative

$$V_d = \boldsymbol{x}_d^T \boldsymbol{R}_d \boldsymbol{x}_d \qquad \dot{V}_d = -\boldsymbol{x}_d^T \boldsymbol{Q}_d \boldsymbol{x}_d. \tag{3.70}$$

Let us select $\boldsymbol{Q}_d$ as unity matrix. Then, for two subsequent switching times t_{i+1+2n} and t_{i+2n},

$$V_d(t_{i+1+2n}) - V_d(t_{i+2+2n}) = -(\underbrace{((x_{d1}^{i+1+2n})^2 - (x_{d1}^{i+2+2n})^2)}_{=0} \tag{3.71}$$

$$+ (x_{d2}^{i+1+2n})^2 - (x_{d2}^{i+2+2n})^2)) < 0, \tag{3.72}$$

which implies $|x_{d2}^{i+1+2n}| > |x_{d2}^{i+2+2n}|$. As the adaptive system tracks the desired system, $|x_{d2}^{i+1+2n}| = |z_{\text{free2}}^{i+1+2n}| > |x_{d2}^{i+2+2n}| = |z_{\text{free2}}^{i+2+2n}|$ holds. Using (3.51) with $\boldsymbol{Q}_{\text{free}}$ as unity matrix, $|z_{\text{free2}}^{i+2+2n}| > |z_{\text{free2}}^{i+3+2n}|$. This condition is now used to prove (3.42) for free space, given that the estimation is converged. Evaluating (3.42) using the Lyapunov function for free space (3.51) for t_{i+1+2n} and t_{i+3+2n} leads to

$$\begin{aligned}
-\Delta V_{\text{free}}(t_{i+3+2n}, t_{i+1+2n}) &= V_{\text{free}}(t_{i+1+2n}) - V_{\text{free}}(t_{i+3+2n}) \\
&= r_{\text{free11}} \underbrace{((z_{\text{free1}}^{i+1+2n})^2 - (z_{\text{free1}}^{i+3+2n})^2)}_{=0} \\
&+ 2r_{\text{free12}} \, (z_{\text{free1}}^{i+1+2n} z_{\text{free2}}^{i+1+2n} - z_{\text{free1}}^{i+2+2n} z_{\text{free2}}^{i+3+2n}) \\
&+ r_{\text{free22}} \, ((z_{\text{free2}}^{i+1+2n})^2 - (z_{\text{free2}}^{i+3+2n})^2) \\
&= 2r_{\text{free12}} \, z_{\text{free1}}^{i+1+2n} (z_{\text{free2}}^{i+1+2n} - z_{\text{free2}}^{i+3+2n}) \\
&+ r_{\text{free22}} \underbrace{((z_{\text{free2}}^{i+1+2n})^2 - (z_{\text{free2}}^{i+3+2n})^2)}_{>0}.
\end{aligned}$$

Selecting $\boldsymbol{Q}_{\text{free}}$ as the unity matrix, the $\boldsymbol{R}_{\text{free}}$ element $r_{\text{free12}} = \frac{m}{2k} > 0$ and $r_{\text{free22}} = \frac{k+m}{2bk} > 0$ as all parameters are restricted to positive values. For the second term to be positive, $z_{\text{free1}}^{i+1+2n}(z_{\text{free2}}^{i+1+2n} - z_{\text{free2}}^{i+3+2n}) > 0$ has to hold. This inequality is satisfied as $\text{sign}(z_1^{i+1+2n}) = \text{sign}(x_e - x_m^*) = \text{sign}(z_{\text{free2}}^{i+1+2n} - z_{\text{free2}}^{i+3+2n})$. Consequently, the condition for multiple Lyapunov stability (3.42) is fulfilled for free space, if the estimation is converged.

Step 2c: Transition Stability for Free Space during Estimation Phase. Finally, transition stability has to be investigated for the estimation phase, where the adaptive system does not track the desired system yet. This proof uses the definition of asymptotic convergence together with the multiple Lyapunov function theory by Branicky [22]. It was shown above that the adaptive system tracks the reference system asymptotically, i.e. $\lim_{t\to\infty} e = 0$ implying that $\lim_{t\to\infty} \boldsymbol{x} = \boldsymbol{x}_d$. Furthermore, the reference system is asymptotically stable such that $\lim_{t\to\infty} \boldsymbol{x}_d = 0$. These two asymptotic convergence properties imply that for every exit time t_{i+1+2n} from free space, there exists another exit time t_{i+k+2n} from free space, where $|x_{d2}^{i+k+2n}| < |x_{d2}^{i+1+2n}|$. As this holds for every exit time, the system will converge to $\boldsymbol{x}^d \to 0$. This concludes the proof for transition stability.

Summarizing, it was shown in this section for the simplified system model B, that model-mediated teleoperation is asymptotically stable for static objects, where transitions between free space and contact can occur. In other words, the teleoperator will remain in contact after a finite number of switches between free space and contact. As it was also shown that the adaptive system for contact tracks the reference system, the system will converge to $\boldsymbol{x} = \boldsymbol{x}_d = \boldsymbol{0}$ asymptotically. This holds for the transient and steady-state

phase as long as $m_a > 0$ and $b_a \geq 0$ and the estimated parameters are constrained to non-negative values.

The comparison with the stability results for system model A in steady-state showed differences for several environment dynamics. The stability regions of system model A are smaller than for system model B. It is therefore an important future step to extend the transition stability proof provided in this section to system model A.

So far, an adaptive identification method and a linear model were assumed for describing and estimating the dynamics of static objects. It would be interesting to investigate stability for other environment models and estimation techniques in future work.

3.4 Fidelity Analysis

The degree of fidelity gives insights into how realistically the remote environment is presented to the operator. In this section, fidelity is analyzed for model-mediated teleoperation and compared to the fidelity that can be achieved when using the classical two-channel FaFa architecture. The degree of fidelity is determined for the parameters that lead to the highest degree of fidelity while guaranteeing asymptotic stability of the system. These parameters are selected based on the results of the robust stability analysis presented in the previous section. As the system models do often not represent exactly the real system, the theoretically derived stability boundaries are often not conservative enough. In order to assess the fidelity of a system more realistically, a new robust fidelity measure is introduced. It takes, to some extent, the realizability of the parameters that optimize the degree of fidelity into account.

3.4.1 Fidelity Analysis for Perfect Environment Reconstruction

Fidelity is investigated for model-mediated teleoperation as well as for the FaFa architecture. Regarding model-mediated teleoperation, it is assumed in this section that the estimation works perfectly such that the reconstructed environment impedance $\hat{Z}_e$ is identical to the real environment impedance Z_e. The transmitted impedances presented in (2.4) can generally be described in terms of the elements of the $\boldsymbol{H}$-matrix as

$$Z_t = \frac{F_h}{sX_m} = \frac{h_{11} + \det \boldsymbol{H}\ Z_e}{1 + h_{22} Z_e}. \tag{3.73}$$

The fidelity analysis is based on system model A, i.e. taking the full system dynamics into account. For model-mediated teleoperation, the transmitted impedance is then given by

$$Z_{t,MM} = h_{11,MM} = \frac{\hat{Z}_{ae} Z_{cm}}{\hat{Z}_{ae} + Z_{PI,m}}, \tag{3.74}$$

while it is given for the FaFa architecture by

$$Z_{t,FaFa} = \frac{h_{11} + \det \boldsymbol{H}\ Z_e}{1 + h_{22} Z_e} \tag{3.75}$$

$$= \frac{Z_{cm} Z_a) Z_{cs} (Z_a + Z_{PI,m}) + Z_{cm} Z_a Z_{aPI} Z_e}{(Z_a + Z_{PI,s})(Z_a + Z_{PI,m}) Z_{cs} + Z_{aPI}(Z_a + Z_{PI,s}) Z_e} \tag{3.76}$$

where $Z_{aPI} = Z_a + Z_{PI,s} + Z_{PI,m}$. Transparency is achieved if $Z_t = Z_e$. It is obvious that this condition is fulfilled for free space, i.e. where $\hat{Z}_e = Z_e = 0$ if

$$Z_{t,MM}|_{\hat{Z}_e=0} = \frac{Z_a Z_{cm}}{Z_a + Z_{PI,m}} \qquad Z_{t,FaFa}|_{Z_e=0} = \frac{Z_a Z_{cm}}{Z_a + Z_{PI,m}}, \tag{3.77}$$

which is guaranteed if

$$Z_a = 0 \Rightarrow m_a = b_a = 0. \tag{3.78}$$

This holds for both architectures equivalently. The fidelity is consequently the same for the FaFa and MM architecture in free space.

In a next step, the effect of contact with objects, i.e. $Z_e \neq 0$, is investigated. The system is assumed to be in steady-state, such that the control parameters are constant. The following section is dedicated to a new robust fidelity measure, while the subsequent section focuses on the fidelity analysis based on the $Z_{\text{diff}}^{\text{abs}}$ measure as introduced in (2.9).

3.4.1.1 Fidelity Analysis based on Robust Fidelity Measure $\mathcal{F}_{\text{robust}}$

Although several effects like sensor and actuator dynamics are taken into account in the full system dynamics described by model A, the true characteristic of the teleoperation system is still not fully captured. Nonlinearities in e.g. actuators, mechanics, or electronics, the discrete nature of the controllers as well as noisy measurements are not incorporated in model A. As a consequence, the control parameters that will stabilize the real system will be different (in this case higher virtual mass and damping) than the theoretical ones. This implies, that taking only the control parameters closest to the optimal ones into account may not be a suitable choice as the real system may not be stable for these control parameters. Thus, the fidelity measure should incorporate the practical realizability in some sense, i.e. it should become more robust to model errors or simplifications. The (in-)stability regions in the parameter space are a good indication of the practical realizability of different control parameters. Consider the comparison of two architectures and assume that the stability region is closed on the admissible parameter domain: first, a larger stability region facilitates to find practically suitable parameters. Thus, a larger stability region should result in a higher degree of robust fidelity. Second, if the stable areas in the parameter space of two architectures are about the same size, a higher degree of fidelity is achieved if the integral of the Z_{error} over the stable region is smaller. Summarizing these considerations, two factors are important for a robust fidelity measure:

i) the stable region should be as large as possible,

ii) the smaller the Z_{error} in the stable region, the better.

This leads to the following definition of robust fidelity:

Definition 3.4.1 (Robust Fidelity $\mathcal{F}_{\mathbf{robust}}$) Given a teleoperation architecture with $\boldsymbol{q} \in D_{\boldsymbol{q}}$ design parameters where $\boldsymbol{q}^s \in D_{\boldsymbol{q}}^s$ represent parameters that lead to a stable system. The set $D_{\boldsymbol{q}}^s \subset \mathbb{R}^n$ is assumed to be compact. A robust fidelity criterion $\mathcal{F}_{\text{robust}}$ is then defined as:

$$\mathcal{F}_{\text{robust}} = \underset{\boldsymbol{q}^s \in D_{\boldsymbol{q}}^s}{\arg\max} \int_{q_1^s} \dots \int_{q_n^s} \frac{1}{Z_{\text{error}}(\boldsymbol{q}^s)} \, \mathrm{d}\, q_n^s \cdots \mathrm{d}\, q_1^s. \tag{3.79}$$

In contrast to the Z-error measure known from literature, it is not sufficient for the robust fidelity measure that there is a single parameter pair where fidelity is minimal, while it is arbitrarily large for all other parameter pairs. On the contrary, as mentioned above, the fidelity should be as small as possible for the whole stability region.

The stability regions change with the environment dynamics. Thus, the fidelity criterion $\mathcal{F}_{\text{robust}}$ is evaluated for different environment dynamics, once for the MM architecture and once for the FaFa architecture. Upper bounds on the admittance parameters were set to $m_{a,\max} = 15$ kg and $b_{a,\max} = 200$ Ns/m. The stable parameter region is discretized and the multiple integral is replaced with a multiple sum. The parameters of the environment dynamics are selected from the sets described in (3.46). The results are presented in Tables 3.1, 3.2, and 3.3 for the MM and FaFa architecture. For the free space condition, $\mathcal{F}_{\text{robust}}^*$ is found as $\mathcal{F}_{\text{robust}}^* = 0.153 \cdot 10^{-3}$ for both architectures.
The $\mathcal{F}_{\text{robust}}$ values for the MM architecture are significantly larger than for the FaFa architecture for all tested objects. These results therefore show that robust fidelity as introduced in this section is superior with model-mediated teleoperation compared to a classical two-channel architecture.

Tab. 3.1: The optimal Z-error, Z_{error}^*, and the introduced robust fidelity measure $\mathcal{F}_{robust}$ for the MM and FaFa architecture for *movable* objects.

Z_e	Z_{error}^*		$\mathcal{F}_{\text{robust}}$	
m_e	MM	FaFa	MM	FaFa
[kg]	$[\cdot 10^{-3}]$	$[\cdot 10^{-3}]$	$[\cdot 10^{3}]$	$[\cdot 10^{3}]$
4	5.010	7.092	1.028	0.086
12	1.869	8.266	6.872	0.832
20	0.192	1000.503	34.347	1.503

3.4.1.2 Fidelity Analysis Based on Original Z-error Measure

The analysis based on the robust fidelity measure showed clearly that model-mediated teleoperation is able to present a more realistic haptic impression of the remote environment to the operator than the classical FaFa architecture. In order to verify these results, fidelity is further investigated based on the well-known Z-error measure presented in Sec. 2.2.1.1.

Tab. 3.2: The optimal Z-error, Z^*_{error}, and the introduced robust fidelity measure $\mathcal{F}_{robust}$ for the MM and FaFa architecture for *static* objects.

Z_e		Z^*_{error}		$\mathcal{F}_{\text{robust}}$	
b_e [Ns/m]	k_e [kN/m]	MM $[\cdot 10^{-3}]$	FaFa $[\cdot 10^{-3}]$	MM $[\cdot 10^{3}]$	FaFa $[\cdot 10^{3}]$
0	5	12.948	25.354	527.593	115.225
50	5	0.027	3.124	231.734	154.800
100	5	40.521	127.321	22.121	15.188
150	5	218.409	388.759	9.352	6.494
200	5	570.293	729.036	4.244	3.319
0	15	76.077	188.379	42.656	16.070
50	15	38.657	135.842	110.165	25.883
100	15	12.517	98.781	751.138	37.032
150	15	2.532	86.290	687.848	42.655
200	15	14.854	99.259	122.992	31.723
0	25	156.496	337.921	21.894	9.144
50	25	123.434	308.778	25.924	11.221
100	25	93.580	285.008	35.891	12.219
150	25	57.185	268.834	58.705	11.432
200	25	41.732	261.184	80.772	11.824

Tab. 3.3: The optimal Z-error, Z^*_{error}, and the introduced robust fidelity measure $\mathcal{F}_{robust}$ for the MM and FaFa architecture for an object characterized by a *mass-spring-damper dynamics*.

Z_e			Z^*_{error}		$\mathcal{F}_{\text{robust}}$	
m_e	b_e	k_e	MM	FaFa	MM	FaFa
[kg]	[Ns/m]	[kN/m]	$[\cdot 10^{-3}]$	$[\cdot 10^{-3}]$	$[\cdot 10^{3}]$	$[\cdot 10^{3}]$
4	0	5	5.276	1000.503	0.001	< 0.001
12	0	5	2.046	1000.503	0.001	< 0.001
20	0	5	0.255	41095.136	0.052	< 0.001
4	100	5	1.372	0.554	2.867	0.647
12	100	5	0.909	5.106	9.634	1.981
20	100	5	0.126	20.037	29.607	2.739
4	200	5	0.567	3.854	7.478	1.575
12	200	5	0.662	3.788	16.453	3.267
20	200	5	0.113	17.159	43.546	4.176
4	0	15	5.868	1000.503	0.001	< 0.001
12	0	15	2.446	1000.503	0.002	< 0.001
20	0	15	0.435	1000.503	0.001	< 0.001
4	100	15	1.791	1.012	2.332	0.589
12	100	15	1.310	4.083	7.241	1.565
20	100	15	0.253	17.503	19.381	2.098
4	200	15	0.709	0.195	7.056	1.826
12	200	15	0.887	2.848	14.500	3.004
20	200	15	0.198	14.829	34.566	3.727
4	0	25	6.519	1000.503	0.001	< 0.001
12	0	25	2.907	1000.503	0.002	< 0.001
20	0	25	0.677	1000.503	0.004	< 0.001
4	100	25	2.088	0.583	2.132	0.595
12	100	25	1.724	3.366	5.978	1.369
20	100	25	0.443	15.338	14.396	1.728
4	200	25	0.843	0.402	7.336	2.209
12	200	25	1.178	2.210	12.944	2.869
20	200	25	0.344	12.790	28.078	3.397

More precisely, the Z-error measure based on $Z_{\text{diff}}^{\text{abs}}(j\omega, \boldsymbol{q}, Z_e)$, see (2.9), will be used in the following analysis. The smaller the Z-error, the higher the degree of fidelity. In other words, the optimum degree of fidelity is found from a set of stable control parameters $\boldsymbol{q}^s \in D_{\boldsymbol{q}}^s$ as the minimum Z_{error} evaluated for a specific environment Z_e

$$\begin{aligned} Z_{\text{error,opt}} &= \arg\min_{\boldsymbol{q}^s \in D_{\boldsymbol{q}}^s} Z_{\text{error}}(\boldsymbol{q}, Z_e) \\ &= \arg\min_{\boldsymbol{q}^s \in D_{\boldsymbol{q}}^s} \underbrace{\frac{1}{\omega_{\max} - \omega_{\min}}}_{\Delta\omega} \int_{\omega_{\min}}^{\omega_{\max}} Z_{\text{diff}}^{\text{abs}}(j\omega, \boldsymbol{q}, Z_e)\, \mathrm{d}\omega. \end{aligned} \tag{3.80}$$

Analytic Fidelity Analysis. In a first step, analytical conditions are derived for solving the optimization problem (3.80). This allows to determine the optimal parameters analytically. This analysis can only be performed for system model B, where several simplifications are assumed. The necessary conditions for the multi-variate static optimization problem (3.80) are given by

$$0 = \frac{\partial}{\partial q_1}(Z_{\text{error}(\boldsymbol{q}, Z_e)}) \tag{3.81}$$

$$\vdots$$

$$0 = \frac{\partial}{\partial q_n}(Z_{\text{error}(\boldsymbol{q}, Z_e)}). \tag{3.82}$$

If $Z_{\text{error}(\boldsymbol{q}, Z_e*)}$ and $\frac{\partial}{\partial q_i} Z_{\text{error}(\boldsymbol{q}, Z_e*)}$ are continuous over a region $[q_{i,\min}; q_{i,\max}] \times [\omega_{\min}; \omega_{\max}]$, the differentiation and integral are commutable according to the Leibniz integral rule [174]:

$$0 = \frac{\partial}{\partial q_i}(Z_{\text{error}(\boldsymbol{q}, Z_e*)}) = \frac{1}{\Delta\omega} \int_{\omega_{\min}}^{\omega_{\max}} \frac{\partial}{\partial q_i} Z_{\text{diff}}^{\text{abs}}(j\omega, \boldsymbol{q}, Z_e)\, \mathrm{d}\omega. \tag{3.83}$$

Using (2.9), (3.83) can be written as

$$0 = \int_{\omega_{\min}}^{\omega_{\max}} \frac{\partial}{\partial q_i} \frac{|Z_t(j\omega, \boldsymbol{q}, Z_e)|^2}{|Z_e(j\omega)|^2}\, \mathrm{d}\omega, \tag{3.84}$$

which can be simplified with $\frac{\partial}{\partial q_i}|Z_e(j\omega)|^2 = 0$ to

$$0 = \int_{\omega_{\min}}^{\omega_{\max}} \frac{\frac{\partial}{\partial q_i}|Z_t(j\omega, \boldsymbol{q}, Z_e)|^2}{|Z_e(j\omega)|^2}\, \mathrm{d}\omega. \tag{3.85}$$

Consequently, the necessary conditions are given by

$$0 = \int_{\omega_{\min}}^{\omega_{\max}} \frac{\frac{\partial}{\partial q_1}|Z_t(j\omega, \boldsymbol{q}, Z_e)|^2}{|Z_e(j\omega)|^2}\,\mathrm{d}\omega \tag{3.86}$$

$$\vdots$$

$$0 = \int_{\omega_{\min}}^{\omega_{\max}} \frac{\frac{\partial}{\partial q_n}|Z_t(j\omega, \boldsymbol{q}, Z_e)|^2}{|Z_e(j\omega)|^2}\,\mathrm{d}\omega. \tag{3.87}$$

Solving these equations leads to the extremum points of Z_{error} with respect to the parameter vector $\boldsymbol{q}$. The next step requires to determine whether the extremum points represent minima or maxima. From functional analysis, it is well known, that an extremum point $\boldsymbol{a}^*$ of a function $f(\boldsymbol{a}), \boldsymbol{a} = [a_1, \ldots, a_n]$ is a local minimum/maximum of $f(\boldsymbol{a})$ if all subdeterminants of the Hessian matrix with elements $\frac{\partial^2}{\partial a_i \partial a_j} f(\boldsymbol{a})$ are positive/negative, see e.g. [174]. These conditions can now be solved for different environment dynamics $Z_e \neq 0$. The admittance parameters minimizing Z_{error} are found for two types of linear environment dynamics:

$$\text{Static: } Z_{e,\text{static}} = b_e + \frac{k_e}{s}, \qquad \text{Movable: } Z_{e,\text{mov}} = m_e\, s \tag{3.88}$$

with $m_e, b_e, k_e \in \mathbb{R}_0^+$. For an object characterized by a mass-spring-damper dynamics $Z_e = m_e\, s + b_e + \frac{k_e}{s}$, the optimality conditions for model-mediated teleoperation cannot be solved analytically. Also, for the FaFa architecture the complexity of the necessary conditions is too high to be solved analytically. Even for the MM architecture, the necessary conditions for the optimal parameters could only be found for simplified dynamics, where the underlying position/velocity controller is assumed to cancel the master dynamics such that the admittance controller can be represented by the admittance only. For these simplified dynamics and $Z_{e,\text{static}}$, the parameters that fulfill the necessary conditions are

$$m_a^*|_{Z_{e,\text{static}}} = -\frac{3\,{b_e}^2\,k_e\,\left(k_e\,\arctan\left(\frac{b_e k_e \Delta\omega}{k_e^2 + b_e^2 \omega_{\min}\omega_{\max}}\right) + b_e\,\Delta\omega\right)}{3\,{k_e}^3\,\arctan\left(\frac{b_e k_e \Delta\omega}{k_e^2 + b_e^2 \omega_{\min}\omega_{\max}}\right) + {b_e}^3\,({\omega_{\min}}^3 - {\omega_{\max}}^3) + 3\,b_e\,{k_e}^2\,\Delta\omega} \tag{3.89}$$

$$b_a^*|_{Z_{e,\text{static}}} = -b_e. \tag{3.90}$$

Negative or zero mass and damping values result in marginal stability or instability. These can consequently not be selected as parameters optimizing fidelity. Generally, small admittance parameters are preferable as the transmitted impedance gets closer to the environment impedance. Consequently, $b_a^*|_{Z_{e,\text{static}}} = 0$ is found as the stable, optimum damping parameter. The optimal mass parameter is found as

$$\lim_{\omega_{\min}\to 0} \lim_{\omega_{\max}\to\infty} m_a^*|_{Z_{e,\text{static}}} = 0. \tag{3.91}$$

For movable objects represented by $Z_{e,\text{mov}}$ the optimal admittance parameters are

$$\begin{aligned} m_a^*|_{Z_{e,\text{mov}}} &= -m_e \\ b_a^*|_{Z_{e,\text{mov}}} &= 0. \end{aligned}$$

Negative or zero mass and damping values result in marginal stability or instability. With these constraints the optimal admittance parameters for the system model B are

$$m_a^*|_{Z_{e,\text{mov}}} > 0 \qquad \text{and} \qquad b_a^*|_{Z_{e,\text{mov}}} = 0. \tag{3.92}$$

For analytically determining the parameters optimizing fidelity for the FaFa architecture, the dynamics had also to be reduced leading to system model B. The MM and FaFa architectures are then identical, such that also the optimal parameters are the same for both architectures, and, at this level of abstraction, both architectures exhibit the same degree of fidelity. A more fair comparison is obtained in the following numerical fidelity analysis where the full system dynamics described by system model A is considered.

Numerical Fidelity Analysis. The Z-error is additionally derived numerically for the full dynamics described by system model A. An optimization algorithm [3] is used to find the optimum with the constraints $m_a \in]0; 10]$ kg and $b_a \in [0; 200]$ Ns/m. Larger mass and damping values are excluded as they would strongly degrade the fidelity for free space and make the system uncomfortable for the operator. The parameters were restricted to the stable regions in the parameter space. The analysis is conducted for static and movable objects, and for objects with a mass-spring-damper characteristic. The parameters of the environment dynamics are selected from the sets described in (3.46). The results are listed for both architectures in Tables 3.1, 3.2, and 3.3.

In free space, the MM and FaFa architecture are equivalent. Consequently, the optimal and stable admittance parameters referred to as $\boldsymbol{p}_a^*$ and the resulting Z_{error} are the same: $m_a^* \ll 1$ μg, $b_a^* = 0.633$ Ns/m, $Z_{\text{error}}^* = 0.141$.

In contrast to the results for the robust fidelity measure, the Z-error is smaller for the FaFa architecture for several objects with MSD characteristics ($m_e = 4$ kg, $b_e = 100$ Ns/m, $k_e = 5000$ N/m, $m_e = 4$ kg, $b_e = 100$ Ns/m, $k_e = 15000$ N/m, $m_e = 4$ kg, $b_e = 200$ Ns/m, $k_e = 15000$ N/m, $m_e = 4$ kg, $b_e = 100$ Ns/m, $k_e = 25000$ N/m). This would imply that the FaFa architecture is superior in fidelity for these cases compared to the MM architecture. It should be noted at this point that numerical inaccuracies weigh much higher for the Z_{error} measure than for the robust fidelity measure: the robust fidelity measure is based on the integration of the Z_{error} over a whole parameter region, the minimum Z_{error} is found as a result from a numerical optimization routine, where the inequality constraints are based on an approximation of the instability regions. Thus and as the majority of tested environments did not reveal discrepancies, the numerical inaccuracies may have led to these differences. Another important aspect is to take the optimal parameters presented in Table C.3 into account. The optimum mass is very small and also the optimum damping is small for the considered experimental setup. In experiments, see e.g. 4.6.2, similar

[3] The Matlab function *fmincon* is used, which is based on sequential quadratic programming and can handle constrained optimization problems.

parameters did not stabilize the real experimental setup. For finally concluding which of the two architectures is superior for the objects with MSD characteristics described above, the minimum mass and damping that results in a stable system should be determined for the real system for both architectures. The Z_{error} can then be determined for these values and it can be finally concluded which architecture is superior.
Summarizing this section, a new fidelity measure was introduced that takes the realizability of the parameters that optimize fidelity into account. The main difference compared to the Z_{error} measure is that the characteristic of the stable parameter space (area and corresponding Z_{error}) affect the introduced robust fidelity measure. The measure is more robust to numerical inaccuracies than the optimum Z-error. The evaluation of robust fidelity showed the superiority of model-mediated teleoperation over the classical two-channel FaFa architecture for all tested environments. The evaluation of the Z_{error} revealed discrepancies for a small set of objects with MSD characteristics, while for the majority of tested environments, the Z_{error} was smaller for the MM architecture. This implies a higher fidelity for the MM architecture compared to the classical architecture. Yet, in order to finally conclude which architecture is superior for the cases with discrepancies in the measures, experimental tests should be performed. The fidelity measure is only defined for a system in steady-state. Statements about the fidelity during the transient phase are not possible with this criterion. An extension of the fidelity criterion to time-varying systems remains therefore future work.

3.4.2 Influence of Stationary Estimation Error on Fidelity

The environment estimation that is used for model-mediated teleoperation can exhibit an offset between estimated and true parameters. This section investigates the influence of such an estimation error on the fidelity of the system. In the previous section, it was shown that model-mediated teleoperation is superior to the classical control architecture FaFa. The assumption was that $\hat{Z}_e = Z_e$. If this assumption does not hold anymore, the question arises how strongly the fidelity and, thus, the quality of model-mediated teleoperation is deteriorated. One possibility to answer this question is to determine the difference in Z_{error} and $\mathcal{F}_{\text{robust}}$ that results from the deterioration of $\hat{Z}_e$. This is achieved by calculating the fidelity for the deteriorated environment impedance according to (3.80) or (3.79) and by comparing it with the fidelity of the classical control architecture. If model-mediated teleoperation is not superior over a classical control architecture in terms of fidelity anymore, it does not make sense to further focus on model-mediated teleoperation, especially due the high implementation effort compared to a classical control architecture.

Another possibility for answering the question of fidelity deterioration due to a stationary estimation error consists in taking the perceptual limitations of the human operator into account. If the operator does not feel the alteration in the reconstructed environment, the perceived fidelity as introduced in Sec. 2.2.1.2 is not influenced at all. As a consequence, the maximum allowed stationary parameter estimation error is found as the parameter vector where the alteration of the environment reconstruction becomes perceivable by the operator. Instead of evaluating the alteration in the reconstructed environment impedance, the alteration in resulting reconstructed forces and torques, $\hat{f}$ and $\hat{\tau}$, is considered in this thesis, see also Sec. 2.2.1.2. Based on the JNDs, which lie between 7% [99]

and 15% [98, 173] for force, and around 13% for torque according to [96, 210, 216], the maximum *stationary* parameter estimation error $\tilde{\boldsymbol{\theta}}_{\max}$ is defined for forces and torques as

$$\tilde{\boldsymbol{\theta}}_{\max,f} = \{\tilde{\boldsymbol{\theta}} \mid \hat{f}(\hat{\boldsymbol{\theta}}) - f = \pm \mathrm{JND}_f\} \tag{3.93}$$

$$\tilde{\boldsymbol{\theta}}_{\max,\tau} = \{\tilde{\boldsymbol{\theta}} \mid \hat{f}(\hat{\boldsymbol{\theta}}) - \tau = \pm \mathrm{JND}_\tau\}, \tag{3.94}$$

where $\hat{\boldsymbol{\theta}}$ is the stationary estimated parameter vector. This method is used in the following chapter in order to evaluate the fidelity of model-mediated teleoperation.

As the title of this section says, statements are only possible for the system in steady-state. It would be interesting to investigate the fidelity of model-mediated teleoperation during the transient phase. If the perceived fidelity is highly deteriorated during the estimation, one possibility would be to feed the estimated parameters back to the master site after the estimation is converged.

3.5 Summary

Stability and fidelity stay in conflict with each other and require an optimal trade-off between them. This chapter focused on environment-related, model-mediated teleoperation, a transparency-oriented, EOT-adapting controller, that provides significant improvements in fidelity compared to a classical, bilateral controller. Based on an estimation of the remote environment dynamics, a haptic map is constructed and the operator is connected to an undelayed, reconstructed copy of this haptic map. Whenever the estimation has converged, the dynamics of the controlled teleoperator and the characteristics of the communication channel do not influence the stability and fidelity of the system. Thus, model-mediated teleoperation is especially beneficial for systems with medium to large ($\geq$ 1 s) time delays and other deficiencies in the communication channel such as packet loss. Most other approaches are applicable up to 0.5 s time delay only.

The known literature on model-mediated teleoperation does not provide a stability proof especially for the transient phase, where the haptic map is estimated. A fidelity analysis based on established fidelity measures is missing, including a comparison with classical control concepts.

This chapter tackled all these aspects. Static and movable objects were considered in the stability and fidelity analyses. The stability analysis was two-folded: first, robust stability was investigated for a detailed system model using the parameter space approach. This analysis is only possible for a time-invariant system, which can be assumed if the estimation is converged. The robustness analysis was performed for model-mediated teleoperation and a classical teleoperation approach. The results revealed stable and unstable parameter regions for static and movable objects as well as for objects with mass-spring-damper characteristics.

Second, the transient phase, where the estimation is active, was investigated. Here, control architecture and remote environment exhibit a time-varying and partly switching character. As long as the dynamics is not switched, the stability of the time-varying system was shown using a stability theorem from adaptive control. Whenever the dynamics becomes switching like for static objects, classical stability analysis tools are not applicable

anymore. Instead, the multiple Lyapunov function approach was employed. In order to derive analytical stability boundaries, the stability analysis for the transient phase was based on a simplified system model.

Based on the results of the robustness analysis, a comprehensive fidelity analysis was conducted in the second part of this chapter. Due to unmodeled dynamics and the neglected discrete nature of the controllers, the numerical stability regions do often not match with real stability regions. Consequently, also the parameters optimizing fidelity may destabilize the real system. Thus, a novel robust fidelity measure was introduced. It takes the realizability of the numerical results into account by accounting for the area of the stable regions and the Z-error integrated over the stable area. The fidelity was determined for different remote objects based on the introduced robust fidelity measure and based on the Z-error measure, known from literature. The results prove the superiority in the introduced robust fidelity of model-mediated teleoperation compared to a classical two-channel architecture.

Concluding this chapter, it was shown that a system based on model-mediated teleoperation is stable and exhibits fidelity improvements compared to a classical control concept. The stability analysis for the transient phase was based on simplified model assumptions. To relax these assumptions and prove transition stability for the full system dynamics is an interesting step for further investigations. As model-mediated teleoperation is especially suited for teleoperation systems with large time delay or packet loss in the communication channel, another important step would be to extend the stability proof to systems with non-negligible deficiencies in the communication channel. Also, the human arm dynamics is assumed to be time-invariant. Whenever models for describing variations of the human arm impedance parameters are available, the stability analysis presented in literature so far should be revised. Finally, the introduced fidelity measure should be applied to other control approaches and validated with experimental results.

The results of this chapter build the foundation of the following chapter where the different implementation possibilities for model-mediated teleoperation are presented and evaluated in simulations and experiments.

4 Transparency-Oriented Control Concept: Design and Evaluation

Among the transparency-oriented, EOT-adapting controllers proposed in literature, model-mediated teleoperation is identified as a promising approach to improve the fidelity of the system. Fidelity is a measure for transparency, that describes how close the system is to absolute transparency. The idea of model-mediated teleoperation is to estimate a haptic map of the remote environment and to reconstruct this map on operator site using local haptic signals. After the estimation has converged, the control loop between the local and remote site is opened. In contrast to most classical approaches, the dynamics of the controlled teleoperator and the deficiencies in the communication channel do not influence the fidelity of the system. Consequently, a significant improvement in fidelity can be expected compared to most classical control concepts for systems with negligible, medium, and large time delays. The key challenges for successfully applying model-mediated teleoperation are i) the determination of appropriate environment (and operator) models, ii) an accurate and fast online parameter identification without impairment of the operator and task execution, iii) a stable reconstruction of the mediated models, and iv) the applicability to a variety of different tasks. Many different modeling, estimation, and reconstruction methods were investigated in the known literature. A clear selection process based on a comprehensive comparison of the different possibilities for modeling, estimating, and reconstructing the haptic map of operator/environment has not been presented so far. Also, teleoperation tasks in full 6 DoF using model-mediated teleoperation have not been realized yet and only static objects were considered. This chapter is dedicated to an intensive investigation and comparison of different design possibilities for model-mediated teleoperation and to the extension of model-mediated teleoperation to a larger class of tasks. This is an important step towards a systematic design process for model-mediated teleoperation.

In the first part of this chapter, environment models and suitable estimation techniques are presented in Sec. 4.2 and 4.3, followed by reconstruction methods in Sec. 4.4. These are especially important for teleoperation systems with time delay. The environment modeling and estimation techniques are based on the work by A. Achhammer [227], and the reconstruction methods were investigated by M. Axenbeck [230].

The second part of this chapter is dedicated to the evaluation of different design possibilities for model-mediated teleoperation. In a first step, suitable modeling approaches are selected for static and movable objects in Sec. 4.5 based on theoretical considerations and simulation results. Using these results, a novel hybrid modeling approach for static objects will be derived. In a next step, a detailed simulation analysis of the estimation techniques allows to select the most suitable one, see Sec. 4.5. It will be shown that a recursive least-squares estimation method with self-perturbation outperforms three other recursive least-squares methods as well as an adaptive identification approach in terms of tracking performance, convergence time, and noise rejection. In a third step, experimental

results using model-mediated teleoperation for full 6 DoF teleoperation tasks prove the effectiveness of the approach. Systems with and without deficiencies in the communication channel as well as the manipulation of static or movable objects in 6 DoF are considered in the experiments, see Sec. 4.6. Based on experimental results provided in Sec. 4.6.3, it will further be shown that a trade-off between safety and fidelity has to be found for systems with time delay in the communication channel. The improvement in fidelity is finally shown in Sec. 4.7.2 based on a comparison with experimental results obtained with a classical control concept, which is presented in Sec. 4.7.

4.1 Overview of Model-mediated Teleoperation Approaches

The main differences between the model-mediated teleoperation approaches presented in literature consist in the algorithm for estimating the parameters of the environment model as well as in the updating or reconstruction procedure of the virtual model. All approaches except for [219] where a mass-spring-damper model is used are based on the linear Kelvin-Voigt model. This model is mainly suited to describe stiff objects. Thus, other modeling techniques for static objects and a variety of parameter estimation techniques are presented and compared with each other in Sec. 4.2 and Sec. 4.3.

The reconstruction procedure becomes an important issue, if non-negligible time delay is present in the communication channel. One reconstruction method consists in generating the virtual model after the first impact between slave and object [37, 139, 200]. First estimation steps to adapt the parameters of the environment model can be performed and the position of the object does not need to be known. However, when the slave touches the object for the first time, the master already passed this point without noticing it due to missing feedback. This can lead to safety problems, i.e. possible damage to remote environment or slave device. One possibility to avoid safety-critical situations is to track the object's position. Then, the virtual model can be shifted to account for the difference in slave and master position [139]. At the second time of contact, the learned contact point is used to present undelayed feedback to the operator. In [140], a distance sensor is used to make this approach applicable in unknown remote environments. In this case, haptic feedback from the virtual model can be provided to the operator at the same moment when contact between slave and object occurs. This feedback may, however, be unrealistic as information of the object's haptic properties is not available yet. These reconstruction methods are presented in detail and compared with each other in terms of advantages and disadvantages in this chapter together with an experimental comparison especially for systems with significant time delay.

The state-of-the-art literature for model-mediated teleoperation does not allow full 6 DoF interaction with remote objects and is focused on the manipulation of static objects. This chapter extends the applicability of model-mediated teloperation to 6 DoF manipulation tasks involving static and movable objects.

4.2 Design: Environment Modeling

Teleoperation is usually performed in unknown and changing environments. Yet, the application area restricts the range of objects and tasks considerably. In addition, different possibilities exist to obtain specific information about objects and/or tasks, either a priori or online. A priori knowledge is e.g. available after a first visual exploration of the remote environment. The operator can then detail the types of objects and main subtasks to be performed. This holds especially for maintenance work. Detailed information about object and task is also available after a first task execution. This knowledge can be used if the same task is performed repeatedly. Even though the first task execution has to be performed without fidelity augmentation, the subsequent trials are facilitated reducing required effort and, consequently, operator fatigue.

Besides a priori knowledge, the required knowledge can also be gained online. One possibility is to use additional contact-free sensors such as cameras, lasers as in [140], or ultrasonic devices in order to detect objects especially in the direction of the teleoperator movement. Another possibility is to obtain this information directly from the operator. A speech recognition system could be used to determine different object properties. This information can facilitate the initialization process of the estimation and thereby improve the first impression of the object. Speech recognition was e.g. used in [52] to trigger different functions in a manipulation task like closing/opening grippers or changing the camera view. The mental workload required for additionally naming and categorizing the manipulated objects is expected to be reasonably small. Another approach would be that the operator selects the best fitting object and task from a menu. This requires, however, a complete interruption of the teleoperation and is therefore a rather time-consuming approach.

In this thesis, it is assumed that the type of object is identifiable a priori, and the focus is on static and movable objects. Interaction with static objects allows to perform peg-in-hole tasks, e.g. replacing a screw, or repairing tasks like screw tightening or palpation tasks, e.g. in minimally invasive surgery. Transportation tasks like removing a broken item and fetching a new one or positioning tasks like aligning an item with an opening requires the manipulation of movable objects. The model assumptions for these two classes of objects are introduced next together with 6 DoF dynamic object models.

4.2.1 Static Objects

The choice of a suitable environment model for static objects is based on the following assumptions about teleoperator and environment:

- The end-effector tool is rigid with a small contact area. Grasping does not occur.
- The objects are static and their surface is smooth. Motions tangential to the surface are not considered, i.e. the geometry of the object is not estimated.
- The dynamics of the remote object is not coupled in different directions of penetration.
- Damping can only occur when pushing into the object. Otherwise, it would be assumed that the robot's tool sticks together with the object.

The Kelvin-Voigt model (KVM), the Hunt-Crossley model (HCM), and the Hammerstein model (HM) fulfill these assumptions and are therefore investigated in this work. Their characteristics are summarized in Table 4.1.

4.2.1.1 Kelvin-Voigt Model

Due to its linearity, the Kelvin-Voigt model is the simplest model. In order to account for the unilateral damping, enforced by the last assumption, the damping term of the original KVM is slightly modified. The mechanical equivalent of this model is the parallel of a spring and a unilateral damper. The object dynamics is described in one translational direction as

$$f = \begin{cases} k_{kv}\,\delta x + b_{kv}\,\delta\dot{x}, & \text{if } \delta x \geq 0 \wedge \delta\dot{x} \geq 0 \\ k_{kv}\,\delta x, & \text{if } \delta x \geq 0 \wedge \delta\dot{x} < 0 \\ 0, & \text{else} \end{cases} \tag{4.1}$$

where f is the measured contact force in one direction and $\delta x \geq 0, \delta\dot{x} > 0$ are penetration depth and velocity into the object, i.e. $\delta x = x_s - x_e$ and $\delta\dot{x} = \dot{x}_s$ ($\delta\dot{x} < 0$ results in motion out of the object). No penetration occurs for $\delta x \leq 0$. The parameters k_{kv} and b_{kv} represent the object's stiffness and damping.

In the original version of the KVM without unilateral damping, the stiffness term vanishes at the beginning and end of contact, as the penetration depth is zero, and the environment is only represented by the damping term. Since the velocity is not necessarily zero at these moments, a non-zero force jump can occur, when contact is established and lost, see Fig. 4.1. This behavior is contradictory to physical observations and becomes evident if the damping is high. In the modified KVM with a unilateral damping as presented above, negative forces at the end of the restitution phase caused by a negative velocity do not occur, see Fig. 4.1. This property avoids a sticky feeling when releasing contact with the object.

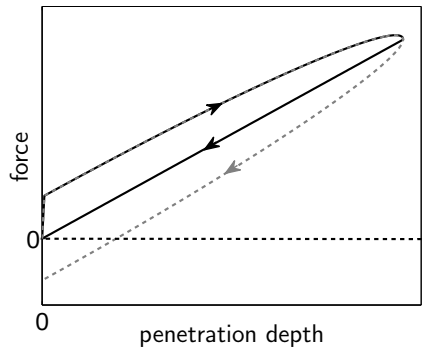

Fig. 4.1: Hysteresis curve of original Kelvin-Voigt model (dashed) and modified Kelvin-Voigt model (solid). The unilateral damping removes the physical inconsistency when releasing contact.

4.2.1.2 Hunt-Crossley Model

The Hunt-Crossley model (HCM) is a nonlinear model. The term that depends on the penetration velocity is a function of the penetration depth such that physical inconsistencies when establishing and releasing contact are avoided, see Fig. 4.2. Also, the nonlinear behavior of soft objects is captured more precisely. Similar to the modification for the Kelvin-Voigt model, a unilateral damping is introduced. The dynamics of the HCM is described in one translational direction as

$$f = \begin{cases} k_{hc}\,(\delta x)^{n_{hc}} + b_{hc}\,(\delta x)^{n_{hc}}\delta\dot{x}, & \text{if } \delta x \geq 0 \wedge \delta\dot{x} \geq 0 \\ k_{hc}\,(\delta x)^{n_{hc}} & \text{if } \delta x \geq 0 \wedge \delta\dot{x} < 0 \\ 0 & \text{else.} \end{cases} \tag{4.2}$$

The exponent n_{hc} reflects contact geometry and material by altering the stiffness depending on the size of the contact area. The parameters k_{hc} and b_{hc} can be regarded as a nonlinear stiffness and damping. Thus, the model can be considered as a nonlinear version of the Kelvin-Voigt model. However, the nonlinear damping and stiffness terms do not represent typical material properties which makes an interpretation of the parameter values difficult.

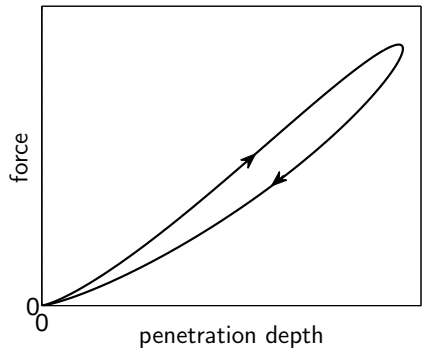

Fig. 4.2: Hysteresis curve of Hunt-Crossley model with unilateral damping. This model does not exhibit any physical inconsistency.

4.2.1.3 Hammerstein Model

Another popular model for describing nonlinear plants is the Hammerstein model, a concatenation of a static nonlinearity and a linear digital filter $G(z^{-1})$, see Fig. 4.3. Regarding

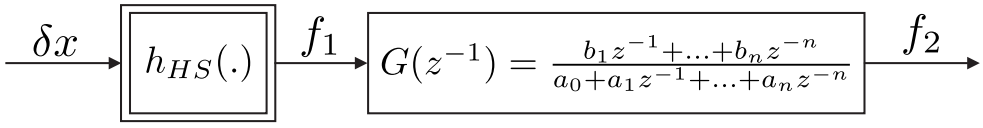

Fig. 4.3: Block diagram of the Hammerstein model

the modeling of static objects, the nonlinearity describes the elastic response force due to a penetration and, given a suitable digital filter, can accurately model static objects. For each translational direction, the input is the corresponding penetration depth δx and the

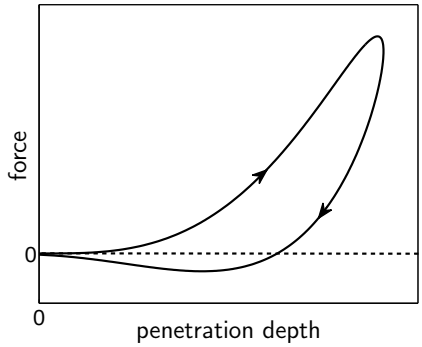

Fig. 4.4: Hysteresis curve of Hammerstein model. This model shows physically inconsistent, negative forces during the restitution phase.

output is the resulting force f. As outlined in [17], two static nonlinearities for elastic objects are mainly used:

$$h_{HS}(\delta x, \delta \dot{x}) = \begin{cases} k_{hs}\, \delta x^{n_{hs}} & \text{if } \delta x \geq 0 \\ 0 & \text{else} \end{cases} \tag{4.3}$$

$$h_{HS}(\delta x, \delta \dot{x}) = \begin{cases} k_{hs}\, e^{n_{hs}\delta \boldsymbol{x}} & \text{if } \delta x \geq 0 \\ 0 & \text{else} \end{cases} \tag{4.4}$$

where k_{hs} and n_{hs} are parameters that depend on material and geometry properties of the object. The first nonlinearity (4.3) represents the nonlinear stiffness term of the Hunt-Crossley model. As described in [227], the model accuracy improves with the filter order. Consequently, for an accurate model a large amount of parameters which are not physically interpretable have to be determined. The model shows physical inconsistencies (negative forces) during the restitution phase, see Fig. 4.4.

Tab. 4.1: Summary of characteristics of the three investigated models for static objects.

Properties	**Kelvin-Voigt**	**Hunt-Crossley**	**Hammerstein**
Physical correspondence	Linear spring-damper	Nonlinear spring-damper	Filtered nonlinear damper
Damping	Unilateral	Unilateral	Bidirectional
Physical consistency	Inconsistent for soft objects	Consistent	Inconsistent for soft objects
# of parameters	2	3	> 3
Parameter interpretability	Material properties	Difficult	Not possible

4.2.2 Movable Objects

The modeling of the dynamics of a movable object is based on the following assumptions, see also Fig. 4.5:

- The teleoperator rigidly grasps the movable object such that it cannot drop.
- The object is rigid, i.e. the relative positions $\boldsymbol{x}$ and orientation represented as Euler angles $\boldsymbol{\varphi}$ between the teleoperator and the object are constant $\boldsymbol{x}_s - \boldsymbol{x}_o = \text{const.}$ and $\boldsymbol{\varphi}_s - \boldsymbol{\varphi}_o = \text{const.}$ This implies that the velocities and accelerations of teleoperator and object are equal.
- The object is lifted, not pushed over the ground such that friction can be neglected.
- The end-effector inertia parameters of the slave are known.

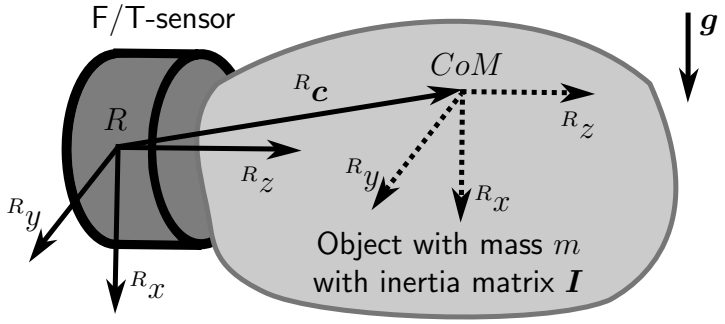

Fig. 4.5: Illustration of rigid object attached to force/torque sensor, see also [111].

The dynamics of a rigid body moved in translational and rotational directions is described in the reference sensor coordinate system $\boldsymbol{R}$, see Fig. 4.5. The dynamics depends on the inertial parameters of the object: mass m, coordinates of the center of mass (CoM) $\boldsymbol{c} = [c_x, c_y, c_z]$, and the inertia matrix $\boldsymbol{I}$:

$$\boldsymbol{I} = \begin{bmatrix} I_{xx} & I_{xy} & I_{xz} \\ I_{xy} & I_{yy} & I_{yz} \\ I_{xz} & I_{yz} & I_{zz} \end{bmatrix}$$

as well as on the linear acceleration ${}^{\boldsymbol{R}}\boldsymbol{a}$ of the reference frame, the angular velocity ${}^{\boldsymbol{R}}\boldsymbol{\omega}$ and acceleration ${}^{\boldsymbol{R}}\boldsymbol{\alpha}$ and the gravity vector ${}^{\boldsymbol{R}}\boldsymbol{g}$. The forces and torques measured in the reference frame, ${}^{\boldsymbol{R}}\boldsymbol{f}$ and ${}^{\boldsymbol{R}}\boldsymbol{\tau}$, are described by the Newton-Euler equations:

$$\begin{aligned} {}^{\boldsymbol{R}}\boldsymbol{f} &= m({}^{\boldsymbol{R}}\boldsymbol{a} - {}^{\boldsymbol{R}}\boldsymbol{g}) + m\,({}^{\boldsymbol{R}}\boldsymbol{\alpha} \times {}^{\boldsymbol{R}}\boldsymbol{c} + {}^{\boldsymbol{R}}\boldsymbol{\omega} \times ({}^{\boldsymbol{R}}\boldsymbol{\omega} \times {}^{\boldsymbol{R}}\boldsymbol{c})) && (4.5) \\ {}^{\boldsymbol{R}}\boldsymbol{\tau} &= {}^{\boldsymbol{R}}\boldsymbol{I}\,{}^{\boldsymbol{R}}\boldsymbol{\alpha} + {}^{\boldsymbol{R}}\boldsymbol{\omega} \times ({}^{\boldsymbol{R}}\boldsymbol{I}\,{}^{\boldsymbol{R}}\boldsymbol{\omega}) + m\,{}^{\boldsymbol{R}}\boldsymbol{c} \times ({}^{\boldsymbol{R}}\boldsymbol{a} - {}^{\boldsymbol{R}}\boldsymbol{g}). && (4.6) \end{aligned}$$

4.3 Design: Environment Estimation

The realization of model-mediated teleoperation requires to estimate the parameters of the selected environment model online. A variety of parameter estimation methods were

presented in the literature leading to the question which one is most suitable for the estimation of static and movable objects in the context of haptic teleoperation. Different recursive least-squares as well as an adaptive estimation technique are investigated and compared with each other for this purpose.

4.3.1 Recursive Least Squares (RLS)

Recursive least square schemes allow for a fast convergence and stable parameter estimation. The model has to be given in the *linear-in-parameter* form

$$y_k = \boldsymbol{\phi}_k^T \boldsymbol{\theta}_k \tag{4.7}$$

with $y_k \in \mathbb{R}$ the system output at a time step k, $\boldsymbol{\phi}_k \in \mathbb{R}^n$ the input regressor, and $\boldsymbol{\theta}_k \in \mathbb{R}^n$ the parameter vector at a time step k. By minimizing the cost function V_k

$$V_k = \frac{1}{2} \sum_{i=0}^{k} e_i^2 \tag{4.8}$$

depending on the estimation error $e_k = y_k - \hat{y}_k$ between measured and estimated system output[1], the estimate of the parameter vector $\hat{\boldsymbol{\theta}}$ minimizing the cost function is found. The solution is a recursive set of equations:

$$\hat{\boldsymbol{\theta}}_k = \hat{\boldsymbol{\theta}}_{k-1} + \boldsymbol{\kappa}_k \left(y_k - \boldsymbol{\phi}_k^T \hat{\boldsymbol{\theta}}_{k-1} \right) \tag{4.9}$$

$$\boldsymbol{\kappa}_k = \boldsymbol{P}_{k-1} \boldsymbol{\phi}_k \left(\lambda \boldsymbol{E} + \boldsymbol{\phi}_k^T \boldsymbol{P}_{k-1} \boldsymbol{\phi}_k \right)^{-1} \tag{4.10}$$

$$\boldsymbol{P}_k = \lambda^{-1} \left(\boldsymbol{E} - \boldsymbol{\kappa}_k \boldsymbol{\phi}_k^T \right) \boldsymbol{P}_{k-1} \tag{4.11}$$

where $\boldsymbol{\kappa}_k \in \mathbb{R}^n$ is referred to as adaptation gain vector and $\boldsymbol{P}_k \in \mathbb{R}^{n \times n}$ as covariance matrix. The parameter $\lambda \in [0; 1]$ is known as forgetting factor. It can be used to weight recent measurements differently to older measurements. If it is set to 1, the RLS algorithm is also referred to as growing window RLS. The algorithm requires initial values for $\hat{\boldsymbol{\theta}}_0$ and $\boldsymbol{P}_0$. A stability proof for the RLS method can be found in [95].

4.3.1.1 Recursive Least Squares with Adaptive Forgetting Factor (RLS-A)

While the growing window RLS allows a good disturbance rejection, it exhibits limited tracking capabilities if the parameters change. With a small forgetting factor parameter changes can be tracked well, but the estimation becomes sensitive to noise. For a better trade-off between tracking performance and disturbance and noise rejection an adaptive forgetting factor as e.g. proposed in [211] can be used. The time-varying forgetting factor is herein defined for a time step k as:

$$\lambda_k = \begin{cases} 1 - \frac{\beta_3}{\pi} \arctan\left(|\rho_k - 1|\right) & \text{if } |\rho_k - 1| \geq \beta_2 \\ \beta_1 + \frac{1}{\pi}(1 - \beta_1) \arctan\left(1 - |\rho_k - 1|\right) & \text{else,} \end{cases} \tag{4.12}$$

[1] An estimated variable p will be denoted as $\hat{p}$.

with

$$\rho_k = \begin{cases} \max\left(\frac{\hat{\boldsymbol{\theta}}_{k-l}[i]}{\hat{\boldsymbol{\theta}}_k[i]}, \frac{\hat{\boldsymbol{\theta}}_k[i]}{\hat{\boldsymbol{\theta}}_{k-l}[i]}\right) & \text{if } \forall\ i \in [0,1,...,m] : \hat{\boldsymbol{\theta}}_{k-l}[i] \cdot \hat{\boldsymbol{\theta}}_k[i] \neq 0 \\ \infty & \text{else.} \end{cases} \tag{4.13}$$

The parameters $l \in \mathbb{N}$, $\frac{1}{3} \leq \beta_1 \leq 1$, $\beta_2 \geq 0$ and $0 \leq \beta_3 \leq 2$ have to be adapted to the specific scenario. A stability proof for the RLS method with time-varying forgetting factor was not provided in [211]. The proof for the RLS with constant forgetting factor is provided in [95]. The requirement is that the input regressor $\boldsymbol{\phi}$ is sufficiently exciting, see also Sec. 4.3.4.

4.3.1.2 Recursive Least Squares with Self-Perturbation (RLS-SP)

In the original RLS, the covariance matrix $\boldsymbol{P}_k$ becomes small, if the estimation error $\boldsymbol{e}_k$ gets small. This in turn leads to a decline of the adaptation gain $\boldsymbol{\kappa}_k$ and the algorithm cannot react on parameter changes anymore. The recursive least squares algorithm with self-perturbation as proposed by Park [152] mitigates this problem by perturbing the covariance matrix whenever a parameter change occurs:

$$\boldsymbol{P}_k \;=\; \left(\boldsymbol{E} - \boldsymbol{\kappa}_k \boldsymbol{\phi}_k^T\right) \boldsymbol{P}_{k-1} + \beta\ \mathrm{NINT}(\gamma e_{k-1}^2)\boldsymbol{E} \tag{4.14}$$

where $\boldsymbol{E}$ is the identity matrix, $\beta > 0$ is a design constant and $\gamma > 0$ is the sensitivity gain. These parameters have to be adjusted with respect to the measurement noise of $\boldsymbol{y}_k$ and $\boldsymbol{\phi}_k$. The function $\mathrm{NINT}(\cdot)$ is defined as a component-wise round-off operator:

$$\mathrm{NINT}(\gamma \boldsymbol{e}_{k-1}^2) = \begin{cases} \gamma e_{k-1}^2, & \text{if } \gamma e_{k-1}^2 \geq 0.5 \\ 0, & \text{else.} \end{cases} \tag{4.15}$$

The algorithm acts like the general RLS algorithm as long as e_{k-1} is within the maximum error bound defined by γ. Otherwise, the self perturbation is activated and $\boldsymbol{\kappa}_k$ increases automatically. A stability proof of this algorithm was not provided. It would be interesting to investigate whether the method can be represented as a special case of covariance resetting where the stability proof is provided in [94].

4.3.2 Adaptive Identification (AI)

One step in the design of an adaptive controller is to derive an estimation of the system model. This step is called adaptive identification and was proposed in [186]. Like many adaptive control theories, it is derived using the Lyapunov theory. The derivation is performed in continuous time space. Similar to the recursive least squares approach the system is described as

$$y(t) = \boldsymbol{\phi}(t)^T \boldsymbol{\theta}(t) \tag{4.16}$$

with $y(t) \in \mathbb{R}$ the system output at time t, $\boldsymbol{\phi}(t) \in \mathbb{R}^n$ the input vector and $\boldsymbol{\theta}(t) \in \mathbb{R}^n$ the parameter vector at time t. The estimated system model is given as:

$$\hat{y}(t) = \boldsymbol{\phi}^T(t)\hat{\boldsymbol{\theta}}(t) \tag{4.17}$$

where $\hat{y}(t) \in \mathbb{R}$ is the estimated system output at time t, and $\hat{\boldsymbol{\theta}}(t) \in \mathbb{R}^n$ the estimated parameter vector at time t. In a first step, a positive definite function $V(t)$ is defined as:

$$V(t) = \frac{1}{2}\tilde{\boldsymbol{\theta}}^T(t)\boldsymbol{\Gamma}\tilde{\boldsymbol{\theta}}(t), \tag{4.18}$$

where $\boldsymbol{\Gamma}$ is a positive definite matrix and $\tilde{\boldsymbol{\theta}} = \hat{\boldsymbol{\theta}} - \boldsymbol{\theta}$. Taking the time derivative of (4.18) leads to

$$\dot{V}(t) = -\tilde{\boldsymbol{\theta}}^T(t)\boldsymbol{\Gamma}\dot{\tilde{\boldsymbol{\theta}}}(t). \tag{4.19}$$

Assuming constant or slowly varying parameters such that $\dot{\boldsymbol{\theta}} \approx 0$, (4.19) can be simplified to

$$\dot{V}(t) = -\tilde{\boldsymbol{\theta}}^T(t)\boldsymbol{\Gamma}\dot{\hat{\boldsymbol{\theta}}}(t). \tag{4.20}$$

The objective is to guarantee asymptotic stability of the estimation, i.e. to guarantee $\lim_{t\to\infty} \tilde{\boldsymbol{\theta}}(t) = \hat{\boldsymbol{\theta}} - \boldsymbol{\theta} = 0$. With the update rule

$$\dot{\hat{\boldsymbol{\theta}}}(t) = -\boldsymbol{\Gamma}^{-1}\boldsymbol{\phi}^T(t)(\underbrace{\hat{y}(t) - y(t)}_{\tilde{y}}) \tag{4.21}$$

equation (4.20) becomes

$$\dot{V}(t) = -\tilde{\boldsymbol{\theta}}^T(t)\boldsymbol{\phi}^T(t)\tilde{y}(t) \tag{4.22}$$

which simplifies with (4.17) to

$$\dot{V}(t) = -\tilde{y}^T(t)\tilde{y}(t) \leq 0. \tag{4.23}$$

Thus, $\dot{V}(t)$ is shown to be negative definite which proves that the estimation error will asymptotically converge to zero. The estimated parameter vector is obtained by integrating (4.21). An initial guess for $\hat{\boldsymbol{\theta}}_0$ has therefore to be given. The positive definite matrix $\boldsymbol{\Gamma}$ is a design parameter and has to be selected a priori.

4.3.3 Adaptation to Environment Models

All estimation methods require the model to be given in the linear-in-parameter form $y = \boldsymbol{\phi}^T\boldsymbol{\theta}$. This paragraph is dedicated to the derivation of the linear-in-parameter form for each of the static and movable object models described in Sec. 4.2.

4.3.3.1 Static Models

Three models are distinguished: the Kelvin-Voigt model, the Hunt-Crossley model and the Hammerstein model. Please note that a model is estimated for each translational

direction separately. Due to its linearity in the parameters, the Kelvin-Voigt model can be transformed into the linear-in-parameter form without further modifications:

$$y = f, \quad \boldsymbol{\theta} = [k_{kv} \;\; b_{kv}], \quad \boldsymbol{\phi} = [\delta x \;\; \delta\dot{x}]^T. \tag{4.24}$$

The nonlinearity of the Hunt-Crossley model requires to linearize the model by taking the natural logarithm of (4.2), see also [74]:

$$\ln(f) = \ln(k_{hc}) + n_{hc}\ln(\delta x) + \ln(1 + k_{hc}^{-1} b_{hc}\delta\dot{x}). \tag{4.25}$$

By assuming that $\ln(1+\alpha) \cong \alpha$ for $|\alpha| \ll 1$ equation (4.25) can be rewritten as:

$$\ln(f) = \ln(k_{hc}) + n_{hc}\ln(\delta x) + k_{hc}^{-1} b_{hc}\delta\dot{x}. \tag{4.26}$$

Equation (4.26) only holds if the term $k_{hc}^{-1} b_{hc}\delta\dot{x}$ is small compared to one. Since, for most robotic applications, the velocity is small during contact with the environment, and the stiffness k_{hc} is commonly larger than the damping b_{hc} this condition can be assumed to be met. The formerly nonlinear system is now expressed by a linear equation and can be rewritten as:

$$y = \ln(f), \quad \boldsymbol{\theta} = [\ln(k_{hc}) \;\; n_{hc} \;\; k_{hc}^{-1} b_{hc}]^T, \quad \boldsymbol{\phi} = [1 \;\; \ln(\delta x) \;\; \delta\dot{x}]^T. \tag{4.27}$$

The structure of the Hammerstein model requires two separate, interconnected estimation steps as shown in Fig. 4.6. The nonlinear system as described in (4.3) is selected. The

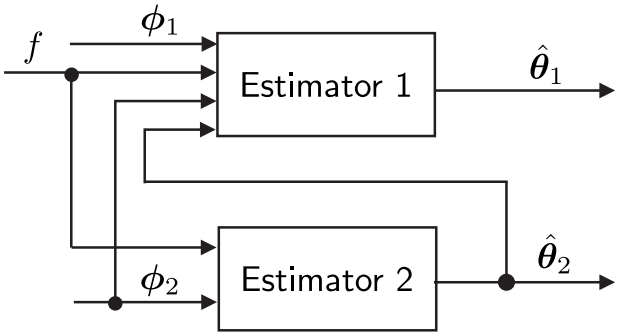

Fig. 4.6: Recursive estimation scheme for the Hammerstein model consisting of two interconnected estimators. Figure modified from [227].

output f_1 of the static nonlinearity is not measurable. It is found by taking the natural logarithm of the difference equation of the linear filter, solved for $f_{1,k-1}$

$$f_{1,k-1} = f_{1,k} - \boldsymbol{\phi}_{2,k}^T \boldsymbol{\theta}_{2,k}. \tag{4.28}$$

Equivalently to the Hunt-Crossley model, the linear-in-parameter form of the static nonlinearity is given by

$$y_1 = \ln(f_{1,k-1}), \quad \boldsymbol{\theta}_1 = [\ln(k_{hs}) \;\; n_{hs}]^T, \quad \boldsymbol{\phi}_1 = [1 \;\; \ln(\delta x)]^T. \tag{4.29}$$

The linear filter of order n is described in linear-in-parameter form at a time step k as

$$y_2 = f_2, \quad \boldsymbol{\theta}_2 = [a_1 \dots a_n \;\; b_1 \dots b_n]^T, \quad \boldsymbol{\phi}_2 = [f_{2,k-1} \dots f_{2,k-n} \;\; f_{1,k-1} \dots f_{1,k-n}]^T. \tag{4.30}$$

4.3.3.2 Movable Objects

The dynamics of a movable object as described in (4.5) and (4.6) is linear in its parameters. Rewriting it in terms of the system output $\boldsymbol{y}$, the parameter vector $\boldsymbol{\theta}$, and the input regressor matrix $\boldsymbol{\phi}$ leads to

$$\boldsymbol{y} = [\boldsymbol{f} \;\; \boldsymbol{\tau}], \quad \boldsymbol{\theta} = [m \;\; m\boldsymbol{c} \;\; \underbrace{I_{xx} \;\; I_{xy} \;\; I_{xz} \;\; I_{yy} \;\; I_{yz} \;\; I_{zz}}_{\boldsymbol{I}_v}], \quad \boldsymbol{\phi} = \begin{bmatrix} \boldsymbol{a}_x - \boldsymbol{g}_x & \boldsymbol{O}_f & \boldsymbol{0}_{3\times 6} \\ \boldsymbol{0}_{3\times 1} & \boldsymbol{O}_{1\boldsymbol{\tau}} & \boldsymbol{O}_{2\boldsymbol{\tau}} \end{bmatrix} \tag{4.31}$$

with

$$\boldsymbol{O}_f = \begin{bmatrix} -\omega_y^2 - \omega_z^2 & \omega_x\omega_y - \alpha_z & \omega_x\omega_z + \alpha_y \\ \omega_x\omega_y + \alpha_z & -\omega_x^2 - \omega_z^2 & \omega_y\omega_z - \alpha_x \\ \omega_x\omega_z - \alpha_y & \omega_y\omega_z + \alpha_x & -\omega_y^2 - \omega_x^2 \end{bmatrix} \tag{4.32}$$

$$\boldsymbol{O}_{1\tau} = \begin{bmatrix} 0 & a_z - g_z & g_y - a_y \\ g_z - a_z & 0 & a_x - g_x \\ a_y - g_y & g_x - a_x & 0 \end{bmatrix} \tag{4.33}$$

$$\boldsymbol{O}_{2\tau} = \begin{bmatrix} \alpha_x & \alpha_y - \omega_x\omega_z & \alpha_z + \omega_x\omega_y & -\omega_y\omega_z & \omega_y^2 - \omega_z^2 & \omega_y\omega_z \\ \omega_x\omega_z & \alpha_x + \omega_y\omega_z & \omega_z^2 - \omega_x^2 & \alpha_y & \alpha_z - \omega_x\omega_y & -\omega_x\omega_z \\ -\omega_x\omega_y & \omega_x^2 - \omega_y^2 & \alpha_x - \omega_y\omega_z & \omega_x\omega_y & \alpha_y + \omega_x\omega_z & \alpha_z \end{bmatrix}, \tag{4.34}$$

where all variables are given in the reference coordinate system R.

4.3.4 Persistent Excitation

According to Yokokohji [218], a teleoperation system is transparent, if the forces on master and slave site as well as the velocities on master and slave site are equal. If master and slave velocities coincide due to e.g. a high-gain position controller and the estimation works perfectly, the reconstructed forces on master and measured forces on slave site will be equal for model-mediated teleoperation. If the position controller is, however, not stiff or if time delay is present in the communication channel, differences between master and slave positions and, thus, velocities may occur. In this case, a high fidelity can only be achieved, if the estimated parameter vector is equal to the true parameter vector. This can be guaranteed, if the input regressor $\boldsymbol{\phi}$ is persistently exciting (PE). This means that the input signal contains enough different frequency components to excite all parameters of the model. According to [95], for a single-input single-output (SISO) system, which is decoupled in the different Cartesian directions, an input signal with $\lceil n/2 \rceil$ distinct non-zero frequencies is sufficiently rich of order n, where n is the number of parameters.

Trajectory design for static objects Regarding static objects, the environment models are of order one. Hence, one non-zero frequency should be contained in the input signal. In

teleoperation, due to the natural tremor of human arm movements, see [65], the operator unconsciously provides input signals with at least one non-zero frequency component and, thus, persistent excitation is guaranteed for these models.

Trajectory design for movable objects The model for movable objects is a multi-input multi-output (MIMO) system, which is coupled in the different Cartesian directions such that the design process for exciting trajectories becomes much more intense. A method for designing ideal input trajectories such that the input regressor matrix excites all 10 parameters of the model is presented in [111]. The measure to be optimized is dependent on the correlation matrix $\boldsymbol{C}$ consisting of N different, concatenated matrices $\boldsymbol{\phi}_k$ determined at a time step k

$$\begin{aligned} \boldsymbol{C} &= \overline{\boldsymbol{\phi}}^T \overline{\boldsymbol{\phi}} && (4.35) \\ \overline{\boldsymbol{\phi}} &= [\boldsymbol{\phi}_1^T \dots \boldsymbol{\phi}_N^T]^T. && (4.36) \end{aligned}$$

In [63, 159], it was shown that the condition number $\iota(\boldsymbol{C})$ of the correlation matrix $\boldsymbol{C}$ should be minimized:

$$\iota(\boldsymbol{C}) = \frac{\mathrm{sing}_{\max}(\boldsymbol{C})}{\mathrm{sing}_{\min}(\boldsymbol{C})} \tag{4.37}$$

where $\mathrm{sing}_{\max}(\boldsymbol{C}), \mathrm{sing}_{\min}(\boldsymbol{C})$ are the maximum and minimum singular values of the matrix $\boldsymbol{C}$. The minimum is consequently $\iota = 1$.

A sine function with amplitude A and frequency f as design parameters is selected for each angular movement ${}^R\alpha, {}^R\beta, {}^R\gamma$ given in the reference frame R:

$${}^R\varphi_x = A_{\varphi_x} \sin(2\pi f_{\varphi_x} t) \quad {}^R\varphi_y = A_{\varphi_y} \sin(2\pi f_{\varphi_y} t) \quad {}^R\varphi_z = A_{\varphi_z} \sin(2\pi f_{\varphi_z} t). \tag{4.38}$$

The linear acceleration is set to zero. The optimal amplitudes and frequencies are found by minimizing the condition number $\iota(\boldsymbol{C})$ using the `fmincon` function from the Matlab Optimization Toolbox.

The optimal excitation is determined for the 6 DoF experimental setup described in Appendix A.6. The frequencies were restricted to a range of 0 to 10 Hz and the amplitudes were allowed to vary between $-\pi/2$ and $\pi/2$. The optimum values are found as

$$\begin{array}{lll} A_{\varphi_x} = 0.0124 & A_{\varphi_y} = -0.0084 & A_{\varphi_z} = 0.0112 \\ f_{\varphi_x} = 8.4662 & f_{\varphi_y} = 7.5898 & f_{\varphi_z} = 6.7899 \end{array} \tag{4.39}$$

and $\iota_{opt} = 7.95$. It would certainly be desirable to run the estimation process simultaneously to the telemanipulation of the object. Due to the complexity of the design process and the resulting input trajectories, it can, however, not be expected that the operator would excite the model in an optimal way. Furthermore, the complex input trajectories cannot be added to the operator commands, as they would significantly change the desired actions of the operator. Consequently, the estimation and reconstruction phase for movable objects have to be separated and the estimation is performed in autonomous mode.

4.4 Design: Environment Reconstruction

Given an environment model and suitable estimation algorithm, the estimated object has to be reconstructed on master site. The reconstruction consequently aims at providing the operator with a virtual model of the remotely manipulated objects. It is described for static and movable objects in this section. The estimated model is transmitted to the operator site where it is reconstructed using local haptic signals, see Sec. 4.4.1. If time delay is present in the communication channel, the first model estimate is received with delay on operator site. This is the most critical aspect for applying model-mediated teleoperation and requires a method how to deal with the delayed model response during first contact. Two approaches differing in the assumptions about a priori available knowledge are presented in Sec. 4.4.2 and advantages and disadvantages are discussed.

4.4.1 Reconstruction for Static and Movable Objects

In order to realize model-mediated teleoperation during contact, the environment parameters have to be estimated on slave site, sent back to the master site, and local external forces and torques have to be generated.

For contact with static objects, it is assumed that only point contacts occur between the teleoperator and the remote objects. Thus, only forces and no torques are measured at the tip of the tool, i.e. in the tool-tip frame (TT), see Fig. 4.7. Using these forces and corresponding positions and velocities as input to the estimation, an estimate of the environment parameters $\hat{\boldsymbol{\theta}}_e$ is obtained for the three translational directions. The reconstructed forces $\hat{\boldsymbol{f}}_{e,r}$ are generated on master site based on the received parameter vector $\hat{\boldsymbol{\theta}}_e$ and the input regressor $\boldsymbol{\phi}_m$:

$$\hat{\boldsymbol{f}}_{e,r} = \hat{\boldsymbol{\theta}}_e \boldsymbol{\phi}_m, \tag{4.40}$$

where $\boldsymbol{\phi}_m$ is calculated using master velocities and positions. The penetration depths are set to zero, if a first estimate is received. It is furthermore assumed that the operator should feel as holding a tool, like a screwdriver for example. Consequently, also torques have to be computed at the grasping point of the tool, i.e. in the wrist frame (WR), see Fig. 4.7. The geometry of the tool mounted on the teleoperator's end-effector and with it

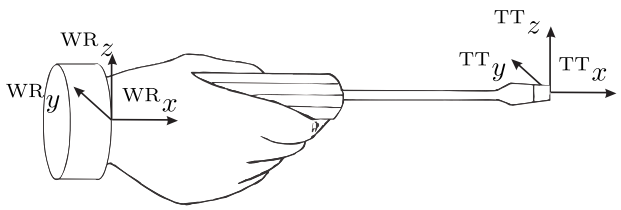

Fig. 4.7: Wrist frame and tool-tip frame. Figure modified from [227].

the distance vector ${}^{\mathrm{WR}}\boldsymbol{d}_{\mathrm{TT}}$ from wrist frame to tool-tip frame, is assumed to be known. Thus, the cross product between ${}^{\mathrm{WR}}\boldsymbol{d}_{\mathrm{TT}}$ and the force vector $\hat{\boldsymbol{f}}_e$ is calculated in order to determine the torque $\hat{\boldsymbol{\tau}}_{e,r}$:

$$\hat{\boldsymbol{\tau}}_{e,r} = {}^{\mathrm{WR}}\boldsymbol{d}_{\mathrm{TT}} \times \hat{\boldsymbol{f}}_{e,r}. \tag{4.41}$$

On master site, it is assumed for a natural feeling of the haptic feedback that the human intuitively grasps the handle at the tool center point, where all axes of rotation intersect. The reconstructed forces and torques $\hat{\boldsymbol{f}}_{e,r}$ and $\hat{\boldsymbol{\tau}}_{e,r}$ then provide the operator with haptic feedback about the interaction between teleoperator and remote object.

Movable objects are reconstructed on master site by simply evaluating the dynamic model (4.5) and (4.6) with the received parameter vector and local haptic signals summarized in the input regressor $\boldsymbol{\phi}_m$. As the controller is based on world coordinates, the resulting forces and torques given in the reference frame R have to be transformed accordingly, see Appendix A.6.0.4.

The reconstruction allows together with a suitably estimated environment model to realize model-mediated teleoperation. As a consequence, the feedback loop from the remote to the local site is closed locally, such that the dynamics on the remote site do not alter the haptic feedback.

4.4.2 Reconstruction for Systems with Non-Ideal Communication

If the time delay in the communication channel cannot be neglected, the first estimation results are received with delay on master site. The estimation and reconstruction phase for movable objects have to be temporally separated, see Sec. 4.3.4, as the operator cannot sufficiently excite the model. Thus, time delay does not influence the reconstruction for these kind of objects. For stiff, fixed objects, on the contrary, estimation and reconstruction are performed simultaneously such that the reconstruction method is important here. It depends essentially on the a priori knowledge of the object's location. This section presents two methods with varying level of a priori knowledge.

4.4.2.1 Reconstruction without Knowledge of the Object Location

If contact-free sensors measuring the distance to the object are not available, the location of the object cannot be determined before first contact. As a consequence, the virtual object is not presented at the location of the true object, see Fig. 4.8. The idea of the first reconstruction method is to shift the object location to the true object location during the release phase of the first contact, see Fig. 4.8 and [139]. This increases the safety for the second contact without deteriorating the fidelity.

The first contact is, however, performed with delayed haptic feedback. If a stiff controller is used on slave site, this can lead to high environment forces especially if the impact velocity is high. Consequently, the slave device and/or remote objects can get damaged. A classic method to deal with this problem is to use a compliant controller on slave site. A virtual mass-spring-damper impedance reduces the forces from the environment by reducing the penetration depth. If the time delay increases, the stiffness/damping on slave site has to be reduced/increased. The disadvantage is a deterioration of fidelity.

4.4.2.2 Reconstruction with Approximate Knowledge of the Object Location

Depending on the application, a distance sensor like a laser range finder as presented in [140] can be used on the remote site. Thus, approximate knowledge about the object's

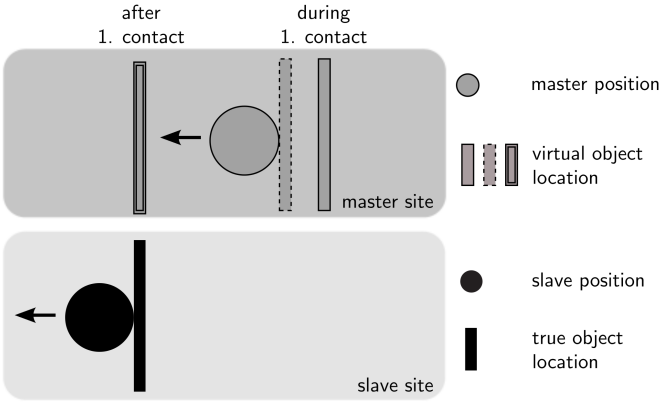

Fig. 4.8: The location of the virtual object is shifted towards the true object location during first contact, see also [230].

location can be obtained a priori. Although the dynamics of the object are unknown during first contact, a haptic resistance can be displayed to the operator at the moment when the object is touched on remote site. This approach can therefore guarantee a safe interaction from the first contact on. Due to noisy measurements, however, only a Gaussian distribution with mean μ and standard deviation σ of the object location is given, see Fig. 4.9. In order to guarantee safety for slave device and environment, high environment forces have to be avoided. This is achieved if the probability that the virtual object is touched before the true one is small. By selecting the object location 3σ in front of the expected object location μ, the probability of penetrating into the true object at first contact is reduced to 0.27%.

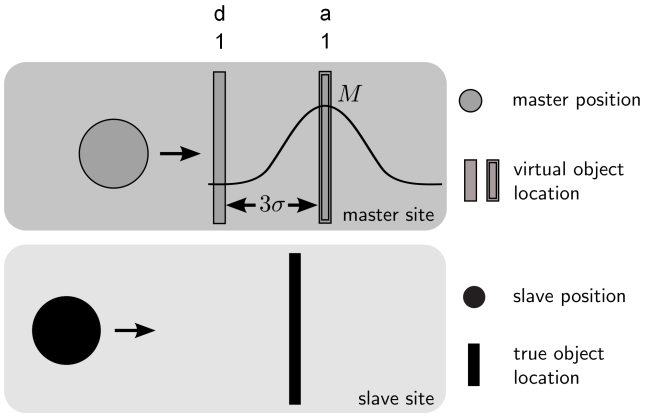

Fig. 4.9: A distance sensor is used to obtain approximate a priori knowledge about the object location. The sensor noise is modeled as a normal distribution with mean μ and standard deviation σ around the true object location.

In addition to the object location, the dynamics of the virtual object has to be selected. If a priori information about the object's mechanical properties is not given, a stiff object prevents penetration and, thus, high environment forces. It is therefore best suited if safety has to be guaranteed. The problem that occurs when presenting stiff objects is that also a

penetration into the object is prohibited, such that the parameters of the true object may not be estimated well. If the operator can provide approximate information characterizing e.g. the stiffness of the object, the dynamics can be adapted correspondingly. In summary, the safety of this reconstruction method is high, but the fidelity depends on the discrepancy between the virtual object dynamics if no estimation is available.

Summarizing this section, the presented reconstruction methods aim at finding a trade-off between fidelity and safety during first contact. As the object location and dynamics of the static object is known after first contact, a high fidelity is provided during the second contact without safety risks.

This section concludes the presentation of design aspects for model-mediated teleoperation. The following part of this chapter is dedicated to the evaluation and comparison of the different implementation possibilities for model-mediated teleoperation.

4.5 Evaluation: Environment Modeling and Estimation

In the first evaluation step, suitable environment models and estimation methods have to be selected out of the three models for static objects and four different adaptation schemes presented in Sec. 4.3. For movable objects, only one model was presented, such that a selection process is not necessary here. The following questions are addressed in this section:

- Which model is suitable for which type of static object and how can the corresponding model be selected online?

- Which of the four adaptation schemes provides the best trade-off between convergence time, noise rejection, and parameter tracking for a) static objects and b) movable objects?

In order to answer these questions, different, virtual 1D static and 6D movable objects were simulated and estimated using the different adaptation schemes. The adaptation schemes were tuned to provide the best trade-off between convergence time, tracking accuracy, and noise rejection possible. For the simulations to be realistic, band-limited white noise was added to the resulting forces and torques. The estimated parameters were initialized with zero, i.e. $\hat{\theta}_0 = \mathbf{0}$ and the diagonal elements of the covariance matrix $\boldsymbol{P}$ were set to $1 \cdot 10^8$. The result of the estimation are the estimated parameters and the estimated forces and torques.

4.5.1 Static Objects

Two different, virtual 1D-objects were simulated with each of the three static object models, Kelvin-Voigt model (KVM), Hunt-Crossley model (HCM), and Hammerstein model

(HSM), see also Sec. 4.2:

KVM[2]	Object I :	$k_{kv} = 4000$ N/m	$b_{kv} = 200$ Ns/m	
	Object II :	$k_{kv} = 10000$ N/m	$b_{kv} = 500$ Ns/m	
HCM	Object I :	$k_{hc} = 40$ N/m	$b_{hc} = 10$ Ns/m	$n_{hc} = 1.5$
	Object II :	$k_{hc} = 80$ N/m	$b_{hc} = 15$ Ns/m	$n_{hc} = 1.1$
HSM	Object I :	$k_{hs} = 20$ N/m	$n_{hs} = 1.6$	$G(z^{-1}) = \frac{z^{-1}}{1.3z^{-1}-0.8z^{-2}}$
	Object II :	$k_{hs} = 10$ N/m	$n_{hs} = 2.5$	$G(z^{-1}) = \frac{z^{-1}}{1.3z^{-1}-0.8z^{-2}}$.

Band-limited white noise with amplitudes of ±3 N (KV), ±0.1 N (HC), ±0.2 N (HS) was added to the resulting forces and torques. In order to investigate how the different estimation approaches can track parameter changes, a switch from object I to II was triggered at $t = 2$ s. The parameters of the objects modeled with KVM and HCM were estimated with the four estimation methods: classic growing-window ($\lambda = 1$) recursive least squares (RLS), RLS with adaptive forgetting factor (RLS-A), RLS with self-perturbation (RLS-SP), and adaptive identification (AI). Due to the recursive structure of the Hammerstein model, the simulated objects were only estimated with the recursive least squares approaches. The parameters of the estimation methods are summarized in the following table, where HSM-E1 and HSM-E2 represent estimator 1 and 2 of the Hammerstein model, see also Sec. 4.3.3.1.

Model	RLS-A				RLS-SP		AI
	α_1	α_2	α_3	l	γ	β	$\mathbf{\Gamma}$
KVM	0.99	1	0.5	5	0.01	$10 \cdot 10^3$	$\begin{bmatrix} 500{\cdot}10^3 & 500{\cdot}10^3 \\ 0 & 500{\cdot}10^3 \end{bmatrix}$
HCM	0.98	10	0.9	0.9	5	500	$\begin{bmatrix} 800 & 1000 & 2000 \\ 400 & 100 & 1000 \\ 100 & 100 & 600 \end{bmatrix}$
HSM-E1	0.99	9	0.5	5	5	50	-
HSM-E2	0.990	500	0.7	5	$1 \cdot 10^{-4}$	500	-

The simulation results are shown in Fig. 4.10, 4.11, and 4.12. The left column shows the simulated (solid and noisy) and estimated (dashed) forces and the estimation error $e = f - \hat{f}$. The right column shows the estimated (solid) and true parameters (dotted).

For the evaluation, the normalized root mean square error between the measured and estimated environment force, f and $\hat{f}$, (NRMSE_f) was determined over the whole estimation horizon, see Appendix B.1. Furthermore, the convergence time for the first object (CT_{O1}) is determined, see Appendix B.3. Table 4.2 summarizes these measures for the different models and estimation methods. These results are used in the following in order to select a suitable estimation method and environment modeling approach.

Selection of Estimation Method for Static Objects: As shown in Table 4.2, all estimation results with the classic RLS show a fast convergence to the true parameter values for the first object. Due to the growing-window character of the approach, a change of the

[2]Please note that the stiffness and damping corresponding to the KVM have a different physical meaning than those of the HCM or HSM.

Tab. 4.2: Normalized root mean square error (NRMSE_f [%]) between simulated and estimated force and convergence time (CT_{O1} [s]) for the different models and estimation methods. E1 stands for estimator 1, E2 for Estimator 2, see also Fig. 4.6. The numbers in bold mark the best, i.e. smallest, NRMSE_f and CT_O1 values for each model.

Model	RLS		RLS-A		RLS-SP		AI	
	NRMSE_f	CT_{O1}	NRMSE_f	CT_{O1}	NRMSE_f	CT_{O1}	NRMSE_f	CT_{O1}
KVM	**2.4**	**0.399**	5.8	1.963	2.3	**0.399**	3.9	∞
HCM	33.6	**0.875**	2.8	∞	**0.6**	**0.875**	1.3	∞
HSM-E1	6.3	**0.028**	2.4	∞	**2.3**	0.04	-	-
HSM-E2	-	**0.283**	-	0.285	-	**0.283**	-	-

object can, however, not be tracked well, see Fig. 4.10(b), 4.11(b) and 4.12(b). Reducing the forgetting factor would result in improved tracking capabilities, but worse noise rejection. An example for a reduced forgetting factor of $\lambda = 0.95$ is shown in Fig. 4.13. The forgetting factor is the only parameter to be tuned.

The RLS method with adaptive forgetting factor shows good tracking properties for both objects. It is, however, sensitive to noise which deteriorates the convergence time. Reducing the sensitivity to noise would result in diminished tracking capabilities, see Fig. 4.14. The tuning effort is high: four parameters have to be determined which, on top, influence each other. Furthermore, not only the convergence time but also the noise rejection and tracking capabilities are influenced by the excitation for this estimation method. Consequently, the parameters of the RLS-A approach should be tuned according to the excitation.

The self-perturbing RLS approach shows fast convergence, good tracking, and good noise rejection. The two parameters can be tuned in an intuitive manner according to the noise characteristics of the force measurement.

The adaptive identification approach reveals the slowest convergence time of all methods. Furthermore, the estimated parameters show noisy behavior. The stability and accuracy of the estimation is very sensitive to the adaptation matrix, which increases with the number of parameters, and therefore requires a very high tuning effort.

In summary, the *self-perturbing RLS algorithm* shows superior performance for all three object models and a small tuning effort compared to the other approaches and will therefore be used for estimating static objects. Regarding movable objects, a high disturbance rejection is important. Furthermore, the estimation for movable objects ran prior to the reconstruction and was therefore triggered externally. Thus, the tracking capabilities of the estimation approach are less important. Due to the good disturbance rejection capabilities, the growing-window RLS and the self-perturbing RLS can therefore be used likewise.

Selection of Environment Models for Static Objects: Regarding stiff objects, the Kelvin-Voigt model may be superior to the Hunt-Crossley or Hammerstein model, as it captures by construction the linearity between $\boldsymbol{f}$ and $\delta\boldsymbol{x}$, which is characteristic for stiff objects. Furthermore, the damping term becomes negligible compared to the stiffness term

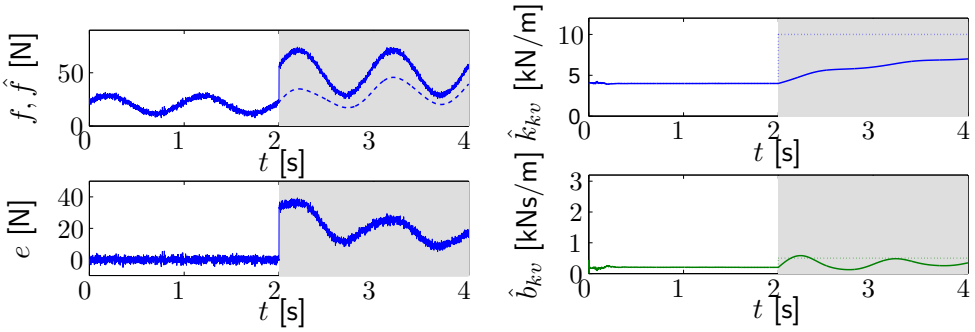

(a) Estimated force with RLS ($\lambda = 1$) (b) Estimated parameters with RLS

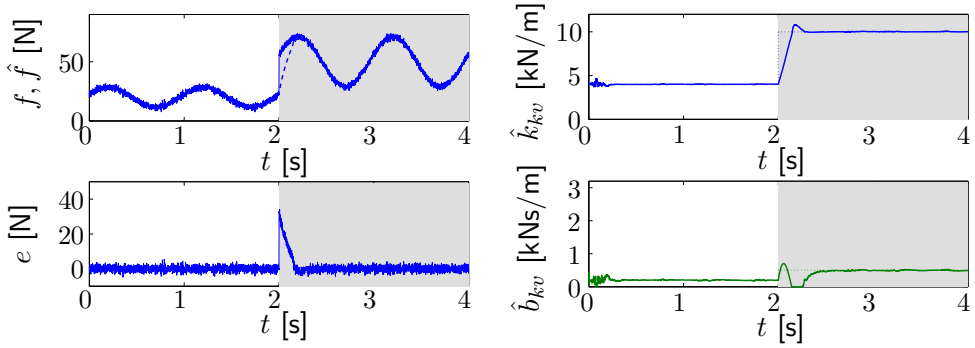

(c) Estimated force with RLS-A (d) Estimated parameters with RLS-A

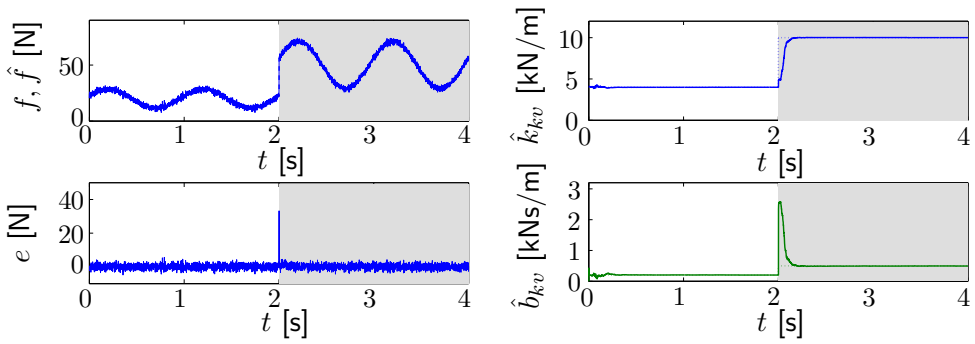

(e) Estimated force with RLS-SP (f) Estimated parameters with RLS-SP

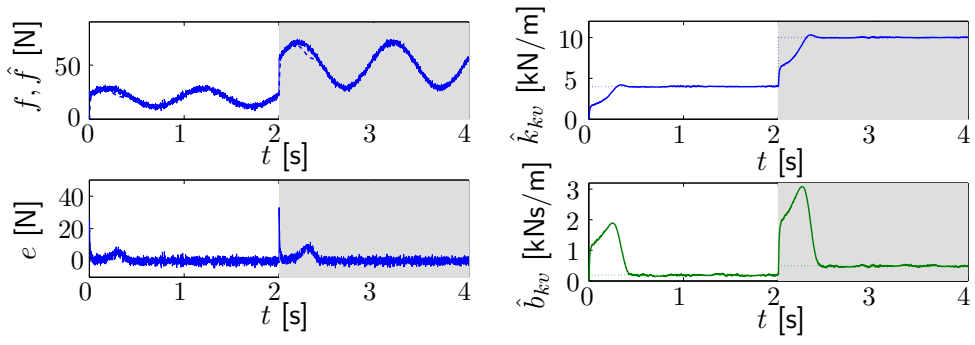

(g) Estimated force with AI (h) Estimated parameters with AI

Fig. 4.10: Estimation results for 2 static objects, switched at $t = 2$ s and modeled with the KVM. Left: Simulated (solid) and estimated (dashed) forces. Right: Estimated (solid/dashed) and true (dotted) parameters.

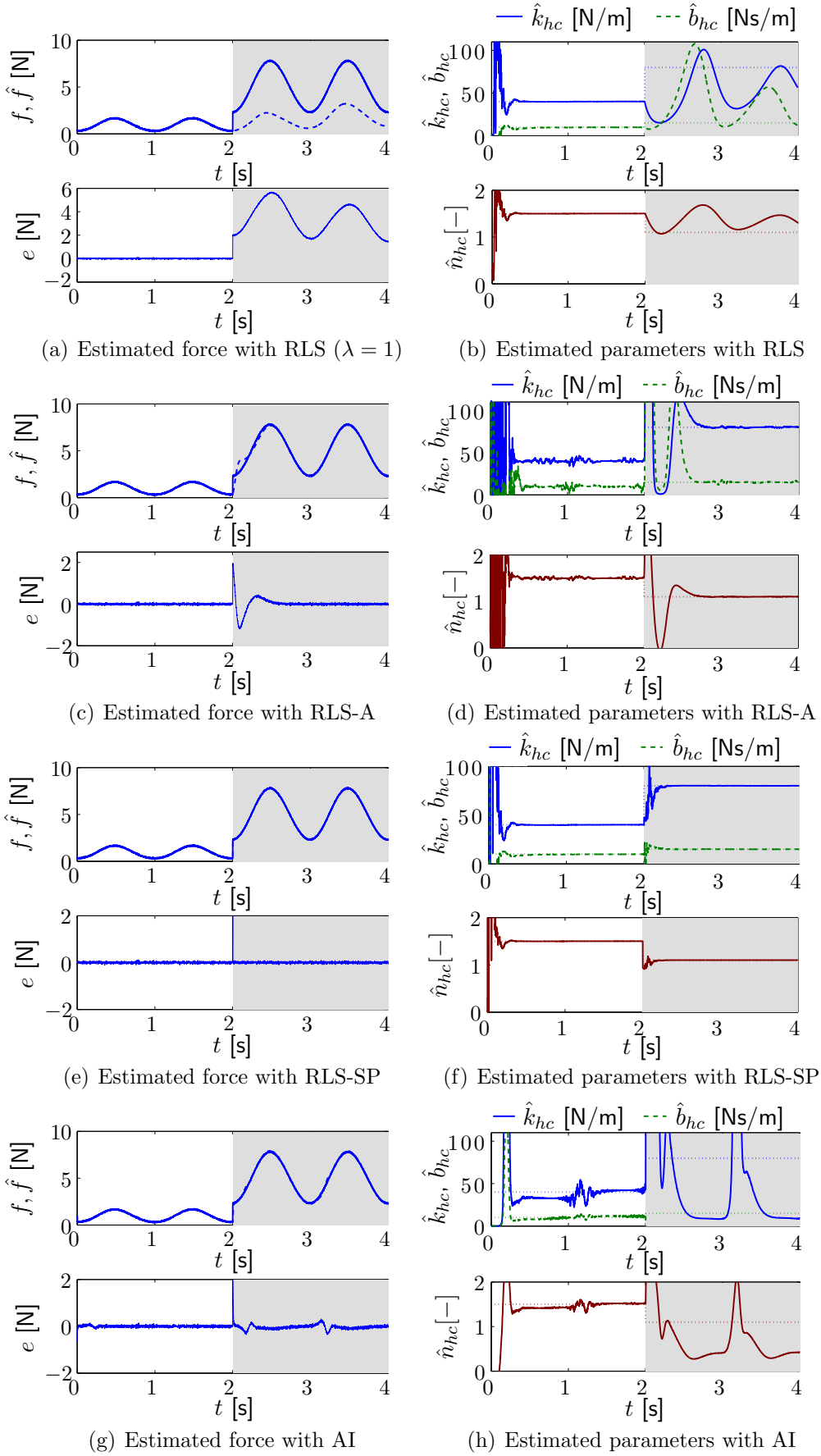

(a) Estimated force with RLS ($\lambda = 1$)
(b) Estimated parameters with RLS
(c) Estimated force with RLS-A
(d) Estimated parameters with RLS-A
(e) Estimated force with RLS-SP
(f) Estimated parameters with RLS-SP
(g) Estimated force with AI
(h) Estimated parameters with AI

Fig. 4.11: Estimation results for 2 static objects, switched at $t = 2$ s and modeled with the HCM. Left: Simulated (solid) and estimated (dashed) forces. Right: Estimated (solid) and true (dotted) parameters.

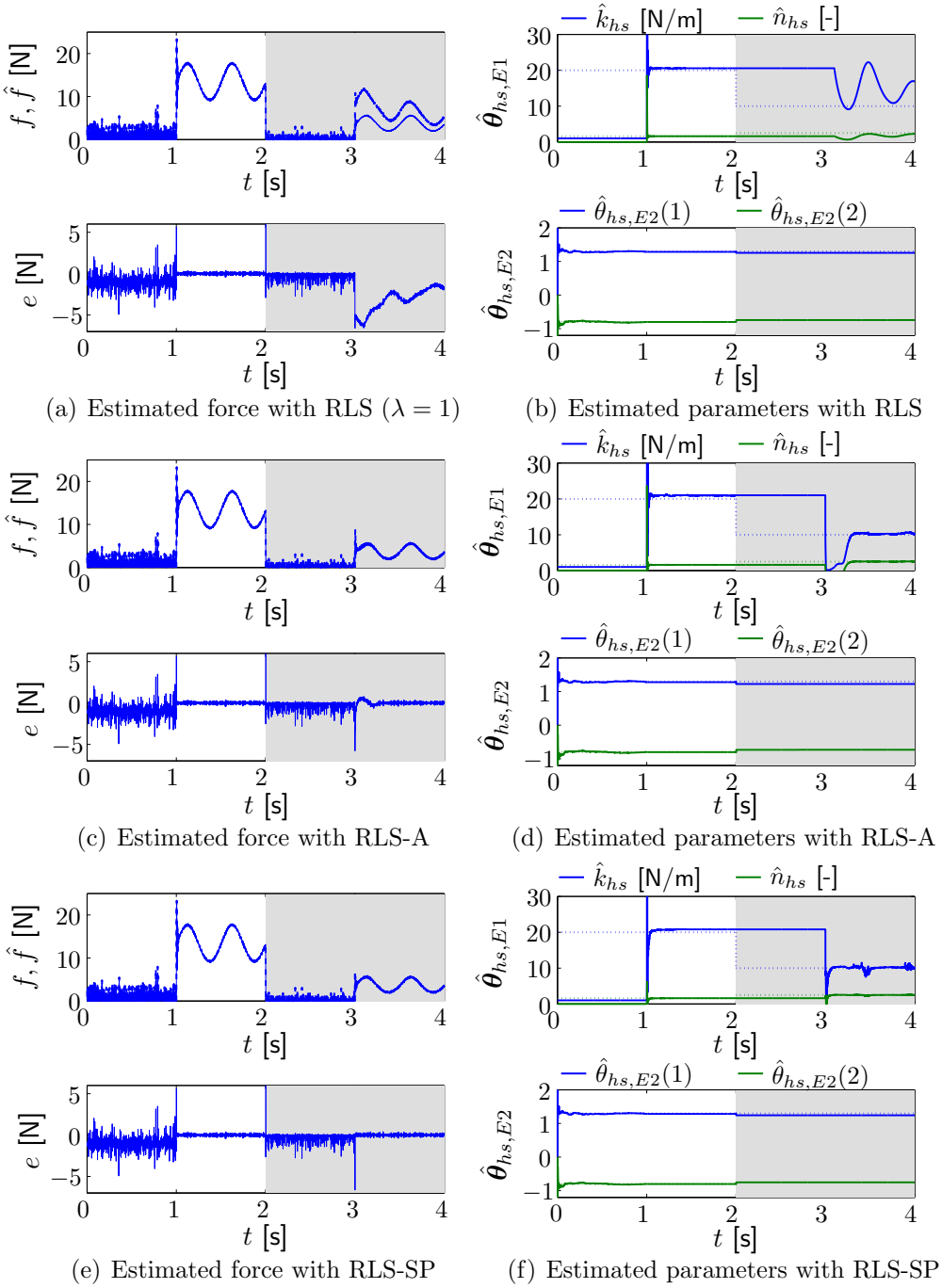

(a) Estimated force with RLS ($\lambda = 1$)

(b) Estimated parameters with RLS

(c) Estimated force with RLS-A

(d) Estimated parameters with RLS-A

(e) Estimated force with RLS-SP

(f) Estimated parameters with RLS-SP

Fig. 4.12: Estimation results for 2 static objects, switched at $t = 2$ s and modeled with the HSM. Left: Simulated (solid) and estimated (dashed) forces. Right: Estimated (solid) and true (dotted) parameters.

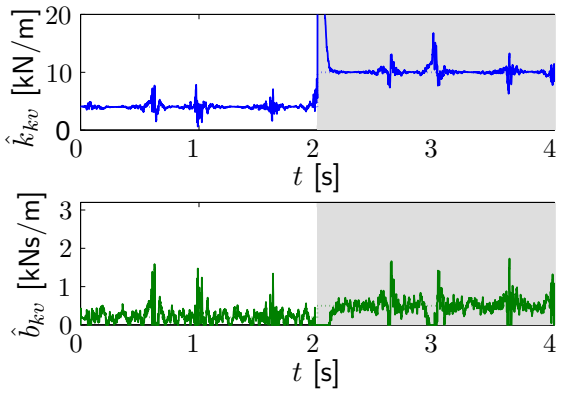

Fig. 4.13: Estimated $\hat{k}_{kv}$ [kN/m] and $\hat{b}_{kv}$ [kNs/m] with RLS and a forgetting factor $\lambda = 0.95$. The solid lines show the estimated parameters, the dotted lines the true parameters.

for these materials, reducing considerably the magnitude of the hysteresis discontinuity at the beginning of contact. The Kelvin-Voigt model is therefore selected when an interaction with a stiff object occurs.

For soft objects, on the contrary, the discontinuity in the hysteresis curve of the Kelvin-Voigt model is not negligible for soft objects and limits its applicability here. Comparing the Hunt-Crossley and Hammerstein model with each other, the simulation results show that the Hunt-Crossley model exhibits superior tracking capabilities compared to the Hammerstein model except for the RLS approach. The concatenation of a digital filter and a static nonlinearity of the Hammerstein model requires two completely different excitation signals. While the estimation converges for the digital filter only, if the excitation is white noise with zero mean, the parameters of the static nonlinearity can be estimated best using a signal with a single frequency and sufficiently large amplitude. As a remedy to this issue, the parameters of the Hammerstein model were estimated in simulations in two phases, one with an excitation for the nonlinearity and one with an excitation for the digital filter. This process is, however, time-consuming and a change in the parameters has to be correctly determined in order to reset the estimation process. Thus, the Hunt-Crossley model is selected for modeling soft objects and the Hammerstein model will not be used further.

As outlined above, the choice of the model depends on the encountered object type. A *hybrid object modeling approach* is therefore proposed, where the Kelvin-Voigt model is selected for stiff objects and the Hunt-Crossley model for soft objects. The estimation runs for both models during contact with an object. As a stiff object is more critical for the system stability, the Kelvin-Voigt model is initially assumed. After a time of 50 ms to check the convergence of both models, a switching between both models occurs if the estimated stiffness of the Kelvin-Voigt model k_{kv} falls below a prespecified threshold k_{th} in one direction. This hybrid switching strategy between the *Kelvin-Voigt model* (kv), and *Hunt-Crossley model* (hc) can be described by a switching operator $\xi(k_{kv})$ in any direction:

$$\xi(k_{kv}) = \begin{cases} kv, & \text{if } k_{kv} \geq k_{th} \\ hc, & \text{else.} \end{cases} \tag{4.42}$$

As the estimation error is small for both models when switching, force discontinuities are not perceivable. As both models are furthermore estimated continuously, a simple switching operator is sufficient here. If the switches were perceivable or the estimation of the models was stopped, a hysteresis could be used instead.

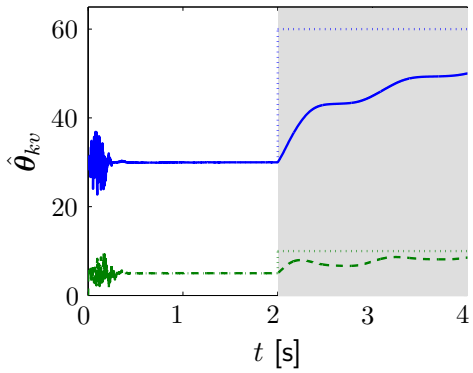

Fig. 4.14: Estimated $\hat{k}_{kv}$ [N/m] (blue, solid) and $\hat{b}_{kv}$ [Ns/m] (green, dashed) with an RLS-A implementation with a small sensitivity to noise. The solid/dashed lines show the estimated parameters, the dotted lines the true parameters.

Based on the theoretical and simulation results, it can be summarized that the Kelvin-Voigt model is best suited to model stiff objects, while the Hunt-Crossley model is superior over the other models for soft objects. The model is selected online using a hybrid switching strategy. The parameters are estimated using the RLS with self-perturbation due to its superior tracking and convergence capabilities as well as a small tuning effort.

4.5.2 Movable Objects

Two virtual, movable objects were simulated, see also (4.5) and (4.6):

Object I	$m = 2$ kg
	$\boldsymbol{c} = [-169 \;\; 0 \;\; -135]$ mm
	$\boldsymbol{I}_v = [5.2 \;\; 0 \;\; 0 \;\; 1.8 \;\; 0 \;\; 3.6] \cdot 10^{-3}$ kg m^2
Object II	$m = 4$ kg
	$\boldsymbol{c} = [11.86 \;\; 12.16 \;\; -77]$ mm
	$\boldsymbol{I}_v = [3.92 \;\; 0.26 \;\; -0.68 \;\; 3.32 \;\; -0.68 \;\; 0.636] \cdot 10^{-3}$ kg m^2

The parameters were estimated with RLS-SP as this method showed superior performance compared to the other approaches. In order to apply this method to multi-input multi-output (MIMO) systems, the NINT function that is required for the self-perturbation was modified to

$$\mathrm{NINT}(\gamma \sum_{i=1}^{n} \hat{\boldsymbol{e}}_{ik-1}^{\,2}) = \begin{cases} \gamma \sum_{i=1}^{n} \hat{e}_{ik-1}^{2}, & \text{if } \gamma \sum_{i=1}^{n} \hat{e}_{ik-1}^{2} \geq 0.5, \\ 0, & \text{else.} \end{cases} \tag{4.43}$$

where n is the order of the output vector $\boldsymbol{y}$. The design constants β and γ were set to

$$\beta = 500 \qquad \gamma = 0.01.$$

The excitation trajectories were selected as described in Sec. 4.3.4. A change from object I to II occurred again at $t = 2$ s. The simulation results are shown in Fig. 4.15. The left plots show the simulated (solid and noisy) and estimated (dashed) forces and torques, and the right plots show the estimated (solid) and true parameters (dotted). The simulation results presented in Fig. 4.15 and a mean NRMSE over all forces and torques of 2.16 % show good tracking performance and noise rejection. However, only if no process noise is added to the simulated forces and torques, all inertia parameters converge within 128 ms. With band-limited white noise with an amplitude of ± 1 N for forces and ± 0.15 Nm for torques, respectively, I_{yy} does not converge within the 2 s estimation time, but the remaining parameters converge within 0.94 s for the first object. The remaining relative estimation error of I_{yy} $\mathrm{REE}_{I_{yy}}$ is found according to Appendix B.2 as 11.5 %. The results show that even though the input trajectories were selected in an optimal way, the estimation of the moments of inertia are difficult. This problem arose as the moments of inertia were so small such that even small process noise deteriorated the signal-to-noise ratio considerably. As a consequence, the convergence time of the estimation increases, especially if convergence is defined with a tracking accuracy of higher or equal than 95%. This result also confirms the expectation that human-generated, task-specific trajectories can be assumed to not provide sufficient excitation for all inertia parameters. It should furthermore be noted here, that joint angle, velocity and acceleration limits of the slave device were not taken into account in this simulation. They further restrict the permissible range of excitation amplitudes and frequencies.

4.6 Evaluation: Model-Mediated Teleoperation

Combining the selected modeling techniques for static and movable objects with a self-perturbing recursive least squares approach, remote objects can be identified online and reconstructed on operator site as described in Sec. 4.4. This section presents experimental results for model-mediated teleoperation using 1 DoF and 6 DoF teleoperation systems together with implementation issues regarding the identifiable range of static object and the estimation excitation for movable objects and limitations of the approach. Besides results for an ideal communication channel shown in Sec. 4.6.2, difficulties arising from a non-ideal communication channel are illustrated with experimental results in Sec. 4.6.3.

4.6.1 Practical Issues

The most critical implementation issues are the identifiable range of parameters for static objects and the excitation for movable objects.

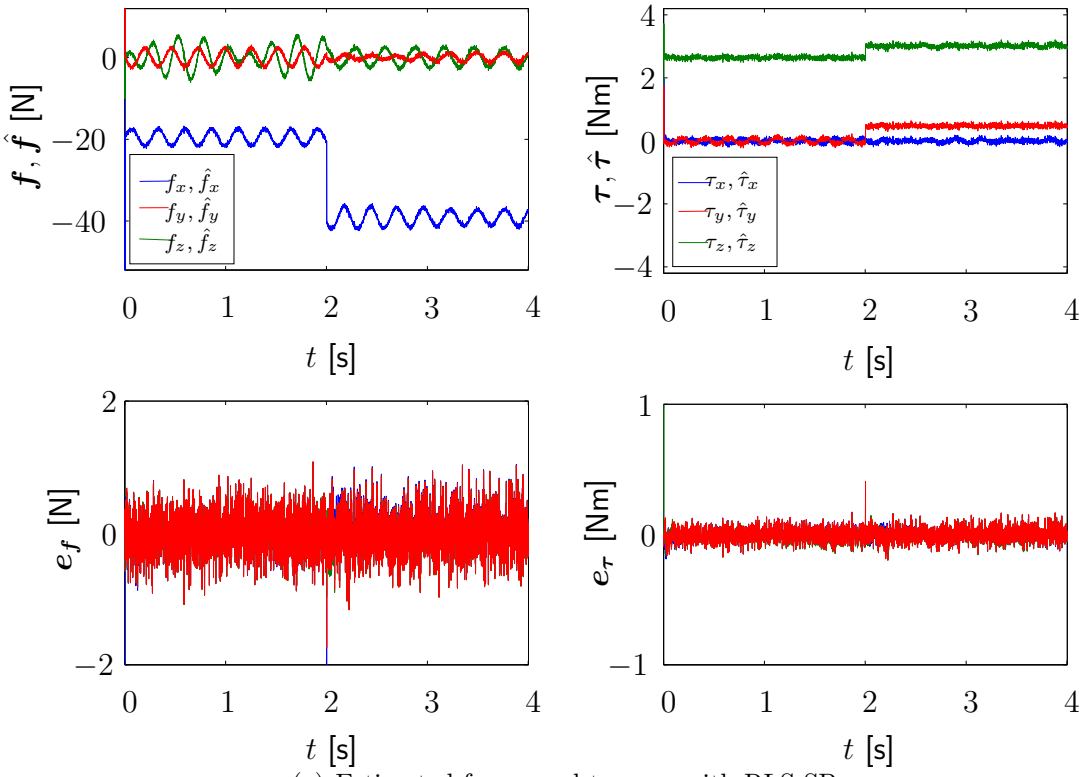

(a) Estimated forces and torques with RLS-SP.

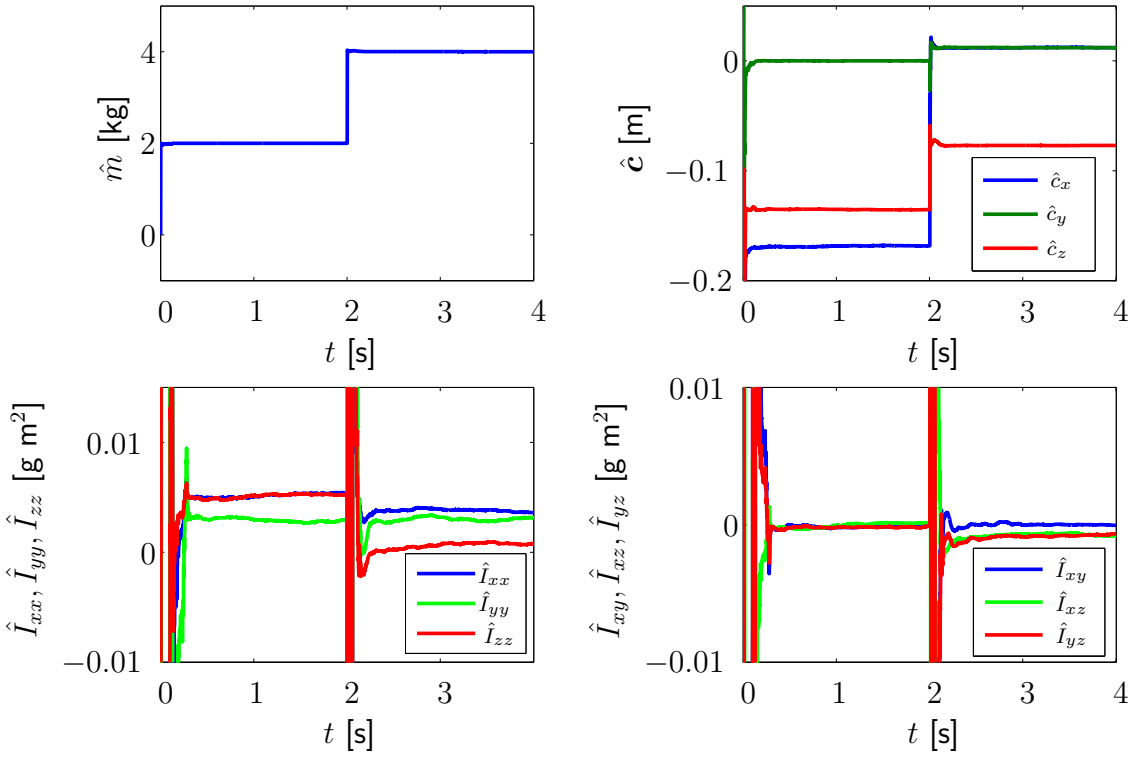

(b) Estimated parameters with RLS-SP.

Fig. 4.15: Estimation results for 2 movable objects, switched at $t = 2$ s. Left: Simulated (solid) and estimated (dashed) forces and torques. Right: Estimated (solid) and true (dotted) parameters.

4.6.1.1 Identifiable Parameter Range for Static Objects.

Regarding the online identification of static object models, an important aspect is the identifiable range of parameters. On the one hand, the force and encoder sensor resolutions and the actuator bandwidths limit the identifiable parameter range. It can, however, be assumed that these components can be selected for a specific application such that the manipulated objects are identifiable regarding sensor and actuator technology. On the other hand, the identifiable parameter range depends on the slave device, that is used for identification, as it is connected in serial with the object. Assuming an admittance-type robot its mechanical structure can be simplified to a spring-damper system denoted by k_s, b_s, interacting with another spring-damper-like object, denoted by $k_{\text{obj}}, b_{\text{obj}}$. The maximum identifiable stiffness is then the serial connection of k_s and k_{obj}, i.e.

$$k_{\max} = \frac{k_s k_{\text{obj}}}{k_s + k_{\text{obj}}}.$$

In the case of an infinitely stiff wall, the identifiable stiffness is consequently limited by the robot's mechanical stiffness. Given persistent excitation, the obtained parameters are therefore not the true values of the object's model alone, but the true values of the interacting robot-object system. These limits have to be considered in the interpretation of the obtained parameter values. For control, this estimation limitation becomes critical only, if the stiffness of the device, where the parameters are applied to, is higher than the stiffness of the device, with which the parameters have been obtained. This is not the case for the experimental setups used in this thesis.

4.6.1.2 Estimation Excitation for Movable Objects.

The parameter estimation for movable objects is limited by the maximum joint angles, velocities, and accelerations of the slave device on the one hand. The sensor bandwidth is assumed to be large enough in order to estimate the desired class of objects. On the other hand, the signal-to-noise ratio for the parameters plays an important role. Often, the moments of inertia are so small compared to the process noise that an accurate estimation is not realizable in an acceptable amount of time even if an optimized regressor matrix is used. This limitation is acceptable as long as the estimation error between reconstructed and measured torques is smaller than the JND for torques.

4.6.2 Model-Mediated Teleoperation with Ideal Communication

This section presents experimental results for model-mediated teleoperation using the 6 DoF experimental setup shown in Fig. 4.16. Further details regarding the experimental setup can be found in Appendix A.6.

The teleoperator is position controlled in joint space using a high-gain PD controller. The desired position and orientation in task space are commanded from the operator. On operator site, a position-based admittance control approach, as described in Sec. 2.3.1, is selected for the given setup. Using a virtual mass-damper system, the difference of forces and torques applied by the operator, $\boldsymbol{f}_h$ and $\boldsymbol{\tau}_h$, and reconstructed forces and torques, $\hat{\boldsymbol{f}}_{e,r}$

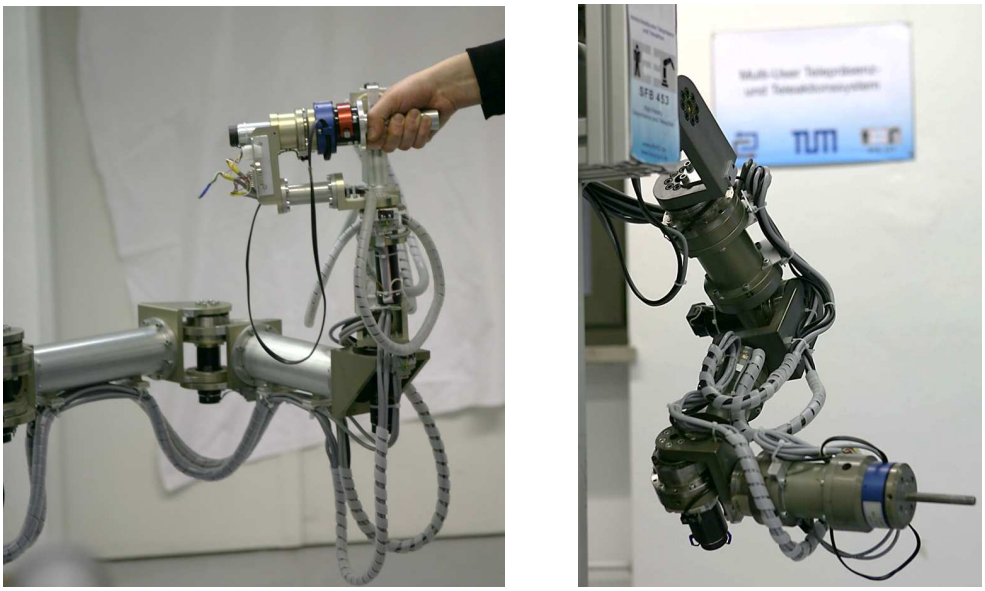

(a) Redundant 7 DoF haptic interface ViSHard7

(b) Redundant 7 DoF teleoperator

Fig. 4.16: 6 DoF experimental setup consisting of a redundant 7 DoF haptic interface and teleoperator. Pictures are taken from [227] and were slightly modified.

and $\hat{\boldsymbol{\tau}}_{e,r}$, are transformed into desired position and orientation, respectively:

$$\boldsymbol{f}_h - \hat{\boldsymbol{f}}_{e,r} = \boldsymbol{M}_a^{\text{trans}} \ddot{\boldsymbol{x}}_m + \boldsymbol{B}_a^{\text{trans}} \dot{\boldsymbol{x}}_m \tag{4.44}$$

$$\boldsymbol{\tau}_h - \hat{\boldsymbol{\tau}}_{e,r} = \boldsymbol{M}_a^{\text{rot}} \dot{\boldsymbol{\omega}}_m + \boldsymbol{B}_a^{\text{rot}} \boldsymbol{\omega}_m, \tag{4.45}$$

where $\boldsymbol{M}_a^{\text{trans}}$ and $\boldsymbol{B}_a^{\text{trans}}$ are diagonal mass and damping matrices for translations, and $\boldsymbol{M}_a^{\text{rot}}$ and $\boldsymbol{B}_a^{\text{rot}}$ are diagonal mass and damping matrices for rotations. The desired positions and orientation are controlled using a high-gain PD-controller in joint space. In order to avoid the dynamics of the underlying position controller, the desired position and orientation are sent to the teleoperator site. As the connection between local and remote site is realized with a local area network (LAN), time delay and packet loss are negligible. For the estimation of static and movable objects, an aluminium bar is used as handle for the operator. For static objects, a steel pin is mounted on the teleoperator's end-effector simulating a rigid tool. Thus, the operator should feel as holding some kind of tool like a screwdriver. For movable objects, a two finger robotic gripper was attached to the teleoperator's end-effector. A potentiometer on operator site allowed to control the gripper's opening and, thus, to grasp an object. The operator had a direct view on the teleoperator site.

Static Objects: The virtual inertia and damping matrices are chosen as $\boldsymbol{M}_a^{\text{trans}} = 5\ \boldsymbol{E}$ kg and $\boldsymbol{B}_a^{\text{trans}} = 1\ \boldsymbol{E}$ Ns/m for translations ($\boldsymbol{E}$ represents the identity matrix) and $\boldsymbol{M}_a^{\text{rot}} = 0.1\ \boldsymbol{E}$ kgm^2 and $\boldsymbol{B}_a^{\text{rot}} = 0.05\ \boldsymbol{E}$ Nms/rad for rotations. The operator remotely established and kept contact with two objects of different material using the model-mediated control approach. In order to show the applicability of the approach to a wide range of

materials, a steel plate and a soft silicone cube were used as objects, see Appendix A.3, and mounted on a solid surface. The true model parameters of these two materials are not known. In the following, estimation results, fidelity, and stability during teleoperation are discussed.

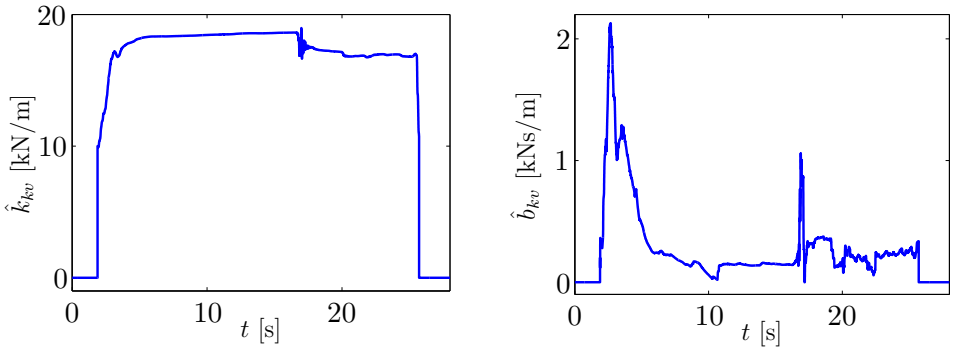

Fig. 4.17: Estimated parameters of Kelvin-Voigt model for contact with the steel plate in the direction of penetration.

For estimation, the parameters were initialized with $\hat{\boldsymbol{\theta}}_{kv} = [10 \cdot 10^3,\ 200]$ and $\hat{\boldsymbol{\theta}}_{hc} = [\log(3000),\ 1/30,\ 1.3]$ and for the self-perturbation the parameters were chosen as $\gamma_{kv} = 1, \beta_{kv} = 50$ and $\gamma_{hc} = 19000,\ \beta_{hc} = 1$. The stiffness threshold for the hybrid estimation approach was set to $k_{th} = 2500$ N/m. The important aspects for the estimation are speed, accuracy, and a correct switching between Kelvin-Voigt and Hunt-Crossley model. In Fig. 4.17 and Fig. 4.18, the estimated model parameters for the steel plate and the soft silicone cube are shown in the direction of penetration.

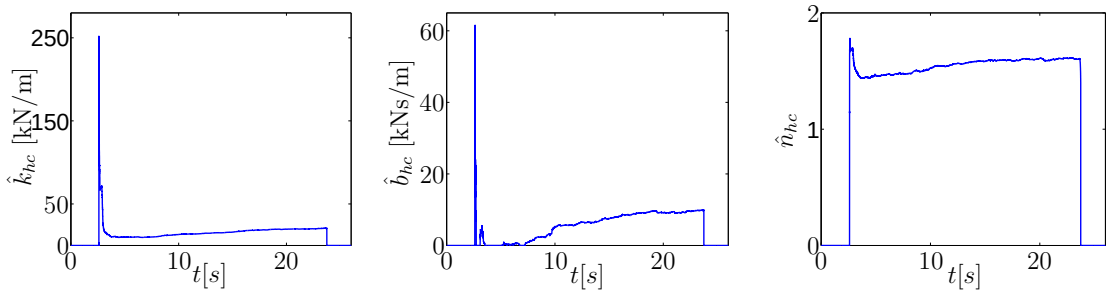

Fig. 4.18: Estimated parameters of Hunt-Crossley model for contact with the silicone cube in the direction of penetration.

The parameters converge in less than 1s, which enables a good rendering of contact forces and torques on master site. For a realistic impression of the object, the time of contact has to be longer than the convergence time of the estimation. Otherwise, a realistic haptic impression of the object cannot be provided to the operator. Furthermore, the $\text{NRMSE}_{\boldsymbol{f}}$ between measured and estimated forces on slave site is calculated in the direction of penetration according to (B.1). It is 1.16% for the steel plate and 1.67% for the silicone cube, which proves a sufficient accuracy of the estimation. As described in Sec. 4.3.4, the stiffness of the Kelvin-Voigt model is the maximum identifiable stiffness of the robot-object interaction. It is consequently limited to the robot's stiffness when touching a rigid

wall. Thus, the estimated value of $k_{kv} \approx 17$ kN/m seems plausible. The initial peak in the damping value occurs due to the combination of a very small penetration depth and large measured forces. As the parameters of the Hunt-Crossley model are not physically interpretable, a statement about the accuracy can hardly be provided. Finally, the hybrid switching technique chose the correct models for the right material, i.e. Kelvin-Voigt for the steel plate and Hunt-Crossley for the silicone cube.

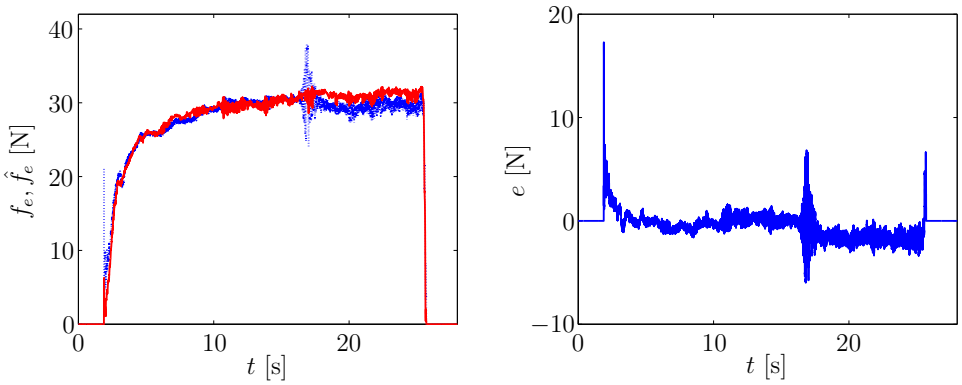

Fig. 4.19: Left plot: Measured force on slave site (solid) and reconstructed force on master site (dashed) for the steel plate, right plot: force error.

For teleoperation, the most important aspects are robustness and fidelity. The observed behavior was always asymptotically stable, i.e. moving in free space and establishing and keeping contact did not lead to oscillations or instabilities. For fidelity evaluation, the force measured at the wrist of the teleoperator's end-effector and the reconstructed force generated in the wrist frame on master site were recorded and are shown in Fig. 4.19 for the steel plate and in Fig. 4.20 for the silicone cube in the direction of penetration. The reconstructed forces generated by both models fit well with the measurements. In steady-state, the force error for the steel plate and the silicone cube is always smaller except for a few peaks than the just noticeable difference for force ($\mathrm{JND}_f \approx 10\%$ for the arm/forearm, see [189]). This means that the estimated forces cannot be distinguished from the measured ones by the operator. Besides force tracking, a high degree of fidelity requires a good position tracking. As the desired master position $\boldsymbol{x}_m^d$ and orientation represented for example as Euler angles $\boldsymbol{\varphi}_m^d$ is tracked on master and slave site using a high-gain PD-controller, the tracking errors between desired and measured position and orientation are small on both site. As a consequence, also the tracking errors between master and slave position and orientation, $\|\boldsymbol{x}_m - \boldsymbol{x}_s\|$ and $\|\boldsymbol{\varphi}_m - \boldsymbol{\varphi}_s\|$, are small. Together with a force and torque error below the JND_f, the system in steady-state is perceived transparent according to the definition in Sec. 2.2.1.2. For the transient phase, further investigations based on a dynamic JND should be performed in future.

Movable Objects: The virtual inertia and damping matrices are chosen as $\boldsymbol{M}_a^{\mathrm{trans}} = 12\ \boldsymbol{E}$ kg and $\boldsymbol{B}_a^{\mathrm{trans}} = 70\ \boldsymbol{E}$ Ns/m for translations and $\boldsymbol{M}_a^{\mathrm{rot}} = 0.2\ \boldsymbol{E}$ kgm^2 and $\boldsymbol{B}_a^{\mathrm{rot}} = 1\ \boldsymbol{E}$ Nms/rad for rotations. After grasping a movable object, the inertia parameters were estimated while the slave was running in autonomous mode. The input trajectories

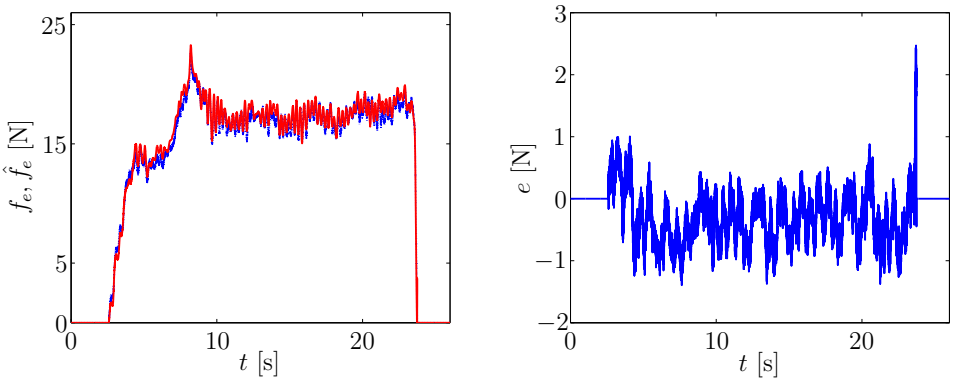

Fig. 4.20: Left plot: Measured force on slave site (solid) and reconstructed force on master site (dashed) for the silicone cube, right plot: force error.

were manually selected to meet the joint limitations, velocities, and accelerations of the device:

$$\begin{array}{lll} A_{\varphi_x} = -\pi/2 \text{ rad} & A_{\varphi_y} = -0.1 \text{ rad} & A_{\varphi_z} = -0.1 \text{ rad} \\ f_{\varphi_x} = \ \ 0.5 \text{ Hz} & f_{\varphi_y} = \ \ 1 \text{ Hz} & f_{\varphi_z} = 0.6 \text{ rad}. \end{array} \tag{4.46}$$

As described in Sec. 4.6.1.2, the excitation of movable objects together with the signal-to-noise ratio of the moments of inertia are critical factors for the online estimation. The 6 DoF experimental setup exhibits strong limitations in terms of joint angles, velocities, and accelerations. If a joint limit is reached, the estimation is stopped as high jerks occur resulting in large force and torque peaks. As a stop in the estimation process retards the convergence and stresses the device, joint limits were avoided as far as possible. A hard drive was selected as movable object, see also [239] for a detailed description of the scenario. The hard drive can be represented as a rectangular box with the parameters

Hard drive	m	$=$	0.62 kg
	$\boldsymbol{c}$	$=$	$[0 \ 0 \ -0.324]$ m
	$\boldsymbol{I}_v$	$=$	$[1.6 \ \ 0 \ \ 0 \ \ 0.55 \ \ 0 \ \ 1.1] \cdot 10^{-3}$ kg m^2.

The estimated inertia parameters are shown in Fig. 4.21. During the first 30 s, the slave was running autonomously in order to estimate the object's parameters. During the time interval from 30 s to roughly 50 s, the operation mode was switched from autonomous mode to teleoperation. Differences between estimated and measured forces/torques were consequently not applied to the system and can be disregarded for the evaluation. From roughly 50 s on, the operator telemanipulated the object. The mass and CoM coordinates show a fast and accurate convergence (within 80 ms) to the true value. The moments of inertia I_{xx} and I_{yy} did, however, not converge. Only I_{zz} converged within 6.6 s. The reason is the small signal-to-noise ratio noise for the moments of inertia. When no measurement noise was added, all parameters converged to the true values.

For the *estimation phase*, where the slave was running autonomously, the mean NRMSE values between measured and estimated forces as well as torques on slave site are determined. All forces and torques are given in the reference frame R. The mean NRMSE is 4.81% for forces and 8.57% for torques.

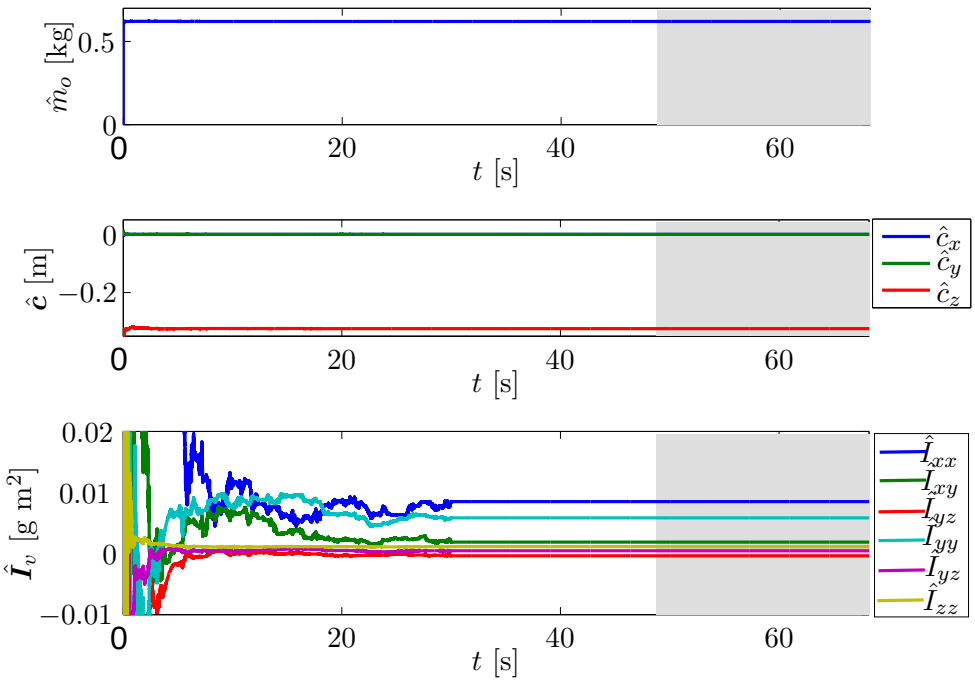

Fig. 4.21: Estimated inertia parameters. During the first 30 s, the inertia parameters were estimated. The excitation was provided by the autonomously running slave. During the reconstruction phase marked in gray, the estimated parameters were used to generate reconstructed forces and torques on master site.

Regarding force and torque tracking during the *reconstruction phase*, where the slave was teleoperated, the simulated forces/torques on slave site and the virtual, reconstructed forces/torques on master site are compared with each other, see the gray part in Fig. 4.22. The NRMSE between measured and reconstructed force is 8.89% for forces and 19.45 % for torques. If the simulated forces and torques were first filtered with a low-pass filter with a cut-off frequency of 10 Hz in order to reduce the influence of the noise, the NRMSE during the reconstruction phase improves to 4.46 % for forces and 8.03 % for torques. The NRMSE values for force and the filtered NRMSE for torques lie below the corresponding just noticeable differences (JND) (10% for force for the arm/forearm, see [189], 12.7% for torques for the forearm, see [96]). Thus, it can be concluded that the estimation is accurate enough such that the operator cannot perceive a difference between true and reconstructed object. A good position tracking is also given as the desired master position and orientation are sent to the slave site and tracked using a high-gain PD-controller. Thus, this system is perceived transparent.

The experimental results presented in this section show that 6 DoF model-mediated teleoperation is realizable for static and movable objects and an experimental setup with an ideal communication channel.

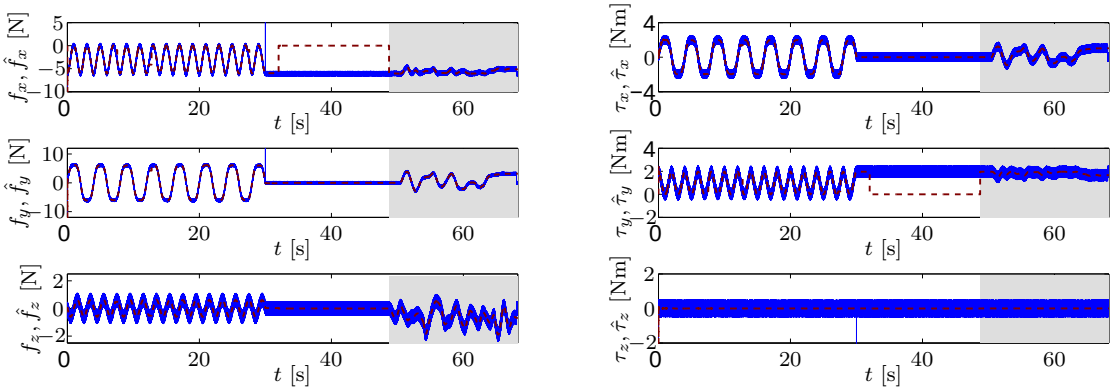

(a) Forces (b) Torques

Fig. 4.22: Simulated forces and torques on slave site (solid) and estimated and reconstructed forces and torques on master site (dashed). During the first 30 s, the slave was running autonomously in order to estimate the object's parameters. During the time interval from 30 s to ca. 50 s, the operation mode was switched from autonomous to teleoperation. From ca. 50 s on, the operator telemanipulated the object.

4.6.3 Model-Mediated Teleoperation with Time Delay

Model-mediated teleoperation is expected to have a main advantage compared to classic control concepts if the communication channel exhibits deficiencies. In this case, it is important to select a suitable reconstruction method for static objects. For movable objects, the choice of the reconstruction method is independent of the deficiencies in the communication channel as the estimation and reconstruction phase are running sequentially, not in parallel. This section therefore presents experimental results for static objects only.

6 DoF Model-Mediated Teleoperation with Small Time Delay: Experimental results were obtained for the connection of the 6 DoF slave device from the Technische Universität München, which was positioned in Munich, Germany, and the 6 DoF light-weight robotic arm from KUKA in Augsburg, Germany.

The experimental setup is shown in Fig. 4.23. Both devices were controlled using position-based admittance controllers. A small time delay of $\approx$ 30 ms was measured between local and remote site, the packet loss was negligible. As the delay was small enough such that stability and safety were not affected, prior knowledge about the object's location was not required nor any compliant behavior for establishing the first contact. Thus, a priori knowledge about the object location was not assumed corresponding to the first reconstruction method presented in Sec. 4.4.2. The experiments were part of the diploma thesis of A. Achhammer [227]. Please refer to this thesis for detailed illustration of measured and reconstructed forces and torques. Three objects were tested: a steel and two silicone cubes. The NRMSE_f for the steel cube (10.53 %, see [227]) was found almost equal to the JND_f for force, the NRMSE_f for the soft silicon cube (4.11 %, see [227]) was found below and the NRMSE_f for the hard silicone cube slightly above the JND. It should, however, be noted that a large range of JNDs is presented in literature ranging

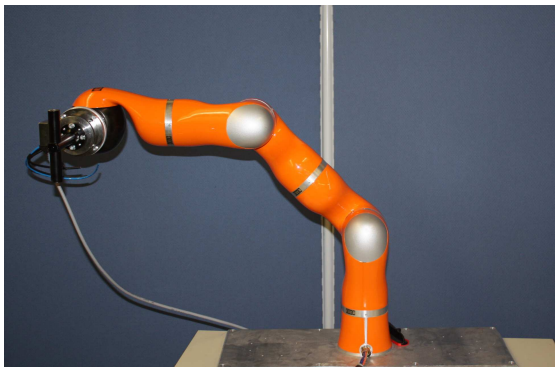

(a) 6 DoF light-weight robotic arm from KUKA

(b) Redundant 7 DoF teleoperator

Fig. 4.23: 6 DoF experimental setup consisting of a 6 DoF light-weight robotic arm from KUKA and a redundant 7 DoF teleoperator from the TU Munich. Pictures are taken from [227] and were slightly modified.

from 7 % [99] up to 15 % [98, 173] for force. It can therefore not be concluded that the operator perceives a difference between real and reconstructed object for the hard silicone cube. The results show that 6 DoF model-mediated teleoperation is realizable over a deficient communication channel with high force and position tracking accuracy and without deteriorating stability.

1 DoF Model-Mediated Teleoperation with Large Time Delay If the time delay becomes large, i.e. above 50 ms, the reconstruction method has to be selected carefully. This section presents experimental results for a 1 DoF experimental setup as shown in Fig 4.24 and compares the two reconstruction methods presented in Sec. 4.4.2. The teleoperator is again position controlled using a high-gain PD controller. The desired position is commanded from the operator. On operator site, a position-based admittance control approach, as described in Sec. 2.3.1, is chosen for the given setup. Using a virtual mass-damper characteristic for the admittance, the difference of the force applied by the operator, f_h, and the reconstructed force, $\hat{f}_{e,r}$, are transformed into a desired position:

$$f_h - \hat{f}_{e,r} \quad = \quad m_a \ddot{x}_m + b_a \dot{x}_m. \tag{4.47}$$

The virtual inertia and damping were chosen as $m_a = 2.3$ kg and $b_a = 0$ Ns/m. An aluminium bar was used as handle for the operator, and a steel pin was mounted on the teleoperator's end-effector simulating a rigid tool. The operator had a direct view on the teleoperator site. The task was to establish contact twice with a silicone cube as shown in Appendix A.3. A constant time delay was simulated, packet loss was neglected.

Reconstruction without Knowledge about Object Location: As the object location is assumed to be unknown, the first contact with the object is risky for the safety of slave device and environment, especially as a stiff position controller is used on slave site.

The approach is therefore applied for a system with a small time delay of 50 ms in the

Fig. 4.24: 1DoF experimental setup consisting of two identical linear direct drive actuators, Thrusttube modules ME2504 from Copley Controls Corp..

forward and backward channel. The object location is determined during first contact and the virtual object is shifted correspondingly such that the virtual object on master site coincides with the remote object from the second contact on. Fig. 4.25(a) shows position and force tracking. While the position tracking is quite accurate, differences in measured and reconstructed environment forces are observable. A small position error of ≈ 5 mm exists, see Fig. 4.25(b), which leads to different penetration depths into the virtual object on master site and the real object on slave site. As the stiffness is large, see Fig. 4.26, these small differences in the penetration depth lead to differences in the measured and reconstructed forces. It can consequently be concluded that the accuracy of force and position tracking for model-mediated teleoperation with static objects is dependent on the accuracy of the object's location. The perceived impedance on master site is, however, not impaired.

In order to increase safety for the first contact, a compliant behavior can be realized on slave site. A mass-spring-damper system with a mass of 2 kg, a stiffness of 8 kN/m and a damping of 400 Ns/m was used. The compliance reduces the penetration depth of the slave device and, consequently, the environment force. The NRMSE of the impedance shows that the realism of the reconstructed object on master site is not impaired, but the master and slave position diverge, see Table 4.3. These experimental results already show that there is a trade-off between fidelity and safety when applying model-mediated teleoperation to systems with time delay.

The experiment is furthermore repeated with time delays of up to 0.5 s, see [230]. Without a compliant behavior during first contact, even small impact velocities lead to large environment forces as the increased delay results in a larger penetration into the object. This issue becomes more severe with increasing stiffness of the objects. For safety reasons, a compliant behavior should therefore be realized on slave site for the first contact. From the moment on when the object location is determined correctly, the interaction with remote objects is safe and a realistic impedance of the remote object is provided to the operator, independent of the time delay and impact velocity. Yet, a small position error is observed which deteriorates force tracking, but is independent of the time delay. For large time delays, a parameter update can further lead to oscillations in the reconstructed forces. It was, however, always possible to establish contact.

Reconstruction with Knowledge about Object Location: If an approximate object location in the form of a Gaussian distribution is given, a safe first contact can be guaranteed

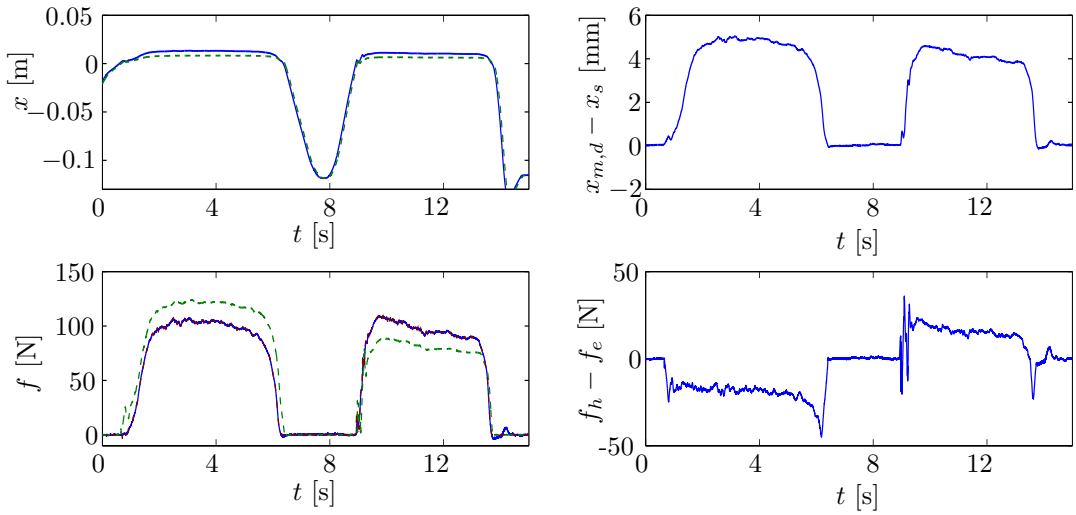

(a) Position and force tracking

(b) Tracking and force error

Fig. 4.25: Experimental results for reconstruction method without knowledge of the object location. Master position and force (blue, solid), slave position and force (green, dashed), and reconstructed force (red, dash-dot) for $T_d = 0.05$ s. The tracking error is determined between delayed master position $x_{m,d} = x_m(t - T_d)$ and slave position.

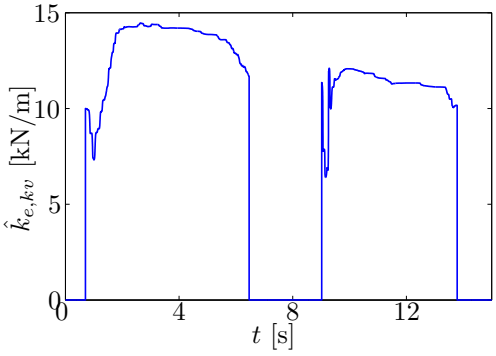

Fig. 4.26: Estimated stiffness of Kelvin-Voigt model for reconstruction method without knowledge of the object location.

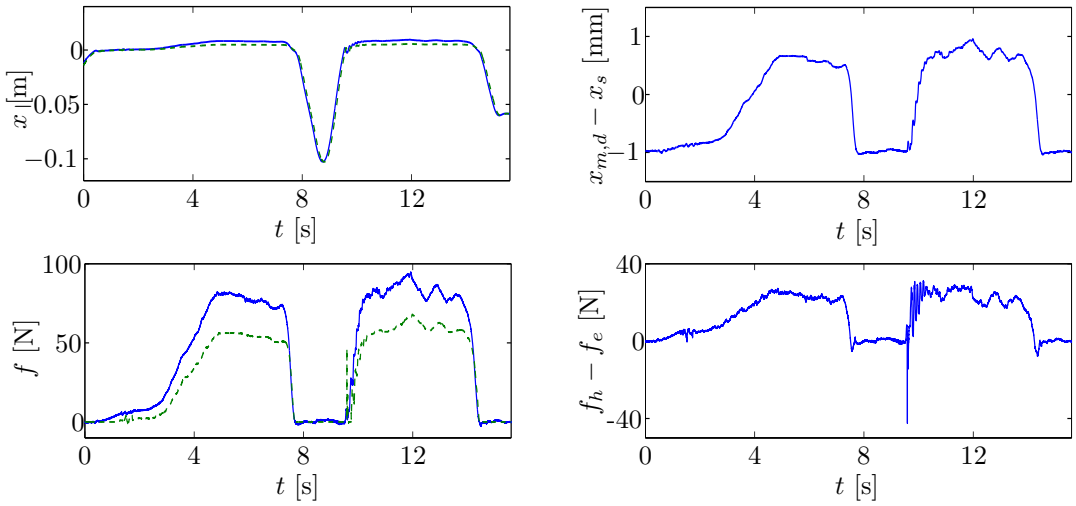

(a) Position and force tracking (b) Tracking and force error

Fig. 4.27: Experimental results for reconstruction method based on approximate knowledge about the object location with $T_d = 50$ ms time delay. Master position and force (blue, solid), slave position and force (green, dashed), and reconstructed force (red, dash-dot). The tracking error is determined between delayed master position $x_{m,d} = x_m(t - T_d)$ and slave position.

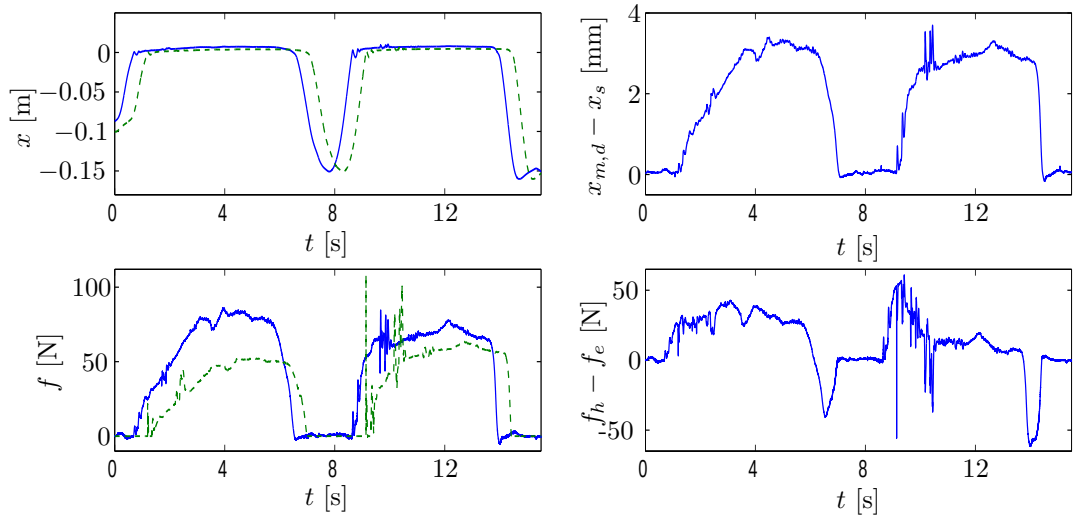

(a) Position and force tracking (b) Tracking and force error

Fig. 4.28: Experimental results for reconstruction method based on approximate knowledge about the object location with $T_d = 500$ ms time delay. Master position and force (blue, solid), slave position and force (green, dashed), and reconstructed force (red, dash-dot). The tracking error is determined between delayed master position $x_{m,d} = x_m(t - T_d)$ and slave position.

with a pre-specified probability, in this case 99.73 %. If contact is not detected at the assumed object location, it is iteratively shifted until contact is established. Fig. 4.27 and 4.28 show position and force tracking for $T_d = 0.05$ s and $T_d = 0.5$ s. A safe interaction is guaranteed with a probability of 99.73% for any time delay and impact velocity. In the bachelor thesis by M. Axenbeck [230], experiments were conducted up to 5 s.

The results show a position error between master and slave site, which is independent of the time delay. The accuracy of the object's location is again the critical factor for the position tracking between master and slave. As the first guess of the object's location was not perfectly corrected, the location of virtual and real object differ also for the second contact. This leads to the position error, which again results in a force error between measured and reconstructed force. As the object location is in most cases presented before first contact is established on slave site and the object dynamics is primarily unknown, the environment force is not tracked well at the beginning of the first contact. This becomes evident for $T_d = 0.5$ s, see Fig. 4.28.

In summary, if time delay is present in the communication channel, the remote objects cannot be presented realistically during the first contact. For the second contact, on the contrary, both reconstruction approaches present the remote object with a high degree of fidelity, as defined by Lawrence [116], to the operator. If the object location cannot be determined a priori, a compliant behavior on slave site and a mis-placed virtual object on master site deteriorate the fidelity. Even though the object location can be measured prior to touching the object, the object dynamics can only be guessed. Regarding safety, the second approach incorporating a priori knowledge about the object is superior to the first one.

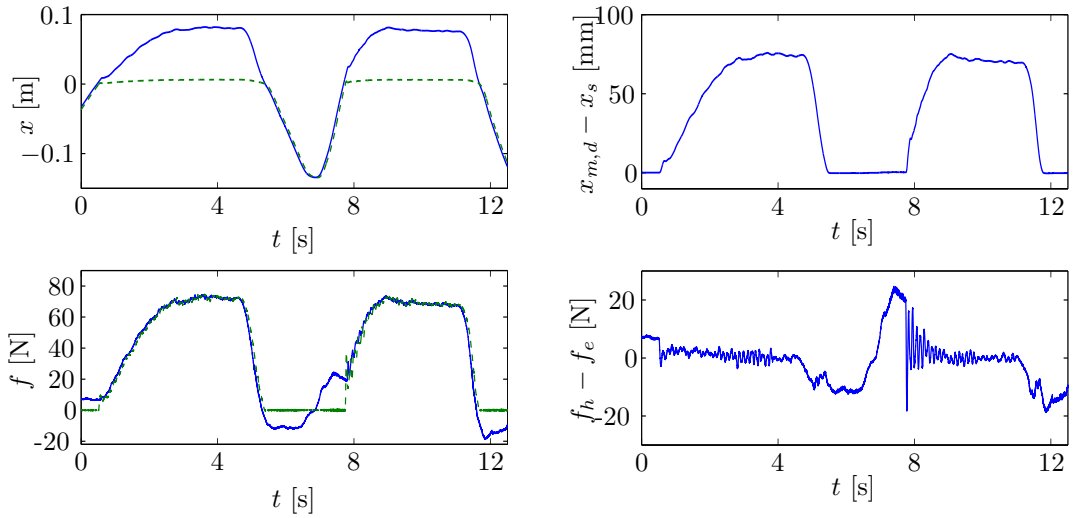

(a) Position and force tracking

(b) Tracking and force error

Fig. 4.29: Classical FaFa architecture with $T_d = 50$ ms and $b_o = 100$ Ns/m: Position and force tracking between local (solid) and remote site (dashed). The tracking error is determined between delayed master position $x_{m,d} = x_m(t - T_d)$ and slave position.

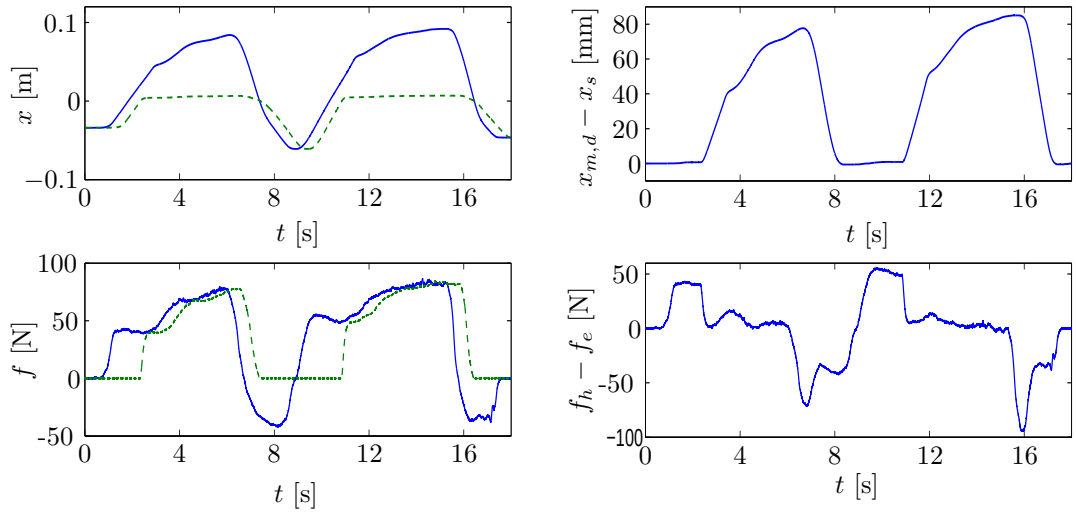

(a) $T_d = 0.05$ s, $b_o = 100$ Ns/m (b) $T_d = 0.5$ s, $b_o = 1000$ Ns/m

Fig. 4.30: Classical FaFa architecture with $T_d = 500$ ms and $b_o = 1000$ Ns/m: Position and force tracking between local (solid) and remote site (dashed). The tracking error is determined between delayed master position $x_{m,d} = x_m(t - T_d)$ and slave position.

4.7 Comparison with Classical Control Concept

In order to allow for a fair and comprehensive conclusion about model-mediated teleoperation, it is compared with a classical, two-channel control concept as presented in Sec. 2.3. The parameters were tuned such that they provide the highest degree of fidelity according to the transparency definition by Lawrence [116] while providing asymptotic stability. First, the experimental results of a classical two-channel architecture with force-force exchange are presented. Subsequently, the results are compared in terms of fidelity with the results for model-mediated teleoperation, see Sec. 4.6. For evaluation, position, force, and impedance tracking properties are determined based on the normalized root mean square error between (artificially) delayed position/force/impedance and slave position/force/impedance, $\text{NRMSE}_{\boldsymbol{Z}}$, $\text{NRMSE}_{\boldsymbol{f}}$ $\text{NRMSE}_{\boldsymbol{x}}$, see also Appendix B.1. The results are furthermore averaged over three trials and summarized for the different approaches in Table 4.3.

4.7.1 Evaluation of Classical Control Concept

One suitable approach for controlling the admittance-type experimental devices is a position-based admittance control as described in Sec. 2.3.2.1. The measured operator and environment forces are sent from master to slave and slave to master, respectively, see Fig. 2.6. For the 6 DoF experimental setup with negligible communication deficiencies as presented in Appendix A.6, the virtual mass and damping matrices of the admittance, which have to be equal on master and slave site, were chosen as $\boldsymbol{M}_a^{\text{trans}} = 10\ \boldsymbol{E}$ kg, $\boldsymbol{B}_a^{\text{trans}} = 10\ \boldsymbol{E}$ Ns/m for translations and $\boldsymbol{M}_a^{\text{rot}} = 0.2\ \boldsymbol{E}$ kgm^2, $\boldsymbol{B}_a^{\text{rot}} = 0.5\ \boldsymbol{E}$ Nms/rad for

rotations. While the contact with the silicone cube was stable, stable contact with the steel plate was only partly achieved. Comparing the admittance parameters with those of the model-mediated teleoperation, see Sec. 4.6, the virtual mass of the FaFa architecture had to be doubled and the virtual damping had to be increased 10 times in order to establish stable contact. As a consequence of the increase in the admittance parameters, higher forces had to be applied in free space compared to model-mediated teleoperation.

Experimental results were also obtained for the 1 DoF experimental setup with time delay in the communication channel. The admittances on both sites exhibit a mass-damper characteristic with an inertia of $m_a = 2.3$ kg and zero damping. These parameters were also used on master site for model-mediated teleoperation. However, even for a small time delay of $T_d = 0.05$ s, a stable contact could not be established. To achieve a stable contact, the virtual damping had to be increased to $b_a = 100$ Ns/m. Position and force tracking for this architecture are shown in Fig. 4.29. While force tracking is very accurate, a position error between master and slave position is observed during contact. This position error can slightly be reduced through an accurate compensation of the end-effector masses. Due to the high virtual damping, this correction will, however, not reduce the position error significantly. Due to a force error at the beginning of contact, see Fig. 4.29(b), and the large virtual damping of $b_a = 100$ Ns/m, the desired master position would result in a large penetration of the remote object. This desired master position can be tracked on master site, while it cannot be tracked on slave site as the device is mechanically constrained by the object. This leads to the position error between master and slave site and leads to a deterioration of the perception of the remote object. An increase in the time delay of up to $T_d = 0.5$ s while being able to establish a stable contact is only possible by increasing the damping to $b_a = 1000$ Ns/m, see Fig. 4.30. Besides the position error during contact, the free space fidelity is highly deteriorated. For this specific setting, a force over 40 N had to be applied in order to accelerate the object.

In summary, stability and fidelity are conflicting objectives regarding the classical control approach, while a trade-off between safety and fidelity has to be found for model-mediated teleoperation. Moreover, the classical approach has a limited applicability for systems with large time delays.

Tab. 4.3: Average root mean square error over several trials between master and slave position $\overline{\text{NRMSE}}_{\boldsymbol{x}}$ [%], master and slave forces $\overline{\text{NRMSE}}_{\boldsymbol{f}}$ [%] as well as between environment and transmitted impedance $\overline{\text{NRMSE}}_{\boldsymbol{Z}}$ [%] for the different reconstruction approaches and the classical control approach.

Control concept	$\overline{\text{NRMSE}}_{\boldsymbol{x}}$ $T_d = 0.05/0.5$ s	$\overline{\text{NRMSE}}_{\boldsymbol{f}}$ $T_d = 0.05/0.5$ s	$\overline{\text{NRMSE}}_{\boldsymbol{Z}}$ $T_d = 0.05/0.5$ s
MM without prior knowledge	30 / 17	15 / 13	15 / 11
MM with prior knowledge	36 / 51	26 / 27	23 / 24
FaFa	870 / 562	2 / 11	39 / 45

4.7.2 Discussion

This section presented experimental results for model-mediated teleoperation and for a classical control concept. The results show the applicability of model-mediated teleoperation to static and movable objects in 6 DoF as well as to teleoperation systems with large time delay in the communication channel. While stability is not a limiting factor here, the first contact with a static remote object can result in safety problems for the slave device and the object due to large forces. As a remedy to this issue, knowledge about the object location can be obtained before first contact using a distance sensor or vision-based object recognition. In this thesis, the object's location was determined based on the measured force on remote site. As this signal is noisy, the object location cannot be determined exactly. As a result, the approach with knowledge of the object's location is not superior to the approach without prior knowledge of the object's location. The accuracy and superiority of the reconstruction method based on prior knowledge of the object's location depends strongly on how accurately the object's location is determined. Especially for stiff objects, small discrepancies between measured and real object location lead to differences in the master and slave position and, as a consequence, also to force errors.

The comparison between model-mediated teleoperation and the classical control concept is based on the NRMSE for positions, forces, and impedances, see Table 4.3. The results show a significantly better position tracking performance for MM teleoperation, but a worse force tracking performance. Thus, the fidelity as defined by Yokokohji [218] cannot be shown to be considerably improved. According to the NRMSE between environment and transmitted impedance, model-mediated teleoperation provides a more realistic representation of the environment than the classical approach. Thus, fidelity as defined by Lawrence [116] is shown to be significantly improved with model-mediated teleoperation. Model-mediated teleoperation is furthermore applicable to systems with time delays of up to several seconds, see also [230].

In summary, the experimental results confirm the theoretically found superiority of model-mediated teleoperation regarding a realistic haptic impression of the remote environment as defined by Lawrence [116] for a large range of time delays.

4.8 Summary

Teleoperation systems are supposed to be stable and to exhibit a high degree of fidelity. However, stability and fidelity, are conflicting objectives. Classical control approaches focus on guaranteeing stability for a wide range of operator behaviors and remote environment dynamics. As a consequence, the degree of fidelity is limited. Considering environment-related model-mediated teleoperation, the focus is shifted from the concern of realizing a stable system to the question of how to improve fidelity without risking oscillations or unstable behavior. The idea of model-mediated teleoperation is to generate a haptic map of the remote environment and to locally connect the operator to a virtual reconstruction of this map. This allows to achieve considerable improvements in fidelity and makes the approach applicable to systems with medium to large ($\geq$ 1 s) time delays. In order to apply model-mediated teleoperation, adequate environment models, fast and accurate es-

timation techniques, and suitable reconstruction methods have to be selected. The known implementations i) lack a comparison and investigation of different implementation possibilities regarding environment modeling, estimation, and reconstruction, and ii) are limited in their applicability to translational DoFs and static objects only.

This chapter addressed these aspects in simulations and experiments. Model-mediated teleoperation is now applicable to 6 DoF manipulation tasks involving static and movable objects. Suitable environment models and estimation technique were identified. Especially for static objects, the classical linear Kelvin-Voigt model was found to be suitable for describing stiff objects, while the nonlinear Hunt-Crossley model can accurately model soft objects. Thus, a hybrid modeling technique was selected for describing static objects. Experimental results confirmed the theoretical finding. Four modifications of recursive least-squares (RLS) and an adaptive identification method were compared with each other for estimating the environment dynamics. It was shown that an RLS approach with self-perturbation outperforms the other estimation techniques in terms of convergence time, tracking performance, and noise rejection. Differences regarding the reconstruction methods were discussed based on an experimental evaluation for systems with medium to large time delays. Depending on the reconstruction method, the system was found to be either completely safe with a small risk of high environment forces, but missing a high degree of fidelity or it was found to be unsafe, but providing a high fidelity. Finally, experiments were performed to show the applicability of model-mediated teleoperation to 6 DoF manipulation tasks involving static and movable objects. The comparison with a classical controller based on experimental results finally proved the superiority of model-mediated teleoperation with respect to fidelity as defined by Lawrence [116]. This result is dependent on how accurately the remote environment can be measured and estimated. Strong discrepancies in the object's location can e.g. lead to position and force errors between master and slave site.

In summary, it was shown that model-mediated teleoperation is a transparency-oriented control concept, that is applicable and superior to classical controllers in terms of fidelity as defined by Lawrence [116]. The approach was shown to be beneficial for systems with negligible, medium, and large time delays up to several seconds. For negligible or small time delays, the classical control approaches have the advantage of a small implementation effort.

Yet, model-mediated teleoperation is only as good as the model is. Also, due to the limited number of presented models only certain classes of manipulation tasks can be performed with the approach so far. One future direction should therefore be directed to further extend the class of objects as well as the online identification of the type of object. This knowledge can be obtained online: i) using additional sensors such as cameras, laser range finders, or ultrasonic devices, ii) employing an intention recognition algorithm with the currently executed task as output, see e.g. [191, 192, 242], or iii) through direct feedback from the operator in the form of e.g. an object selection from a menu or via speech. Another interesting aspect would be to combine classical control approaches with model-mediated teleoperation. When selecting a classical control concept whenever a suitable object model cannot be found, any teleoperation task can be realized. The degree of fidelity will certainly be reduced if an unknown object/task is manipulated/performed, but it will be high for known objects/tasks. The limiting factor for applying classical control

concepts is the time delay: stabilizing control parameters could not be found for large time delays. Especially for stiff objects, the object was penetrated strongly as long as the operator did not receive haptic feedback due to time delay, such that large force peaks occurred.

The first part of this thesis was dedicated to transparency-oriented control concepts. Besides transparency, performance is an important design objective for haptic teleoperation systems. The following chapter presents an advanced performance-oriented control concept. The integration of transparency- and performance-oriented controllers into one multi-criteria control concept will be presented subsequently.

5 Performance-Oriented Control Concept

The connection of the operator with a local, remote, or virtual environment via a haptic device offers the possibility to continuously combine human actions with computer-generated haptic commands. The extrema of the resulting shared control system are *manual control*, where the human influences solely the actions of the system, and *autonomous control*, where the machine has complete authority over the system [182]. Between these extrema, there is a continuum of haptic shared control between human and machine, see Fig. 5.1. In aviation and automation, the term H-metaphor and its implementation, H-mode, is often used in order to describe the possibilities for sharing the control between a human and a fully automated system, see [58, 67]. The H-metaphor refers to the example of horse riding. If a horse is given a direction where to go, it will autonomously find its path to follow this direction without running into trees, people, or other obstacles. Simultaneously, it continuously perceives changes in the human behavior and can react to them. The rider, on the other hand, can concentrate on choosing the optimal direction while being aware of the horse's actions. It can let the horse go or take over control.

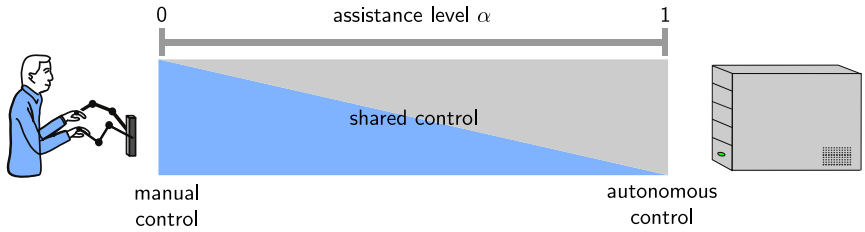

Fig. 5.1: Haptic shared control system: human and assistance share the authority over the system's actions, see also [57].

Haptic assistance is the most prominent approach for a performance-oriented controller design for teleoperation systems. The objective of haptic assistance is to improve performance beyond performance of manual control, i.e. to facilitate manipulation tasks in terms of e.g. reduced task completion time, control effort, or mental workload or to teach a human how to perform a certain task. Typical shared control systems can be found e.g. in directly operated microsurgery [15, 108] or in teleoperated applications like minimally invasive surgery [1] or maintenance [205]. All tasks are quite demanding for the user. Another important application is training or rehabilitation of motor skills [48, 109, 110, 120, 131, 207], where haptic assistance can be used to continuously transfer a motor skill to a human. Further application areas can be found in vehicle control, see also [3, 4]. Haptic assistance has been added e.g. to mobility aids for elderly people like walking support systems [36, 221] or powered wheelchairs [40, 208] and recently was also introduced for aircrafts [58, 67, 182] and automobiles [59, 71, 145].

This chapter introduces a design space for adaptive, user- and task-adapted haptic assistances, which is unique in the known literature. Special focus lies on the authority

distribution between human and machine. When analyzing current design possibilities for the authority policy of a haptic assistance, two main research directions can be distinguished:

1. Approaches, where the assistance is supposed to behave human-like. The system should be experienced as a human partner and task performance should be similar to one observable in human-human collaboration, see e.g. [54]

2. Approaches, where the superior *technical* capabilities of machines, high speed, precision, payload, and a constant performance are combined with the superior *cognitive* capabilities of humans in handling unknown situations in varying or unstructured environments. The capabilities of the haptic device are exploited in order to achieve a task performance beyond manual control or human-human collaboration.

This thesis focuses on the latter approach and aims at developing haptic assistances for considerably facilitating manipulation tasks from a quantitative and qualitative point of view.

As a first step towards a systematic formulation and exploration of haptic assistances, a general framework is introduced, see Fig. 5.2. It shows the identified functional units and their interdependencies of a haptic assistance. According to this framework, a haptic assistance can be represented as a concatenation of a *path planning*, a *control*, and an *interaction design unit*. The interaction design unit is responsible for analyzing the actual scene as well as for estimating human intentions, cognitive, and mental states and to finally decide on the activated assistance. The selected assistance is then realized by the path planning and control unit. Having a closer look into the control unit two units are again distinguished: *assistance control* and *assistance policy*. The assistance controller processes the desired path and calculates a tentative assisting force or motion. As shown in Fig. 5.1, the assistance policy unit decides on the assistance level α, and, thus, on the authority distribution between human and machine. The assistance level is then passed to the assistance control unit where it modifies the control parameters or the assisting force/motion and, thus, decides how the assistance influences the operator's commands.

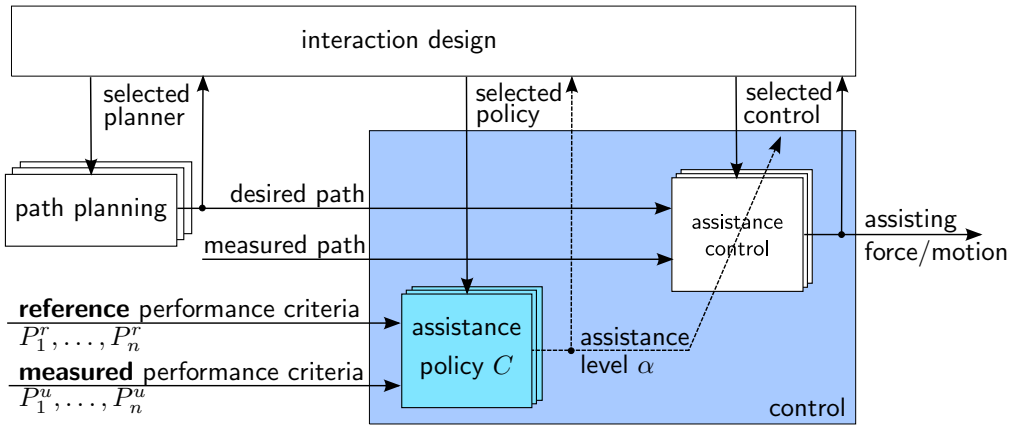

Fig. 5.2: Haptic assistance consisting of interaction design, path planning, and control unit.

A variety of concepts for designing the path planning and control unit of a haptic assistance have already been proposed, see Sec. 2.4.2.2 and [162, 238] for an overview. In

these cases, a constant assistance level is selected and the constant output of the assistance policy unit is multiplied with the output of the assistance controller. With these assistance concepts, the performance can be significantly improved. In [172] it was e.g. shown that performance improvements of up to 70 % can be achieved for the selected performance criteria. Yet, the assistance level has to be selected carefully: a too small assistance does not facilitate the task for the user, and a too large assistance does not keep the user in control such that his/her cognitive attentiveness may drop during task execution, see also [207]. So far, the assistance levels are mostly designed heuristically and with respect to one performance criterion only. Thus, one performance criterion may be improved while another probably equally important criterion may be deteriorated. Another disadvantage of a constant assistance is that it cannot react to unknown situations. Moreover, it is known from human-human collaborative manipulation, that the workload sharing between two humans is changing during task execution and that they take over different roles, see [166]. Current research focuses therefore on the development of time-varying assistance policies that adapt to the task and/or user [48, 120, 121, 150, 206, 221]. Employing adaptive assistance policies, it can be expected that a similar task performance as with constant assistance is achieved while effort and failure rates are reduced. If designed correctly, it can furthermore be hypothesized that an adaptive haptic assistance can result in a higher acceptance by the human operator. In summary, there exist constant and adaptive assistance policies in the known literature. A systematic design tool and a systematic extension of known assistance policies does, however, not exist.

This chapter introduces a design space for systematically analyzing and exploring the assistance policy unit. The proposed design space not only allows to classify state-of-the-art implementations, but also to systematically expand them. The introduced design space proposes three orthogonal design criteria. This allows to systematically select constant and adaptive assistance policies for a specific application. The second contribution is the implementation, evaluation, and comparison of so far unexplored areas in the introduced design space. Special emphasis is given to implementations that optimize more than a single performance criterion and/or dynamically changing assistances. So far, only one approach by Urdiales et al. [206] investigated a multi-criteria assistance policy for powered wheelchairs. This chapter presents a similar approach as in [206] together with two new multi-criteria assistance policies. In contrast to [206], the assistance policies are applied to haptic manipulation tasks. Some of the proposed approaches for designing the assistance policy unit are tuned according to a user study with constant assistance levels. The results from this user study are important for analyzing the effect of the assistance level on different performance measures. Based on these results, a multi-criteria performance measure is developed. Furthermore, a measure for determining whether human and assistance agree or disagree in their task is introduced. As will be shown in experiments, this measure is especially useful for making haptic assistances adaptive and flexible in situations that are unknown to the system. The extensions of the design space were tested in a haptic shared control system, where a user interacts with a virtual haptic assistance to manipulate an object in a virtual environment. It is analyzed a) which assistance policy leads to the best performance as well as highest user comfort and acceptance, b) which role plays the selection of the reference in this context, and c) whether approaches evaluating multiple

performance criteria can outperform approaches based on a single criterion. These research questions are addressed by means of a case study for qualitatively comparing the different implementations and by means of a user study that statistically evaluates the implementations of the design space from a quantitative and qualitative point of view.

The remainder of this chapter is organized as follows: Sec. 5.1 is devoted to the introduction of the design space and the analysis of the identified design criteria. In order to classify current implementations into the proposed framework, related work is presented and discussed in Sec. 5.2. The resulting classification of current implementations allows to identify so far unexplored areas in the design space. These are exploited in a user study. The research questions are formulated in Sec. 5.3 and the scenario is presented in Sec. 5.4. The chapter finishes with a detailed evaluation of the experimental findings in Sec. 5.6.4 and a summary in Sec. 5.7.

5.1 Design Space for Assistance Policy Module

As shown in Fig. 5.2, the output of the assistance policy module is the assistance level α. The assistance level strongly influences the authority distribution between human operator and assistance. In order to design the authority of the assistance in a suitable manner, this section presents a design space for the assistance policy module. The design tool allows to exploit different designs for adaptive, user- and task-adapted assistances and to determine the most promising approach.

The assistance policy module can be regarded as a controller. The controller output is the assistance level α. The assistance should take over control if the performance gets worse and vice versa. The performance is consequently the reference for the controller. As reference performance, either a single performance criterion or a combination of multiple performance criteria can be selected. Moreover, the reference can be *external* relating to e.g. the performance of a trainer. Or, it can be *internal*, if only the user performance is used for determining the assistance level. For all types of references, the controller type can finally be selected. It can range from *constant* over *switching* to *continuously-adapting* linear and nonlinear control strategies or assistance policies. These three aspects for the design of the assistance policy module, the performance criteria, the reference, and the assistance policy represent the three axes of the design space, see Fig. 5.3.

Technically speaking, the assistance policy module of a haptic assistance determines a proper assistance level α out of the actual user performance $P^u = f(P_1^u, \ldots, P_n^u)$ that is related to a certain reference performance $P^r = f^r(P_1^r, \ldots, P_n^r)$. The design process for the assistance level α involves i) to select the performance criteria $P_1, \ldots, P_n$ and to decide on their combination into a single measure P ii) to select the reference performance P^r and iii) to decide on the actual assistance policy C. This problem can be formulated as follows:

$$\alpha(t) = C(P^r, P) = C(f^r(P_1^r, \ldots, P_n^r), f(P_1^u, \ldots, P_n^u)). \tag{5.1}$$

The three axes i) performance criteria, ii) reference performance and iii) assistance policy are independent from each other, such that any combination in this design space can be realized. In the following sections each of the three axes will be discussed in detail.

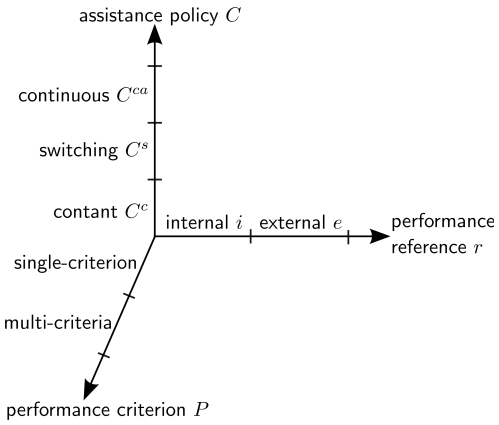

Fig. 5.3: Design space of assistance policy module. The performance criteria, the reference performance, and the control policy span the three orthogonal axes of the design space.

5.1.1 Performance Criteria

A series of qualitative and quantitative performance measures can be considered when designing haptic assistances. In the following section some of the most important performance measures P_i that can be considered in this context are listed. A discussion on differences between a single- and a multi-criteria performance measure follows.

5.1.1.1 Performance Measures

A) Task Performance: One of the main objectives for the design of a haptic assistance is high task performance. A variety of task performance measure are listed in [147]. High task performance can be achieved by shifting control to the haptic assistance if the action plans of human and assistance are consistent and the haptic assistance is provided with all required information to perform the task. This, however, can lead to a strong dependence of the human on the assistance as shown in [131]. Consequently, the user will have difficulties in performing the task without assistance and may be poorly prepared for unexpected situations. It is therefore desired to keep the human in the loop and provide only as much assistance as needed. This point is especially important for training and rehabilitation scenarios.

B) Effort: Effort represents the physical workload that is required for performing the task. Mostly, measures based on the evaluation of forces or energy are used. In order to avoid fast fatigue of the operator, it is desired to keep the effort applied by the operator low. This can be achieved by increasing the authority of the assistance.

C) Agreement: Human and assistance can disagree on their action plan, e.g. i) if events that are unknown to the system take place and no suitable haptic assistance is available, ii) if human intentions are not or wrongly recognized and an unsuitable assistance is selected, iii) if obstacles are not correctly detected by the assistance, or iv) if the user induces unexpected changes in his/her action plan. In all these cases, the system should

be able to recognize these situations and to react with a reduced assistance level α, such that the user is not hindered by the haptic assistance, but rather has the freedom to modify the action plan. Otherwise, a considerable degradation in task performance or even task failure can occur.

D) Smoothness: Smoothness is a further criterion to be considered for the design of haptic assistances as jerky movements induced by the assistance may affect task performance negatively. Smoothness and assistance level α can stay in different relationships to each other depending on the context of the task to be considered: At the beginning of a rehabilitation or motor learning task for example, users can be imcapable of performing smooth movements and, thus, strong support by the machine is beneficial. As the user's movements become smoother, the assistance level can be reduced. On the other hand, a high level of assistance in manipulation or vehicle driving tasks can result in very jerky movements if the human changes his action plan unexpectedly due to e.g. suddenly appearing obstacles. In such a case, the assistance level should be reduced if non-smooth movements are detected.

E) Perceived Workload: Perceived workload plays an important role when designing haptic assistances. Depending on the human cognitive and mental state a reduction of the workload can be desirable. This can be achieved by increasing the assistance level of the haptic assistance and, thus, shifting the control towards the machine. Physiological signals can be used to give online indications of the user's perceived workload. Alternatively, the user can be asked while executing the task about the perceived workload and using speech recognition (instead of using intention recognition) his/her answer can be mapped to a suitable assistance level. An offline way of determining perceived workload are questionnaires.

F) Efficiency: Efficiency relates performance to effort or perceived workload, see e.g. [25]. Either a quantitative effort measure such as mechanical work or a qualitative measure such as the perceived workload described above can be used. A small effort/workload and a high performance result in a high efficiency. As the haptic assistance is supposed to facilitate the task for the user, i.e. to reduce the effort/workload and increase the performance, a low efficiency can be improved by shifting the control and consequently also the workload/effort to the haptic assistance.

5.1.1.2 Single- vs. Multi-criteria Performance Measures

Sometimes a single performance criterion is of utmost importance and should consequently be selected as the only performance criterion when designing the assistance policy. If, however, no performance criterion has an outstanding priority, the main goal is to achieve a good trade-off between the most important criteria. As only one parameter, the assistance level, is influenced, the single measures have to be incorporated into one quantity P that can be used to adjust the assistance level:

$$P = f(P_1, \ldots, P_n) \tag{5.2}$$

where $P_1, \ldots, P_n$ and the resulting performance P can be constant or time-varying. Time-varying performance measures will be denoted by $P_i(t)$ while performances measures that remain constant over the whole task are referred to as $\overline{P}_i$.

5.1.2 Performance Reference

The reference performance P^r to the assistance policy module is another design parameter. An external and internal reference performance denoted as P^e and P^i, respectively, are distinguished in this work. Thus, the set from which the reference performance can be selected is given by $P^r \in \{P^e, P^i\}$.

5.1.2.1 External Reference Performance

If the haptic assistance is used for training or learning purposes, an external reference performance in the form of e.g. an expert behavior, the behavior of a user group or an artificially designed reference such as minimum-jerk movements is often used for the assistance policy module. Whenever the user gets close to the external reference performance P^e, the assistance level is reduced and vice versa.

5.1.2.2 Internal Performance Reference

When assisting everyday activities like walking with mobility aids, performing a task at distance using teleoperation technology or steering a vehicle, such an external reference performance is often not available. Moreover, the environment may change such that the reference performance becomes unsuitable. In this case, the user performance over time is the only available reference. It will be referred to as internal reference performance P^i and corresponds to the user performance P^u: $P^i = P^u$.

External as well as internal references can be either determined offline and represent the mean performance over the whole trial. Or, they are evaluated online: an external reference performance is represented by a recorded performance curve over time, the internal reference performance is calculated for each time step online. Offline references are denoted as $\overline{P}^r$, online references are referred to as $P^r(t)$.

5.1.3 Assistance Policies

The third axis in the proposed design space is the assistance policy. It can be selected arbitrarily ranging from a constant over linear to nonlinear, and switching assistance policies. The class of assistance policies considered in this work are a constant assistance denoted as C^c, a switching assistance referred to as C^s and continuously adapting assistances denoted as C^{ca}.

5.1.3.1 Constant Assistance Policy

The constant assistance policy sets the assistance level α to a constant. The constant value is selected depending on the offline reference performance $\overline{P}^r$, and can be based on

an average mean performance from a user group (external reference performance) or from one or several training trials of the user him-/herself (internal reference performance):

$$\overline{\alpha} = C^c(\overline{P}^r) = \text{const.} \tag{5.3}$$

5.1.3.2 Switching Assistance Policy

A switching assistance policy selects the assistance level from a discrete set of constant assistance levels $\alpha \in \{\overline{\alpha}_1, \ldots, \overline{\alpha}_n\}$. The switching between the different conditions $S \in \{S_1, \ldots, S_n\}$ depends on the performance criteria $P^u(t)$ and P^r. While $P^u(t)$ is tracked over time, P^r can be either calculated offline or online. This leads to the assistance policy

$$\alpha(t) = \begin{cases} \overline{\alpha}_1 & \text{if } \xi_1(P^u(t), \overline{P}^r \text{ or } P^r(t)) = \mathsf{true} \\ \vdots & \\ \overline{\alpha}_n & \text{if } \xi_n(P^u(t), \overline{P}^r \text{ or } P^r(t)) = \mathsf{true}. \end{cases} \tag{5.4}$$

5.1.3.3 Continuously-Adapting Assistance Policy

A third possibility is to continuously modify the assistance level depending on the reference performance $P^r(t)$, and the user performance $P^u(t)$ over time. Linear and nonlinear adaptation laws can be realized to achieve adaptive and proactive assistance behavior:

$$\alpha(t) = C^{ca}(P^r(t), P^u(t)). \tag{5.5}$$

5.2 Categorization of Related Work

In this section state-of-the-art implementations of the assistance policy module are reported and classified according to the introduced design space, see Fig. 5.4.

Marayong & Okamura [133] proposed a *constant assistance level* based on an *external reference performance*. Mean performance of a user group served as the reference. For selecting the constant assistance level, they investigated the relationship between assistance level and task performance of a user group for a path following task as well as for off-path targeting and an obstacle avoidance task. The assistance was designed for the path following task and was not aware of other targets or obstacles. As expected, if user and assistance did not agree, i.e. in the investigated off-path targeting task and the obstacle avoidance task, task performance of the user group was found to be worse with increasing assistance level. For the path following task, this relationship was inverted. As a solution, Marayong & Okamura [133] proposed a constant assistance level yielding an optimal trade-off between the performance curves for tasks performed in agreement and tasks performed in disagreement with the haptic assistance.

As shown in [131], the user easily gets dependent on a constant assistance level. Thus, Esen [48] proposed a *proportional-type controller with an external reference performance* in the area of motor skill learning. A virtual trainer performance was used as reference and guidance was applied proportional to the difference between the user and trainer performance. The guidance was applied to force tasks and the user felt if the applied force

was diverging from the trainer's force. Information about how to correct the applied force was not given. Only the best performance (of the trainer) was taken into account, while a worst reference performance was not used.

For improving a mobility aid for elderly people Yu et al. [221] employed an *external reference performance* as well and combined it with a *nonlinear assistance policy*. An ideal system behavior, more specifically an ideal path, an ideal velocity, and an acceleration profile were used as reference. The assistance level was selected as a nonlinear function of the performance difference between user and ideal system behavior. A forgetting factor determined the responsiveness of the system to the user. As in [48], a worst case system behavior was not taken into account.

Another interesting shared-control approach for powered wheelchairs was presented recently by Urdiales et al. [206]. The authority between human and machine was decided online by evaluating the efficiency of human and machine on a *continuous scale*. Efficiency was determined as a combination of three criteria: smoothness, directness, and safety. Each criterion was weighted equally. The criteria for adaptation were dependent on the current direction, on (partial) goals and obstacles, and, thus, represent an *external reference performance*. The main objective of their continuous control sharing strategy was to keep the human in the loop and, thus, to preserve the "residual capabilities" of the operator as named in [206]. A large user study was conducted in order to evaluate the proposed approach. A statistical analysis was, however, not provided. The performance of the proposed shared-control approach was improved compared to manual and autonomous control. The main conclusion was that the performance became similar between participants with different disabilities.

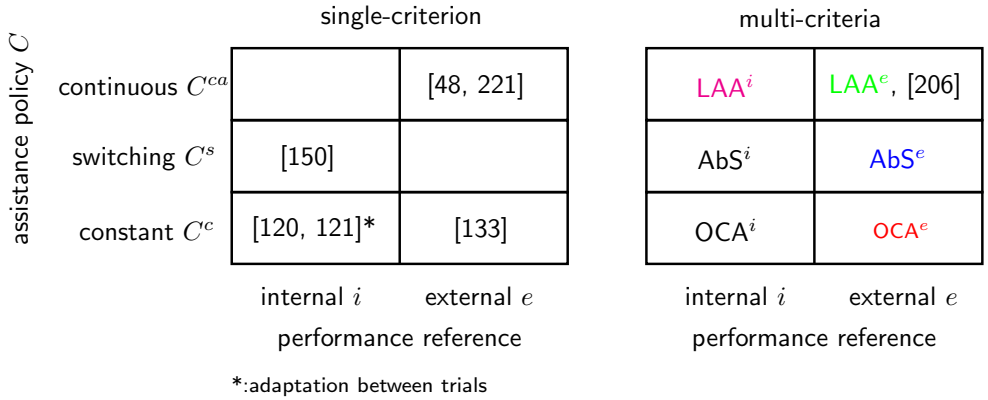

Fig. 5.4: Classification according to introduced design space: State-of-the-art and case study implementations of the assistance policy module. OCA stands for optimal constant assistance, AbS for agreement-based switching, and LAA for linear-adapting assistance. A detailed description of the case study implementations are provided in Sec. 5.4.3.

The question how to design the behavior of an adaptive haptic assistance is also relevant in the area of physical human-robot interaction, aviation, and automation of vehicles. In the area of physical human-robot interaction, Oguz et al. [150] proposed a *switching controller* in the form of a finite state machine with three assistance behaviors: a non-dominant behavior corresponding to a small assistance level, a role-blending behavior and

a dominant behavior corresponding to a high assistance level. Roles of the machine were designed in a discrete way. The user force was used to trigger the transitions between the behaviors. The user force was hereby compared with a threshold that was online adapted to the user as we know from discussions with the authors. This represents an *internal reference performance*. A justification for the selection of the human force measure or the thresholds was not given. Compared to discrete switches between assistance levels, a linear continuous role blending between a passively following robot and an actively guiding robot was proposed in [51]. However, a suitable performance metric for adapting the role of the system has not been proposed so far. Goodrich et al. [66] presented a switching control policy employing a binary user-triggered logic for aviation. As stated in [66], firm inputs by the pilot triggers the transition to a low-authority mode, i.e. the pilot is mainly in control of the system, while loose inputs make the system take over most of the control.

For motor skill learning, Li et al. [120, 121] proposed adapting the assistance level with a *proportional-type controller based on user performance changes*: if task performance became better over trials, the assistance level was decreased. The adaptation process was performed offline, between training trials. The results showed that performance-dependent assistance was more effective than a constant assistance for the considered motor skill learning task.

Few approaches (Esen [48], Yu et al. [221], and Urdiales et al. [206]) adapt the assistance level on a continuous scale and within trials. The approach by Urdiales et al. [206] is the only approach so far where a multi-criteria measure was proposed for adapting the authority between human and machine. This shows that the design space for haptic assistances is not fully exploited yet. Thus, the following section will investigate so far unexplored fields in the proposed design space by employing multiple performance measures and combining them with different assistance policies and references, see the abbreviations in Fig. 5.4 (right).

5.3 Research Questions

Having identified the design space for the assistance policy unit, the remaining part of the chapter will investigate so far unexplored fields in the proposed design space by moving from single to multiple criteria performance measures and combining them with different assistance policies as well as external and internal reference performance. The objective of the assistance policy unit is to suitably combine human and machine capabilities. This implies that a high performance is achieved without impairing the user's comfort and acceptance when working with the system. This is especially important if situations occur that are unknown to the assistance. These aspects are addressed for the different design possibilities based on the following research questions:

RQ I: Which assistance policy leads to the highest performance, user comfort, and acceptance? More precisely:

(a) Do assistances with online adaptive assistance level (adaptation taking place within trials and not between trials) outperform assistances with constant assistance level?

(b) Do switching or continuously adapting assistance policies lead to higher performance, user comfort, and acceptance?

RQ II: Which role plays the selection of the reference performance? Does an approach with internal or external reference performance better suit a task where unexpected events are likely to occur? Such tasks resemble a very important class that can be found e.g. whenever the human intention is detected wrongly and an unsuitable assistance mechanism is selected, or the user induces intentional changes in his/her action plan that are unforeseeable for the assistance.

RQ III: Can approaches evaluating multiple performance criteria outperform approaches based on a single criterion? Does a potential benefit come without cost?

These research questions are discussed for a maze scenario, presented in the following section.

5.4 Exploring the Design Space for a Maze Scenario

The categorization of related work clearly showed that especially assistance policies based on a multi-criteria performance measure are rarely investigated. Furthermore, a comparison between the different design aspects is missing in the current literature. This section is therefore dedicated to explore the area of the design space, where multiple performance measures are used. More precisely, the colored design possibilities in Fig. 5.4 are implemented for a specific scenario and compared with each other in terms of quantitative and qualitative performance. The effect on performance, user comfort, and acceptance is investigated together with the effect of the type of reference performance (internal vs. external) and whether approaches evaluating multiple performance criteria can outperform approaches based on a single criterion. These research questions are targeted qualitatively based on the results of a case study and by means of a user study that allows for a statistical evaluation.

This section starts with the scenario and experimental setup in Sec. 5.4.1. The design of the path planning and assistance control unit is presented in Sec. 5.4.2. Finally, the design space for the selected scenario is spanned in Sec. 5.4.3 followed by the different implementations of the assistance policy module in Sec. 5.4.3.

5.4.1 Scenario and Experimental Setup

Haptic assistances are designed task-dependent and the parameter selection of the assistance controller is dependent on the underlying control architecture. This section introduces the scenario, the control, and the experimental setup.

5.4.1.1 Scenario

The scenarios used for the evaluation were selected to represent abstract versions of tasks found in everyday life. More precisely, a transportation task was selected as standard scenario. A two-dimensional maze (width: 38.2 cm, length: 19.1 cm) was designed, where a virtual object (width: 1 cm, length: 0.7 cm) had to be moved through, see Fig. 5.5 (left).

The virtual object, a square box, was simulated as a mass pushed over the ground. The objective was to move the object as quickly as possible from the start to the end position without touching walls. The haptic assistance is programmed for this standard scenario denoted by SC_{agree}. Restrictions of free space areas due to suddenly appearing walls exist in almost any real environment. Compared to often considered path-following tasks, the scenarios selected for this work leave the user some freedom to move and do not restrict him/her to one specific path to be followed.

In order to evaluate the flexibility of haptic assistances, they were furthermore tested in a second scenario, the assistance is not programmed for. In this second scenario denoted by SC_{disagree}, obstacles in the form of additional rectangular boxes on the path of the haptic assistance were introduced, see Fig. 5.5 (right). The task was not only to avoid touching the virtual walls, but also the obstacles while moving as fast as possible. Since the assistance is not informed about the location of obstacles, it is expected that the user disagrees with the assistance around these obstacles. Unexpected events are likely to occur in real-life situations as the perception system may fail or the human may intentionally change his/her action plan.

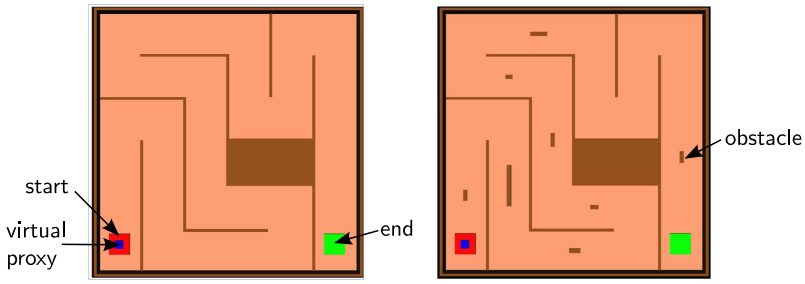

Fig. 5.5: Scenario 1 SC_{agree} (left): maze without obstacles, scenario 2 SC_{disagree} (right): maze with obstacles. The task was to move as quickly as possible from start to end without touching the walls or obstacles.

5.4.1.2 Control, Haptic Rendering and Apparatus

A position-based admittance controller as proposed in [157] was used to render a mass-damper dynamics simulating a box pushed over the ground. Spring-damper models were implemented to haptically render the walls of the maze. In order to achieve a stiff haptic rendering, desired position and velocity $\boldsymbol{x}^d, \dot{\boldsymbol{x}}^d$ of the haptic interface were used instead of the measured position/velocity. If a penetration into an object or wall occurs, the resulting force from the virtual environment was calculated as $\boldsymbol{f}_e = k_e(\boldsymbol{x}^d - \boldsymbol{x}_e) + d_e\dot{\boldsymbol{x}}^d$ where $\boldsymbol{x}_e$ is the position vector where contact with the wall occurs and $k_e = 7000$ N/m, $d_e = 500$ Ns/m for each direction.
The sum of the forces from the haptic assistance $\boldsymbol{f}_{\text{assist}}$, see (5.14), from the haptic rendering of the virtual walls $\boldsymbol{f}_e$, and the forces applied by the human $\boldsymbol{f}_h$ are the input for the admittance filter:

$$\boldsymbol{f}_h - \boldsymbol{f}_e + \boldsymbol{f}_a = m_a\ddot{\boldsymbol{x}}^d + d_a\dot{\boldsymbol{x}}^d \tag{5.6}$$

where m_o, d_o are virtual mass and damping, respectively, and $\ddot{\boldsymbol{x}}^d$ is the desired acceleration of the haptic interface. The desired position was tracked using a high-gain PD-controller. A virtual mass of 5 kg and a virtual damping of 20 Ns/m were chosen for both directions.

The apparatus, a 2 DoF admittance-type haptic device is presented in Appendix A.5. It allows translational motions in the horizontal plane only. The virtual environment was displayed to the user via a monitor.

5.4.2 Implementation of Path Planning and Assistance Control

Guiding virtual fixtures with a computer-generated reference path as shown in Fig. 2.8(a) are a promising haptic assistance regarding quantitative and qualitative performance for the considered scenario. This assistance tries to compensate human-induced errors when performing a task by leading the user towards an error-free path. Rosenberg described virtual fixtures in [172] as perceptual overlays to improve performance. The way of operation is similar to using a ruler when drawing a straight line, as outlined in his paper.

In the *path planning module* of this assistance, the desired path is designed. For the given scenario, the centerline of the maze was used as the desired path for straight movements, while a circular movement was chosen for the curves. In real-world environments, additional sensors such as cameras or laser scanners together with path planning algorithms would be required to define desired paths towards a goal.

The *assistance control module* is responsible for tracking the desired path of the assistance. Task-relevant motions are supported, while deviations from the desired path are constrained. Guiding virtual fixtures are generally realizable on the position and force level.

Remark (Force and Position Decomposition) Figure 5.6 illustrates the following derivations. The reference path is represented by a discrete number of R points:

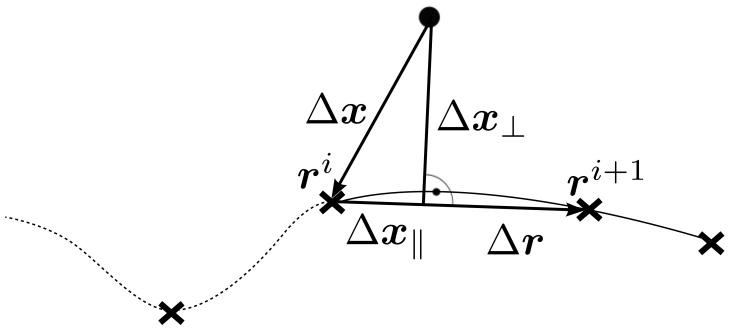

Fig. 5.6: Illustration of position and force decomposition into components tangential and perpendicular to the reference path $\boldsymbol{r}$.

$\boldsymbol{r} \in \{\boldsymbol{r}^1, \ldots, \boldsymbol{r}^R\}$. Assume that the reference point with minimal distance to the position of the remote device is $\boldsymbol{r}^i$. Then, the vector pointing from the current to the next point on the reference path is given by $\Delta\boldsymbol{r} = \boldsymbol{r}^{i+1} - \boldsymbol{r}^i$ and the difference between the current device position and reference point is $\Delta\boldsymbol{x} = \boldsymbol{r}^i - \boldsymbol{x}$. With the normalized vector tangential to the reference path

$$\boldsymbol{n}_\parallel^{\text{trans}} = \frac{\Delta\boldsymbol{r}}{\|\Delta\boldsymbol{r}\|} \tag{5.7}$$

the difference vector to the reference path can be decomposed into a tangential and a perpendicular component:

$$\Delta \boldsymbol{x}_{\parallel} = (\boldsymbol{n}_{\parallel}^{\text{trans}})^T \; \Delta \boldsymbol{x} \; \boldsymbol{n}_{\parallel}^{\text{trans}} \qquad \Delta \boldsymbol{x}_{\perp} = \Delta \boldsymbol{x} - \Delta \boldsymbol{x}_{\parallel}. \tag{5.8}$$

The normalized vector perpendicular to the reference path can consequently be written as

$$\boldsymbol{n}_{\perp} = \frac{\Delta \boldsymbol{x}_{\perp}}{\|\Delta \boldsymbol{x}_{\perp}\|}. \tag{5.9}$$

Similarly, the operator forces can be decomposed into a tangential and a perpendicular component:

$$\boldsymbol{f}_{\parallel} = (\boldsymbol{n}_{\parallel}^{\text{trans}})^T \; \boldsymbol{f} \; \boldsymbol{n}_{\parallel}^{\text{trans}} \qquad \boldsymbol{f}_{\perp} = \boldsymbol{f} - \boldsymbol{f}_{\parallel}. \tag{5.10}$$

The same considerations hold for torques and a respective reference path given in Euler coordinates.

For each of the two directions (tangential/perpendicular), two types of virtual fixtures can be distinguished: active and passive ones. This leads to four different types of virtual fixtures: active or passive in both directions referred to as *active virtual fixture* and *passive virtual fixture*, respectively, as well as active in tangential and passive in perpendicular direction or vice versa, which is referred to as *active*$_{\parallel}$*-passive*$_{\perp}$ or *active*$_{\perp}$*-passive*$_{\parallel}$ *virtual fixture*. A passive virtual fixture scales the applied operator force in order to drive the human back to the desired path [6]. Thus, if the operator does not apply any force, the device does not move either. It is assumed that the reference path has to be followed in a specific direction. Forces in this direction are therefore amplified, while forces in the opposite direction are diminished:

$$\boldsymbol{f}_{vf\parallel} = \begin{cases} \boldsymbol{U}_{\parallel} \; \boldsymbol{f}_{\parallel} & \text{if } (\boldsymbol{n}_{\parallel}^{\text{trans}})^T \; \boldsymbol{f} \geq 0 \\ \boldsymbol{D}_{\parallel} \; \boldsymbol{f}_{\parallel} & \text{else} \end{cases} \quad \boldsymbol{f}_{vf\perp} = \begin{cases} \boldsymbol{U}_{\perp} \; \boldsymbol{f}_{\perp} & \text{if } (\boldsymbol{n}_{\perp})^T \; \boldsymbol{f} \geq 0 \\ \boldsymbol{D}_{\perp} \; \boldsymbol{f}_{\perp} & \text{else} \end{cases} \tag{5.11}$$

where $\boldsymbol{U}_{\parallel}$, $\boldsymbol{U}_{\perp}$ are diagonal matrices with positive elements ≥ 1 for amplification, if $\boldsymbol{n}^T \boldsymbol{f} \geq 0$, and $\boldsymbol{D}_{\parallel}$, $\boldsymbol{D}_{\perp}$ are diagonal matrices with positive elements < 1 for diminishing.

Active virtual fixtures, on the other hand, apply additional forces directed towards and along the desired path [158]. Thus, even if the operator does not apply any force, the assistance would accomplish the task. Often, a spring or spring-damper is fixed between the position of the remote device and the reference path:

$$\begin{aligned} \boldsymbol{f}_{vf\parallel} &= \boldsymbol{K}_{\parallel}^{\text{trans}} \Delta \boldsymbol{x} + \boldsymbol{B}_{\parallel}^{\text{trans}} \Delta \dot{\boldsymbol{x}} \\ \boldsymbol{f}_{vf\perp} &= \boldsymbol{K}_{\perp}^{\text{trans}} \Delta \boldsymbol{x} + \boldsymbol{B}_{\perp}^{\text{trans}} \Delta \dot{\boldsymbol{x}} \end{aligned} \tag{5.12}$$

where $\boldsymbol{K}_{\parallel}$, $\boldsymbol{K}_{\perp}$, $\boldsymbol{B}_{\parallel}$, and $\boldsymbol{B}_{\perp}$ are diagonal matrices with positive elements. In order to avoid excessive forces, the assistance is only activated if the difference is within a predefined distance $d_{\max}$ to the reference path

$$\boldsymbol{f}_{vf} = \begin{cases} \boldsymbol{f}_{vf\parallel} + \boldsymbol{f}_{vf\perp} & \text{if } \|\Delta \boldsymbol{x}\| \leq d_{\max} \\ 0 & \text{else.} \end{cases} \tag{5.13}$$

Another possibility would be to use a nonlinear stiffness, see e.g. [144]. It is important to note at this point that for virtual fixtures applied in translational and rotational directions, the position and orientation of the remote device are coupled. To each reference position, there exist a corresponding orientation. This implies that the selection of the current reference position and orientation have to match. This aspect is, however, only relevant for active virtual fixtures as a passive virtual fixture is independent of the distance to the reference path.

For the considered scenario, only an active virtual fixture perpendicular to the path allows to track the desired path well enough. In order to give the operator the freedom to select the speed tangential to the path, a passive virtual fixture was used for motions along the path, such that the device does not move if no forces are applied on the device. The motion towards the goal was facilitated through force up-scaling, while motions away from the goal were impeded through down-scaling of the applied user force. The force up-scaling reduces the mass-damper dynamics which facilitates to drive with high speed and, thus, decreases the task completion time. In summary, an active$_\perp$-passive$_\parallel$ virtual fixture was used. As active component of the virtual fixture, a virtual spring with stiffness $k_{vf} = 1500$ N/m was fixed between virtual object and path, see (5.12). The scaling parameters of the passive component tangential to the path were set to $U_x^{\text{trans}} = U_y^{\text{trans}} = 0.5$, $D_x^{\text{trans}} = D_y^{\text{trans}} = -0.9$, see also (5.11). The concept of the resulting haptic assistance is illustrated in Fig. 5.7.

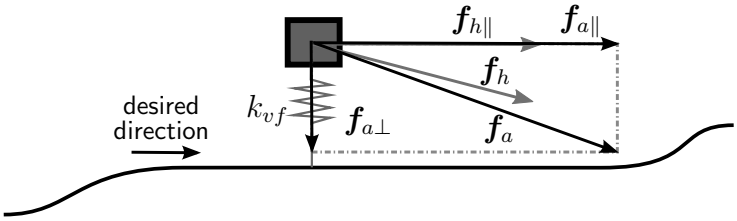

Fig. 5.7: Concept of active$_\perp$-passive$_\parallel$, guiding virtual fixture. Motions perpendicular to the reference path are actively constrained while motions tangential to the reference path are facilitated or impeded through force up- or down-scaling.

The control actions of the haptic assistance were fused with the assistance level from the assistance policy module by independently scaling the force components $\boldsymbol{f}_{vf\parallel}, \boldsymbol{f}_{vf\perp}$ with assistance levels $\alpha_\parallel$ and $\alpha_\perp$, respectively. The components were scaled independently, as the performance criteria for tangential adaptation are different from the performance criteria for perpendicular adaptation, see Sec. 5.4.3.1. The assistance levels were allowed to vary between 0 and 1. The sum of the scaled force components leads to the applied assistance forces

$$\boldsymbol{f}_a = \alpha_\parallel \boldsymbol{f}_{\parallel vf} + \alpha_\perp \boldsymbol{f}_{\perp vf}. \tag{5.14}$$

If both assistance levels were 0, the user had complete freedom over the actions of the system, while maximum haptic support is provided for $\alpha_\parallel = \alpha_\perp = 1$.

5.4.3 Spanning the Design Space

In this section, the three design axes, performance measures, reference performance, and control policy are specified for the considered scenario. Important performance measures are task performance, effort, agreement, smoothness, perceived workload, or efficiency. These can be either combined into a multi-criteria performance measure or a single criterion can be selected. The reference performance can be either external from e.g. a trainer or internal if the user performance only is used. Finally, three classes of control policies are distinguished in the design space: constant, switching, and continuously-adapting. For the selection of a multi-criteria performance measure and for tuning the parameters of some of the proposed approaches the effects of the assistance level on the performance measures are important. A user study with five distinct, constant assistance levels $\alpha_{\parallel} = \alpha_{\perp} = \alpha_c \in \mathcal{A}_c = \{0, 0.25, 0.5, 0.75, 1\}$ was conducted in order to determine these effects. An opportunity sample of 13 participants conducted the experiment. Details on the experimental design, the method of this user study, and the statistical results are provided in Appendix D.1. The results are used for the design of the assistance policies in this section.

5.4.3.1 Performance Measures

In this section, performance criteria, that were identified for the given scenario and assistance, are introduced. They are then combined into a multi-criteria performance measure. As the design of the assistance policy module is based on the selected performance criteria, their selection and combination into a multi-criteria performance measure is one of the most critical steps. If they are not designed properly, the assistance may adapt in a non-intuitive or obstructive way. This can make the task more difficult and irritating for the user and can also lead to performance degradation. For the considered scenario, task performance and human-assistance agreement were identified as important and online quantifiable objectives for the design of the assistance policy module. The goal is to facilitate the manipulation tasks for the operator whenever the operator agrees with the assistance. Otherwise, the operator should take over control. Consequently, both criteria are equally important for the considered task and a multi-criteria performance measure will be used. Offline and online versions for both measures are discussed in the following subsections.

In order to combine measures with different scales (time-, force-based) into a single measure, they are normalized denoted by $N(x)$. The resulting metric does consequently not have a unit. For offline evaluation, all measures are normalized with the maxima found in the dataset with constant assistance levels, as the results from the user study with constant assistance levels are used for tuning some of the approaches. Please note that the maximum value was derived from all V participants, all constant assistance levels $\alpha_c \in \mathcal{A}_c$, and both scenarios summarized in the set Ω_c:

$$\Omega_c = \{v \in \{1, \dots V\}; \alpha_c \in \mathcal{A}_c; SC \in \{SC_{\text{agree}}; SC_{\text{disagree}}\}\}. \tag{5.15}$$

For online evaluation, there are two possibilities for determining the maximum value. Either a worst case estimate is known or assumed or the maximum value is tracked over

time. A worst case estimate requires prior knowledge about the task. As this knowledge was not assumed to be given, the maximum value was tracked online. Offline calculated measures are averaged over the whole trial, while online calculated measures are averaged over an observation window in order to reduce noise. The length L of the observation window was set to 200 samples for the given setup.

Task Performance: There exist a variety of task performance measures, see [147] for an overview. The objective of the task considered in this work is to complete the task as fast as possible and without wall/obstacle contacts.

The time to complete the task was measured offline and determined as the task completion time TCT [s], see also Table 2.1. For online adaptation, relative performance changes during task execution were needed. A suitable measure is the speed tangential to the path $\dot{x}_{\parallel}$ of the assistance as a fast movement in this direction results in a low task completion time. The speed was averaged over an observation window of L samples. For one out of V participants the normalized offline task completion time measure $N(\mathrm{TCT})$ and the normalized online speed measure $N(\overline{\dot{x}})$ are given by

$$N(\mathrm{TCT}) = \frac{\mathrm{TCT}}{\max_V(\mathrm{TCT})} \qquad N(\overline{\dot{x}}) = \frac{\mathrm{mean}_L\, \dot{x}_{\parallel}}{\max_V(\mathrm{mean}_L\, \dot{x}_{\parallel})}. \tag{5.16}$$

The second objective is to minimize contact with the walls of the maze. The normalized collision time with walls or obstacles $N(\mathrm{ET})$ [s] was used as offline measure, see also Table 2.1. For online evaluation, the number of time samples of wall/obstacle contacts C_E within an observation window of L samples was tracked and normalized:

$$N(\mathrm{ET}) = \frac{\mathrm{ET}}{\max_V(\mathrm{ET})} \qquad N(C_E) = \frac{C_E}{L}. \tag{5.17}$$

The normalized task performance $N(P)$ which is to be minimized was selected as the weighted sum of normalized task completion time and normalized error time

$$N(P) = a_1\ N(\mathrm{TCT}) + a_2\ N(\mathrm{ET}). \tag{5.18}$$

In accordance with the task considered in this work speed and error were equally weighted, i.e. $a_1 = a_2 = 0.5$.

Agreement: The agreement measure is based on interactive forces $\boldsymbol{f}_{\mathrm{int}}$ between human and assistance, see also Sec. 2.2.2 for a detailed explanation. Continuous agreement A and disagreement D as introduced in Sec. 2.2.4.2 is calculated separately for the tangential and the perpendicular component. Both, offline and online versions, are denoted by $D = N(\overline{f}_{\mathrm{int}})$ and $A = 1 - N(\overline{f}_{\mathrm{int}})$. The offline interactive forces are averaged over the whole trial with K samples, while the online interactive forces are averaged over a window

of L samples. Disagreement is defined for any direction by

$$D_{\parallel} = N(\overline{f}_{\text{int}\parallel}) = \frac{\text{mean}_{K/L}(|f_{\text{int}\parallel}|)}{\max_V(\text{mean}_{K/L}(|f_{\text{int}\parallel}|))} \tag{5.19}$$

$$D_{\perp} = N(\overline{f}_{\text{int}\perp}) = \frac{\text{mean}_{K/L}(|f_{\text{int}\perp}|)}{\max_V(\text{mean}_{K/L}(|f_{\text{int}\perp}|))}. \tag{5.20}$$

Multi-criteria Performance Measure: We use task completion time, error time, and agreement as criteria for the multi-criteria performance measure, i.e. $P_1 = N(\text{TCT})$, $P2 = N(\text{ET})$, $P3 = D$. Optionally, smoothness, workload, efficiency, and assistance level could be taken into account as well. The objectives differ for the two force components of the haptic assistance (tangential and perpendicular). Objectives to be considered for $\alpha_{\parallel}$ are a short task completion time and a low disagreement. These objectives are summarized in an offline and online multi-criteria performance measure. For $\alpha_{\perp}$, contacts with walls should be avoided resulting in a low error time. As for $\alpha_{\parallel}$, also disagreement should be minimized. If human-assistance agreement is high, the objective of $\alpha_{\perp}$ is furthermore to decrease task completion time. With a large $\alpha_{\perp}$, the risk to make errors, i.e. touching the walls, is low and, thus, the user can increase speed. If human-assistance agreement is low, this objective is negligible compared to the other objectives. Consequently, the objective task completion time was weighted with agreement.

These considerations can be summarized in the following, offline multi-criteria performance measures:

$$\overline{P}_{\parallel} = a_{\parallel 1}\, N(\text{TCT}) + a_{\parallel 2}\, N(\overline{D}_{\parallel}) \tag{5.21}$$

$$\overline{P}_{\perp} = a_{\perp 1}\,(1 - N(\overline{D}_{\perp})) \cdot N(\text{TCT}) + a_{\perp 2}\, N(\overline{D}_{\perp}) + a_{\perp 3}\, N(\text{ET}). \tag{5.22}$$

If the measure is calculated online, it has furthermore to be distinguished whether the performance metrics are tracked from the beginning of the trial and integrated up to the current time, $P_{\int}$, or whether they are calculated over an observation window referred to as $P(t)$. Integrating the multi-criteria performance over time ($P_{\int}$) is used whenever an external reference performance is available, as this allows to use the global task knowledge coded in the external reference performance. If an internal reference performance is used, where only changes in the user behavior are evaluated, the multi-criteria performance averaged over an observation window $P(t)$ is used. The multi-criteria performance measures were determined online by

$$P_{\parallel \int}(t) = a_{\parallel 1}\, N(t) + a_{\parallel 2}\, N(D_{\parallel \int}) \tag{5.23}$$

$$P_{\perp \int}(t) = a_{\perp 1}\,(1 - N(D_{\perp \int})) \cdot N(t) + a_{\perp 2}\, N(D_{\perp \int}) + a_{\perp 3}\, N(C_E) \tag{5.24}$$

$$P_{\parallel}(t) = a_{\parallel 1}\, N(\dot{\overline{x}}) + a_{\parallel 2}\, N(\overline{D}_{\parallel}) \tag{5.25}$$

$$P_{\perp}(t) = a_{\perp 1}\,(1 - N(\overline{D}_{\perp})) \cdot N(\dot{\overline{x}}) + a_{\perp 2}\, N(\overline{D}_{\perp}) + a_{\perp 3}\, N(C_E), \tag{5.26}$$

where

$$N(t) = \frac{t}{T_{\max}}, \quad N(D_{\int}) = \frac{\text{mean}_{[0;t]}(|D|)}{D_{\max}}, \quad N(C_E) = \frac{C_E}{C_{E,\max}},$$

and $T_{\max}$, $C_{E,\max}$, and $D_{\max}$ are the a priori determined normalization constants for task completion time, wall/obstacle contacts, and disagreement.

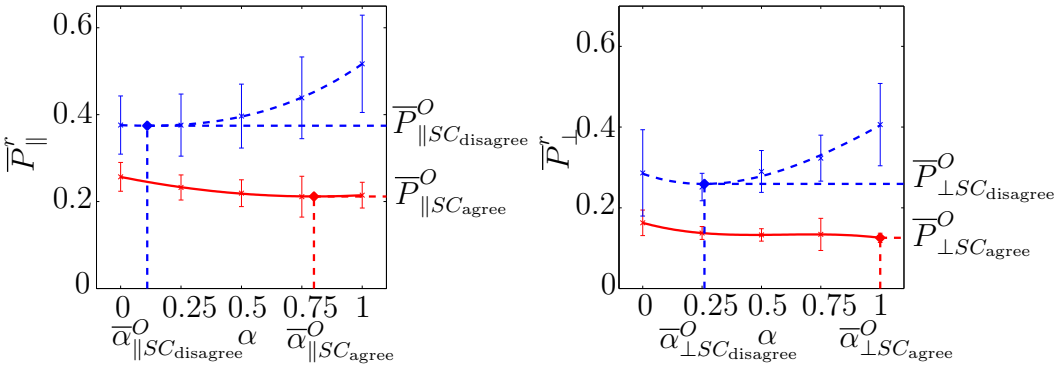

Fig. 5.8: Third-order polynomials [1] fitted to multi-criteria performance data, separately for the two scenarios: SC_{agree} (solid) and SC_{disagree} (dashed). Mean and standard deviation from user study with constant assistance levels. Constant assistance levels $\overline{\alpha}^O$ and corresponding performance values $\overline{P}^O$ minimizing multi-criteria performance.

The weighting of the different components can be decided as desired. In this work, it is proposed to use the normalized standard deviations of the performance components as weights to reflect the importance given by the user or alternatively also a group, such that a weight a_i out of I weights is given by:

$$a_i = \frac{\sigma_i}{\sum_{k=1}^{I} \sigma_k}. \tag{5.27}$$

The required standard deviations can be derived from training trials or a reference user group. Alternatively, all criteria can be weighted equally or they can be designed according to their importance for the task.

The results for multi-criteria performance are shown for the user study with constant assistance levels in Fig. 5.8 for the two scenarios separately and in Fig. 5.9 for both scenarios combined. They allow to determine assistance levels for best and worst performance. There are two possibilities for their selection: i) on a continuous scale (denoted by subscript c) as the minima/maxima of the third-order polynomials shown in Fig. 5.8 and 5.9, or ii) out of the five discrete assistance levels (see subscript d) that lead to the best/worst performance averaged over the V participants, $\underset{V}{\text{mean}}(\bar{P})$, i.e.

$$\overline{\alpha}^b_c = \arg\min_{\alpha\in[0;1]}(\pi(\bar{P},\alpha)) \qquad \overline{\alpha}^b_d = \arg\min_{\alpha\in\mathcal{A}_c} \underset{V}{\text{mean}}(\bar{P}(\alpha)) \tag{5.28}$$

$$\overline{\alpha}^w_c = \arg\max_{\alpha\in[0;1]}(\pi(\bar{P},\alpha)) \qquad \overline{\alpha}^w_d = \arg\max_{\alpha\in\mathcal{A}_c} \underset{V}{\text{mean}}(\bar{P}(\alpha)). \tag{5.29}$$

The best and worst, continuous and discrete, assistance levels, that are determined from the third-order polynomials, are summarized in Table 5.1.

The results show, that if task performance and agreement are equally important, the

[1] The root-mean squared fitting errors are: $e_{\parallel SC_{\text{agree}}} = 0.092$, $e_{\parallel SC_{\text{disagree}}} = 0.082$, $e_{\perp SC_{\text{agree}}} = 0.024$, and $e_{\perp SC_{\text{disagree}}} = 0.073$.

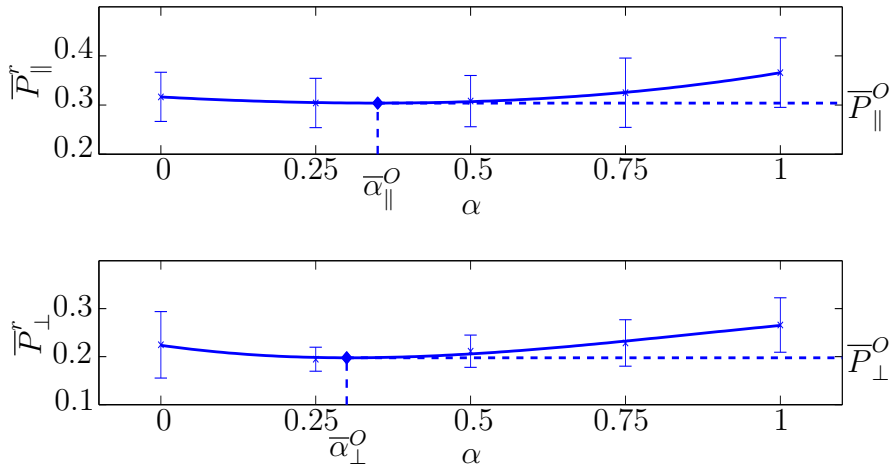

Fig. 5.9: Third-order polynomials fitted to multi-criteria performance data with $a = 0.5$ for both scenarios combined. Mean and standard deviation from user study with constant assistance levels. Constant assistance levels $\overline{\alpha}^O$ and corresponding performance values $\overline{P}^O$ minimizing multi-criteria performance.

Tab. 5.1: Assistance levels leading to best and worst multi-criteria performance. They are determined on a continuous and discrete scale and listed for each scenario separately and for both scenarios combined.

	SC_{agree}		SC_{disagree}		$SC_{\text{agree}} + SC_{\text{disagree}}$	
	Best	Worst	Best	Worst	Best	Worst
Cont.	$\overline{\alpha}^b_{\parallel} = 0.8$	$\overline{\alpha}^w_{\parallel} = 0$	$\overline{\alpha}^b_{\parallel} = 0.11$	$\overline{\alpha}^w_{\parallel} = 1$	$\overline{\alpha}^b_{\parallel} = 0.35$	$\overline{\alpha}^w_{\parallel} = 1$
	$\overline{\alpha}^b_{\perp} = 1$	$\overline{\alpha}^w_{\perp} = 0$	$\overline{\alpha}^b_{\perp} = 0.26$	$\overline{\alpha}^w_{\perp} = 1$	$\overline{\alpha}^b_{\perp} = 0.3$	$\overline{\alpha}^w_{\perp} = 1$
Discrete	$\overline{\alpha}^b_{\parallel} = 0.75$	$\overline{\alpha}^w_{\parallel} = 0$	$\overline{\alpha}^b_{\parallel} = 0.25$	$\overline{\alpha}^w_{\parallel} = 1$	$\overline{\alpha}^b_{\parallel} = 0.25$	$\overline{\alpha}^w_{\parallel} = 1$
	$\overline{\alpha}^b_{\perp} = 1$	$\overline{\alpha}^w_{\perp} = 0$	$\overline{\alpha}^b_{\perp} = 0.25$	$\overline{\alpha}^w_{\perp} = 1$	$\overline{\alpha}^b_{\perp} = 0.25$	$\overline{\alpha}^w_{\perp} = 1$

assistance levels should be set to $\overline{\alpha}_{\parallel} = 0.8$ and $\overline{\alpha}_{\perp} = 1$ for SC_{agree} and to $\overline{\alpha}_{\parallel} = 0.11$ and $\overline{\alpha}_{\perp} = 0.26$ for SC_{disagree}. The assistance levels that lead to an optimal trade-off in multi-criteria performance for both scenarios are $\overline{\alpha}_{\parallel} = 0.35$ and $\overline{\alpha}_{\perp} = 0.3$.

5.4.3.2 Reference Performance

The second axis in the design space for the assistance policy module of a haptic assistance is concerned with the type of reference performance.

An internal reference performance corresponds to the user performance either determined offline as the performance mean over a trial $\overline{P}^{i} = \overline{P}^{u}$ or tracked online over time $P^{i}(t) = P(t)^{u}$. In case of an external reference performance more considerations have to be taken into account. In the following paragraphs the procedure is explained that was adopted to determine an offline and an online external reference performance.

Offline External Performance Reference $\overline{P}^{e}$: External reference behaviors can be obtained in different ways. In this work, the results from a user study were used, where the participants performed the task in SC_{agree} and SC_{disagree} several times with five distinct, constant assistance levels $\alpha_{\parallel} = \alpha_{\perp} \in \mathcal{A}_c$. The performance measure was the multi-criteria performance P defined in (5.21) and (5.22) for both assistance components. For the offline reference performance, the mean multi-criteria performance was determined over the whole dataset. The mean and standard deviations of the offline reference performance $\overline{P^{e}_{\parallel}}$ and $\overline{P^{e}_{\perp}}$ are shown together with the third-order polynomials in Fig. 5.8 for the two scenarios separately and averaged over the two scenarios in Fig. 5.9.

Online External Performance Reference $P^{e}_{\int}(t)$: For the online external reference performance, the multi-criteria performance was integrated over time as defined in (5.23) and (5.24). To model the whole user group, it was decided to extract the performance data of best and worst user as all the other user performances lie between these two extrema. The assistance level α is scaled within these two bounds: if the user is close to the best user performance, the control is switched or shifted to the human, while the assistance has to take over the control if the user performance is close to the worst user performance.

The participant (out of V participants), who achieved best offline performance $\overline{P}^{e}$ without being assisted, was selected as the best or expert user B. The worst user W was selected as the user who achieved worst offline performance $\overline{P}^{e}$ corresponding to $\overline{\alpha}^{W}$, where $\overline{\alpha}^{W}$ is the discrete assistance level that resulted in the worst mean performance averaged over all participants from the pre-study, i.e.

$$B = \arg\min_{N} \overline{P}^{e}(\overline{\alpha}_c = 0) \qquad W = \arg\max_{N} \overline{P}^{e}(\overline{\alpha}^{W}). \tag{5.30}$$

The online best/worst performance data, $P^{e,B}_{\int}(t)$ and $P^{e,W}_{\int}(t)$, were determined at 30 distinct positions in the maze. Thus, for each time step the position of the recorded best/worst performance samples with minimal Euclidean distance to the current user position was determined first. Then, the performance values that corresponded to this position were

selected as the current best/worst performance. By using a spatial measure (the Euclidean distance), the reference does not change if the operator does not move.

5.4.3.3 Assistance Policies

All approaches presented in the following can be used with an external or internal performance reference, such that it will be referred to the performance reference with P^r only. It is assumed that the performance is to be minimized. The assistance level α can take values in the interval $[0; 1]$ and is assumed to facilitate the task for the user.

Optimal Constant Assistance (OCA): The first approach denoted as optimal constant assistance (OCA) is based on the approach by Marayong & Okamura [133]. As presented in Sec. 5.2, they found inverted relationships between assistance level and task performance in scenarios where human and assistant agree and one where they disagree. Disagreement can occur due to unexpected or unknown events, due to a false intention recognition, or due to unexpected changes in the user's action plan. In order to achieve an optimal trade-off in task performance for scenarios of agreement and disagreement, Marayong & Okamura proposed to use the assistance level, that corresponds to the intersection of the performance curves for both types of scenarios. This point corresponds to the best overall task performance for both scenarios.

In this work, a generalized version of the method by Marayong & Okamura [133] is introduced that i) holds also for non-intersecting performance curves, see Fig. 5.10, and ii) incorporates multiple performance measures. An optimal performance for a scenario of agreement SC_{agree} and disagreement SC_{disagree} is obtained by selecting the assistance level as

$$\overline{\alpha}^O = \underset{\alpha \in [0;1]}{\arg\min}(w\, \overline{P}^r_{SC_{\text{agree}}}(\alpha) + (1-w)\, \overline{P}^r_{SC_{\text{disagree}}}(\alpha)). \tag{5.31}$$

The importance between the two scenarios can be regulated with the weight $w \in [0; 1]$. As mentioned earlier, an internal reference performance can be obtained from several trials of one user. Using an external reference performance, different sources can be used: i) it can be an average performance over several trials of one expert user, ii) it can be represented by the mean performance of a user group, or iii) it can be determined based on an ideal system behavior. In this thesis, option (ii) was selected as already detailed in Sec. 5.4.3.2.

Agreement-based Switching (AbS) Assistance: A switching assistance policy as introduced in Sec. 5.1.3 represents a possibility for avoiding human-assistance disagreement without task performance degradation. Here, a performance-optimal constant assistance level $\overline{\alpha}_{SC_{\text{agree}}}$ is selected for SC_{agree} and one denoted as $\overline{\alpha}_{SC_{\text{disagree}}}$ for SC_{disagree}. The switching is triggered depending on the currently measured disagreement $D(t)$ and a pre-defined constant reference threshold $\overline{D}^r$. For agreement, the role of the the assistance is one of an active leader while it changes to a role of a passive follower for human-assistance disagreement. The main objective of this approach is to avoid human-assistance disagreement while keeping task performance as high as possible by applying a high assistance level in

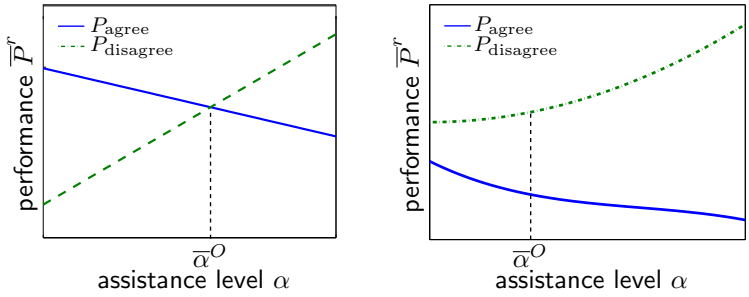

Fig. 5.10: Determination of $\overline{\alpha^O}$ for intersecting (left) and non-intersecting (right) multi-criteria performance curves. $\overline{\alpha^O}$ represents the assistance level that allows for an optimal trade-off between the performance curves (equal weighting of task performance and agreement ($w = 0.5$)) for a scenario of agreement (blue solid) and disagreement (green dashed).

case of human-assistance agreement.

Given a constant reference threshold $\overline{D}^r$ for separating agreement from disagreement, an online update rule for the assistance level can be established, see Fig. 5.11. A hysteresis with switch-on point $\overline{D}^r$ and switch-off point 0 is applied to D. The switch-off point of the hysteresis is set to 0, as this indicates that user and assistance operate in the same direction. The resulting assistance level is furthermore filtered with $G(s)$. The filter $G(s)$ is required, as the user cannot damp the jump between two different assistance levels arbitrarily fast.

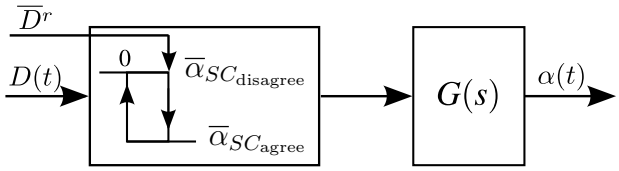

Fig. 5.11: Structure of agreement-based switching: Disagreement is the measured performance, and $\overline{D^r}$ is the constant reference representing the threshold for the hysteresis.

Consequently, the switching condition $\xi(\overline{D}^r, D(t))$ as introduced in (5.4) corresponds to a hysteresis operator $H_{\overline{D}^r}(.)$ with switch-on point $\overline{D}^r$ and switch-off point 0. The assistance level is determined by

$$\alpha(t) = \begin{cases} G(s)\overline{\alpha}_{SC_{\text{agree}}} & \text{if } H_{\overline{D}^r}(D(t)) = 0 \\ G(s)\overline{\alpha}_{SC_{\text{disagree}}} & \text{if } H_{\overline{D}^r}(D(t)) = 1 \end{cases} \tag{5.32}$$

The agreement-based switching has the advantage that high human-assistance agreement is achieved. The performance is not expected to be impaired. One disadvantage may be the discrete switching between two considerably different assistance levels. Although the transition is smooth due to a strong filter applied to the jump of the assistance level, the user still has to adapt to these different assistance levels which may lead to a rather high mental workload.

Linear-Adapting Assistance (LAA): Also, a linear-adapting assistance policy is proposed where the assistance level changes continuously in dependence of the performance P. As described earlier, various types of controllers are possible. The focus in this work is on an adaptation method similar to the gradient search method. Classic gradient-search is applicable, but does not lead to the desired behavior as sketched in Appendix D.2. The main problem is, that the adaptation fluctuates around a constant α whenever the costs increase. In order to avoid this behavior, a proportional-type controller is used:

$$\alpha(t) = \alpha_c + K_p(t)(P^r(t) - P^u(t)) \tag{5.33}$$

where $\alpha_c \in [0; 1]$ is a constant assistance level offset, and $K_p(t) > 0$ is the proportional, possibly time-varying gain. With this approach, a 1:1 mapping between assistance level and performance is obtained and the desired behavior is achieved: the user is supported whenever the performance degrades, while giving him/her as much freedom as possible whenever the performance improves. As a combination of arbitrary measures can be integrated into the measure P^r, a trade-off between all criteria is achieved for every time instant. It should be noted, that due to the restriction of α to the interval $[0; 1]$, upper and lower bounds for P are needed to guarantee a linear mapping between assistance level and performance. In [48], on the contrary, the assistance level was not assumed to be upper bounded.

It is expected that the linear adapting assistance policy will lead to different results depending on the selected reference performance.

If an external reference performance is used, the user behavior is evaluated with respect to a desired/undesired behavior, and, thus, gives a clear feedback about the current performance to the user. The disadvantage is that an approach based on an external reference performance cannot deal with unexpected changes in the environment. This disadvantage can be reduced if scenarios of agreement can be distinguished from scenarios of disagreement and reference knowledge is available for both scenarios (agreement/disagreement). The references and parameters can then be selected for each scenario separately. This should lead to an overall better performance compared to selecting one parameter set optimal for both scenarios (agreement/disagreement).

Using an internal reference performance, the progress of the user performance is evaluated. This can be an advantage if e.g. the environment changes unexpectedly. As the user performance changes, a controller with internal reference performance would adapt the assistance level. The disadvantage of the missing external reference performance is mainly observable in training scenarios. If the user performance does not change anymore, the assistance level is not adapted independent of whether the absolute difference to a trainer performance is small or large.

5.4.4 Extracting Examples from the Design Space: Conditions

Combining all possible assistance policies with either internal or external reference performance would lead to a total of six conditions. In order to reduce the time a subject needed to perform the whole experiment, the number of tested conditions was reduced to four out of these six conditions. Each type of assistance policy was combined with an external ref-

erence. Additionally one condition with internal reference performance was added leading to the final four conditions: OCA^e, AbS^e, LAA^e, and LAA^i.

5.4.4.1 1. Optimal Constant Assistance Policy with External Reference (OCA^e):

The optimal constant assistance level was determined according to (5.31). To equally weigh situations of agreement and disagreement the gain was set to $w = 0.5$. The multi-criteria performance measure P presented in Sec. 5.4.3.1 was used as performance criterion and was evaluated for the reference user group. The assistance levels for an overall best performance were extracted from Fig. 5.9 as $\overline{\alpha}^O_{\parallel} = 0.35$ in tangential direction and $\overline{\alpha}^O_{\perp} = 0.3$ in perpendicular direction.

5.4.4.2 2. Agreement-based Switching Assistance Policy with External Reference (AbS^e):

Following (5.32) the assistance level was switched between two different α-values depending on the actual measure for disagreement $D(t)$. Interactive forces as introduced in [72] were employed as agreement measure. For $\overline{\alpha}_{SC_{\text{agree}}}$ the optimal assistance level for SC_{agree} and for $\overline{\alpha}_{\text{disagree}}$ the optimal assistance level for SC_{disagree} were chosen. Both parameters were extracted from the performance curves of the reference user group shown in Fig. 5.8 and are given by $\overline{\alpha}_{\parallel SC_{\text{agree}}} = 0.75$, $\overline{\alpha}_{\parallel \text{disagree}} = 0.25$ as well as $\overline{\alpha}_{\perp SC_{\text{agree}}} = 1$ and $\overline{\alpha}_{\perp \text{disagree}} = 0.25$.

The external reference threshold $\overline{D}^e$ was furthermore chosen to optimally separate the two distributions of agreement and disagreement. The two thresholds for the tangential and perpendicular assistance were calculated to be $\overline{D}^r_{\parallel} = 2.31$ N and $\overline{D}^r_{\perp} = 4.73$ N. The procedure for determining these thresholds is explained step-by-step in Appendix D.3.

5.4.4.3 3. Linearly-Adapting Assistance Policy with External Reference performance (LAA^e):

Following (5.33) a linear adaptation policy to online adapt the assistance level was implemented. The parameters for the user study were optimally tuned for both scenarios combined. A time-varying adaptation gain $K_p(t)$ was selected as

$$K_p(t) = \frac{\overline{\alpha}^O}{P^{e,B}_{\int}(t) - P^{e,W}_{\int}(t)}$$

where $\overline{\alpha}^O$ was extracted from Fig. 5.9 and is given by $\overline{\alpha}^O_{\parallel} = 0.3$, $\overline{\alpha}^O_{\perp} = 0.35$. These assistance levels guarantee that if the user is performing worse than the worst user, the assistance level is selected that leads to the best performance for both scenarios combined. For the qualitative design space evaluation, $\overline{\alpha}^O$ was extracted from Fig. 5.8 and is given by $\overline{\alpha}^O_{\parallel SC_{\text{agree}}} = 0.8$, $\overline{\alpha}^O_{\perp SC_{\text{agree}}} = 1$ and $\overline{\alpha}^O_{\parallel SC_{\text{disagree}}} = 0.26$, $\overline{\alpha}^O_{\perp SC_{\text{disagree}}} = 0.11$. $P^{e,B}_{\int}(t)$ and $P^{e,W}_{\int}(t)$ represent online tracked best and worst performances of the reference user group that was determined for each time step as detailed in Sec. 5.4.3.2.

5.4.4.4 4. Linearly-Adapting Assistance Policy with Internal Reference (LAA^i):

The linear-adapting assistance policy was furthermore combined with an internal reference performance, where the assistance level was adapted according to (5.33) with $P^r(t) = P^u(t-1)$. Initial values for the assistance levels $\alpha_{\parallel 0}$ and $\alpha_{\perp 0}$ were set to 1 as this corresponds to the assumption of worst user performance. The parameter K_i was set to -1.

5.4.4.5 Filter

For the agreement-based switching approach, it became evident, that the user cannot react within 1 ms (controller sampling time) to large changes in the assistance level, as a smooth transition in the behavior, typical for humans, is not possible anymore. As a remedy to this problem, the changes in the assistance level are filtered with $G(s)$. As even the slope of a strong 1st order low-pass filter was found to be too large to sufficiently damp the overshoots, a 2nd order critically damped low-pass with a natural frequency of 5 Hz $G(s) = \frac{1}{(0.1s+1)^2}$ was used. The rising time of this filter is 0.48 s, which is at the upper end of human response times according to [26]. For better comparison, this filter was applied to all tested assistances.

5.5 Qualitative Evaluation

To give the reader an impression how the different introduced implementations of the assistance policy module affect the assistance level α and how results change when moving along the axes of the defined design space, a single user was asked to perform the task under different conditions. These experiments only allow a qualitative comparison of the different implementations. The systematic statistical evaluation and comparison is presented in the subsequent sections.

5.5.1 Internal vs. External Reference

First, the differences resulting from using an external versus an internal reference performance are investigated. As the differences are most evident for the linear-adapting assistance policy, this control policy was implemented with both types of reference performance. Details about the parametrization of the two implementations were presented in the previous section 5.4.4. Fig. 5.12 shows the evolution of the performance (left) and the corresponding assistance level $\alpha_{\parallel}$ (right) over time for SC_{agree}. The user was instructed and trained to behave similarly in the following experiments: he/she was asked to perform well at the beginning of the trial, to strongly degrade in performance between the third and fifth curve, and to improve again considerably towards the end. With external reference performance, $\alpha_{\parallel}$ is around 0 at the beginning of the trial as the user performance is superior to the best reference performance. Then, the difference between user and reference performance and consequently also the assistance level increases up to the maximum of $\overline{\alpha}_{\parallel}^{W} = 0.8$ as $P_{\parallel} \geq P_{\parallel}^{e,W}$. Although the user improves towards the end ($P_{\parallel}^{e,B} < P_{\parallel} < P_{\parallel}^{e,W}$), the best performance cannot be reached anymore, such that $\alpha_{\parallel}$ does not totally decrease to

zero. With internal reference performance, see Fig. 5.12(b), the assistance level is adapted according to changes in the user performance. It can be observed that $\alpha_{\parallel}$ increases strongly in the middle of the trial as the user performance became worse, but it is reduced immediately as the user performance improves again. The absolute difference to a best/worst performance does not play a role for this approach.

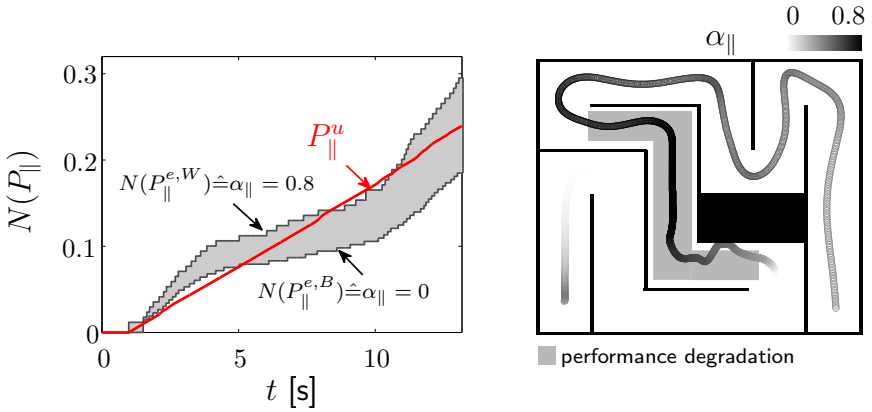

(a) External reference performance

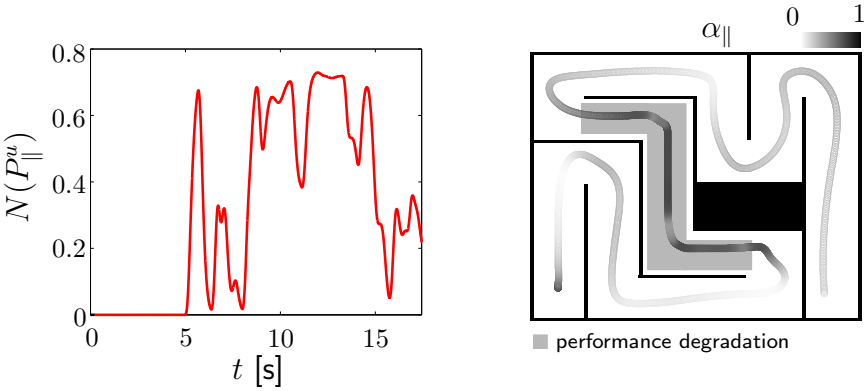

(b) Internal reference performance

Fig. 5.12: Comparison between external and internal reference performance: Time-series of representative $P_{\parallel}$ (left) and $\alpha_{\parallel}$ (right) using LAA for SC_{agree}.

Fig. 5.13 shows the evolution of $\alpha_{\perp}$ for SC_{disagree}. As the multi-criteria performance measure incorporates a measure for agreement and additionally an internal reference performance was used that reacts to changes in the user behavior, $\alpha_{\perp}$ is reduced around the obstacles, where the user behavior changes (speed decreases and disagreement increases). If an external reference performance is used, such a behavior cannot be observed: Only if the user performance is considerably worse than the best performance, the assistance level is increased independently of the environment.

If an external reference performance is used for adaptation, the absolute skill level of the user is evaluated. On the contrary, if the adaptation is based on an internal reference performance, the progress of the user is used for adaptation. Summarizing, it can be concluded that an external reference performance is beneficial for training scenarios, where haptic support should be provided if the user performance decreases with respect to the reference performance, while an internal reference performance is especially suited for

scenarios where unexpected events are likely to occur.

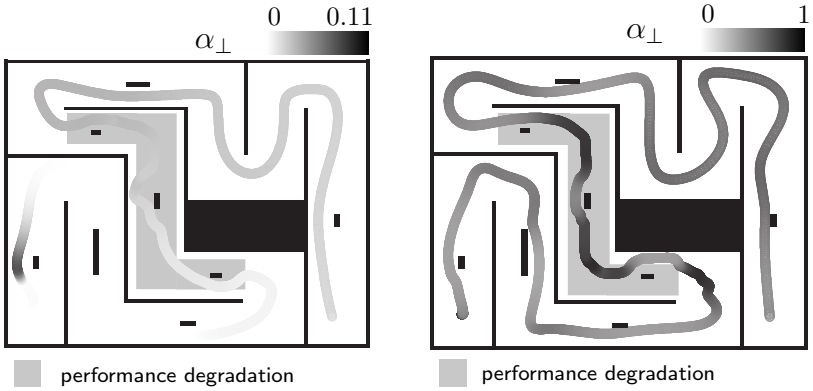

(a) External reference performance

(b) Internal reference performance

Fig. 5.13: Assistance $\alpha_\perp$ for SC_{disagree} using LAA with external and internal reference performance.

5.5.2 Single- vs. Multi-Criteria Performance

Finally, the last axis in the design space is devoted to performance measures. For the considered case study, the most important ones were considered to be task performance and agreement. Fig. 5.14 shows how these two measures are influenced by different constant

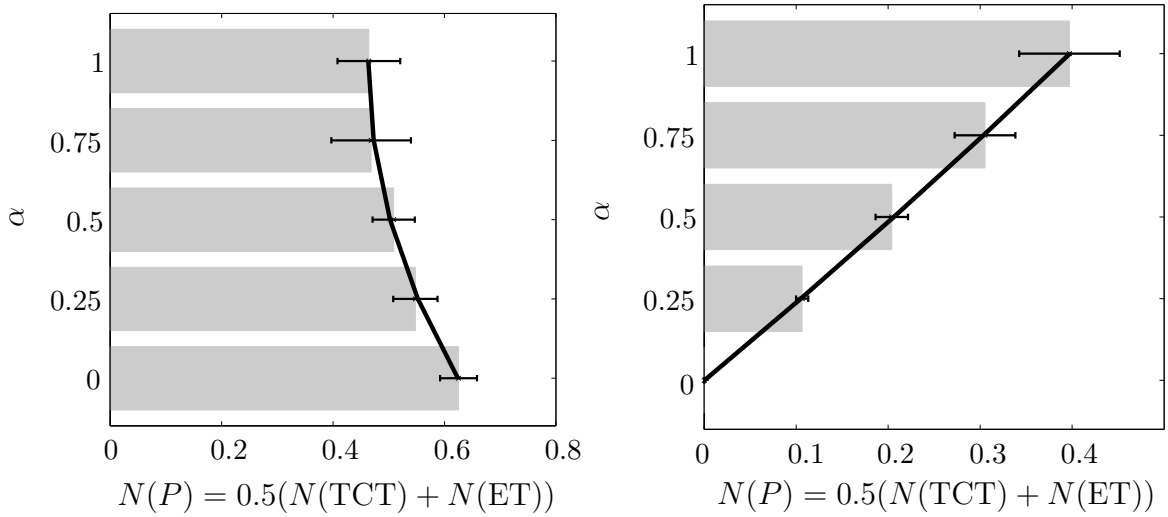

(a) Normalized task performance

(b) Disagreement

Fig. 5.14: Mean and standard deviation of normalized task performance and disagreement depending on the assistance level.

assistance levels [2]. The axes were flipped to better illustrate which assistance level would be selected if task performance or agreement were the only performance measures. A good task

[2]The results were obtained from the user study with constant assistance levels, see also Sec. 5.4.3.1

performance (small $N(P)$) can be achieved with the highest assistance level, while a low disagreement would call for no assistance at all. As a consequence, if the assistances were tuned according to a single criterion (task performance or disagreement), the respective other criterion would be seriously deteriorated. Only a multi-criteria measure as introduced in this work allows to achieve a compromise between the two conflicting measures.

5.5.3 Switching vs. Continuously-Adapting Assistance

The next investigation is concerned with differences due to the assistance policy. As the behavior is obvious for the optimal constant assistance, the agreement-based switching and the linear-adapting assistance policies are compared with each other. The implementations with external reference performance were selected for a better comparison.

5.5.3.1 Agreement-based Switching (AbS^e):

The objective of the switching controller is to achieve a high human-assistance agreement without degrading task performance. The controller switches online between two considerably different assistance levels depending on the switching condition. The resulting behavior is presented for SC_{disagree} as the switching condition (disagreement) is triggered mainly around the obstacles of this scenario. A curve of both α components (tangential/perpendicular to the path) is shown in Fig. 5.15. As expected, $\alpha_\perp$ is switched to the lower assistance level around the obstacles resulting in smaller interactive forces and, thus, a high degree of human-assistance agreement. In all other situations, the assistance level $\alpha_\parallel$ is set to the higher assistance level around 0.75. Deviations from the higher assistance levels are very short in time such that no negative influence on task performance is expected.

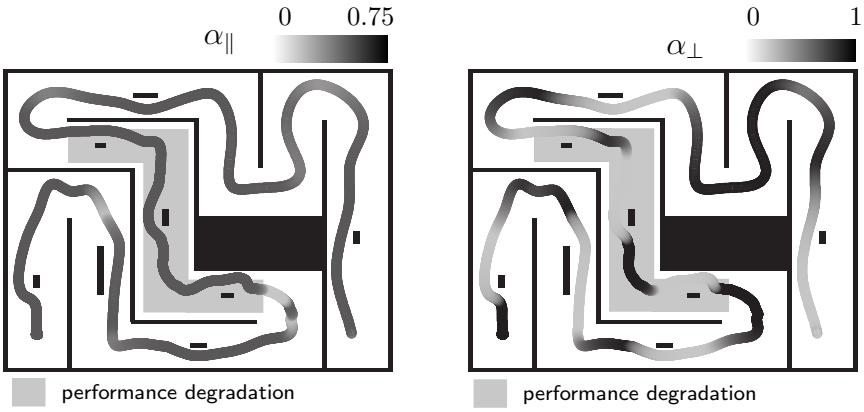

Fig. 5.15: Assistance levels for SC_{disagree} using AbS^e.

5.5.3.2 Linear-adapting Assistance (LAA^e):

Results for the linear-adapting assistance are shown in Fig. 5.16 for the tangential and perpendicular direction. As can be observed the user pays a lot more attention to maximizing speed than minimizing errors. The user performance is close to the best performance in the

tangential direction indicating a high speed, which leads again to small assistance levels $\alpha_{\parallel}$ for this direction, while in perpendicular direction it approaches and even undershoots the worst performance leading to a high assistance level $\alpha_{\perp}$. This effect is pronounced towards the end of the trial. As expected, both assistance levels change continuously during task execution and proportional to the difference between user performance and external upper/lower reference performance.

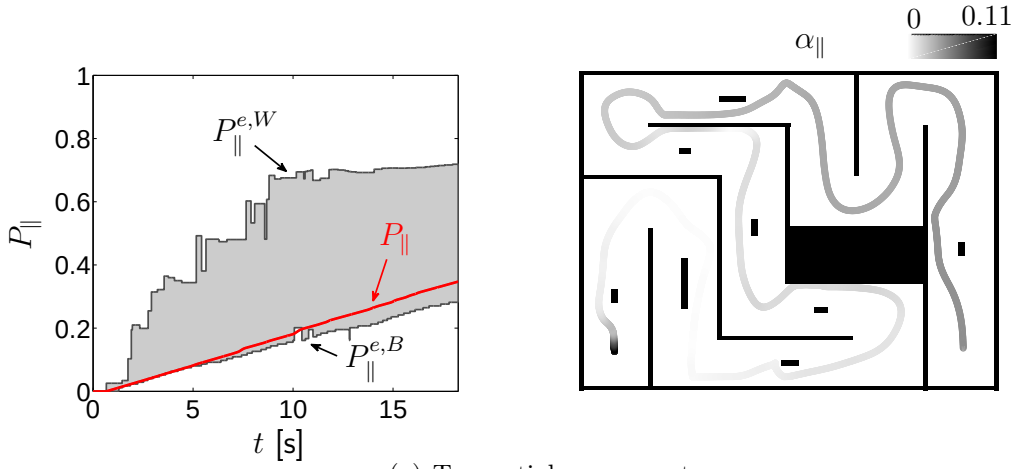

(a) Tangential component

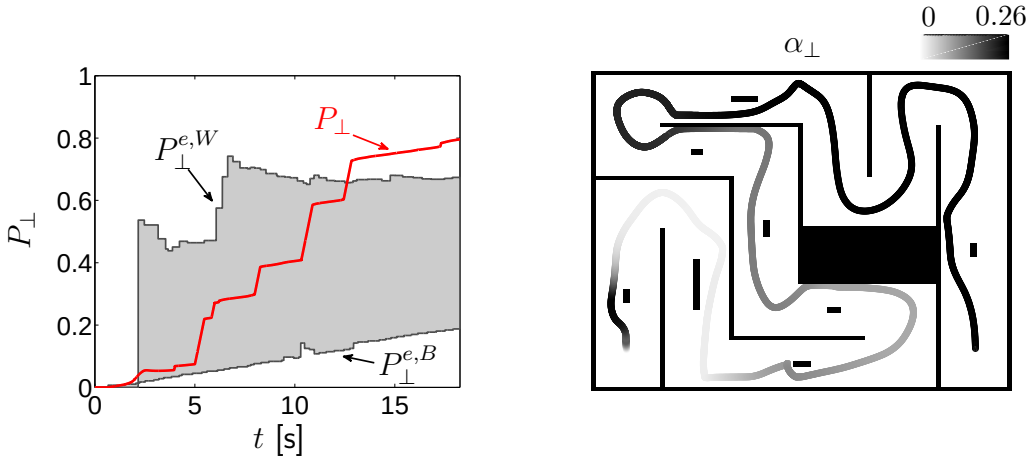

(b) Perpendicular component

Fig. 5.16: Time-series of performance data and assistance levels for SC_{disagree} using LAA^{e}.

5.5.4 Discussion

The three independent axes of the design space reveal a variety of different concepts for designing the assistance policy module of a haptic assistance. However, not all possibilities are suitable for every scenario and application. Also, different advantages and disadvantages may be experienced. The expectations which can be derived from the qualitative results are summarized for each of the three axes in Table 5.2. This table is a first point of orientation when designing the assistance policy module for a specific haptic assistance, application, and task.

Tab. 5.2: Summary of differences regarding the three design axes of the assistance policy module of a haptic assistance.

	Advantages(+)/Disadvantages(−)	**Best suited**
Performance		
Single-criterion	+ Clear feedback to user	if priority(P_i)>>priority(P_k), $\forall\ k \neq i$
Multi-criteria	+ Trade-off between several objectives	if importance(P_1)≈ importance(P_2) ≈ ... ≈ importance(P_n)
Reference		
External	− Prior knowledge required	for Training/Learning
Internal	− Independent of difference to reference	for Mobility Aids/Vehicles/ Teleoperation
Control Policy		
Constant	+ Predictability	for Mobility Aids/Vehicles/
	+ Small tuning effort	for Teleoperation
	− User dependence on assistance [131]	
Switching	+ Two-criteria optimization	for Mobility Aids/Vehicles/
	o Medium tuning effort	for Teleoperation
	− Strong assistance changes	
Continuous	+ Reference tracking for each time step	for Training/Learning (external reference)
	+ Small tuning effort (internal reference)	for Mobility Aids/Vehicles/
	− High tuning effort (external reference)	for Teleoperation (internal reference)

5.6 Statistical Evaluation

In order to allow for a statistical comparison, the specific implementations of the design space introduced in Sec. 5.4.3 are evaluated in a user study. This section presents the method, evaluation criteria, results, and a discussion, where the research question described in Sec. 5.3 are answered.

5.6.1 Method

This section presents the experimental design, the method, and the experimental results of the user study. The different implementations detailed in Sec. 5.4.4 were compared with each other in this study.

5.6.1.1 Experimental design

The experiment featured a 4 (assistance) x 2 (scenario) repeated-measures within-subjects experimental design.

5.6.1.2 Procedure

The participants were first given the opportunity to familiarize themselves with the experimental setup and the task requirements prior to the experimental trials. Thus, they were allowed to practice both scenarios with $\alpha_{\parallel} = \alpha_{\perp} = 0$ as well as $\alpha_{\parallel} = \alpha_{\perp} = 1$. It was emphasized to avoid contact with walls and obstacles while moving as quickly as possible. After the test trials, the four different assistances, see Sec. 5.4.4, were presented in randomized order as blocks consisting of three consecutive trials with SC_{agree} and SC_{disagree}, respectively. The sequence of scenarios per type of assistance was again randomized. Hence, each block consisted of six trials with one type of assistance and both scenarios. As the first two trials of SC_{agree} and SC_{disagree} represented training trials for the particular condition, only the third trial was used for the analysis. After completing a scenario using a certain type of assistance, subjects had to fill in a questionnaire to assess the perceived workload.

5.6.1.3 Participants

An opportunity sample of 16 subjects (12 men and 4 women, all right-handed) with a mean age of 24.5 years (std. deviation: 3.3 years) and sparse experience in the handling of haptic devices (mean(experience) = 1.50, scale ranging from *1 = no experience* to *5 = much experience*) took part in the experiment.

5.6.2 Performance Criteria

Quantitative and qualitative performance criteria were evaluated in the user study. Task performance and agreement as described in Sec. 5.4.3.1 build the quantitative measures together with smoothness. From a qualitative point of view, mental workload was determined. Finally, efficiency correlating task performance and perceived workload, was evaluated. The measures for smoothness, mental workload, and efficiency are introduced next.

5.6.2.1 Smoothness

In order to quantify the smoothness S of the movements through the maze, the spectral metric proposed in [13] was used. It is based on the frequency spectrum of the velocity signal and independent of the time scaling of movements. Compared to [13], in this work, the frequency spectrum was not normalized in order to make the metric independent of the amplitude, as the amplitude should have an influence on the smoothness measure. Given a velocity signal $\dot{\boldsymbol{x}}$ the frequency spectrum $X(\omega)$ was determined using the Fast Fourier transformation fft:

$$\boldsymbol{X}(\omega) = \text{fft}(\tilde{\dot{\boldsymbol{x}}}) \tag{5.35}$$

where $\tilde{\dot{\boldsymbol{x}}}$ is the zero-padded version of $\dot{\boldsymbol{x}}$. In order to reduce noise in the measure, a cutoff frequency ω_c was determined above which all amplitudes are below a threshold T_S, i.e.

$$\omega_c = \min_{\omega \in]0; \frac{\omega_s}{2}]} |\boldsymbol{X}(\omega)| < T_S \quad \forall\, \omega > \omega_c \tag{5.36}$$

with ω_s the sampling frequency and T_S is selected as $T_S = 0.01$. The smoothness was finally determined from the remaining frequency spectrum $\tilde{\boldsymbol{X}}(\omega),\ \omega \in [-\omega_c; \omega_c]$ as

$$S = -\sum \max(\tilde{\boldsymbol{X}}). \tag{5.37}$$

The spectral method has the main advantage that the position signal has to be differentiated only once compared to e.g. classical smoothness measures like jerk where the fourth derivative of the position has to be determined.

5.6.2.2 Qualitative Measure

From a qualitative point of view, the perceived workload was investigated, which was assessed using the NASA TLX questionnaire [93]. Further details regarding this questionnaire are provided in Sec. 2.2.4.2.

5.6.2.3 Efficiency

Besides purely quantitative and qualitative measures both measures should also be correlated. This can be assessed with an efficiency measure E between a task performance measure P and an effort/workload measure W as introduced in Sec. 2.2.4.1.

As performance is used in the efficiency measure, it has to be maximized. Thus, the inverse of the normalized task performance was used $\text{inv}(N(P)) = 1-(N(\text{TCT})+N(\text{ET}))$, such that low TCT and ET resulted in a high performance $\text{inv}(N(P))$. The perceived workload from the NASA TLX questionnaire as introduced in Sec. 2.2.4.2 functioned as effort measure.

5.6.3 Results

Except for collision time, values of qualitative and quantitative measures were found to be normally distributed according to the results of Kolmogorov-Smirnov tests. Hence, statistical analyses were performed parametrically for these measures, while the analyses

for collision time were based on the non-parametric Friedman ANOVA. In line with the experimental design, variables were evaluated with two-factorial repeated measurement analyses of variance (ANOVA) to investigate the influence of the assistance and type of scenario. All statistical tests were conducted on a 5% significance level. Outliers with more than three standard deviations away from the mean were replaced with the mean value.

5.6.3.1 Task Completion Time

Concerning TCT, the factors *assistance* ($F_{Greenhouse-Geisser:1.71,25.71} = 5.461,\ p = .014,\ \eta_p^2 = .267$), *scenario* ($F_{Greenhouse-Geisser:1,15} = 67.71,\ p < .001,\ \eta_p^2 = .819$), and their *interaction* ($F_{3,45} = 3.752,\ p < .017,\ \eta_p^2 = .2$) reach significance, see Fig. 5.18. Derived from the distribution of means, task completion time for SC_{disagree} is worse than for SC_{agree}. Investigating the found interaction a significant simple effect was found for SC_{agree} ($F_{Greenhouse-Geisser:1.82,27.31} = 16.067,\ p < .001,\ \eta_p^2 = .517$). Paired, Bonferroni-corrected comparisons reveal significant differences between LAA^e and AbS^e ($p \leq .001$) and LAA^i ($p \leq .001$).

5.6.3.2 Collision Time

The factor *scenario* reaches significance ($Z = -5.892,\ p < .001$). Friedman's ANOVA found a significant assistance main effect on collision time for SC_{agree} ($\chi^2(3) = 8.589$, $p = .035$), but fails significance for SC_{disagree}. Wilcoxon post-hoc comparisons with Bonferroni corrections for multiple comparisons (accepted α-level of $p < .008$) do not reveal significant differences.

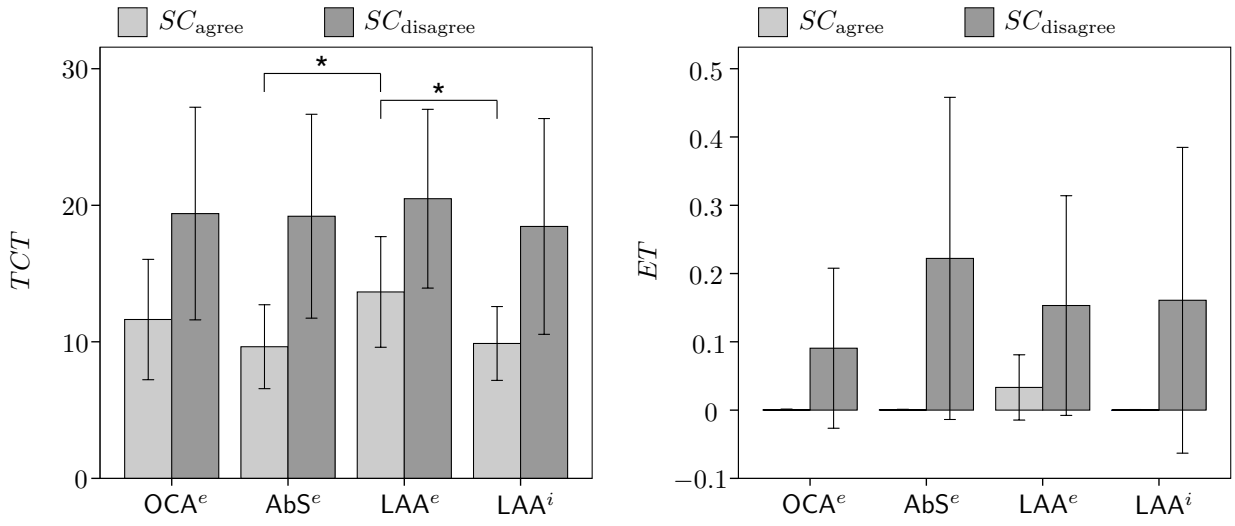

Fig. 5.17: Mean and standard deviation of task completion time and error time depending on assistance and scenario. * marks significant differences.

5.6.3.3 Task Performance

Concerning normalized task performance $N(P)$, see Fig. 5.18, the factor *assistance* does not reach significance, while *scenario* ($F_{Greenhouse-Geisser:1,15} = 243.826,\ p < .001,\ \eta_p^2 = .942$)

and their *interaction* ($F_{Greenhouse-Geisser:1.75,26.22} = 3.539$, $p = .049$, $\eta_p^2 = .191$) reach significance. Derived from the distribution of means, task performance with obstacles is worse than without. Investigating the found interaction a significant simple effect was found for SC_{agree} only ($F_{Greenhouse-Geisser:1.87,28} = 23.244$, $p < .001$, $\eta_p^2 = .608$). Paired, Bonferroni-corrected comparisons reveal significant differences between LAA^e and all other approaches (OCA^e: $p = .010$, AbS^e and LAA^i: $p < .001$).

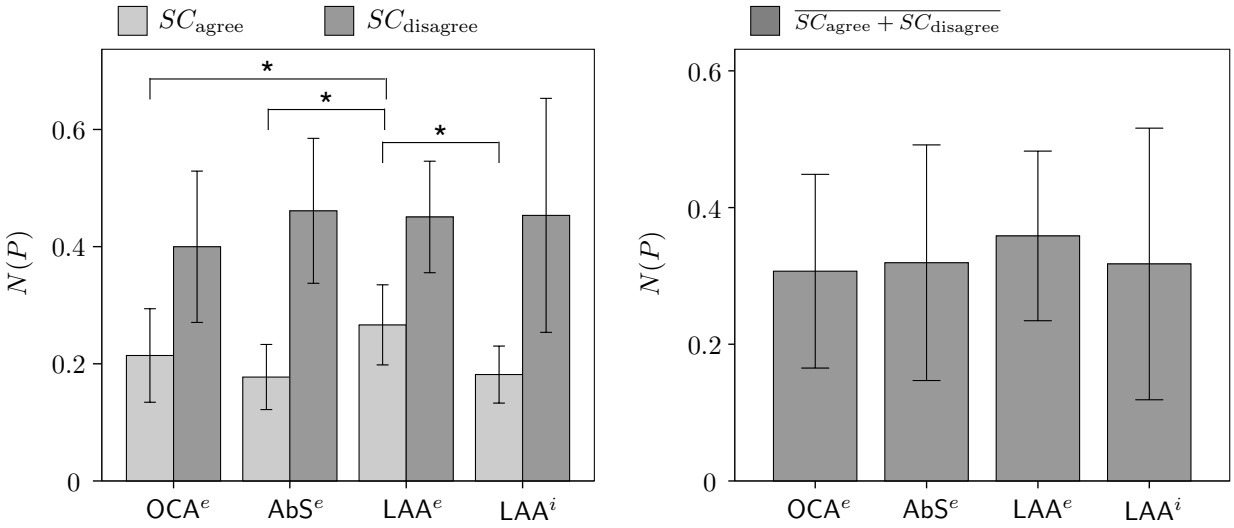

Fig. 5.18: Mean and standard deviation of normalized task performance depending on assistance and scenario (left) and independent of scenario (right). * marks significant differences.

5.6.3.4 Disagreement

By evaluating the norm of the internal forces, significant effects with very large effect sizes of *assistance* ($F_{3,45} = 180.342$, $p < .001$, $\eta_p^2 = .923$), *scenario* ($F_{Greenhouse-Geisser:1,15} = 1221.438$, $p < .001$, $\eta_p^2 = .988$), and their *interaction* ($F_{3,45} = 150.167$, $p < .001$, $\eta_p^2 = .909$) are found. Investigating the found interaction significant simple effects were found for SC_{agree} ($F_{3,45} = 52.041$, $p < .001$, $\eta_p^2 = .776$) and SC_{disagree} ($F_{3,45} = 217.924$, $p < .001$, $\eta_p^2 = .936$). For SC_{agree} paired, Bonferroni-corrected comparisons reveal significant differences between all approaches except AbS^e vs. LAA^i (OCA^e vs. AbS^e: $p = .005$, OCA^e vs. LAA^i: $p = .004$, $p < .001$ else). For SC_{disagree} all comparisons were found to be significant ($p < .001$) except OCA^e vs. AbS^e. For both scenarios combined, a significant main effect was found as well ($F_{3,45} = 180.342$, $p < .001$, $\eta_p^2 = .923$), where Bonferroni-corrected comparisons reveal significant differences between all approaches ($p \leq .002$).

5.6.3.5 Smoothness

The smoothness of the movements S_{xy} is significantly affected by the *assistance* ($F_{2.25,33.72} = 12.397$, $p < .001$, $\eta_p^2 = .452$), the *scenario* ($F_{1,15} = 29.694$, $p < .001$ $\eta_p^2 = .664$),

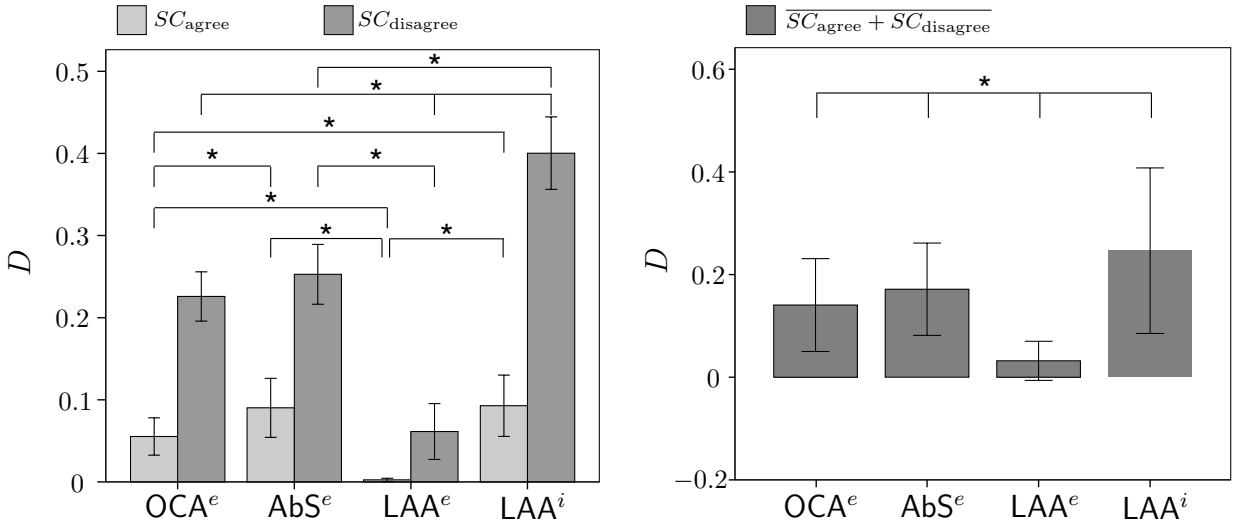

Fig. 5.19: Mean and standard deviation of disagreement depending on assistance and scenario (left) and independent of scenario (right). * marks significant differences.

and their *interaction* ($F_{3,45} = 18.387$, $p < .001$, $\eta_p^2 = .551$). Investigating the found interaction a significant simple effect was found for SC_{agree} ($F_{Greenhouse-Geisser:1.91,28.62} = 3.685$, $p = .04$, $\eta_p^2 = .197$) and SC_{disagree} ($F_{3,45} = 20.440$, $p < .001$, $\eta_p^2 = .577$). For SC_{agree}, paired, Bonferroni-corrected comparisons reveal significant differences between OCA^e vs. AbS^e ($p = .039$) and OCA^e and LAA^i ($p = .011$). For SC_{disagree}, paired, Bonferroni-corrected comparisons reveal significant differences between all approaches except AbS^e and LAA^i (LAA^e vs. OCA^e: $p = .006$, OCA^e vs. AbS^e: $p = .035$, $p \leq .001$ else). A significant main effect was furthermore found for both scenarios combined ($F_{Greenhouse-Geisser:2.26,33.84} = 10.764$, $p < .001$, $\eta_p^2 = .418$). Bonferroni-corrected comparisons reveal significant differences between all approaches except LAA^e vs. OCA^e and AbS^e and LAA^i (LAA^e vs. AbS^e: $p = .007$, LAA^e vs. LAA^i: $p = .01$, OCA^e vs. AbS^e: $p = .041$, OCA^e vs. LAA^i: $p < .001$).

5.6.3.6 Perceived Workload

The perceived workload in this experiment strongly depends on the type of *scenario* ($F_{Greenhouse-Geisser:1,15} = 38.249$, $p < .001$, $\eta_p^2 = .718$), but not *assistance*. The ordinal *interaction* of these factors reaches significance ($F_{3,45} = 6.283$, $p = .001$, $\eta_p^2 = .295$) as well, indicating generally higher workload in SC_{disagree}. Investigating the found interaction a significant simple effect was found for SC_{agree} only ($F_{Greenhouse-Geisser:2.11,31.62} = 6.359$, $p = .004$, $\eta_p^2 = .298$). Paired, Bonferroni-corrected comparisons reveal significant differences between LAA^e and LAA^i ($p = .007$). Descriptively, AbS^e and LAA^i result in least workload within SC_{agree}, while LAA^e produces most. In contrast, the least workload in SC_{disagree} is found for LAA^e.

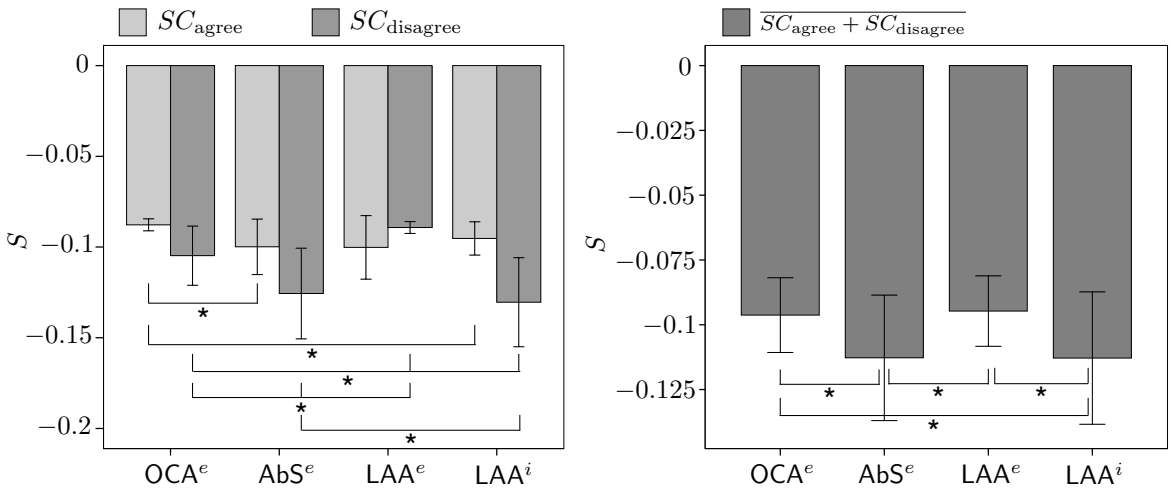

Fig. 5.20: Mean and standard deviation of movement smoothness depending on assistance and scenario (left) and independent of scenario (right). * marks significant differences.

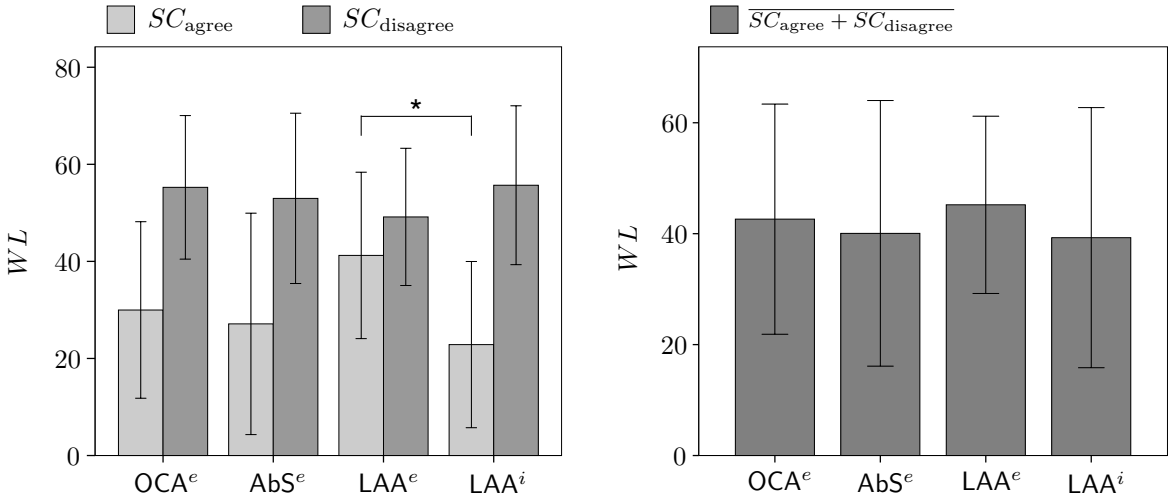

Fig. 5.21: Mean and standard deviation of perceived workload depending on assistance and scenario (left) and independent of scenario (right). * marks significant differences.

5.6.3.7 Efficiency

Efficiency is not significantly affected by the *assistance*, but the *scenario* ($F_{Greenhouse-Geisser:1,15} = 93.413$, $p < .001$, $\eta_p^2 = .862$), with higher efficiency values within SC_{agree} overall. Also, the *interaction* between assistance and scenario ($F_{3,45} = 5.871$, $p = .002$, $\eta_p^2 = .281$) reaches significance. Investigating the found interaction a significant simple effect was found for SC_{agree} only ($F_{3,45} = 10.864$, $p < .001$, $\eta_p^2 = .420$). Paired, Bonferroni-corrected comparisons reveal significant differences between AbS^e and LAA^e ($p = .005$) and between LAA^i and LAA^e ($p < .001$) for SC_{agree}. In this scenario, AbS^e and LAA^i also descriptively outperform OCA^e.

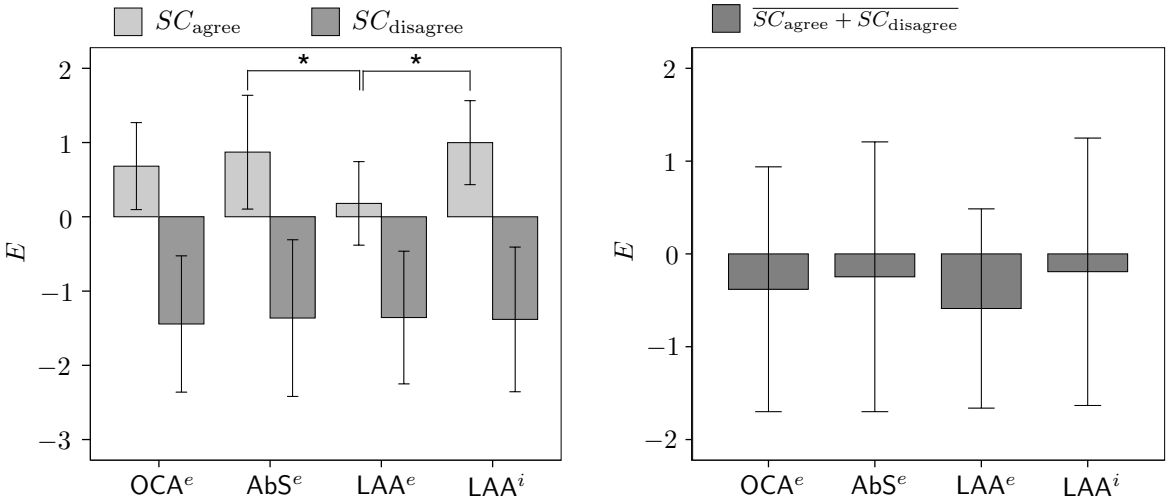

Fig. 5.22: Mean and standard deviation of efficiency depending on assistance (left) and assistance and scenario (right). * marks significant differences.

5.6.3.8 Assistance Level

To determine the typical amount of applied assistance per approach, the mean $\alpha = \text{mean}(\alpha_{\parallel}, \alpha_{\perp})$ value is evaluated. In a first evaluation step, the inequality of the mean α values against 0 and 1 is tested with one sample t-tests, where significance is reached overall (p values $\leq .001$). The two-factorial repeated measures ANOVA for the α_a values shows the *assistance* ($F_{\text{Greenhouse-Geisser:1.98,29.71}} = 1909.526$, $p < .001$, $\eta_p^2 = .992$), and the *interaction* ($F_{1.73,25.88} = 147.311$, $p < .001$, $\eta_p^2 = .908$) to be significant. Investigating the found interaction a significant simple effect was found for SC_{agree} ($F_{1.84,27.52} = 1858.528$, $p < .001$, $\eta_p^2 = .992$). Also for SC_{disagree} a significant simple effect was found ($F_{1.92,28.83} = 678.153$, $p < .001$, $\eta_p^2 = .978$). Paired, Bonferroni-corrected comparisons reveal significant differences between all approaches ($p < .001$) for both scenarios. The factor *scenario* does not reach significance. The mean values are shown in Fig. 5.23.

5.6.4 Discussion

In Sec. 5.1.1 the following objectives, that can be used to compare different implementations of haptic assistances, were identified: a) task performance, b) human-assistance agreement,

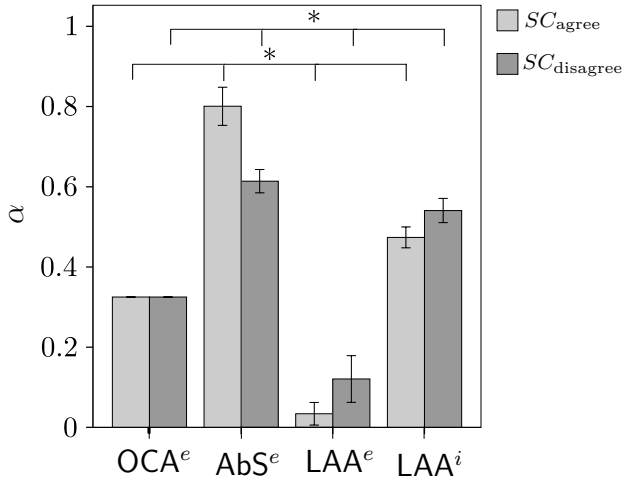

Fig. 5.23: Mean and standard deviation of adaptive assistance levels depending on scenario. * marks significant differences.

c) perceived workload, d) efficiency, e) and smoothness of movements. In this section, the different implementations will be compared with respect to these measures with the final aim of finding answers for the research questions formulated in Sec. 5.3. Furthermore, the tuning effort of the single implementations and the generalizability of obtained results will be discussed.

5.6.4.1 RQ Ia: Adaptive vs. Constant Assistance

Although a haptic assistance with optimally selected constant assistance level provides a trade-off between different, conflicting performance criteria, this paragraph investigates whether haptic assistances implementing an online adaptive assistance level have the potential to outperform such an assistance.

Looking at the results reported in Sec. 5.6.3 a trend of AbS^e and LAA^i to outperform OCA^e in terms of task performance, workload, and efficiency for SC_{agree} is found. For the same pairs and SC_{disagree}, no differences in terms of task completion time, workload, and efficiency were observed, but due to reduced collision times a slightly better normalized task performance was observed for OCA^e. OCA^e significantly outperforms LAA^i in terms of agreement for both scenarios and AbS^e for SC_{agree}.

LAA^e was found to be significantly superior over OCA^e in terms of agreement. Yet, normalized task performance, collision time, perceived workload for SC_{agree}, and efficiency, tended to be better with OCA^e, which can be explained by the small assistance levels realized by LAA^e.

All approaches with adaptive assistance level were found to be less smooth than OCA^e. It should be noted, however, that even though movements were found to be less smooth, approaches with adaptive assistance level did not lead to a significantly higher mental workload, which indicates that the changes in the assistance level can be well interpreted by the user and do not harm the collaboration.

Summarizing, it can be concluded that the approaches AbS^e and LAA^i with adaptive

assistance levels show a trend to be superior to an optimal constant assistance in all evaluation criteria except agreement and task performance for SC_{disagree}. For the considered type of task, it is consequently proposed to favor them especially if a efficiency and low perceived workload and, for scenarios without unexpected events, a high task performance are of concern. In terms of agreement and for SC_{disagree}, AbS^e performs only slightly worse than OCA^e, while the effect is more pronounced for LAA^i. Thus, AbS^e represents an interesting alternative to OCA^e. LAA^e should only be preferred if human-assistance agreement is the most important design factor.

5.6.4.2 RQ Ib: Switching vs. Continuously-Adapting Assistance

Knowing that assistances with adaptive assistance levels have the potential to outperform assistances with optimal constant assistance levels, it is now interesting to investigate whether assistances with switching or continuously adapting assistance levels should be preferred. To answer this research question each of the quantitative and qualitative performance criteria is analyzed separately.

The AbS^e approach tries to improve the trade-off between task performance and human-assistance agreement by switching between two different assistance levels that have been optimally selected for the two scenarios SC_{agree} and SC_{disagree}. Compared to LAA^i this enables high human-assistance agreement in both scenarios without degradation in task performance. Yet, the low disagreement levels of the LAA^e approach which lead to a slightly worse task performance cannot be reached. Thus, if human-assistance agreement is the main design criterion, LAA^e should be preferred. In case task performance is of equal importance, then AbS^e should be selected as it achieves a slightly better task performance than LAA^e at a still lower disagreement than LAA^i.

AbS^e and LAA^i tend to outperform LAA^e in terms of mental workload, especially for SC_{agree}. The assistance levels for SC_{agree}, see Fig. 5.23, were found to be small such that control over the actions of the system was shifted to the user. A consequence of the low mental workload for AbS^e and LAA^i is a superior efficiency. The two approaches AbS^e and LAA^i perform similarly in terms of perceived workload and efficiency and should thus, be again favored over LAA^e.

Due to the strong assistance levels and the high speeds resulting in high task performance, movements were more jerky with AbS^e and LAA^i compared to LAA^e. Thus, a high task performance is achieved at the cost of reduced smoothness. As this did, however, not significantly deteriorate the perceived workload and efficiency, AbS^e and LAA^i should be nevertheless preferred over LAA^e.

The results indicate that the assistance with switching assistance levels can be superior to assistances with continuously adapting assistance in achieving an overall good trade-off between task performance and agreement without deteriorating perceived workload and efficiency. Moreover, the disagreement measure was used in a discrete way differentiating only agreement and disagreement, while it was used in a continuous way for the continuously adapting assistances. Considering agreement as a continuous measure may not be appropriate in all situations, since humans might also apply passive resistance in form of inertia. On the other hand, assistances with continuously adapting assistance levels can be tuned to achieve various performance criteria with different importance, while there are

few possibilities to tune the AbS^e approach.

5.6.4.3 RQ II: Internal vs. External Reference

Further, the difference between assistances with external and internal reference is analyzed. While assistances with external reference evaluate the difference between the user and the reference performance, approaches with internal reference react on changes in user performance only. Consequently, approaches with internal reference performance provide assistance, whenever the user performance changes, which can be due to the task in general (e.g. the need for slowing down in curves or speeding up on straight paths) or due to unexpected events. On the other hand, approaches with external reference provide assistance if the user behavior significantly degrades from the reference independently from the desired behavior changes introduced by the task. Thus, a generally low assistance will be provided if the user performs similar to the reference. Unexpected events, on the other hand, can lead to a drastic increase of the error between user and reference behavior and thus, to an increase in the assistance level. This might be undesired as the assistance does not know about potential, unexpected obstacles and consequently would drag the user towards them. Based on these considerations approaches with internal reference should be preferred over approaches with external reference if unexpected events are likely to occur.

In this specific evaluation, it was found that the user group performed very close to the reference and, thus, experienced very low assistance levels in LAA^e throughout the whole task. Even around obstacles, the assistance increased only moderately so that the expected negative effect of of an external reference when combined with unexpected events was not very pronounced. The general low assistance levels explain also the unexpectedly higher agreement found for LAA^e compared to LAA^i. In order to realize a higher general support by this assistance, maximum assistance levels would need to be revised, which however would come along with the negative effects introduced above. Beside the unexpected findings for agreement, LAA^i clearly outperformed LAA^e in terms of task performance, perceived workload, and efficiency for SC_{disagree} and should consequently be preferred when unexpected events for the assistance are likely to occur.

5.6.4.4 RQ III: Single- vs. Multi-Criteria Performance

The last research question focuses on performance differences observed for implementations based on single or multi-criteria performance measures. As conditions with single performance measures were not included in this evaluation study, only the results achieved in the pre-study with constant assistance levels are considered. There, we found that task completion time improved with increasing assistance level, while agreement was significantly deteriorated for SC_{disagree}. Collision time again increased significantly at low and high assistance levels. If the assistance levels were tuned according to a single criterion (task performance, collision time, or disagreement), the respective other criterion would be seriously deteriorated. A multi-criteria performance measure, on the contrary, can provide a trade-off between multiple measures by still preserving their relative importance through weighting. Consequently, one criterion should only be taken into account if it is of superior priority over all others. Such scenarios can be found for example in rehabilitation or when

learning motor skills, where smoothness of movements or the accuracy are more important than speed, disagreement, or mental workload. This user study focused on a manipulation task without learning or training background. For the selected maze scenario, the criteria task performance and disagreement are equally important. Thus, realizing a good trade-off between them is of utmost importance, and can be realized using a multi-criteria performance measure.

The benefit of providing a trade-off between multiple performance measures comes at the cost of a potentially unclear haptic feedback as it is not coded into the feedback signal which of the multiple measures requires improvement. This is illustrated in Fig. 5.24 for a continuously adapting assistance policy. In situation *a*, the assistance level changes due to a change in the user's speed, while it changes in situation *b* due to an increase in disagreement. Disagreement and speed increase together in situation *c* leading also to a decrease in the assistance level. The reason for the change in the assistance level may, however, not be evident to the user. If the user starts to explore the reason for the increased assistance level, this can again induce disagreement. This can also explain the higher disagreement observed for LAA^i compared to OCA^e where the assistance level is fixed druing the whole trial (for LAA^e smaller disagreement is found due to the rather small assistance levels in consequence of the user group performing very close to the reference). Perceived workload and performance and consequently also efficiency of LAA^i, however, were not found to be negatively affected.

Thus, it is concluded that if the multi-criteria performance measure and weightings are selected with respect to the task and the haptic assistance, no negative effects are expected from using a multi-criteria performance measure. A slight mistake in the design phase of the multi-criteria performance measure can, however, significantly worsen the situation as the behavior of the assistance might not seem logical to the user. The selection of the performance criteria for AbS^e is more straight-forward such that AbS^e clearly outperforms $\text{LAA}^{i/e}$ in this respect. AbS^e still optimizes multiple performance measures, but provides a much more clear feedback to the user as it switches between two assistance levels triggered by disagreement only.

5.6.4.5 Tuning Effort and Required Knowledge

A final criterion for the selection of the haptic assistance is the tuning effort. LAA^i requires the least tuning effort. The initial values are the only parameters that have to be tuned, which can be easily achieved based on the results of a few training trials. Required knowledge for the application of LAA^i are the task objectives like speed, accuracy, and agreement and their importance with respect to each other, if a multi-criteria performance measure was used. Moderate tuning effort is required for the assistance implementing an optimal constant assistance level and agreement-based switching. While OCA^e requires knowledge about the optimum assistance levels for the two different scenarios, AbS^e requires the threshold separating agreement from disagreement. Both can be determined from a series of training trials or alternatively can be calculated and updated online during task execution. Precise task knowledge in the form of best/worst reference curves and best/worst assistance levels is required for the linear-adapting assistance with external reference performance. Consequently, this last approach requires the most tuning effort.

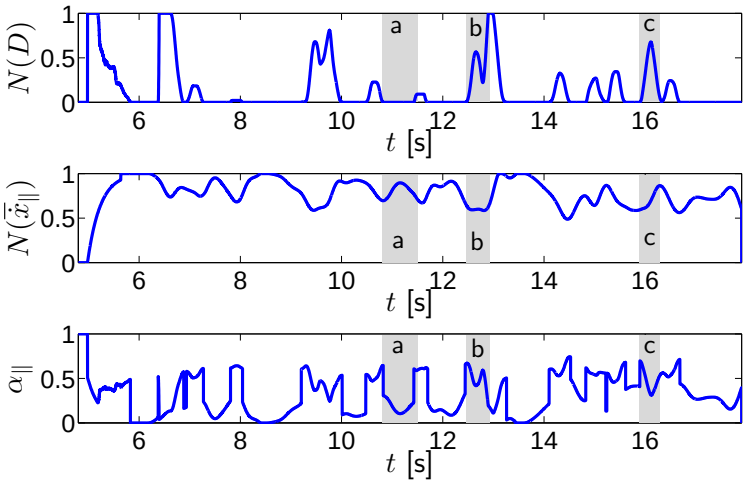

Fig. 5.24: Time-series of normalized disagreement, normalized tangential speed, and unfiltered assistance levels [3] for SC_{agree} using LAA^i.

5.6.4.6 Generalizability

Finally, generalizability of found results to different scenarios and setups is important. Although the idea behind LAA^i and LAA^e is very general and consequently has huge potential for generalization, these approaches strongly rely on a proper selection of the multi-criteria performance measure according to the specific task and objectives. In this context special attention has to be paid to causal dependencies of measures and assistance levels. Not taking into account causal dependencies can easily lead to non-intended behavior of the assistance. Having defined the multi-criteria performance measure properly, LAA^i can be expected to outperform OCA^e due to the continuous and multi-criteria adaptation. Causal dependencies can be easily extracted from a few test trials performed under constant assistance levels. The performance of LAA^e strongly relies on the selection of the best/worst references and the behavior of the specific user group. Finally, AbS^e is supposed to outperform OCA^e if scenarios of agreement and disagreement can be clearly distinguished and the assistance levels for the two scenarios are significantly different.

Table 5.3 summarizes the results of this discussion and highlights the favorite approach(es) for each measure and scenario.

5.7 Summary

Haptic assistances allow to augment the performance beyond manual control performance by combining the capabilities of machines with those of humans. Haptic assistances belong consequently to the class of performance-oriented control concepts for teleoperation systems. In this chapter, a general framework for designing haptic assistances was introduced and functional units and their interdependencies were derived. In this thesis, a haptic assistance is described as a combination of an interaction design unit, a path planning

[3] Please note that these measures are evaluated online, see Sec. 5.4.3.1.

Tab. 5.3: Recommended approaches depending on performance criterion.

	SC_{agree}	SC_{disagree}	$SC_{\text{disagree+agree}}$
Task performance	AbS^e, LAA^i	AbS^e, LAA^i	AbS^e, LAA^i
Agreement	OCA^e, AbS^e, LAA^e, LAA^i	LAA^e	LAA^e, AbS^e, OCA^e
Smoothness	OCA^e	LAA^e	LAA^e
Workload	LAA^i	LAA^e	AbS^e, LAA^i
Efficiency	AbS^e, LAA^i	AbS^e, LAA^i	AbS^e, LAA^i

unit, and a control unit. The interaction design unit analyzes the current scene and the cognitive and mental state of the operator. Machine learning approaches are often used in this context. The focus of this chapter was, however, on the control unit. The control unit is again decomposed into an assistance controller and an assistance policy unit. Regarding the path planning and assistance control unit, a lot of research exists while only few approaches propose concepts for the assistance policy unit taking into account more than one performance criterion.

The main contribution is the introduction of a design space for the assistance policy unit that decides on the applied assistance level. The assistance level influences the authority distribution between assistance and human operator. A three-dimensional design space spanned by the three independent axes i) performance measures, ii) reference performance, and iii) assistance policy was defined. Categorizing state-of-the-art implementations into this design space clearly showed a series of so far unexplored areas that can be systematically explored by designing new haptic assistances. Especially implementations that optimize multiple performance measures and realize dynamically changing assistances have rarely been investigated. A discussion of the introduced design space shows that a multi-criteria performance measure can be advantageous when a compromise between multiple, contradictory measures should be achieved. This benefit comes at the cost of a potentially unclear haptic feedback, since it is not coded in the feedback signal which of the multiple measures requires improvement. Comparing implementations with internal and external reference performance, it is expected that external references are well suited for training scenarios, while internal references better perform for scenarios where unexpected events are likely to occur. These expectations were investigated in detail in a qualitative and statistical evaluation.

More precisely, a variety of so far unexplored possibilities in the design space were developed and implemented for a specific virtual environment scenario. As the scenario considered in this thesis is designed such that task performance is the main objective, virtual fixtures were selected as haptic assistance scheme. For improving several performance measures simultaneously, a weighted sum of multiple performance measures was introduced as multi-criteria performance measure. The three different axes of the design space were

then experimentally explored. External and internal references were considered and tested assistance policies ranged from constant over switching to linear-adapting implementations. First, qualitative results showed significant differences in the behavior of the implemented assistance control policies. From the results, it could be hypothesized that constant assistances are highly predictable, but may lead to user dependence. The switching policy introduces fast changes in the assistance behavior and, thus, it remained unclear after the qualitative investigation whether such changes will deteriorate user acceptance and comfort. Finally, the qualitative evaluation showed that the linear-adapting approach provides continuous and performance-adapted assistance, but did not allow conclusion with respect to task performance, user comfort, and acceptance.

In order to answer these open questions, a user study was conducted in a second step. Several quantitative performance metrics like performance, agreement, and smoothness as well as qualitative performance metrics like perceived workload were analyzed along with an efficiency measure that correlates them. Due to the introduced multi-criteria performance measure, a trade-off between multiple, also contradicting performance measures was achieved. It was found that a single-criterion performance measure should only be applied if one performance criterion has superior priority over all others.

Assistances with an adaptive assistance level were found to have the potential to outperform assistances with constant assistance policy in terms of multiple performance measures. The same conclusion was drawn by Li et. al [120, 121] for a motor skill learning task. Switching assistance policies were found advantageous over continuously adapting assistance policies. This is because switching assistance policies are able to achieve an overall good trade-off between task performance and agreement, while continuously-adapting assistance policies provide more flexibility in prioritizing different measures. In contrary to the proposed switching assistance policy that only evaluates the agreement measure online and otherwise switches between fixed assistance levels, the proposed continuously-adapting assistance policy evaluates all performance measures online. Although this can be considered an advantage of the latter over the former, it does not come without cost. The feedback provided to the user can be unclear as it is not coded into the feedback signal which of the multiple measures requires improvement. This problem was found to be overcome by the agreement-based switching assistance policy as it still optimizes multiple performance measures, but provides a much clearer feedback to the user: it switches between the two assistance levels triggered by disagreement only, while a high task performance is guaranteed by the respective assistance levels selected for agreement and disagreement.

The analysis of internal versus external reference performance showed that an external reference performance is best suited for training or learning scenarios where the task is well defined, while in real-world scenarios an internal reference performance allows for a suitable adaptation of the assistance level also in case of unexpected events.

For future work, it would be interesting to evaluate different control policies for scenarios where single-criteria performance measures are best suited such as rehabilitation or training. Moreover, training effects and user dependency on the different proposed implementations should be evaluated.

Another interesting research aspect is to analyze physical and cognitive dominance as proposed in [73]. One of two haptically interacting partners is physically dominant

if he/she determines to a higher degree how to follow a desired trajectory, see [73]. A partner is cognitively dominant if he/she decides on the desired trajectory. As outlined in [73], physical dominance is a force-based measure, cognitive dominance a position-based measure. Thus, the cognitive dominance of the assistant is regulated within the trajectory planning unit of the haptic assistant, while the physical dominance of the assistant is determined within the assistance policy unit. In the current implementations, physical and cognitive dominance were tightly coupled. For future work, it would be interesting to design separate assistance policies and path planning strategies for physical and cognitive dominance of haptic assistants.

Although this thesis focuses on haptic teleoperation systems, it is worth mentioning that the proposed performance-oriented control concepts can be directly transferred to physical human-robot interaction where a human and a robot perform a joint manipulation task, e.g. transporting a heavy or bulky object. The two often implemented extreme behaviors are to passively follow the human or to take over control and lead the performed actions. As introduced in [51], also a continuous blending between these two behaviors or roles of a passive follower and an active leader is thinkable. The changing of the robot dominance corresponds directly to the regulation of α discussed here in form of different implementations of the assistance policy unit. Recent work on designing roles for an autonomous robot interacting with a human are given in [115, 142]. The transfer of the proposed design space and the investigated implementations to physical human-robot interaction is interesting and important to be investigated in future work.

This thesis presented so far a transparency- and a performance-oriented control concept. The idea of the following chapter is to combine transparency- and performance-oriented controller into a novel multi-criteria control concept.

6 Towards Multi-Criteria Control Concepts

In order to allow a human operator to successfully and efficiently perform manipulations in a remote place, haptic teleoperation systems should be designed such that a high degree of fidelity close to transparency, a high task performance, a strong feeling of presence, and a high usability are achieved. Technical deficiencies of e.g. the devices, the communication channel, or the controllers limit, however, the realizability of these objectives. Moreover, some of the objectives like transparency stay in conflict with robust stability, a requirement that has to be fulfilled for any teleoperation system. In order to mitigate these conflicts and to get closer to the ideal teleoperation system, a variety of control concepts were presented in the telerobotics literature. In order to improve fidelity, a transparency-oriented control concept can be employed. It aims at minimizing the error between the dynamics of the remote environment transmitted and presented to the operator and the real dynamics of the environment. The objective of a performance-oriented control concept is that a high task performance in terms of e.g. high speed, high accuracy, or small required energy is realizable. Control concepts that online evaluate the feeling of presence or usability in order to improve these objectives are not found in the current telerobotics literature, mainly as quantitative and online evaluable measures for feeling of presence and usability are only partly available.

So far, this thesis investigated transparency- and performance-oriented control concepts separately with significant improvements found for fidelity or task performance. In the first part of this thesis, model-mediated teleoperation was investigated as a transparency-oriented control concept that can significantly improve fidelity as defined by Lawrence [116] for systems with negligible, medium, and large time delays (> 0.5 s). The second part of this thesis was dedicated to the design of flexible, user- and task-adapted haptic assistances that improve task performance beyond manual control performance by augmenting the operator commands through computer-generated commands. New, user- and task-adapted assistances were proposed, that find a trade-off between multiple performance criteria.

Ideally, controllers of a teleoperation system would optimize all objectives at the same time. Or, if this is not realizable, it is desired to find an optimal trade-off between the objectives. This chapter is dedicated to multi-criteria control concepts for haptic teleoperation systems. Two main control concepts are distinguished: 1) control concepts derived from multi-criteria optimization and 2) concepts that are based on a suitable integration of controllers that improve a single objective (single-objective controller). While the first class of control concepts is well-known in telerobotics literature, the second class has not been fully exploited yet and will be the focus of this chapter.

More precisely, one concept for integrating single-objective controllers is presented as a novel type of multi-criteria control concept for haptic teleoperation systems. Related work was only found in the field of autonomous robotics by Ganesh et al. [62]. The novel multi-criteria control concept is expected to achieve a superior multi-criteria per-

formance compared to multi-criteria optimization approaches especially as the parameters are adapted at each time step to improve the single criteria and the performance-oriented controllers can be designed in an active or proactive way. This chapter presents one design concept and the resulting control architectures for the integration of a selected class of adaptive, single-objective controllers into one system. Possibilities for keeping the system stable during task execution are presented and discussed. Furthermore, a first adaptive, multi-criteria controller with similar properties to [62] is designed and evaluated in a proof-of-concept study. The result is a novel, adaptive, multi-criteria system. The effectiveness of the multi-criteria controller is shown in experiments. Experimental results and comparisons with single-objective controllers are presented to confirm the expected improvement in the two investigated objectives, fidelity (transparency) and task performance.

As the design of multi-criteria controllers for haptic teleoperation systems has not been fully exploited yet, the chapter concludes with numerous open research questions, that have been identified and that are supposed to motivate further research in this direction.

The chapter introduces first the state-of-the-art control concepts derived from multi-criteria optimization and sketches the extension to multi-criteria control for haptic teleoperation. In Sec. 6.2, the integration of existing single-objective controllers into one system is presented and discussed. The proof-of-concept study of a selected multi-criteria controller is presented in Sec. 6.3. The chapter further provides a discussion of future research aspects in Sec. 6.4 and finishes with a summary and conclusion in Sec. 6.5.

6.1 Related Work

The state-of-the-art in multi-criteria control for haptic teleoperation systems focused so far on control approaches, that are based on multi-criteria optimization. One prominent approach for deriving a controller that optimizes several performance criteria is H_∞ control, see e.g. [69]. The resulting controller is guaranteed to be robustly stable with time-invariant parameters. H_∞ control has been also researched for teleoperation systems in order to find an optimal trade-off between fidelity and robust stability, see [39, 89, 90, 101, 119, 195, 217]. The performance criteria for the H_∞ optimization routine were related to transparency, e.g. based on force or position errors between master and slave. By extending the H_∞ approach and taking additionally task performance measures like the operator speed, forces, or energy as criteria for the optimization routine into account, the resulting controller is expected to provide an optimal trade-off between transparency and task performance while guaranteeing robust stability.

The advantages of H_∞ control are that the resulting controllers are guaranteed to be stable with respect to the considered perturbations in operator behavior, remote environment, and task, and that an optimal trade-off between different criteria is found. The resulting system is, however, only optimal for the considered scenario. If the operator, environment, or task changes in an unexpected way during teleoperation, optimality is not guaranteed anymore. As a consequence, the expected improvement in the different objectives may not be reached. Also, it is often difficult to interpret the resulting control parameters especially if the controller is of high order. This can lead to a high tuning effort. For performance improvements, it may be desired to actively guide the operator

by means of active or pro-active haptic assistance. With an (pro-)active haptic assistance, the operator can follow paths easier, i.e. faster and without collisions, or he/she can be warned against entering forbidden regions in the workspace. An H_∞ controller cannot provide (pro-)active haptic assistance. These drawbacks inspired to some extent the idea of integrating single-objective controllers into one system.

As mentioned above, the work by Ganesh et al. [62] in the field of autonomous robotics presents an approach where multiple single-objective controllers are combined into one system. Ganesh et al. [62] proposed a human-inspired adaptation strategy. This work showed that humans adapt their feedforward and feedback control strategy when learning new motor tasks in order to achieve multiple objectives: successful task execution and high performance with minimal control effort and movement error. Based on a minimization problem, an adaptation law was derived which was shown to reduce the costs as desired. This approach will be the baseline for the multi-criteria controller that will be presented in the proof-of-concept study.

6.2 Multi-Criteria Control Concept

The problem statement for a multi-criteria control concept can be described as the minimization of multi-criteria system costs J over all stabilizing control parameters $C \in \mathbb{C}$. The minimization of the costs J is given as the weighted sum of the costs for each optimization criterion, in this case transparency J_t, and performance J_p

$$\min_{C \in \mathbb{C}} J = \min_{C \in \mathbb{C}} (w_t \, J_t + w_p \, J_p), \tag{6.1}$$

where w_t and w_p represent weights for transparency and performance. All concepts are certainly expendable to incorporate further objectives as long as they are quantifiable. At the moment, quantifiable measures are mostly available for transparency and task performance, see Sec. 2.2. Although transparency is dependent on the environment dynamics, the measure, e.g. the transparency error, remains the same. The performance measures, on the contrary, may change depending on the tasks that are performed during teleoperation. Path-following or transportation tasks, for example, require high motion accuracy and/or speed, tasks involving contact with objects often require an accurate force tracking. If the task consists of subtasks with different performance objectives, i) either the system costs are determined for each subtask separately or ii) the different performance criteria are incorporated into a single cost function. Given the cost function and the system dynamics, the desired control concept and corresponding implementation have to be selected.

Generally, two classes of multi-criteria control concepts are identified: i) one controller, that provides an optimal trade-off between the different objectives, is derived based on the cost function (6.1) or ii) specific, compatible control concepts are selected for each criterion and combined into one system. This chapter focuses on the second class of control concepts, which has been rarely investigated in telerobotics literature so far. More precisely, one integration concept and the resulting control architectures are introduced in this section. The proposed multi-criteria control architecture is especially suitable if promising single-objective controllers were identified and their effectiveness was shown.

The proposed control architecture is designed for the admittance-type experimental setups considered in this thesis. The local controllers on master and slave site are therefore restricted to force or admittance/impedance controllers. The communication channel is assumed to be lossless and latency-free. An extension to other controller classes remains future work. The integration strategy will vary with the selected single-objective controllers. In this thesis, it is introduced based on the following classes of transparency- and performance-oriented controller: In the overview of state-of-the-art transparency-oriented controllers for fidelity augmentation, see Sec. 2.4.1.2, it was found that most approaches adapt the control parameters according to estimated characteristics of the remote environment. This class of controllers is selected as the basic transparency-oriented control concept for the multi-criteria controller. Regarding performance augmentation, virtual fixtures were identified as one class of popular and promising performance-oriented approaches, see Sec. 2.4.2.2. They belong to the class of haptic assistances and will be used in the multi-criteria control concept for improving performance.

The objective of virtual fixtures is to modify the operator commands either on the force or position level such that the resulting actions improve performance. They rather act as a trajectory planning unit than as a control unit. As integration concept, it is therefore proposed to combine the single-objective controllers by *cascading* them, see Fig. 6.1. Alternatives like combining the controllers in a parallel connection or switching between them may be suitable for other classes of controllers. They are not subject of research in this work. If the virtual fixtures act on the force level, they run in the outer cascade and provide (together with the operator command) the desired force for the transparency-oriented controller, running in the inner cascade. If the virtual fixtures act on the position level, the cascade structure is inverted, i.e. a desired trajectory is generated by the transparency-oriented controller and fed into the virtual fixtures. In order for the operator to get continuous haptic feedback from the virtual fixtures, it is more suitable to use them on the master site only. The transparency-oriented controller, that is adaptive to changes in the remote environment, can be implemented on master site, slave site, or on both sites. The architecture connecting local and remote site can be implemented as known from the classical four- and two-channel architectures.

Both single-objective control concepts are well understood. Thus, it can be analyzed how they will influence each other and when critical situations especially for the stability of the system may occur. A short discussion aims at illustrating the interactions between the controllers. If the virtual fixture runs in the outer cascade, see Integration I in Fig. 6.1, it essentially acts as an impedance and provides assisting forces depending on the distance between measured master position x_m and reference position r^*_{assist}. The advantage of this architecture is that the operator will directly feel the actions of the virtual fixture. The most critical aspect is to guarantee stability. Stability-critical situations can occur, if large forces from the virtual fixture are fed into a stiff transparency-oriented force controller or a transparency-oriented admittance controller with small target dynamics. As long as the parameters of the controllers are adapted in these situations, both controllers can run simultaneously. As a consequence, the fidelity-augmenting control parameters and the assisting forces of the virtual fixture are perceived by the operator and lead to an improvement in both objectives.

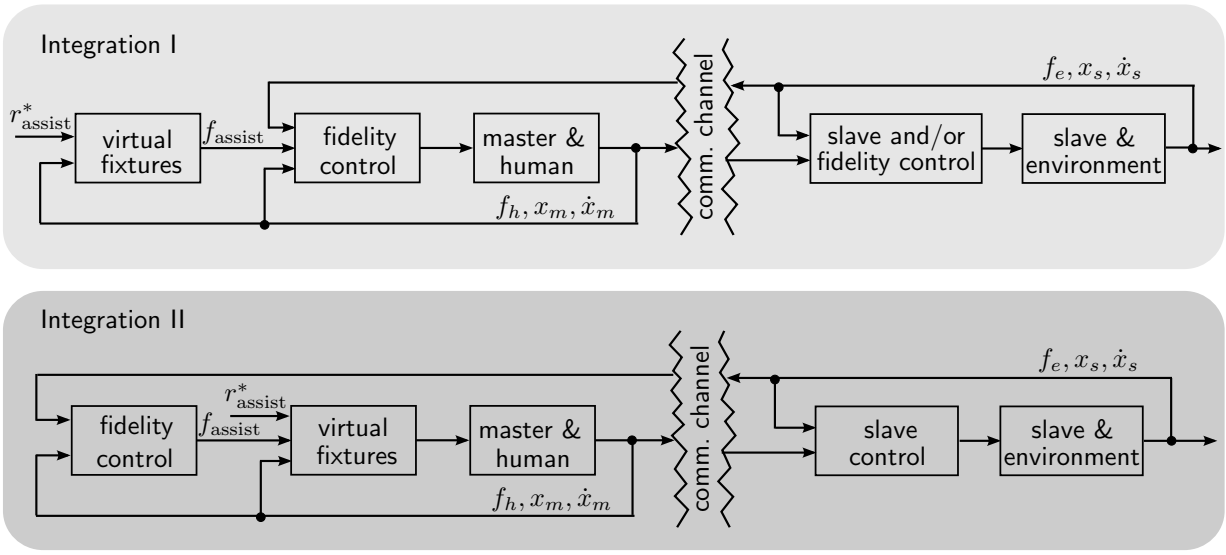

Fig. 6.1: Multi-objective control concept: adaptive transparency-oriented controllers referred to as fidelity control is cascaded with virtual fixtures, the considered performance-oriented controller. Regarding integration I, virtual fixtures run in the outer loop, while the fidelity controller runs in the inner loop. This structure is inverted for integration II. Force or admittance/impedance controllers are assumed as local controllers and as basis for the fidelity controller.

If the virtual fixture runs in the inner cascade, it will modify the desired trajectory. This has, however, no consequence for the transparency-oriented controller as will be shown in the proof of concept study. This type of cascade structure referred to as Integration II in Fig. 6.1 is therefore less critical for instabilities. The disadvantage is that the operator does not directly feel the commands from the virtual fixture. He/she will only see the modified trajectory.

In the above discussion, it became evident that stability is a critical aspect for multi-criteria control. Two ways for adapting the parameters and keeping the system stable are identified: i) the parameters of each controller are determined a priori such that the overall system is stable or ii) a stability observer is introduced that adapts the control parameters online if an undesired, oscillating behavior is detected.

The first method for guaranteeing stability is to select the control parameters such that the closed-loop integrated system is (robustly) stable. This is achieved by analyzing the safety-critical situations. Considering the proposed multi-criteria control architecture, stability-critical situations can occur if e.g. the virtual fixture provides strong assisting forces in free space and the transparency-oriented controller increases the stiffness (force control) or reduces the target dynamics (admittance control) in order to improve fidelity. Thus, the parameters of the single-objective controllers have to be adapted accordingly. Yet, the resulting stability regions may be more conservative than those of the single-objective controllers. In consequence, a trade-off is typically accepted between the different objectives. This implies that improvements in all objectives are achieved but they may not be as large as for the single-objective controllers individually. It is important to note that the classical stability analysis tools are not applicable as the transparency-oriented

controller class is time-varying. In this case, advanced stability analysis tools like Lyapunov theory, see e.g. [95, 146] for their application in adaptive control, or methods as presented in [44, 193] for second-order linear time-varying (LTV) systems can be used if the assumptions are met. As these stability proofs are difficult and often only possible for simplified model dynamics, a second possibility for guaranteeing stability is presented in the following.

Instead of determining the control parameters off-line such that the resulting system is guaranteed to be stable, the control parameters can be adapted online if undesired, oscillatory behavior is observed. This reduces the tuning effort. One possibility for a fast suppression of undesired, oscillatory behavior during teleoperation is to augment the integrated system with a stability observer and controller as proposed in [175]. The idea is not to prevent the system from oscillations, but to detect and suppress them by adapting the control parameters accordingly. The approach proposed by Ryu et al. [175] is based on the frequency spectrum of the master and/or slave motions. If master and slave positions are tightly coupled, the analysis of one of these positions is sufficient in order to detect oscillations in the system. Thus, only the master position x_m is analyzed in the remainder of this section. The discrete Fourier transformation with a window length of N samples is used to online calculate the frequency spectrum of x_m. The sampling time is denoted by T_a. The selection of the window length and sampling frequency is of utmost importance for a fast and reliable detection of oscillations. A detailed analysis of these parameters is provided in [175]. By defining a frequency f_u above which the motions are considered as oscillatory, a stability index R can be calculated according to [175] by summing the amplitudes of the frequency spectrum H above f_u and dividing it by the sum of all amplitudes

$$R = \frac{\sum_{f \geq f_u} H(f)}{\sum_f H(f)}. \tag{6.2}$$

The stability measure R is continuous and restricted to the interval $[0; 1]$. It is assumed that the effect of the single-objective controllers on stability is known. Thus, using this stability index, the control parameters of the transparency- and performance-oriented controllers can be adapted accordingly. Taking an admittance controller with mass-damper dynamics as example, an increase in R corresponding to an increase of oscillations in the system can be diminished by increasing the two admittance parameters (either one of the two or both depending on the implementation). This approach is especially suitable if the controllers influence each other or if an a priori stability analysis can only be performed for strong assumptions regarding the system dynamics such that the resulting parameters do not guarantee to stabilize the real system. As the stability observer only reacts if some oscillatory behavior occurs, these oscillations can be perceived by the human operator.

The approach based on a stability observer and controller only diminishes the fidelity- and performance-augmenting actions if undesired, oscillatory behavior is observed. As long as oscillations occur only rarely and are of small amplitude, this approach may lead to high multi-criteria performance. The tuning effort is smaller than for the H_∞ control and the performance-oriented controller can be of active or proactive nature.

Concluding this section, a novel multi-criteria control concept was presented for a selected class of single-objective controllers. It is proposed to cascade the single-objective controllers such that either the performance- or transparency-oriented controller runs in

the inner loop, while the respective other runs in the outer loop. The idea of combining single-objective controllers into one system has only been investigated in the field of autonomous robotics. The advantages compared to classical multi-criteria optimization-based approaches like H_∞ are i) a high flexibility of the system to unexpected events as the controllers can be selected in an adaptive way taking online gained knowledge about environment, operator, and task into account, ii) significant improvements in task performance as an active or pro-active performance-oriented control concept can be implemented, and iii) high multi-criteria improvement as the parameters are adapted at each time step to improve fidelity and performance. One drawback of the introduced control approach is that rigorous stability proofs for interconnected and adaptive controllers are difficult especially compared to an H_∞ approach, where robust stability is guaranteed for the resulting controller.

6.3 Proof of Concept

The following study provides a first evidence that the proposed multi-criteria controller concept is applicable to haptic teleoperation systems and leads to an improvement in all considered objectives compared to single-objective controllers.

The proof-of-concept study is based on a bachelor thesis by A. Spenninger, see [241]. A multi-criteria cost function as in (6.1) is used to evaluate the integrated system. As presented in the previous section, an adaptive transparency-oriented controller and virtual fixtures are selected as single-objective controllers. The adaptation strategy is similar to the one in [62]. The transparency-oriented controller does not only adapt the control parameters in order to improve fidelity but it also keeps the integrated system stable. Thus, it essentially incorporates a stability observer and controller. The basic control architecture for this study is the FaFa architecture, which will be shortly reviewed in the following section. For evaluating the effectiveness of the integrated system, the costs are determined for the multi-criteria and for the classical FaFa control architecture. As the fidelity improves with smaller admittance parameters, see Chap. 3, the admittance parameters for the classical control architecture were tuned manually as small as possible without risking instabilities for the selected task. The task consisted of free space and contact phases with a stiff object. Thus, a good trade-off between stability and fidelity/task performance was achieved for the classical controller.

This section starts with the description of the basic control architecture, followed by the control concepts for transparency and performance. Experimental results are then presented for the integrated as well as the classical control concept. The subsequent evaluation and discussion finishes the section.

6.3.1 Basic Control Architecture

The master and slave devices used in this thesis are of admittance-type. A suitable control architecture for these setups is the FaFa architecture, where position-based admittance controllers on master and slave site are connected with each other over the communication channel through a bilateral force exchange, see also Sec. 2.3.1. The dynamics of

the FaFa architecture is given by (2.24). This dynamics can be modified to incorporate transparency- and performance-oriented controllers, which is illustrated in the following for one translational direction.

The main idea regarding environment-related transparency-oriented controllers is to increase the fidelity of the system by adapting the control parameters according to the estimated environment dynamics $\hat{Z}_e$. In the following, only the admittance parameters are adapted:

$$\begin{aligned} 0 &= \tilde{f}_h - \tilde{f}_e + g_{am}(\boldsymbol{X}_m^d, \boldsymbol{p}_{am}, \hat{Z}_e) \\ 0 &= \tilde{f}_h - \tilde{f}_e + g_{as}(\boldsymbol{X}_s^d, \boldsymbol{p}_{as}, \hat{Z}_e), \end{aligned} \tag{6.3}$$

where $\tilde{f}_h$ and $\tilde{f}_e$ represent measured forces including sensor dynamics, and $g_{am}(\boldsymbol{X}_m^d, \boldsymbol{p}_{am}, \hat{Z}_e)$ and $g_{as}(\boldsymbol{X}_m^d, \boldsymbol{p}_{am}, \hat{Z}_e)$ represent time-varying admittance mappings on master and slave site, respectively. The admittance parameters are summarized in the parameter vectors $\boldsymbol{p}_{am}$ and $\boldsymbol{p}_{as}$, while the vectors $\boldsymbol{X}_m^d$ and $\boldsymbol{X}_s^d$ are composed of the desired master/slave position, velocity, and acceleration. The adaptation of the admittance is dependent on the estimated environment impedance $\hat{Z}_e$. Stability can e.g. be investigated using analysis tools from adaptive control, which are mostly based on Lyapunov theory.

A haptic assistance represents a performance-oriented control concept for haptic teleoperation systems. It acts either on the force or position level. The assistance force/position, f_{assist} or x_{assist}, can depend on the human input force, the environment force, the state of master and slave, and on a state-independent position/force reference trajectory r^*_{assist}. When acting on a force level, an additional assistance force is added to the input force from operator and environment on master and slave site:

$$\begin{aligned} 0 &= \tilde{f}_h - \tilde{f}_e + f_{\text{assist}}(f_h, f_e, \boldsymbol{X}_m, r^*_{\text{assist}}) + g_{am}(\boldsymbol{X}_m^d, \boldsymbol{p}_{am}) \\ 0 &= \tilde{f}_h - \tilde{f}_e + f_{\text{assist}}(f_h, f_e, \boldsymbol{X}_s, r^*_{\text{assist}}) + g_{as}(\boldsymbol{X}_s^d, \boldsymbol{p}_{as}). \end{aligned} \tag{6.4}$$

If the assistance is provided on the position level, the desired master and slave positions are the sum of assisted and desired, operator-commanded position, which are then tracked using PD-controllers:

$$\begin{aligned} 0 &= f_m + K_{pm}(x_{am}^d - x_m) + K_{dm}(\dot{x}_{am}^d - \dot{x}_m) \\ 0 &= f_s + K_{ps}(x_{as}^d - x_s) + K_{ds}(\dot{x}_{as}^d - \dot{x}_s) \end{aligned} \tag{6.5}$$

with $x_{am}^d = x_m^d + x_{\text{assist}}(f_h, f_e, \boldsymbol{X}_m, r^*_{\text{assist}})$ and $x_{as}^d = x_s^d + x_{\text{assist}}(f_h, f_e, \boldsymbol{X}_s, r^*_{\text{assist}})$ and $\dot{x}_{am}^d$ and $\dot{x}_{as}^d$ the corresponding time derivatives. Integrating the transparency-oriented control concept (6.3) and the force-based haptic assistance (6.4) into a multi-criteria system leads to a time-varying and nonlinear dynamics:

$$\begin{aligned} 0 &= \tilde{f}_h - \tilde{f}_e + f_{\text{assist},m}(f_h, f_e, \boldsymbol{X}_m, r_a^*) + g_{am}(\boldsymbol{X}_m^d, \boldsymbol{p}_{am}, \hat{Z}_e) \\ 0 &= \tilde{f}_h - \tilde{f}_e + f_{\text{assist},s}(f_h, f_e, \boldsymbol{X}_s, r_a^*) + g_{as}(\boldsymbol{X}_s^d, \boldsymbol{p}_{as}, \hat{Z}_e). \end{aligned} \tag{6.6}$$

As the performance-oriented control runs in the outer cascade, this multi-criteria control architecture corresponds to integration type II in Fig. 6.1. It can be seen from the last two equations that the assistance force f_{assist} enters the adaptive admittance together with the forces from the operator and the environment. The adaptive admittance controller

(transparency-oriented control) and the haptic assistance (performance-oriented control) influence each other and the stability regions will not remain the same as for each controller separately.

Similarly to (6.6), the adaptive admittance controller (6.3) can be combined with a haptic assistance acting on the position level, see (6.5), to form a multi-criteria system. This corresponds to the second multi-criteria control architecture shown in Fig. 6.1. As will be illustrated in an example in the subsequent section, these two single-objective controllers do not influence each other as one is acting on the signal level and one on the parameter level. These single-objective controllers can consequently be combined without further modifications. It can therefore be concluded, that it depends on the implementation whether single-objective controllers influence each other when being integrated into one system.

6.3.2 Transparency-oriented Controller

In a first step, a transparency-oriented controller known from literature is selected. In order to improve the fidelity of the system and to keep the system stable, an adaptive admittance controller is chosen. An overview of state-of-the-art adaptive controllers can be found in [238] and Sec. 2.4. A linear time-varying mass-damper dynamics is selected for the master and slave admittance where $\boldsymbol{p}_{am}(t) = \boldsymbol{p}_{as}(t) = [m_a(t), b_a(t)]$:

$$g_{am} = m_a(t)\ddot{x}_m^d + b_a(t)\dot{x}_m^d \qquad g_{as} = m_a(t)\ddot{x}_s^d + b_a(t)\dot{x}_s^d. \tag{6.7}$$

As proposed in [62], the minimization of the admittance parameters corresponds to a minimization of human effort and an improvement of fidelity. A significant reduction of the admittance parameters may, however, result in oscillations especially if the human behavior or environment dynamics change. The idea for adapting the admittance parameters is based on the following human behavior: the human adapts his/her arm impedance according to the amplitude (P) and to the changes of the amplitude (D) of an error signal ϵ, see [62, 196]. In other words, a human adapts his/her arm impedance depending on a feedback error ϵ. This feedback error is generated from a proportional-derivative (PD) controller with gains $K_{p,T}$ and $K_{d,T}$ and a control error e as input:

$$\epsilon = K_{p,T}e + K_{d,T}\dot{e}. \tag{6.8}$$

This idea is used to adapt the admittance parameters. The feedback error ϵ is designed to detect changes in human/environment dynamics incorporated in the control error e. Prominent examples for the selection of e are the difference between master and slave position or force or the environment force only.

Given the feedback error ϵ, the admittance parameters $\boldsymbol{p}_{am}$ and $\boldsymbol{p}_{as}$ are selected to improve fidelity:

$$\dot{\boldsymbol{p}}_{am} = \beta_m|\epsilon_m| - \gamma_m \qquad \dot{\boldsymbol{p}}_{as} = \beta_s|\epsilon_s| - \gamma_s, \tag{6.9}$$

where β and γ are design parameters. Whenever ϵ is small, the parameter γ reduces the admittance parameters and thereby improves fidelity. Whenever a significant feedback error is detected, the admittance parameters are increased. Thus, oscillations are suppressed.

The benefit of this controller is an increased degree of fidelity while avoiding oscillatory or unstable behavior. Yet, the changes in the admittance parameters may be perceivable for the operator. Especially when releasing contact, the fast but maybe not fast enough decrease of the parameters can lead to a sticky feeling. Also, as for any adaptive controller, the benefit is dependent on the parameter tuning. Especially the derivative gain $K_{d,T}$ has to be selected carefully in order to avoid a too high sensitivity to changes, that may result in permanent parameter changes or even instability. If it is selected too small, the adaptation may be too slow.

6.3.3 Performance-Oriented Controller

The second step for a multi-criteria controller for haptic teleoperation systems is to select a performance-oriented controller, in this case a haptic assistance. The most prominent approach are virtual fixtures as presented in Sec. 2.4.2.2. They are used to reduce human effort, and to increase speed and accuracy. Virtual fixtures drive the human operator to a reference path r^*_{assist} by either applying an assisting force or modifying the desired position. In this study, the desired master and slave position x^d_m is modified such that the reference is followed, see also (6.5). In order to allow a cooperative interaction between the haptic assistance and the operator and to guarantee a successful and safe task execution, the reference path should be adaptable to the human behavior. If it were not, the human operator cannot change the task as desired and sudden changes in the environment would lead to collisions. Thus, an adaptive law for the reference path is to be developed. It is selected similar to the adaptation approach of the admittance parameters described in the previous subsection and, thus, is related closely to the feed-forward adaptation proposed by Ganesh et al. [62]. The reference path is followed as long as the human operator does not intervene. If the path is left, but the operator is moving towards the reference path, a relaxation process can be started which drives the system back to the reference path. The resulting reference path velocity $\tilde{\dot{r}}^*_{\text{assist}}$ is determined according to the adaptation law

$$\tilde{\dot{r}}^*_{\text{assist}} = \begin{cases} \alpha_P \, (1+\mu) \, \dot{r}^*_{\text{assist}} & \text{if } \operatorname{sign}(\dot{r}^*_{\text{assist}}) = \operatorname{sign}(r^*_{\text{assist}} - x_m) \text{ and } \|r^*_{\text{assist}} - x_m\| \geq d_{r_{\text{assist}}} \\ \alpha_P \, \dot{r}^*_{\text{assist}} & \text{else} \end{cases} \tag{6.10}$$

with

$$\dot{\alpha}_P = \beta_P |\epsilon_P| - \gamma_P \tag{6.11}$$

and

$$\epsilon_P = K_{p,P} f_h + K_{d,P} \dot{f}_h. \tag{6.12}$$

The adaptation parameter α_P is restricted to the interval $[0; 1]$. It reduces the reference velocity whenever the human operator intervenes. In this case, the virtual fixture becomes inactive and the operator can perform the change in the task as desired without having to counteract the haptic assistance. Whenever he/she reduces the force, the haptic assistance will be activated again such that the original reference path would then be followed at

the new location. The relaxation process is triggered if the device is moved towards the reference path and the distance between reference and device position exceeds a pre-defined distance $d_{r_{\text{assist}}}$. A movement towards the reference path is interpreted as the operator's intention to continue with the original task. Returning to the original task is facilitated through amplification of the reference velocity by the factor μ. The parameter μ determines the convergence time to the original path. It has to be selected in order to meet the bandwidth limitations of the device.

The benefit of the introduced virtual fixture is a significant reduction of the human effort. However, this is only achieved if the operator does not deviate from the learned task. Shifting the operating point of the task to another area in the workspace requires the same effort as without virtual fixture. As the task modification cannot be anticipated by the haptic assistance, a support is not possible here. In order to increase the applicability of the haptic assistance, an intention recognition unit would be required such that the reference path can be reset or another haptic assistance can be selected. Thus, it can be concluded, that the haptic assistance is mainly beneficial if a task is performed repeatedly.

6.3.4 Experimental Results

For evaluating the transparency- and performance-oriented controllers, the 1 DoF experimental setup described in Appendix A.4 is used.

6.3.4.1 Transparency-oriented Controller

In order to provide stability during free space as well as contact with stiff static objects, the admittance parameters are restricted to the intervals $m_a \in [1;4]$ kg, $b_a \in [5;10]$ Ns/m. These parameter intervals were determined experimentally to guarantee stability for contact with the investigated objects. The objective of the adaptive admittance controller is to improve the fidelity of the system as long as changes in the human operator or environment dynamics do not lead to oscillations. Thus, the feedback signal e is selected as the difference between filtered operator and environment force $e = \tilde{f}_h - \tilde{f}_e$. In order to track changes in the feedback signal and its derivative fast enough, but without oscillations, $K_{p,T}$ and $K_{d,T}$ were experimentally set to

$$K_{pm,T} = K^a_{ps,T} = 1 \qquad K_{dm,T} = 0.15 \cdot 10^{-3}, K^a_{ds,T} = 3 \cdot 10^{-3}. \tag{6.13}$$

The parameters of the adaptation laws (6.9) were experimentally tuned to provide fast adaptation to errors as well as a fast decay whenever the error gets small:

$$\beta_m = 5 \quad \beta_s = 4 \quad \gamma_m = \gamma_s = 10. \tag{6.14}$$

The results shown in Fig. 6.2(a) and Fig. 6.2(b) illustrate that the admittance parameters are increased whenever oscillations induced by the operator or high interaction forces from contact with a stiff object occur. Whenever contact is released, the parameters return fast to small values. The adaptive admittance controller allows to reduce the virtual mass by 80 % and the damping by 50 % (if e is small) compared to a non-adaptive FaFa architecture. Thus, the fidelity of the system is improved considerably, especially in free

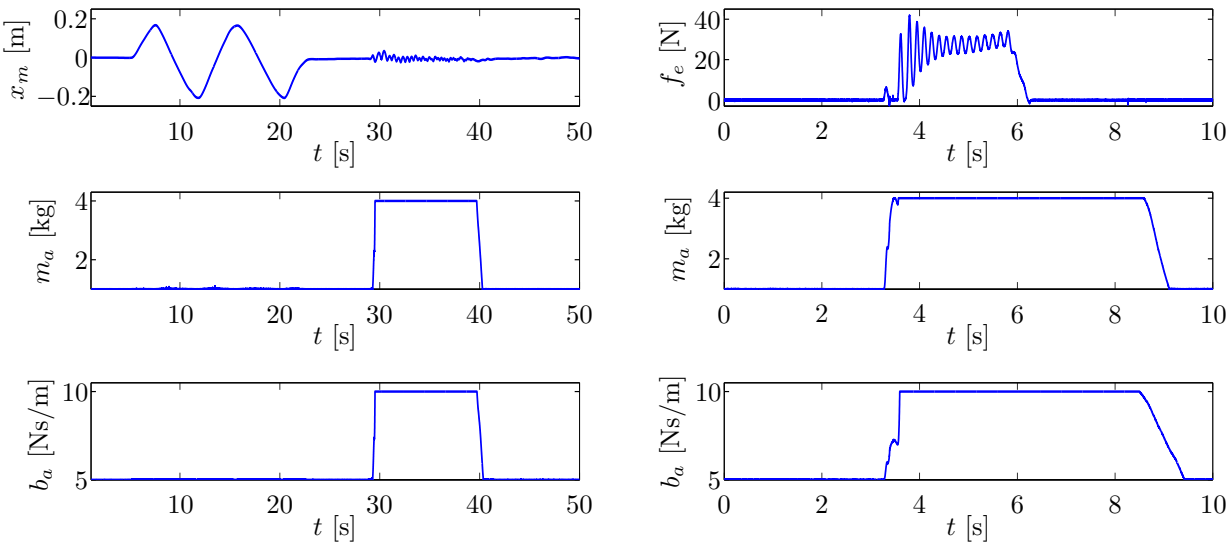

(a) Operator-induced high-frequent oscillations.

(b) Contact with a stiff wall.

Fig. 6.2: Experimental results for adaptive admittance controller. Pictures are taken from [241] and were slightly modified.

space. The adaptation of the admittance parameters was perceived if the admittance parameters were not reduced fast enough when relasing contact. A sticky feeling may occur in this case. This effect can, however, be diminished when detecting movements out of the object and reducing the admittance parameters accordingly. The strong increase in the admittance parameters when establishing contact was not felt.

6.3.4.2 Performance-oriented Controller

For the performance-oriented controller, it is assumed that the task is performed repeatedly and not known a priori. Consequently, a reference path can only be learned after a first task execution. A limited number of master positions were recorded and transformed into a smooth trajectory through a nonlinear interpolation, see [241] for details. As the path corresponds to a human-performed path, it is safe to apply it to the system and will not introduce any oscillations or instabilities. The admittance parameters were set to constant values, $m_a = 3$ kg, $b_a = 10$ Ns/m. It was found in experiments, that changes in the operator force can be detected fast enough without evoking oscillations in ϵ with

$$K_{p,P} = 1 \qquad K_{d,P} = 0.01. \tag{6.15}$$

The parameters for the adaptation of α and μ were experimentally set to realize a fast increase in α in case of an increasing feedback error and a fast decay of α whenever the feedback error decreases:

$$\beta_P = -3.9 \quad \gamma_P = -3.5 \quad \mu = 0.3. \tag{6.16}$$

The initial value for $\alpha_P = \alpha_{P0} + \int \tilde{\alpha}_P \, \mathrm{d}t$ is set to $\alpha_{P0} = 1$. Fig. 6.3(a) shows that the operator can arbitrarily modify the operating point of the task. The haptic assistance

is essentially deactivated such that the operator does not have to apply extra forces for leaving the reference path. As mentioned above, also a relaxation process can be started

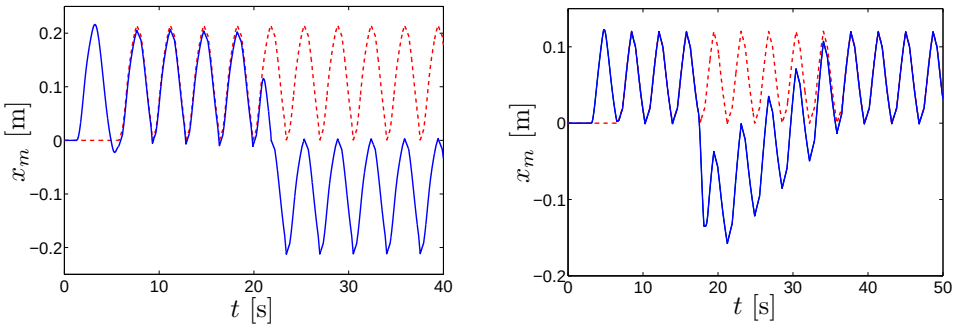

(a) Modification of operating point

(b) Relaxation to the original operating point

Fig. 6.3: The solid line represents the realized master position, while the dashed line shows the reference trajectory of the haptic assistance. a) The operator changes the operating point of the task without additional effort. b) If desired, the assistance drives the system back to the original operating point.

for driving the system back to the original operating point. The position of the master device is shown together with the reference position in Fig. 6.3(b). The operator leaves the reference path at $t = 17.5$ s and releases the device when reaching the desired new position. Thus, the haptic assistance is again activated and would perform the original task at the new position. As the relaxation process was activated, the master device is, however, accelerated towards the original reference path and reaches it after several task repetitions. The number of repetitions depends on the distance between original and modified operating point as well as on the parameter μ. This parameter has to be selected such that the bandwidth limitations of the device are not exceeded. Comparing the costs J_P of the performance-oriented controller with those of the FaFa architecture, see Table 6.1, a considerable reduction in the required effort is observable. The augmentation of the operator commands through computer-generated commands from a haptic assistance is consequently effective for this scenario.

6.3.5 Integrated System

The transparency- and performance-oriented controllers presented in the previous section can now be integrated into one system. In a first step, it is investigated whether the performance- and transparency-oriented controllers can run simultaneously without counteracting each other.

Two versions of virtual fixtures are analyzed: i) the reference path r^*_{assist} is added to the desired master position or ii) a virtual spring is attached between desired master position and reference path leading to an assistance force. Only the master site is analyzed and actuator dynamics and the bandwidth limitation of the force sensor are neglected. The state is defined as $\boldsymbol{x} = [x^d_m, \dot{x}^d_m, x_m, \dot{x}_m]$. The integrated system dynamics is then given for

the assistance on position level by

$$\dot{\boldsymbol{x}} = \boldsymbol{A}\boldsymbol{x} \tag{6.17}$$

$$= \begin{bmatrix} 0 & 1 & 0 & 0 \\ -\frac{K_p}{m_m} & -\frac{K_d+b_m}{m_m} & \frac{K_p}{m_m} & \frac{K_d}{m_m} \\ 0 & 0 & 0 & 1 \\ \frac{m_h K_p}{\hat{m}_a m_m} - \frac{k_h}{\hat{m}_a} & \frac{m_h(K_d+b_m)}{m_m \hat{m}_a} - \frac{b_h}{\hat{m}_a} & -K_p \frac{m_h}{\hat{m}_a m_m} & -K_d \frac{m_h}{\hat{m}_a m_m} - \frac{\hat{b}_a}{\hat{m}_a} \end{bmatrix} \boldsymbol{x} + \begin{bmatrix} 0 \\ \frac{1}{m_m} r^*_{PDa} \\ 0 \\ \frac{1}{\hat{m}_a} f^\star_h - \frac{m_h}{m_m \hat{m}_a} r^*_{PDa} \end{bmatrix} \tag{6.18}$$

with $r^*_{PDa} = K_p r^*_{\text{assist}} + K_d \dot{r}^*_{\text{assist}}$ and $\hat{m}_a = m_a(\hat{k}_e), \hat{b}_a = b_a(\hat{k}_e)$. If the assistance acts on the force level, the element a_{41} of the system matrix $\boldsymbol{A}$ changes to $\frac{m_h K_p}{\hat{m}_a m_m} - \frac{k_h + k_a}{\hat{m}_a}$. Without any further investigations, it can be seen that due to the differences in element a_{41} the stability regions will be different for the two systems. A virtual fixture acting on the position level does not alter the system matrix and consequently has no influence on the stability of the system. On the contrary, the virtual spring k_a added to the admittance leads to a change in the system matrix. In this case, the two controllers influence each other such that the corresponding parameters cannot be selected independently. As the haptic assistance is designed to act on the position level, the single-objective controllers do not interfere with each other. Thus, the same control parameters as presented in the previous subsections 6.3.2 and 6.3.3 can be used. The system dynamics is given by:

$$\begin{aligned} 0 &= -f_m + K_{pm}(x^d_{am} - x_m) + K_{dm}(\dot{x}^d_{am} - \dot{x}_m) \\ 0 &= \tilde{f}_h - \tilde{f}_e + m_a(f_h, f_e)\ddot{x}^d_m + b_a(f_h, f_e)\dot{x}^d_m \\ 0 &= \tilde{f}_h - \tilde{f}_e + m_a(f_h, f_e)\ddot{x}^d_m + b_a(f_h, f_e)\dot{x}^d_m. \end{aligned} \tag{6.19}$$

with $x^d_{am} = x^d_m + x_{am}(f_h, f_e, \boldsymbol{X}_m, r^*_{\text{assist}})$ and $\dot{x}^d_{am}$ the corresponding time derivative.

The FaFa architecture without any augmenting controller is investigated as basic architecture for a 1 DoF haptic teleoperation system with admittance-type devices. The admittance parameters mass and damping were set to $m_a^{FaFa} = 5$ kg and $b_a^{FaFa} = 10$ Ns/m.

6.3.6 Evaluation

The multi-criteria control concept and the classical FaFa architecture were tested in three different scenarios. The results are compared in terms of overall costs as well as costs for fidelity and performance separately. All costs should be minimized. The overall costs J are the sum of the costs for fidelity, J_T, and for performance, J_P:

$$J = J_T + J_P = j_f \ \text{RMSE}_{f_h - f_e} + j_{\dot{x}} \ \text{RMSE}_{\dot{x}_m - \dot{x}_s} + j_P \ W. \tag{6.20}$$

where $j_f, j_{\dot{x}}$, and j_P represent weights.

The procedure was the same in all scenarios: the slave device was brought into contact with the steel cube, see Appendix A.3, and moved back to the initial position. This task was repeated several times. Fig. 6.4 shows one evaluation trial with the integrated system. The same procedure was performed for the FaFa architecture.

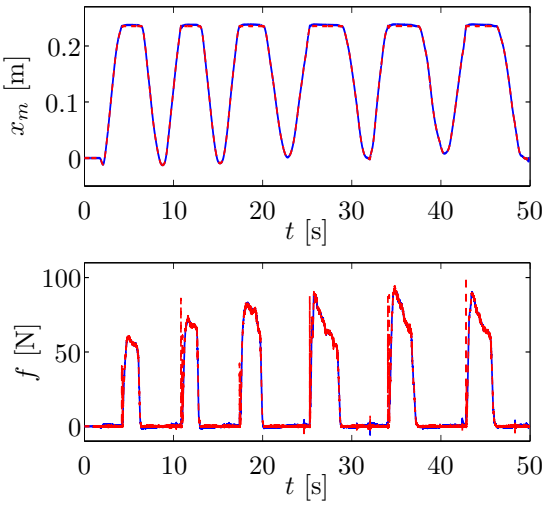

Fig. 6.4: Master (solid) and slave (dashed) position and force for one evaluation trial with the integrated system. The task consisted in repeatedly establishing contact with a steel cube and returning to the initial position.

6.3.6.1 Scenario 1: Transparency-oriented Controller

The costs of this controller are determined according to the transparency definition by Yokokohji [218], see Sec. 2.2.1, as the weighted sum of force and velocity tracking performance between master and slave site:

$$J_T = j_f \ \mathrm{RMSE}_{f_h - f_e} + j_{\dot{x}} \ \mathrm{RMSE}_{\dot{x}_m - \dot{x}_s}. \tag{6.21}$$

The parameters j_f and $j_{\dot{x}}$ were selected as $j_f = 1$ 1/N and $j_{\dot{x}} = 500$ s/m to balance different scales of the two components and RMSE is the root mean square error without normalization as presented in Appendix B.1.

In this scenario, only the adaptive admittance controller was active. The resulting costs are provided in Table 6.1 for the transparency-oriented controller and for the FaFa architecture. The reduction in the costs for fidelity compared to those of the FaFa architecture are mainly due to the reduction of the admittance parameters in free space. The admittance parameters only increased if high interaction forces were measured. Although no statistical comparison could be performed as only one operator performed the task, the results provide a first evidence that the transparency-oriented controller is effective.

6.3.6.2 Scenario 2: Performance-oriented Controller

The main objective of the virtual fixture is to reduce the physical workload W for the human operator, which is given for one trial by

$$W = \mathrm{RMSE}_{f_h \dot{x}_m}. \tag{6.22}$$

The costs of this controller are determined as:

$$J_P = j_P \mid W \mid, \tag{6.23}$$

where j_P was selected as $j_P = 20\text{s/Nm}$ to balance different scales when combining these costs with those of the transparency-oriented controller.

For this scenario, only the virtual fixture provided assistance to the operator. The costs J_P for the performance-oriented controller and the FaFa architecture in Table 6.1 indicate, that the virtual fixture can considerably reduce the physical workload for the human operator when moving in free space.

6.3.6.3 Scenario 3: Integrated System without Relaxation

Finally, both controllers were activated resulting in a multi-criteria controller. The relaxation process was deactivated. Comparing the costs, see Table 6.1, with those of the non-adaptive FaFa architecture, the costs for fidelity and for performance are considerably reduced with the multi-criteria control concept. The result also shows that the single controllers are integrated in a suitable manner, as each cost component and, thus, also the overall costs are improved. Again, a user study would be required to statistically prove this result.

Tab. 6.1: Costs for transparency J_T, for performance J_P, and overall costs J averaged over several trials. The task was performed by one operator.

		J_T	J_P	J
Classic FaFa		9.99	6.17	16.16
Integrated System	Transparency-oriented Control	3.51	-	3.51
	Performance-oriented Control	-	2.80	2.80
	Transp.- and Perf.-oriented Control	4.59	2.54	7.13

Summarizing this section, a haptic teleoperation system combining a transparency- and performance-oriented controller into an integrated system was developed. The adaptation approach of force, trajectory, and impedance by Ganesh et al. [62] was used as baseline for the control concepts. The transparency-oriented controller was designed such that not only the degree of fidelity was improved, but that also oscillatory behavior was avoided such that the system remained stable. As the performance-oriented controller does not interfere with the transparency-oriented controller regarding stability, both controllers could be activated at the same time. For evaluation, suitable cost functions were defined. Preliminary experimental results for each of the single-objective controllers as well as for the integrated system reveal smaller costs than for a classical two-channel architecture. This is a strong indication that an integrated system can improve several design objectives for haptic teleoperation systems simultaneously. A user study for statistically proving the found results remains future work.

6.4 Open Research Questions

Besides the implementation of specific single-objective controllers, several research questions for the design of multi-criteria controllers for haptic teleoperation systems are still open:

1. The interaction between the single controllers should be further investigated. Usually, an intention recognition unit decides about the type of virtual fixture. Thus, the performance-oriented controller may change during task execution. It is therefore important to investigate stability of the switching between different controllers and of the interaction between the different performance- and transparency-oriented controllers.

2. Similar to the design space introduced for haptic assistances in the previous chapter, it is important to derive general guidelines and independent design criteria for the selection of single-objective controllers such that they can be integrated into a multi-criteria control architecture.

3. The proof-of-concept reveals a considerable decrease in the costs of the integrated system compared to a classical control architecture. For a general statement about this multi-criteria control concept, a user study would be necessary. Further, the integrated control concept employing a stability observer and controller was only sketched and the described advantages and disadvantages are not proven. Developing, evaluating, and comparing this control concept with classical control architectures is necessary and important in order to show the potential of the proposed multi-criteria controller.

4. It is not clear how an adaptive multi-criteria system is perceived by the operator and whether it is accepted and preferred over a classical or single-objective control concept. Due to the various, often simultaneous adaptation processes, the intention of the machine may not become evident to the operator. If irritations are observed, new strategies for improving the man-machine interaction should be developed.

5. The examples and the proof-of-concept was performed for admittance-type haptic devices only. An extension to impedance-type devices is of high interest as they are often used in teleoperation. Furthermore, deficiencies in the communication channel were neglected. It is an open research question, whether a multi-criteria control concept is superior over a classical control architecture in the presence of packet loss or time delay.

6. Besides transparency and performance, feeling of presence and usability are important design criteria for haptic teleoperation systems. Whenever quantifiable and online evaluable measures for these objectives are available, it is of great interest to also incorporate those in the design of multi-criteria controllers.

6.5 Summary

Transparency and performance are two important and quantifiable design objectives for haptic teleoperation systems. Control concepts such as model-mediated teleoperation and adaptive haptic assistances as presented in this thesis were shown to drive the system closer to one of the two design objectives compared to classical control concepts. Similarly, current single-objective control concepts, see e.g. [238] for an overview, can be used to improve one of these objectives. Concepts for combining transparency- and performance-oriented controllers into one integrated system and thereby improving multiple objectives simultaneously have, however, not yet been considered in telerobotics. Only multi-criteria optimization approaches such as H_∞ control were proposed to derive an optimal trade-off between transparency and stability. In this thesis, stability is considered as optimization constraint rather than as design objective. Thus, also optimization-based approaches have to be extended to incorporate multiple design objectives.

This chapter was dedicated to control concepts improving multiple objectives. Multi-objective controllers represent an interesting future research field for haptic teleoperation systems. Two classes of concepts for designing multi-criteria controllers were identified: 1) a controller design based on multi-criteria optimization or 2) the suitable integration of existing single-objective controllers into one system. The H_∞ method is one possibility for designing controllers based on multi-criteria optimization. This approach can be extended to incorporate performance-related criteria like operator speed, force, or workload as further costs in the optimization, such that an optimal trade-off between these objectives can be achieved.

As controllers based on multi-criteria optimization are well-known in telerobotics literature, a novel design concept for multi-criteria controllers was proposed in this chapter. The concept was introduced for popular classes of transparency- and performance-oriented controllers. It is furthermore restricted to teleoperation architectures based on force or admittance/impedance controllers. For this class of systems, it is proposed to cascade the single-objective controllers, such that either the transparency- or performance-oriented controller is running in the outer control loop, while the respective other controller runs in an inner control loop. The main challenge is to guarantee stability of the integrated system. This is achieved by either determining the control parameters based on an a priori stability analysis or by adapting the parameters online if undesired oscillations are observed, see e.g. the stability observer and controller approach by Ryu et al. [175]. The multi-criteria control concept proposed in this thesis is expected to achieve a superior multi-criteria performance compared to e.g. an H_∞ approach as i) the parameters can be tuned in an intuitive way, ii) the controller is able to react to unexpected situations, iii) assistance can be provided in an active or proactive manner, and iv) a high multi-criteria improvement can be achieved as the parameters are adapted at each time step to improve the single criteria. The main drawback of the introduced concept is that a systematic synthesis approach for other classes of single-objective controllers is missing so far. An important aspect for future work is therefore to derive general guidelines for the selection of the single-objective controllers and for the integration into a multi-criteria teleoperation system.

One possibility for integrating single-objective control concepts into one multi-criteria

system is to combine an adaptive admittance controller improving fidelity with a virtual fixture improving performance. This integrated system was experimentally evaluated in a proof-of-concept study. The parameters were tuned a priori such that the resulting system remained stable during teleoperation. The results of the case study are a first evidence that a multi-criteria control concept is realizable for haptic teleoperation systems and that the costs of the multi-criteria controller can be considerably reduced compared to those of single-objective controllers and those of a classical teleoperation architecture.

While the proof-of-concept study gives a clear indication, that multi-criteria control concepts are beneficial for teleoperation systems, a variety of aspects regarding the generalizability to different tasks and environments, the usability of the system, and the comparison with other multi- and single-objective control concepts are missing. Further experimental results and user studies are required to confirm the advantages and disadvantages of the different multi-criteria control concepts. Another important aspect is the selection of suitable single-objective controllers, which do not negatively influence each other. Otherwise, improvements in multiple objectives cannot be realized simultaneously. A systematic design tool for the introduced control concept is therefore an important future step.

Besides the improvements in multiple objectives, this research area can also bring different research fields closer together: while the design of transparency-oriented controllers is mainly concerned with control-theoretic aspects, performance-oriented control concepts focus mainly on the human-machine interaction aspects. The ideal teleoperation system can, however, only be approached by considering aspects of both fields.

7 Conclusions and Future Work

This thesis focused on the synthesis, evaluation, and integration of transparency- and performance-oriented control concepts for haptic teleoperation systems. Transparency means an undisturbed haptic feedback to the operator, i.e. the operator feels as directly interacting with the remote environment. Fidelity is a measure for determining how close the system is from being transparent. The objective of a transparency-oriented control concept is to increase the fidelity of the system, while performance-oriented control concepts aim at achieving a superior task performance compared to concepts without performance augmentation. Adaptive control concepts were used throughout this thesis to realize improvements in fidelity and task performance. Besides transparency and performance, feeling of presence and usability are two further design objectives for haptic teleoperation systems. As quantifiable and online evaluable measures are only partly available so far, purely presence- and usability-oriented control concepts were not considered. This chapter summarizes the results and contributions of this thesis and addresses future research directions.

7.1 Conclusions

The research directions of this thesis were selected based on a classification and overview of current state-of-the-art control concepts for haptic teleoperation systems. EOT-adapting control concepts were defined in this thesis to incorporate online gained knowledge from the human operator, the remote environment, and the task, while classical controllers were defined to not be adaptive to this online gained knowledge. The literature review showed that EOT-adapting controllers can considerably improve fidelity and performance compared to classical control concepts. This thesis therefore focused on EOT-adapting controllers. The literature research showed furthermore that most control concepts focus on one design objective (transparency or performance) only. One interesting research aspect considered in this thesis was therefore the integration of single-objective controllers into one multi-criteria system.

The first part of this thesis was dedicated to single-objective controllers. The first objective was to realize improvements in fidelity without loss of stability. The control approach model-mediated teleoperation achieves this by coupling the operator to a local, estimated, haptic map of the remote environment. This thesis extended the state-of-the-art on model-mediated teleoperation with respect to the following aspects: i) a comprehensive stability analysis including the steady-state and estimation phase, ii) a theoretical, numerical, and experimental fidelity analysis including the proposition of a novel fidelity measure and the comparison with a classical controller, iii) an extensive summary and comparison of modeling, estimation, and reconstruction methods for static and movable objects, and iv) the extension of model-mediated teleoperation to 6 DoF manipulation tasks.

The second considered objective was to achieve significant improvements in task performance through haptic assistance. An important design aspect for fully exploiting human and machine capabilities is the selection of the assistance level of a haptic assistance. The assistance level strongly influences the authority and workload distribution between human and machine. This thesis presented a design space for the assistance policy module, which determines the assistance level. The design space allows not only to classify current implementations but also to explore novel design possibilities. In this thesis, several of the unexplored approaches were implemented and evaluated for a specific scenario. It was found that most assistances that are adaptive to the user and the task should be preferred over non-adaptive assistances, where the authority distribution remains unchanged during task execution.

Finally, the development of an integrated multi-criteria teleoperation system, which achieves improvements in fidelity and performance simultaneously, was explored. Two classes of control concepts for multi-criteria controllers were distinguished in this context. The first class of multi-criteria control concepts is well-known in telerobotics literature and has only to be extended to incorporate performance criteria. The second class of multi-criteria controllers is based on the idea of integrating single-objective controllers into one system, such that the resulting system benefits from each controller. Different implementation possibilities were proposed and illustrated with examples. In a proof-of-concept study, it was shown that the novel multi-criteria control concept is superior to single-objective controllers and to a classical control approach.

The remainder of this section presents a detailed summary and conclusion for each part of the thesis.

Transparency-Oriented Control

Model-mediated teleoperation was investigated as a promising transparency-oriented control approach. The operator interacts with a local, estimated, haptic map of the environment. Whenever the online estimation of this map is converged, the control loop between local and remote site is opened. Thus, the dynamics of the communication channel and the controlled slave device do not influence the fidelity of the system. This leads to significant fidelity improvements for systems with negligible, medium, and large time delays compared to classical control approaches. Model-mediated teleoperation is known in literature but missed so far a rigorous and comprehensive stability and fidelity analysis, a comparison with other architectures and was limited in its applicability to translational DoFs and static objects.

This thesis contributed to the state-of-the-art by proving stability using model-mediated teleoperation for systems with negligible communication deficiencies. Both, the the steady-state and estimation (transient) phase were analyzed for movable and static objects. A robust stability analysis based on the parameter space approach illustrated stable and unstable parameter regions. These results were the basis for the fidelity analysis. For the transient phase, methods and theorems from adaptive control as well as the multiple Lyapunov function approach were used to prove stability for the time-varying and switched dynamics.

The known literature was furthermore extended by a detailed fidelity analysis, where aspects regarding human perception limitations and realizability of theoretical stability boundaries were taken into account. The analysis investigated how realistically the remote environment is presented to the operator using model-mediated teleoperation and using a classical control concept. Due to modeling and hardware-related uncertainties, the numerically determined stable parameters are not necessarily stable when applied to the real system and the expected degree of fidelity is found to be unrealizable. This deteriorates also the comparison of different architectures with respect to fidelity. A robust fidelity measure was introduced in order to take the practical realizability into account. Numerical and experimental results showed the superiority of model-mediated teleoperation with respect to the introduced fidelity measure compared to a classical control concept.

A comprehensive comparison and selection of suitable modeling, estimation, and reconstruction techniques addressed important design aspects for model-mediated teleoperation. The applicability of model-mediated teleoperation was limited as it was only applied to estimate and reconstruct static objects in translational DoFs so far. The control concept was extended to tasks comprising the manipulation of static and movable objects in 6 DoF. Profound experimental evaluations confirmed the applicability and effectiveness of model-mediated teleoperation to systems with negligible, medium, and large time-delays in the communication channel and to 6 DoF manipulations of static and movable objects. Summarizing, the potential of model-mediated teleoperation for improving the fidelity of haptic teleoperation systems was shown and the applicability was significantly extended compared to current implementations.

Performance-Oriented Control

Besides transparency, a high task performance should be achieved with a teleoperation system. One possibility for considerably facilitating teleoperated manipulation tasks for the operator is to continuously combine operator-generated with computer-generated commands from a haptic assistance. This mode of operation is referred to as shared control. If the authority over the actions of the system is distributed in a suitable, user- and task-adapted manner between man and machine, the capabilities of human and machine are most beneficially exploited. As a result, the performance of teleoperated manipulation tasks can be improved beyond purely manual control. The authority distribution can be influenced by the assistance level, which is controlled by the assistance policy module. So far, the authority distribution and, consequently, the physical and cognitive workload between human and machine was fixed. Different situations require, however, different authority distributions. Thus, it is important to carefully design the assistance policy module.

This thesis introduced a design tool for the assistance policy module of a haptic assistance. Based on a classification of current implementations, novel assistance policies were developed and evaluated for a specific scenario. The application of this design tool is not restricted to teleoperation systems, but to any system where human and machine share the control over the actions of a system, like in human-robot interaction, aviation, or automation of vehicles. The design tool consists of a three-dimensional design space for selecting the assistance level. Performance measures, the type of performance reference, and the assistance policy were identified as the three axes of the design space. The proposed design

space allows i) to investigate the main components when designing a flexible, user- and task-adapting haptic assistance, ii) to classify the current implementations, iii) to identify unexplored areas and iv) to compare different assistance policies.

Based on a detailed analysis and classification of current implementations of haptic assistances, new performance measures and control policies for selecting the assistance level of a haptic assistance were proposed. These comprise the combination of multiple performance criteria into one multi-criteria performance measure as well as constant, switching, and linearly adapting assistance policies.

These novel assistance concepts were implemented in a typical scenario encountered in real-environment teleoperation tasks and evaluated based on the results of a user study. The experimental results showed that all assistances improved task performance and agreement between human and assistance. Furthermore, most haptic assistances that varied the authority distribution during task execution should be preferred over assistances with a fixed authority distribution. It was also found that a multi-criteria performance measure allows to achieve a trade-off between the different criteria, in this case task performance and agreement between human and assistance. Finally, it was concluded that the reference performance should be selected according to the application area: external knowledge from e.g. an expert is preferable for learning or training scenarios, as the patient/student can be assisted according to the distance between the performance of the trainer/expert and the patient/student. Adapting the assistance level without external knowledge is beneficial for real-world scenarios. As the assistance level is selected depending on changes in the operator performance, the assistance is more flexible to react to unexpected events or changes in the operator intention. In summary, the introduced design space builds a first systematic tool for developing and comparing flexible, user- and task-adapted haptic assistances.

Multi-criteria Control

In order to achieve improvements in several design objectives such as fidelity and task performance, multi-criteria control concepts were investigated in this thesis. Contrary to classical or single-objective control concepts, multi-criteria controllers aim at simultaneously improving several objectives like fidelity and performance. This topic represents an important and interesting research aspect for the controller design of haptic teleoperation systems. A state-of-the-art analysis revealed that multi-criteria control design has not been fully investigated for haptic teleoperation systems yet.

This thesis distinguished two classes of multi-criteria control concepts. These include i) controllers based on multi-criteria optimization and ii) the integration of single-objective controllers such that improvements in all criteria are achieved. H_∞ control belongs to the former class of approaches and can be easily extended to incorporate further performance criteria. The latter class of multi-criteria control concepts represents a novel approach for a multi-criteria control design.

The novel multi-criteria control concept was studied in detail and an integration approach for well-known classes of transparency- and performance-oriented controllers was proposed leading to two different control architectures. As guaranteeing stability is an important aspect, two possibilities for a stable implementation were proposed and illustrated by examples. A qualitative discussion of advantages and disadvantages of the proposed

multi-criteria controller was provided. It showed that the integration of single-objective controllers has several advantages compared to an H_∞ control design: i) the parameters can be tuned in an intuitive way, ii) the controller is able to react to unexpected situations, iii) active or proactive assistances can be integrated, and iv) a high multi-criteria improvement can be achieved due to online adaptation of the parameters. The introduced multi-criteria controller can only be effective, if the single-objective controllers do not compete each other. In order to generalize the introduced integration concept, it is an important future step to introduce a systematic synthesis approach, which guarantees compatibility between the controllers and, thus, improvements in all desired objectives.

The applicability and effectiveness of the novel multi-criteria control concept was shown in a proof-of-concept study. The multi-criteria controller achieved considerably lower costs with respect to fidelity and task performance compared to the single-objective controllers and a classical control approach. As multi-criteria control design has not been fully exploited for haptic teleoperation systems yet, several open research aspects were identified. These include a profound experimental evaluation of the proposed concept also in terms of usability, a stability proof for the novel multi-criteria control concept, and the investigation of further integration concepts like connecting the single-objective controllers in parallel or switching between them. Summarizing, the applicability and effectiveness of a novel multi-criteria control concept showed the potential of this research aspect and provides therefore a basis for further investigations towards a transparent, high-performant, immersive, and comfortable teleoperation system.

In summary, novel concepts and contributions regarding transparency- and performance-oriented control concepts as well as an integrated multi-criteria controller advance the state-of-the-art for haptic teleoperation systems considerably. The results of this thesis are expected to build a good basis for further research not only for teleoperation but also for other applications involving physical human-robot interaction.

7.2 Future Research Directions

Several future research directions ranging from further exploiting the concepts presented in this thesis to completely new research areas emerge from this work:

- *Extension and Transfer of Model-Mediated Teleoperation to Novel Teleoperation Setups:* As model-mediated teleoperation was shown to be a promising transparency-oriented control concept, its extension to further classes of objects and manipulation tasks is an interesting research aspect. Furthermore, encounter-type haptic devices were proposed as novel master devices for teleoperation systems for the interaction in real and virtual remote environments, see e.g. [61, 87, 128, 137]. These systems allow the human operator to freely move around the local site, while providing haptic feedback if contact with an object and/or another human in the remote place occurs. Thus, motions in free space are transparent. The model-mediated teleoperation approach with the idea of gathering and replicating a haptic map of the remote environment on the local site is a promising approach for this setup.

- *Transfer of Design Space to Further Shared-Control Applications:* The introduced design tool for haptic assistances is not limited to teleoperation systems but is applicable to all haptic shared-control systems. Applications range therefore from vehicle control, mobility aids, powered wheelchairs over rehabilitation and training scenarios to the interaction of humans with autonomous robots. All these areas can benefit from the introduced design space for haptic assistances. A further interesting aspect is to develop concepts for separately adapting the physical and cognitive dominance [73] of haptic assistances.

- *Investigation of Multi-Criteria Control Concepts:* The integration of single-objective controllers and the development of multi-criteria control concepts was proposed as an innovative research field in this thesis. Significant advances are expected when further exploring this topic. This concerns especially the integration of single-objective controllers into a multi-criteria teleoperation system. An important future step is hereby the introduction of a design tool for the selection and integration of the single controllers. This design tool would allow to generalize the approach to a variety of different teleoperation tasks.

- *Incorporation of Advances in Autonomous Robotics:* The advances of the last years in the fields of perception, planning, reasoning, and learning for autonomous robots have not been fully integrated in haptic teleoperation setups yet. Incorporating the state-of-the-art technologies can have a significant impact for transparency-oriented control concepts, that are based on online gained knowledge from the remote environment, for shared control, and for semi-autonomous teleoperation.

The individual concepts as well as the main idea of this thesis are expected to motivate further developments towards user-oriented, high-performant, immersive, and transparent haptic teleoperation systems, and to inspire the development of approaches for novel teleoperation setups and shared-control systems.

A Modeling and Experimental Setups

A.1 Human Operator Model

The human operator is modeled as a force or position source and an arm impedance $Z_h = \frac{f_h}{\dot{x}_h} = \frac{m_h s^2 + b_h s + k_h}{s}$. In order to guarantee robust stability, the impedance parameters are selected in a conservative way. They are selected as large as possible, as large impedance parameters increase the instability regions for admittance-type haptic devices, see [155]. In [198], the hand impedance parameters were estimated for subjects grasping a haptic interface. This is an important aspect as it was shown in [198] that stiffness and viscosity increase when grasping a handle. The maximum estimated impedance was extracted from the experimental results and the corresponding standard deviations were added to each parameter.

	mass/inertia m_h [kg]	damping b_h [Ns/m]	stiffness k_h [N/m]
6 DoF	$1.260 + 0.107$	$26.030 + 0.790$	$340.480 + 8.277$

A.2 Dynamic Model of Position-based Admittance Control with Force-Force Exchange (FaFa)

The control laws for position-based admittance control with force-force exchange denoted as FaFa is given in Laplace domain as:

$$f_{cm} = Z_{PI,m}(\dot{x}_m^d - \dot{x}_m) = Z_{PI,m}(Y_a(f_h - f_e) - \dot{x}_m) \quad (A.1)$$

$$f_{cs} = Z_{PI,s}(\dot{x}_m^d - \dot{x}_s) = Z_{PI,s}(Y_a(f_h - f_e) - \dot{x}_s) \quad (A.2)$$

such that according to (2.18)

$$C_m = Z_{PI,m}, \quad C_s = Z_{PI,s}, \quad C_1 = C_4 = 0 \quad (A.3)$$

$$C_2 = C_6 = Z_{PI,s}Y_a, \quad C_3 = C_5 = Z_{PI,m}Y_a. \quad (A.4)$$

With $Z_m + Z_{PI,m} = Z_{cm}$ and $Z_s + Z_{PI,s} = Z_{cs}$ the elements of the $\boldsymbol{H}$-matrix are found as

$$\boldsymbol{H} = \begin{bmatrix} \frac{Z_{cm}Z_a}{Z_a+Z_{PI,s}} & \frac{Z_{PI,s}}{Z_a+Z_{PI,s}} \\ -\frac{Z_{PI,m}Z_{cm}}{(Z_a+Z_{PI,m})Z_{cs}} & \frac{Z_a+Z_{PI,s}+Z_{PI,m}}{(Z_a+Z_{PI,m})Z_{cs}} \end{bmatrix}. \quad (A.5)$$

Substituting the elements of the $\boldsymbol{H}$-matrix into (2.23) leads to the closed-loop transfer function for the FaFa architecture G_{FaFa}.

A.3 Objects

Figure A.1 shows a steel and a silicone cube that were used for experimental evaluation of model-mediated teleoperation.

(a) Steel cube (b) Silicone cube

Fig. A.1: Stiff and soft remote objects.

A.4 1 DoF Teleoperation System: Linear Devices Thrusttubes

The teleoperation system with one degree of freedom consists of two identical linear direct drive actuators, Thrusttube modules ME2504 from Copley Controls Corp., see Fig. A.2. The continuous and peak forces of the motors are 43.3 N and 312 N, respectively. Each of the devices is equipped with an optic position encoder (resolution 1 μm) and a 1 DoF force sensor from Burster, Model 8245. The slave device is furthermore equipped with a 1 DoF acceleration sensor (BG 2166, Mikrotechnik + Sensorik GmbH). The workspace size is 1612 mm. In order to realize free space movements as well as contact situations, a steel plate was mounted on slave site. Different kind of objects can be attached to it via a permanent magnet. A multichannel analog and digital I/O card (Sensoray S626) connects the software with an electronic box. This box contains the power supply, the motor amplifier, the measurement amplifier for force signals, and a safety system. The latter includes a watchdog timer monitoring the PC, a velocity limit based on the position signal, and an emergency button for immediate shutdown of the motor current.

The controllers for both devices as well as the simulation of the communication channel were implemented in `MATLAB/SIMULINK`. Standalone real-time capable code was generated from the SIMULINK model on a standard Linux PC with Real Time Application Interface (RTAI). The control ran at a sampling frequency of 1 kHz.

A.5 2 DoF Teleoperation System: Linear Devices Thrusttubes

A 2 DoF haptic interface as shown in Fig. A.3 consisting of two linear actuators, where a Thrusttube module ME2504 from Copley Controls Corp. is mounted at a right angle on

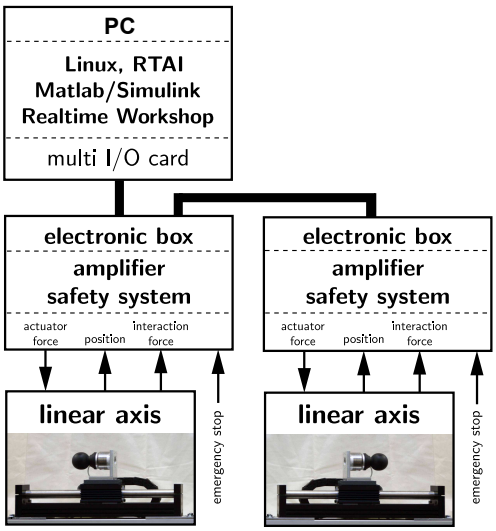

Fig. A.2: Experimental 1 DoF teleoperation setup.

Tab. A.1: Parameters of 1 DoF teleoperation setup.

parameter	value
$m_{m,s}$	2.498 kg
$b_{m,s}$	20 Ns/m
K_p	70 kN/m
K_d	500 Ns/m
T_a	0.65 ms
T_f	$1/(2\pi \cdot 500)$ s

top of a second Thrusttube module ME2510 was used for the evaluation of performance-oriented control concepts. Each of the actuators is equipped with an optical position encoder (resolution 1 μm). A 6 DoF JR3 force sensor and a handle were mounted on the upper actuator. The control ran at a sampling frequency of 1 kHz. Experimental data (positions, human/assistance forces, task completion time, collision time with walls) were recorded at the same frequency.

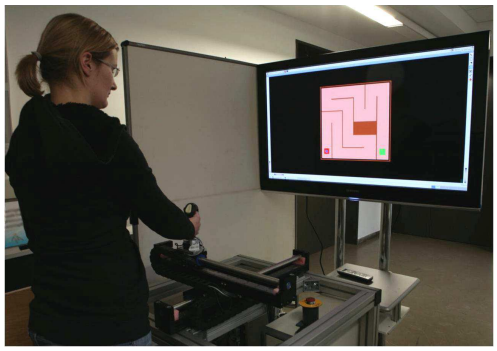

Fig. A.3: Apparatus: A 2 DoF haptic interface.

A.6 6 DoF multi-modal Teleoperation System: Haptic Interface ViSHaRD7 and Mobile Teleoperator MTO

For the demonstration of the methods on multi-DoF systems, two haptic interfaces, two redundant 7 DoF robotic arms referred to as ViSHaRD7 [156], see Fig. A.4(a), were available. The arms have a large, singularity-free workspace and a high force output capability, see the respective references for a detailed analysis of design and performance. Two anthropomorphic 7 DOF robotic arms [188] were used as teleoperator. All devices are of the admittance-type, and are, thus, characterized by a relatively large, human-like workspace, and a high force output capability. The redundancy on operator site is used to decouple translational from rotational movements, while on teleoperator site it is used to avoid singular configurations. 6 DoF JR3 force/torque sensors are mounted at the end-effector of the devices. The end-effector pose consisting of positions and orientation was obtained by applying the forward kinematics to the measured joint angles. Gravity forces of the end-effectors were compensated in the force measurements.

The controllers for both devices were implemented in `MATLAB/SIMULINK`, compiled into real-time capable code and ran on standard Linux PCs with Real Time Application Interface (RTAI). The sampling frequency was 1 kHz. A local area network (LAN) was used to establish the communication between the haptic interface and the teleoperator, such that time delay and packet loss were negligible.

An aluminum bar mounted at the end-effector of the haptic interface was used as handle for the operator. On the teleoperator's end-effector, different tools can be mounted: A two finger robotic gripper is available to grasp objects. The gripper opening was controlled by opening and closing a potentiometer on master site. Or, for exploring the remote environment, a steel pin was mounted on the teleoperator's end-effector.

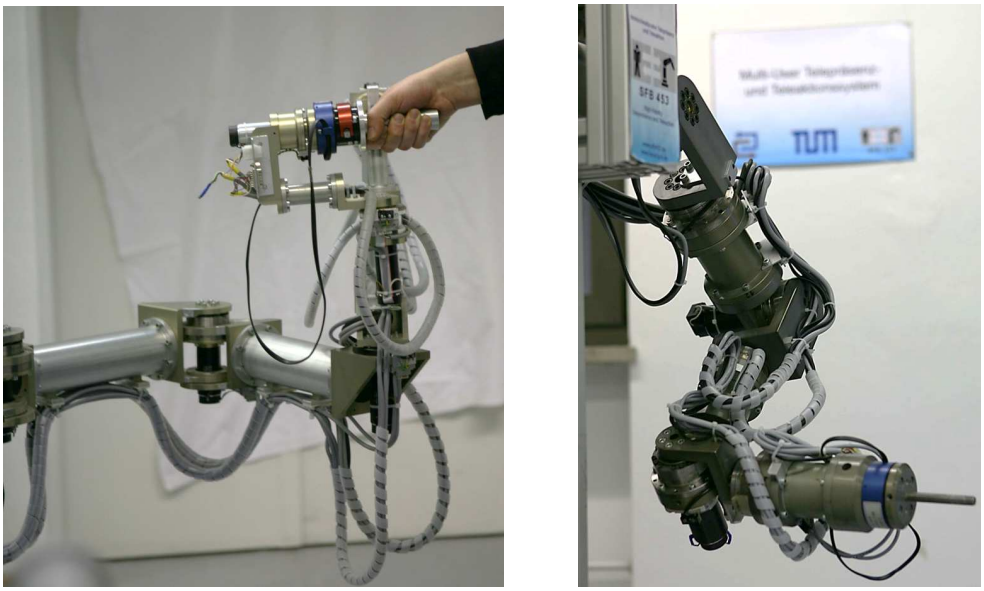

(a) Redundant 7 DoF haptic interface ViSHard7

(b) Redundant 7 DoF teleoperator

Fig. A.4: 6 DoF experimental setup consisting of a redundant 7 DoF haptic interface and teleoperator. Pictures are taken from [227] and slightly modified.

For stability analysis and simulations, the parameters as described in Table A.2 were used, see also [155].

Tab. A.2: Parameters of 6 DoF teleoperation setup.

parameter	value
m_m	23.334 kg
b_m	20 Ns/m
m_s	15.4 kg
b_s	20 Ns/m
K_p	3250 kN/m
K_d	13 kNs/m
T_{act}	0.0003 s
T_{sensor}	$1/(2\pi \cdot 500)$ s

A.6.0.4 Rotation Matrix from Force-Torque Sensor to World Coordinates

The rotation matrix from the force-torque sensor coordinate system R to the world coordinate system W is given for the teleoperator, see Appendix A.6, by

$$\boldsymbol{T}_R^W = \begin{bmatrix} r_{11} & r_{12} & r_{13} \\ r_{21} & r_{22} & r_{23} \\ r_{31} & r_{32} & r_{33} \end{bmatrix} \tag{A.6}$$

where

$$
\begin{aligned}
r_{11} &= c_6(s_1s_3s_4 + c_4c_1s_2 + c_1c_2c_3s_4) + s_5s_6(s_3c_1c_2 - s_1c_3) - c_5s_6(s_1s_3c_4 + c_1c_2c_3c_4 - s_4c_1s_2)\\
r_{12} &= (s_1s_3s_4 + c_4c_1s_2 + c_1c_2c_3s_4)s_6s_7 + (s_3c_1c_2 - s_1c_3)(c_5c_7 - s_7s_5c_6)\\
&\quad +(s_1s_3c_4 + c_1c_2c_3c_4 - s_4c_1s_2)(s_5c_7 + s_7c_5c_6)\\
r_{13} &= (s_1s_3s_4 + c_4c_1s_2 + c_1c_2c_3s_4)s_6c_7 + (s_3c_1c_2 - s_1c_3)(-c_5s_7 - c_7s_5c_6)\\
&\quad +(s_1s_3c_4 + c_1c_2c_3c_4 - s_4c_1s_2)(c_7c_5c_6 - s_5s_7)\\
r_{21} &= c_6(c_4s_1s_2 + s_1c_2c_3s_4 - c_1s_3s_4) + s_5s_6(c_1c_3 + s_3s_1c_2) - c_5s_6(s_1c_2c_3c_4 - c_1s_3c_4 - s_4s_1s_2)\\
r_{22} &= (c_4s_1s_2 + s_1c_2c_3s_4 - c_1s_3s_4)s_6s_7 + (c_1c_3 + s_3s_1c_2)(c_5c_7 - s_7s_5c_6)\\
&\quad +(s_1c_2c_3c_4 - c_1s_3c_4 - s_4s_1s_2)(s_5c_7 + s_7c_5c_6)\\
r_{23} &= (c_4s_1s_2 + s_1c_2c_3s_4 - c_1s_3s_4)s_6c_7 + (c_1c_3 + s_3s_1c_2)(-c_5s_7 - c_7s_5c_6)\\
&\quad +(s_1c_2c_3c_4 - c_1s_3c_4 - s_4s_1s_2)(c_7c_5c_6 - s_5s_7)\\
r_{31} &= c_6(s_2c_3s_4 - c_2c_4) + s_5s_6s_2s_3 - c_5s_6(s_2c_3c_4 + c_2s_4)\\
r_{32} &= (s_2c_3s_4 - c_2c_4)s_6s_7 + s_2s_3(c_5c_7 - s_7s_5c_6) + (s_2c_3c_4 + c_2s_4)(s_5c_7 + s_7c_5c_6)\\
r_{33} &= (s_2c_3s_4 - c_2c_4)s_6c_7 + s_2s_3(-c_5s_7 - c_7s_5c_6) + (s_2c_3c_4 + c_2s_4)(c_7c_5c_6 - s_5).
\end{aligned}
$$

B Model Evaluation Tools

B.1 Normalized Root Mean Square Error (NRMSE)

The normalized root mean square error between a time series of estimated parameters/variables $\hat{\boldsymbol{a}} = [\hat{a}_0, \ldots, \hat{a}_N]$ and a time series of measured parameters/variables $\boldsymbol{a} = [a_0, \ldots, a_N]$ determines the accuracy of the estimation:

$$\mathrm{NRMSE}_{\boldsymbol{a}} = \frac{1}{a_{\max} - a_{\min}} \frac{\|\boldsymbol{a} - \hat{\boldsymbol{a}}\|}{\sqrt{N}} \cdot 100\% \tag{B.1}$$

where $a_{\max} = \max(\boldsymbol{a})$ and $a_{\min} = \min(\boldsymbol{a})$.

B.2 Relative Estimation Error (REE)

In order to evaluate the accuracy of an estimated parameter $\hat{p}$, the relative estimation error with respect to the true parameter p (REE_p) can be calculated:

$$\mathrm{REE}_p = \frac{|p - \hat{p}|}{p} \cdot 100\%. \tag{B.2}$$

Please note that this measure is determined for the last estimated parameter value, i.e. at a single time step.

B.3 Convergence Time (CT)

Given the true parameter $\boldsymbol{p} \in \mathbb{R}$ and the vector $\hat{\boldsymbol{p}} \in \mathbb{R}^N$ containing the time series of the estimated parameter vector. The convergence time of an estimation is determined as the time instance from which on the parameter errors $\boldsymbol{e} = \boldsymbol{p} - \hat{\boldsymbol{p}}$ remain within a 5 % bound. For a sample time TA, the convergence time is determined as

$$\mathrm{CT} = \{n \cdot TA | \ \ |\boldsymbol{e}(i)| < 0.05 \quad \forall\, i \geq n\}. \tag{B.3}$$

C Fidelity Analysis: Stable Parameters Optimizing Fidelity

The stable admittance parameters optimizing fidelity, m_a^{*s} and b_a^{*s}, are determined for different movable and static objects as well as for different objects with mass-spring-damper characteristics. The results are presented in Tables C.1, C.2, and C.3.

Tab. C.1: Stable optimal parameters $m_a^{s*} \in D_{\boldsymbol{q}}^s$ [kg],$b_a^{s*} \in D_{\boldsymbol{q}}^s$ [Ns/m] for MM and FaFa architecture for *movable* objects.

Z_e	Stable Optimum MM		Stable Optimum FaFa	
m_e [kg]	m_a^* [μg]	b_a^* [Ns/m]	m_a^* [mg]	b_a^* [Ns/m]
4	> 0	0	0.861	3.472
12	> 0	0	< 0.001	9.066
20	> 0	0	< 0.001	84.608

Tab. C.2: Stable optimal parameters $m_a^{s*} \in D_{\boldsymbol{q}}^s$,$b_a^{s*} \in D_{\boldsymbol{q}}^s$ for MM and FaFa architecture for *static* objects.

Z_e		Stable Optimum MM		Stable Optimum FaFa	
b_e [Ns/m]	k_e [kN/m]	m_a^* [g]	b_a^* [Ns/m]	m_a^* [g]	b_a^* [Ns/m]
0	5	699.287	200.000	< 0.001	200.000
50	5	145.756	< 0.001	< 0.001	0.635
100	5	< 0.001	< 0.001	0.001	3.196
150	5	< 0.001	89.505	< 0.061	1.585
200	5	< 0.001	200.000	0.001	6.506
0	15	696.599	200.000	13.588	200.000
50	15	419.169	200.000	40.968	200.000
100	15	169.567	200.000	687.667	200.000
150	15	988.631	< 0.001	648.725	200.000
200	15	< 0.001	< 0.001	659.651	94.287
0	25	694.152	200.000	< 1.648	200.000
50	25	420.766	200.000	13.340	200.000
100	25	170.914	200.000	687.389	200.000
150	25	10000.000	200.000	648.157	200.000
200	25	10000.000	200.000	676.863	200.000

Tab. C.3: Stable optimal parameters $m_a^{s*} \in D_{\boldsymbol{q}}^s$ kg, $b_a^{s*} \in D_{\boldsymbol{q}}^s$ Ns/m for MM and FaFa architecture for an object characterized by a *mass-spring-damper dynamics*.

Z_e			Stable Optimum MM		Stable Optimum FaFa	
m_e [kg]	b_e [Ns/m]	k_e [kN/m]	m_a^* [g]	b_a^* [Ns/m]	m_a^* [mg]	b_a^* [Ns/m]
4	0	5	0.229	0.0	< 0.001	73.383
12	0	5	0.271	0.0	< 0.001	81.071
20	0	5	1.440	0.0	< 0.001	14.708
4	100	5	153.416	0.035	< 0.001	3.440
12	100	5	204.670	0.0	< 0.001	9.066
20	100	5	122.377	0.0	< 0.001	14.709
4	200	5	240.134	0.516	236.465	12.411
12	200	5	271.755	0.0	< 0.001	9.066
20	200	5	161.421	0.0	< 0.001	14.708
4	0	15	0.150	0.0	< 0.001	71.091
12	0	15	0.520	0.0	< 0.001	79.235
20	0	15	0.206	0.0	0.001	34.534
4	100	15	112.147	3.419	$\lessdot$49.471	5.313
12	100	15	168.567	0.602	< 0.001	9.066
20	100	15	115.988	0.512	0.001	14.708
4	200	15	188.311	6.320	5.088	3.633
12	200	15	253.908	0.938	< 0.001	9.066
20	200	15	170.828	0.781	< 0.001	14.708
4	0	25	< 0.001	0.0	< 0.001	27.574
12	0	25	0.482	0.0	< 0.001	9.081
20	0	25	0.534	0.0	< 0.001	46.118
4	100	25	77.057	6.447	< 0.001	3.440
12	100	25	144.806	1.836	< 0.001	9.066
20	100	25	110.203	1.200	< 0.001	14.708
4	200	25	132.154	11.580	54.129	5.493
12	200	25	231.137	3.261	< 0.001	9.067
20	200	25	172.062	2.083	< 0.001	14.708

D Aspects concerning the Design Space of Haptic Assistances

D.1 User Study with Constant Assistance Levels

D.1.1 Experimental design

The assistance level α_c in the pre-test was varied on five discrete levels: $\alpha_c = \alpha_{c\parallel} = \alpha_{c\perp} \in \{0, 0.25, 0.5, 0.75, 1\}$. The experiment featured consequently a 5 (assistance) x 2 (scenario) repeated-measures within-subjects experimental design.

D.1.2 Procedure

The participants were first given the opportunity to familiarize themselves with the experimental setup and the task requirements prior to the experimental trials. Thus, they were allowed to practice both scenarios with $\alpha_c = 0$ as well as $\alpha_c = 1$. It was emphasized to avoid contact with walls and obstacles while moving as quickly as possible. After the test trials, the different assistance levels were presented in randomized order as blocks consisting of three consecutive trials with SC_{agree} and SC_{disagree}, respectively. The sequence of scenarios per type of assistance was again randomized. Hence, each block consisted of six trials with one assistance level and both scenarios. Only the third trial was used for the analysis. After completing a scenario using a certain type of assistance, subjects had to fill in a questionnaire to assess the perceived workload.

D.1.3 Participants

An opportunity sample of 13 subjects (8 men and 5 women, all right-handed) with a mean age of 23.6 years (std. deviation: 2.2 years) and little experience in the handling of haptic devices (mean(experience) = 1.00, scale ranging from *1 = no experience* to *5 = much experience*) took part in the study.

D.1.4 Evaluation Results

Values of qualitative and quantitative measures were found to be normally distributed according to the results of Kolmogorov-Smirnov tests. Hence, statistical analyses were performed parametrically. In line with the experimental design, variables were evaluated with two-factorial repeated measurement analyses of variance (ANOVA) to investigate the influence of the assistance and type of scenario. All statistical tests were conducted on a 5% significance level. Outliers with more than three standard deviations away from the mean were replaced with the mean value.

D.1.4.1 Task Performance

For both scenarios, the *assistance level* has a significant influence on this measure ($F_{4,48} = 11.16,\ p < .001,\ \eta_p^2 = .482$) leading to better performance with increasing assistance level. Furthermore, $N(P)$ values significantly differ between scenarios ($F_{1,12} = 63.41$, $p < .001$, $\eta_p^2 = .841$).

D.1.4.2 Disagreement

There is a clear distinction of disagreement between the scenarios. The effect of *scenario* ($F_{1,12} = 532.123, p < .001, \eta_p^2 = .978$), *assistance* ($F_{\text{Greenhouse-Geisser:1.31,15.66}} = 188.24$, $p < .001$, $\eta_p^2 = .94$) as well as their (hybrid) *interaction* ($F_{\text{Greenhouse-Geisser:1.65,19.79}} = 245.47$, $p < .001$, $\eta_p^2 = .953$) reach significance. Disagreement is higher in SC_{disagree}.

D.1.4.3 Multi-criteria Performance

The multi-criteria performance P is significantly affected by the *assistance* level as well as the *scenario* (assistance: $F_{4,48} = 9.5$, $p < .001$, $\eta_p^2 = .442$; scenario: $F_{1,12} = 210.7$, $p < .001$, $\eta_p^2 = .946$). Due to a significant, hybrid *interaction* of these factors ($F_{2.515,30.184} = 25.82$, $p < .001$, $\eta_p^2 = .683$) only the influence of obstacles can be interpreted in terms of worse performance in SC_{disagree}.

D.1.4.4 Smoothness

The smoothness of the movements S_{xy} is significantly affected by the *assistance* as well as the *scenario* (assistance: $F_{4,48} = 4.237,\ p = .005,\ \eta_p^2 = .261$; scenario: $F_{1,12} = 15.268$, $p = .002$, $\eta_p^2 = .56$). Due to a significant, hybrid *interaction* of these factors ($F_{4,48} = 10.887$, $p < .001$, $\eta_p^2 = .476$) the effect of assistance can be better interpreted by looking at the scenarios separately. All except $\alpha_c = 0$ show a higher smoothness in SC_{agree} than in SC_{disagree}.

D.1.4.5 Perceived Workload.

The factor *scenario* has a significant, large effect on perceived workload ($F_{1,12} = 35.18$, $p < .001,\ \eta_p^2 = .746$). Though the factor *assistance* fails to reach significance, a significant *interaction* effect is evident ($F_{4,48} = 9.05,\ p < .001,\ \eta_p^2 = .43$). Hence, the effect of adding obstacles is not the same for different α_c. While the perceived workload is higher in SC_{disagree} with obstacles to drive past, for SC_{agree}, the minimal value is reached for $\alpha_c = 1$, while for SC_{disagree}, medium assistance levels have a lower workload than no or full assistance.

D.1.4.6 Efficiency

Finally, efficiency depending on task performance and perceived workload is significantly influenced by *assistance* ($F_{4,48} = 5.49,\ p = .001,\ \eta_p^2 = .31$) and *scenario* ($F_{1,12} = 69.97$,$p < .001,\ \eta_p^2 = .85$). Due to the significant *interaction* between these factors ($F_{4,48} = 4.39,\ p = .004,\ \eta_p^2 = .268$), the assistance effect can be better interpreted by

looking at the scenarios independently: for SC_{agree}, efficiency clearly improves with increasing assistance values, while for SC_{disagree}, medium assistances are more appropriate than no or full assistance.

D.2 Classical Gradient Search

The idea of a gradient search method is to treat the performance metric P incorporating all important objectives as a cost function and to reduce the cost for every time step such that an optimal trade-off between the performance criteria is found. The terms performance and cost will be used equally. Consequently, this method could lead to an overall better performance than achievable with a constant assistance level. Assuming the optimization problem

$$\min \|P(\alpha)\|, \qquad \text{where } \alpha \in [0;1], \tag{D.1}$$

the update rule of the assistance level at time step k for a gradient-search method, see e.g. [20], would be

$$\alpha_k = \alpha_{k-1} - \gamma \ \operatorname{sign}(\alpha_{k-1} - \alpha_{k-2}) \ (P_{k-1} - P_{k-2}), \quad \gamma > 0 \tag{D.2}$$

and the costs are guaranteed to decrease

$$\begin{aligned} P_{k+1} &= P_k + \frac{\partial P}{\partial \alpha}(\alpha_k - \alpha_{k-1}) \\ \text{with (D.2)} \quad &\approx P_k - \underbrace{\gamma \frac{(P_{k-1} - P_{k-2})^2}{|\alpha_{k-1} - \alpha_{k-2}|}}_{>0} \end{aligned}$$

This holds only, if α is the only factor influencing P. In a haptic shared control system, however, the user and the environment have a strong, direct influence on performance and, thus, on the costs P. The classic gradient-search method is therefore not suitable as illustrated with the following example: Assume the speed of the manipulated object as a cost function with internal reference. The higher the speed, the lower are the costs and vice versa. Assume further, that the user reduces the speed of the object, independent of what the assistance proposes. Then, the assistance level will not change anymore as shown in the following example. If $\operatorname{sign}(\delta\alpha_k) = 1$ with $\delta\alpha_k = \alpha_k - \alpha_{k-1}$ and $\delta P_k = P_k - P_{k-1}$

$$\begin{aligned} \alpha_{k+1} &= \alpha_k - \gamma \underbrace{\delta P_k \ \operatorname{sign}(\delta\alpha_k)}_{>0} && \Rightarrow \alpha_{k+1} < \alpha_k \\ \Rightarrow \alpha_{k+2} &= \alpha_{k+1} - \gamma \underbrace{\delta P_{k+1} \ \operatorname{sign}(\delta\alpha_{k+1})}_{<0} && \Rightarrow \alpha_{k+2} > \alpha_{k+1}. \end{aligned}$$

This is contradictory to the expectation, that the assistance level increases α whenever the user performance degrades (speed reduction in this case). Thus, a gradient-like search was used, see Chap. 5.

D.3 Disagreement Threshold

In order to apply agreement-based switching, thresholds for distinguishing agreement from disagreement have to be known. We propose the following procedure to determine these thresholds:

1. Determine performance-optimal discrete assistance levels $\overline{\alpha}^{O}_{\parallel,d}$ and $\overline{\alpha}^{O}_{\perp,d}$ for SC_{agree} and SC_{disagree} separately.
2. Calculate mean and standard deviations of agreement data for each assistance level and scenario: $\overline{\alpha}_{\parallel\text{agree},d}, \overline{\alpha}_{\perp\text{agree},d}, \overline{\alpha}_{\parallel\text{disagree},d}, \overline{\alpha}_{\perp\text{disagree},d}$.
3. Prove separability of distributions for SC_{agree} and SC_{disagree}.
4. Find threshold $\overline{D^r}$ according to (D.3).

Step 1. As we need the agreement distributions in step 3, only discrete assistance levels were selected for α^O instead of continuous assistance levels. They correspond to $\overline{\alpha}^{O}_{\parallel\text{agree},d}, \overline{\alpha}^{O}_{\parallel\text{disagree},d}, \overline{\alpha}^{O}_{\perp\text{agree},d}, \overline{\alpha}^{O}_{\perp\text{disagree},d}$.

Step 2. As presented in Sec. 2.2.4.3, we use the interactive forces as disagreement measure. More specifically, we proposed in [236] to use the offline calculated mean normed interactive force $N\overline{F_i}$ distributions to distinguish agreement from disagreement. When testing this approach, it was found, that the mean of the interactive forces is not a good measure for online agreement determination, as the maxima of $\overline{F_i}$ are considerably higher especially around obstacles compared to the average, see Fig. D.1. Furthermore, for the determination of $\overline{D^r}$ the interactive force data of all assistance levels were taken into account. This is not necessary, as only two assistance levels are activated in this approach. As shown in Fig. D.1, the important criterion for switching between agreement and disagreement should be based on the high levels of interactive forces. Otherwise, the error of identifying SC_{disagree} while SC_{agree} is correct is high and can lead to a considerable increase in error time. Thus, in contrast to our earlier work [236] we propose to use the mean of the upper quartile of the absolute values of the interactive force components, $|f^{U25}_{i\parallel}|$ and $|f^{U25}_{i\perp}|$, respectively. The upper quartile are the highest 25 % of the force data within a trial [88].

Regarding step 3, the distributions of the interactive force data that have to be separated for SC_{agree} are those for $\overline{\alpha}_{\perp\text{agree}} = 1$,$\overline{\alpha}_{\parallel\text{agree}} = 0.75$ and $\overline{\alpha}_{\perp\text{disagree}} = 1$,$\overline{\alpha}_{\parallel\text{disagree}} = 0.75$. The assumption that there are significant differences between the distributions for SC_{agree} and SC_{disagree} is proven with paired t-tests revealing significant differences with large effect sizes ($|f^{U25}_{\parallel\text{agree}}|$: $t_{12} = -3.281$, $p = .007$, $d_z = 0.91$, $|f^{U25}_{\perp\text{agree}}|$: $t_{12} = -13.88$, $p < .001$, $d_z = 3.86$).

The final step 4 asks for determining the agreement threshold $\overline{D}^{r}_{\parallel\text{agree}}$ and $\overline{D}^{r}_{\perp\text{agree}}$ separating the distributions of upper quartile interactive forces corresponding to human-assistant agreement from those corresponding to disagreement. As proposed in our previous work [236], an optimal separating threshold is given by

$$\overline{D}^{r} = -\frac{\bar{\chi}_1 {s_2}^2 - \bar{\chi}_2 {s_1}^2 + s_1 s_2 \sqrt{2\ln\left(\frac{s_1}{s_2}\right)\left({s_1}^2 - {s_2}^2\right) + (\bar{\chi}_1 - \bar{\chi}_2)^2}}{{s_1}^2 - {s_2}^2} \tag{D.3}$$

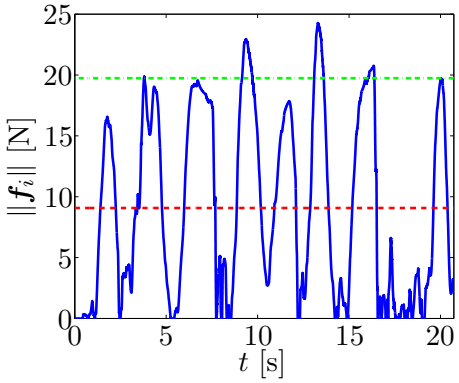

Fig. D.1: Time series (solid) and mean of norm of interactive force vector (dashed) for $\alpha_c = 1$ and SC_{disagree}

where $\bar{\chi}_1, \bar{\chi}_2$, s_1, s_2 are the mean and standard deviations of the upper quartile interactive forces of the two distributions.

Bibliography

[1] D. Aarno, S. Ekvall, and D. Kragic. Adaptive virtual fixtures for machine-assisted teleoperation tasks. In *IEEE International Conference on Robotics and Automation*, pages 1139–1144, 2005.

[2] D. A. Abbink. *Neuromuscular analysis of haptic gas pedal feedback during car following*. PhD thesis, Delft University of Technology, 2006.

[3] D. A. Abbink and M. Mulder. Exploring the dimensions of haptic feedback support in manual control. *Journal of Computing and Information Science in Engineering*, 9:011006–1 – 9, 2009.

[4] D. A. Abbink, M. Mulder, and E. R. Boer. Haptic shared control: smoothly shifting control authority? *Cognition, Technology & Work*, 14:19–28, 2012.

[5] J. J. Abbott. *Virtual Fixtures for Bilateral Teleoperation*. PhD thesis, The Johns Hopkins University, Baltimore, MD, USA, 2005.

[6] J. J. Abbott, P. Marayong, and A. M. Okamura. Haptic virtual fixtures for robot-assisted manipulation. *Robotics Research*, 28:49–64, 2007.

[7] J. Ackermann. *Robust Control: The Parameter Space Approach*. Springer, London, 2nd edition, 2002.

[8] R.J. Adams and B. Hannaford. Stable haptic interaction with virtual environments. *IEEE Transactions on Robotics and Automation*, 15:465–474, 1999.

[9] P. Aigner and B. McCarragher. Human integration into robot control utilising potential fields. In *IEEE International Conference on Robotics and Automation*, pages 291–296, 1997.

[10] O.M. Al-Jarrah and Y. F. Zheng. Intelligent compliant motion control. *IEEE Transactions on Systems, Man, and Cybernetics, Part B: Cybernetics*, 28:116–122, 1998.

[11] M. Ammi and A. Ferreira. Robotic assisted micromanipulation system using virtual fixtures and metaphors. In *IEEE International Conference on Robotics and Automation*, pages 454–460, 2007.

[12] R.J. Anderson and M. W. Spong. Bilateral control of teleoperators with time delay. *IEEE Transactions on Automatic Control*, 34(5):494–501, May 1989.

[13] S. Balasubramanian, R. Wei, R. Herman, and J. He. Robot-measured performance metrics in stroke rehabilitation. In *International Conference on Complex Medical Engineering*, pages 1–6, 2009.

[14] A.K. Bejczy, W. S. Kim, and S. C. Venema. The phantom robot: predictive displays for teleoperation with time delay. In *IEEE International Conference on Robotics and Automation*, pages 546–551, 1990.

[15] A. Bettini, P. Marayong, S. Lang, A. M. Okamura, and G. D. Hager. Vision-assisted control for manipulation using virtual fixtures. *IEEE Transactions on Robotics*, 20:953–966, 2004.

[16] N. Bevan. Measuring usability as quality of use. *Software Quality Journal*, 4:115–130, 1995. 10.1007/BF00402715.

[17] L. Biagiotti, C. Melchiorri, P. Tiezzi, and G. Vassura. Modelling and identification of soft pads for robotic hands. In *IEEE/RSJ International Conference on Intelligent Robots and Systems*, pages 2786–2791, 2005.

[18] R. C. Bonitz and T. C. Hsia. Internal force-based impedance control for cooperating manipulators. *IEEE Transactions on Robotics and Automation*, 12:78–89, 1996.

[19] D. Botturi, S. Galvan, and C. Secchi. A force dependent scaling for improving the human perception in bilateral teleoperation. In *Workshop on New Vistas and Challenges in Telerobotics, ICRA 2008*, 2008.

[20] S. Boyd and L. Vandenberghe. *Convex Optimization*. Cambridge University Press, 2004.

[21] M. S. Branicky. Stability of switched and hybrid systems. In *IEEE Conference on Decision and Control*, pages 3498–3503, 1994.

[22] M. S. Branicky. Multiple lyapunov functions and other analysis tools for switched and hybrid systems. *IEEE Transactions on Automatic Control*, 43:475–482, 1998.

[23] T. Burkert, J. Leupold, and G. Passig. A photorealistic predictive display. *Presence: Teleoperators & Virtual Environments*, 13:22–43, 2004.

[24] M. Buss, A. Peer, T. Schauss, N. Stefanov, U. Unterhinninghofen, S. Behrendt, J. Leupold, M. Durkovic, and M. Sarkis. Development of a multi-modal multi-user telepresence and teleaction system. *International Journal of Robotics Research*, 29(10):1298–1316, 2010.

[25] G. Camp, F. Paas, R. Rikers, and J. van Merrienboer. Dynamic problem selection in air traffic control training: a comparison between performance, mental effort and mental efficiency. *Computers in Human Behavior*, 17:575 – 595, 2001.

[26] S. K. Card, T. P. Moran, and A. Newell. *The psychology of human-computer interaction*. Lawrence Erlbaum Associates, 1983.

[27] A. Casals, J. Fernandez, and J. Amat. Augmented reality to assist teleoperation working with reduced visual conditions. In *IEEE International Conference on Robotics and Automation*, pages 235–240, 2002.

[28] M. C. Cavusoglu, W. Williams, F. Tendick, and S. S. Sastry. Robotics for telesurgery: Second generation berkeley/UCSF laparoscopic telesurgical workstation and looking towards the future applications. *Industrial Robot, Special Issue on Medical Robotics*, 30:22–29, 2003.

[29] B. Chebbi, D. Lazaroff, F. Bogsany, P. Liu, L. Ni, and M. Rossi. Design and implementation of a collaborative virtual haptic surgical training system. In *IEEE International Conference of Mechatronics and Automation*, pages 315–320, 2005.

[30] Y. Cheung and J. H. Chung. Adaptive force reflecting teleoperation with local intelligence. In *Industrial Robot: An International Journal*, pages 201–210, 2007.

[31] P. Chiacchio, S. Chiaverini, and B. Siciliano. Cooperative control schemes for multiple robot manipulator systems. In *IEEE International Conference on Robotics and Automation*, pages 2218–2223, 1992.

[32] H. C. Cho and J. H. Park. Impedance control with variable damping for bilateral teleoperation under time delay. *JSME International Journal Series C*, 48:695–703, 2005.

[33] N. Y. Chong, S. Kawabata, K. Ohba, T. Kotoku, K. Komoriya, K. Takase, and K. Tanie. Multioperator teleoperation of multirobot systems with time delay: Part I - aids for collision-free control. *Presence: Teleoperators & Virtual Environments*, 11:277–291, 2002.

[34] N.Y. Chong, T. Kotoku, K. Ohba, K. Komoriya, and K. Tanie. Exploring interactive simulator in collaborative multi-site teleoperation. In *10th IEEE International Workshop on Robot and Human Interactive Communication*, pages 243–248, 2001.

[35] G. A. V. Christiansson. *Introduction to Analysis and Control in Haptic Teleoperation*. http://sunet.dl.sourceforge.net/project/hapticanalysis/IntroductionToTeleoperation/1.00/IntroductionToTeleoperation1.00.pdf, 2007.

[36] O. Chuy, Y. Hirata, and K. Kosuge. A new control approach for a robotic walking support system in adapting user characteristics. *IEEE Transactions on Systems, Man, and Cybernetics, Part C: Applications and Reviews*, 36(6):725 –733, nov. 2006.

[37] S. Clarke, G. Schillhuber, M. F. Zaeh, and H. Ulbrich. Prediction-based methods for teleoperation across delayed networks. *Multimedia Systems*, 13:253–261, 2008.

[38] C. L. Clover, G. R. Luecke, J. J. Troy, and W. A. McNeely. Dynamic simulation of virtual mechanisms with haptic feedback using industrial robotics equipment. In *IEEE International Conference on Robotics and Automation*, pages 724–730, 1997.

[39] J. E. Colgate, P. E. Grafing, M. C. Stanley, and G. Schenkel. Implementation of stiff virtual walls in force-reflecting interfaces. In *IEEE Virtual Reality Annual International Symposium*, pages 202–208, 1993.

[40] R.A. Cooper. Intelligent control of power wheelchairs. *IEEE Engineering in Medicine and Biology Magazine*, 14(4):423–431, jul/aug 1995.

[41] B. Corteville, E. Aertbelien, H. Bruyninckx, J. De Schutter, and H. Van Brussel. Human-inspired robot assistant for fast point-to-point movements. In *IEEE International Conference on Robotics and Automation*, pages 3639–3644, 2007.

[42] R.Q. Van der Linde, P. Lammertse, E. Frederiksen, and B. Ruiter. The hapticmaster, a new high–performance haptic interface. In *Eurohaptics*, pages 1–5, 2002.

[43] R.V. Dubey, S. E. Everett, N. Pernalete, and K. A. Manocha. Teleoperation assistance through variable velocity mapping. *IEEE Transactions on Robotics and Automation*, 17:761–766, 2001.

[44] L. H. Duc, A. Ilchmann, S. Siegmund, and P. Taraba. On stability of linear time-varying second-order differential equations. *Quarterly of applied mathematics*, 64:137–151, 2006.

[45] V. Duchaine and C. M. Gosselin. General model of human-robot cooperation using a novel velocity based variable impedance control. In *WorldHaptics*, pages 446–451, 2007.

[46] V. Duchaine and C. M. Gosselin. Safe, stable and intuitive control for physical human-robot interaction. In *IEEE International Conference on Robotics and Automation*, pages 3383–3388, 2009.

[47] E. J. Dumon. Making best use of performance measures and information. *International Journal of Operation & Production Management*, 14:16–31, 1994.

[48] H. Esen. *Training in Virtual Environments via a Hybrid Dynamic Trainer Model*. PhD thesis, Technische Universität München, Munich, Germany, 2006.

[49] S.E. Everett and R. V. Dubey. Model-based variable position mapping for telerobotic assistance in a cylindrical environment. In *IEEE International Conference on Robotics and Automation*, pages 2197–2202, 1999.

[50] P. Evrard and A. Kheddar. Homotopy-based controller for physical human-robot interaction. In *18th IEEE International Symposium on Robot and Human Interactive Communication*, pages 1–6, 2009.

[51] P. Evrard and A. Kheddar. Homotopy switching model for dyad haptic interaction in physical collaborative tasks. In *Proceedings of the World Haptics - Third Joint EuroHaptics conference and Symposium on Haptic Interfaces for Virtual Environment and Teleoperator Systems*, pages 45–50, 2009.

[52] P. Evrard, N. Mansard, O. Stasse, A. Kheddar, T. Schauß, C. Weber, A. Peer, and M. Buss. Intercontinental, multimodal, wide-range tele-cooperation using a humanoid robot. In *Proceedings of the 2009 IEEE/RSJ International Conference on Intelligent Robots and Systems*, pages 5635 – 5640, 2009.

[53] L. Fabiani, G. Burdea, N. Langrana, and D. Gomez. Human interface using the rutgers master ii force feedback interface. In *Proceedings of the IEEE Virtual Reality Annual International Symposium*, pages 54–59, 1996.

[54] D. Feth, R. Groten, A. Peer, and M. Buss. Haptic human-robot collaboration: Comparison of robot partner implementations in terms of human-likeness and task performance. *Presence*, 20:173–189, 2011.

[55] D. Feth, A. Peer, and M. Buss. Incorporating human haptic interaction models into teleoperation systems. In *IEEE/RSJ International Conference on Intelligent Robots and Systems*, pages 4257 – 4262, 2010.

[56] T. Flash and N. Hogan. The coordination of arm movements: An experimentally confirmed mathematical model. *The Journal of Neuroscience*, 5:1688–1703, 1985.

[57] F. Flemisch, M. Heesen, T. Hesse, J. Kelsch, A. Schieben, and J. Beller. Towards a dynamic balance between humans and automation: authority, ability, responsibility and control in shared and cooperative control situations. *Cognition, Technology & Work*, 14:3–18, 2012.

[58] F. Flemisch, A. Schieben, J. Kelsch, and C. Löper. Automation spectrum, inner / outer compatibility and other potentially useful human factors concepts for assistance and automation. *Human Factors for assistance and automation*, pages 1–16, 2008.

[59] B. A. C. Forsyth and K. E. MacLean. Predictive haptic guidance: Intelligent user assistance for the control of dynamic tasks. *IEEE Transactions on Visualization and Computer Graphics*, 12:103–113, 2006.

[60] R. A. Frazer and W. J. Duncan. On the criteria for the stability of small motion. *Proceedings of the Royal Society, A*, 124:642–654, 1929.

[61] K. Fujita, P. Weangsima, and T. Honda. A study of haptic representation of virtual plain wall. In *IEEE International Conference on Robotics and Biomimetics*, pages 323–327, 2004.

[62] G. Ganesh, A. Albu-Schäffer, M. Haruno, M. Kawato, and E. Burdet. Biomimetic motor behavior for simultaneous adaptation of force, impedance and trajectory in interaction tasks. In *IEEE International Conference on Robotics and Automation*, pages 2705–2711, 2010.

[63] M. Gautier and W. Khalil. Exciting trajectories for the identifcation of base inertial parameters of robots. *The International Journal of Robotics Research*, 11:362–375, 1992.

[64] J. J. Gibson. *The senses considered as perceptual systems.* Houghton Mifflin, Oxford, England, 1966.

[65] J. G. Gonzalez, E. A. Heredia, T. Rahman, K. E. Barner, and G. R. Arce. A customized optimal filter for eliminating operator's tremor. In *Proceedings SPIE's International Symposium on Intelligent Systems and Advanced Manufacturing - Telemanipulator and Telepresence Technologies II*, pages 131–142, 1995.

[66] K. Goodrich, P. C. Schutte, and R. A. Williams. Piloted evaluation of the H-mode, a variable autonomy control system, in motion–based simulation. In *AIAA Proceedings*, pages 1–15, 2008.

[67] K. H. Goodrich, P. C. Schutte, F. O. Flemisch, and R. A. Williams. Application of the H-mode, a design and interaction concept for highly automated vehicles, to aircraft. In *IEEE/AIAA 25th Digital Avionics Systems Conference*, pages 1 – 13, 2006.

[68] S. Grange, F. Conti, P. Rouiller, P. Helmer, and C. Baur. Overview of the delta haptic device. In *Eurohaptics*, 2001.

[69] M. Green and D. J. N. Limebeer. *Linear Robust Control*. Prentice Hall, 1994.

[70] W. B. Griffin. *Shared Control for Dexterous Telemanipulation with Haptic Feedback*. PhD thesis, Stanford University, Palo Alto, CA, USA, 2003.

[71] P. Griffiths and R. B. Gillespie. Shared control between human and machine: Haptic display of automation during manual control of vehicle heading. In *12th international conference on Haptic interfaces for virtual environment and teleoperator systems*, pages 358–366, 2004.

[72] R. Groten, D. Feth, H. Goshy, A. Peer, D. A. Kenny, and M. Buss. Experimental analysis of dominance in haptic collaboration. In *The 18th International Symposium on Robot and Human Interactive Communication*, pages 723–729, 2009.

[73] R. K. Groten. *Haptic Human-Robot Collaboration: How to Learn from Human Dyads*. PhD thesis, Technische Universität München, 2011.

[74] A. Haddadi and K. Hashtrudi-Zaad. A new method for online parameter estimation of hunt-crossley environment dynamic models. In *IEEE/RSJ International Conference on Intelligent Robots and Systems*, pages 981–986, 2008.

[75] B. Hannaford. A design framework for teleoperators with kinesthetic feedback. *IEEE Transactions on Robotics and Automation*, 5:426–434, 1989.

[76] B. Hannaford and R. Anderson. Experimental and simulation studies of hard contact in force reflecting teleoperation. In *IEEE International Conference on Robotics and Automation*, pages 584–589, 1988.

[77] S.C. Hart and C. Wickens. *Manprint, an approach to systems integration*. Van Nostrand Reinhold, New York, 1990.

[78] K. Hashtrudi-Zaad and S. E. Salcudean. Analysis of control architectures for teleoperation systems with impedance/admittance master and slave manipulators. *The International Journal of Robotics Research*, 20:419–445, 2001.

[79] K. Hashtrudi-Zaad and S.E. Salcudean. Adaptive transparent impedance reflecting teleoperation. In *IEEE International Conference on Robotics and Automation*, pages 1369 –1374, 1996.

[80] S. Hirche. *Haptic Telepresence in Packet Switched Communication Networks*. PhD thesis, Technische Universität München, 2005.

[81] S. Hirche and M. Buss. Human-oriented control for haptic teleoperation. *Proceedings of the IEEE*, 100:623–647, 2012.

[82] G. Hirzinger, N. Sporer, A. Albu-Schäffer, M. Hähnle, R. Krenn, A. Pascucci, and M. Schedl. Dlr's torque–controlled light weight robot III – are we reaching the technological limits now? In *IEEE International Conference on Robotics and Automation*, pages 1710–1716, 2002.

[83] N. Hogan. Impedance control - an approach to manipulation. I - theory. *ASME, Transactions, Journal of Dynamic Systems, Measurement and Control*, 107:1–24, 1985.

[84] N. Hogan. Stable execution of contact tasks using impedance control. In *IEEE International Conference on Robotics and Automation. Proceedings*, pages 1047–1054, 1987.

[85] N. Hogan. Controlling impedance at the man/machine interface. In *IEEE International Conference on Robotics and Automation*, pages 1626–1631, 1989.

[86] P. F. Hokayem and M. W. Spong. Bilateral teleoperation:an historical survey. *Automatica*, 42:2035 – 2057, 2006.

[87] R. L. Hollis, Y. Yokokohji, and T. Kanade. What you can see is what you can feel. In *Proceedings of the Virtual Reality Annual International Symposium*, pages 46–53, 1996.

[88] D. C. Howell. *Fundamental Statistics for the Behavioral Sciences, 7th Edition*. Linda Schreiber, 2011.

[89] Z. Hu, S. E. Salcudean, and P. D. Loewen. Optimization-based teleoperation controller design. In *IFAC World Congress*, 1996.

[90] Z. Hu, S.E. Salcudean, and P.D. Loewen. Robust controller design for teleoperation systems. In *IEEE International Conference on Systems, Man and Cybernetics*, pages 2127 –2132, 1995.

[91] L. Huijun and S. Aiguo. Virtual-environment modeling and correction for force-reflecting teleoperation with time delay. *IEEE Transactions on Industrial Electronics*, 54:1227–1233, 2007.

[92] R. Ikeura and H. Inooka. Variable impedance control of a robot for cooperation with a human. In *IEEE International Conference on Robotics and Automation*, pages 3097–3102, 1995.

[93] NASA TLX: Task Load Index. http://human-factors.arc.nasa.gov/groups/tlx/.

[94] P. Ioannou and B. Fidan. http://www.siam.org/books/dc11/.

[95] P. Ioannou and B. Fidan. *Adaptive Control Tutorial*. Society for Industrial and Applied Mathematics, 2006.

[96] L. Jandura and M. A. Srinivasan. Experiments on human performance in torque discrimination and control. *Dynamic Systems and Control*, 1:369–375, 1994.

[97] N. Jarrasse, J. Paik, V. Pasqui, and G. Morel. How can human motion prediction increase transparency? In *IEEE International Conference on Robotics and Automation*, pages 2134–2139, 2008.

[98] L. A. Jones. Matching forces: Constant errors and differential thresholds. *Perception*, 18:681–687, 1989.

[99] L. A. Jones and I. W. Hunter. Human operator perception of mechanical variables and their effects on tracking performance. *ASME Advances in Robotics*, 42:49–53, 1992.

[100] D.B. Kaber, J.M. Riley, R. Zhou, and J.V. Draper. Effects of visual interface design, and control mode and latency on performance, telepresence and workload in a teleoperation task. In *Proceedings of the XIVth Triennial Congress of the International Ergonomics Association/44th Annual Meeting of the Human Factors and Ergonomics Society*, pages 503–506, 2000.

[101] H. Kazerooni, T.-I. Tsay, and K. Hollerbach. A controller design framework for telerobotic systems. *IEEE Transactions on Automatic Control*, 1:50–62, 1993.

[102] F. Keyrouz and K. Diepold. Binaural source localization and spatial audio reproduction for telepresence applications. *Presence Teleoperators and Virtual Environments*, 16:509–522, 2007.

[103] B. Khademian and K. Hashtrudi-Zaad. A four-channel multilateral shared control architecture for dual-user teleoperation systems. In *IEEE/RSJ International Conference on Intelligent Robots and Systems*, pages 2660–2666, 2007.

[104] H. K. Khalil. *Nonlinear Systems*. Prentice Hall Inc., 2000.

[105] O. Khatib. Real-Time Obstacle Avoidance for Manipulators and Mobile Robots. *The International Journal of Robotics Research*, 5:90–98, 1986.

[106] W.S. Kim and A.K. Bejczy. Demonstration of a high-fidelity predictive/preview display technique for telerobotic servicing in space. *IEEE Transactions on Robotics and Automation*, 9:698–702, 1993.

[107] K. Kosuge, M. Koga, K. Furata, and K. Nosaki. Coordinated motion control of robot arm based on virtual internal model. In *IEEE International Conference on Robotics and Automation*, pages 1097–1102, 1989.

[108] D. Kragic, P. Marayong, M. Li, A. M. Okamura, and G. D. Hager. Human-machine collaborative systems for microsurgical applications. *The International Journal of Robotics Research*, 24:731–741, 2005.

[109] H. I. Krebs, J. J. Palazzolo, L. Dipietro, M. Ferraro, J. Krol, K. Rannekleiv, B. T. Volpe, and N. Hogan. Rehabilitation robotics: Performance-based progressive robot-assisted therapy. *Autonomous Robots*, 15(1):7–20, 2003.

[110] A.B. Kuang, S. Payandeh, Bin Zheng, F. Henigman, and C.L. MacKenzie. Assembling virtual fixtures for guidance in training environments. In *12th International Symposium on Haptic Interfaces for Virtual Environment and Teleoperator Systems, HAPTICS*, pages 367 – 374, 2004.

[111] D. Kubus, T. Kröger, and F. M. Wahl. On-line rigid object recognition and pose estimation based on inertial parameters. In *IEEE/RSJ International Conference on Intelligent Robots and Systems*, pages 1402–1408, 2007.

[112] K. J. Kuchenbecker and G. Niemeyer. Canceling induced master motion in force-reflecting teleoperation. In *Proceedings of IMECE - ASME International Mechanical Engineering Congress and RD&D Expo*, 2004.

[113] K.J. Kuchenbecker and G. Niemeyer. Modeling induced master motion in force-reflecting teleoperation. In *IEEE International Conference on Robotics and Automation*, pages 348–353, 2005.

[114] K.J. Kuchenbecker and G. Niemeyer. Improving telerobotic touch via high-frequency acceleration matching. In *IEEE International Conference on Robotics and Automation*, pages 3893–3898, 2006.

[115] M. Lawitzky, A. Mörtl, and S. Hirche. Load sharing in human-robot cooperative manipulation. In *19th IEEE International Symposium on Robot and Human Interactive Communication*, pages 185–191, 2010.

[116] D. A. Lawrence. Stability and transparency in bilateral teleoperation. *IEEE Transactions on Robotics and Automation*, 9:624–637, 1993.

[117] S. W. Lawson, J. R. G. Pretlove, A. C. Wheeler, and G. A. Parker. Augmented reality as a tool to aid the telerobotic exploration and characterization of remote environments. *Presence*, 11:352–367, 2002.

[118] S. Lee and K. Jeong. Design of robust time delayed teleoperator control system. In *IEEE/RSJ/GI International Conference on Intelligent Robots and Systems*, pages 1413 –1420, 1994.

[119] G.M.H. Leung, B.A. Francis, and J. Apkarian. Bilateral controller for teleoperators with time delay via μ–synthesis. *IEEE Transactions on Robotics and Automation,*, 11:105–116, 1995.

[120] Y. Li, J. C. Huegel, V. Patoglu, and M. K. O'Malley. Progressive shared control for training in virtual environments. In *WorldHaptics*, pages 332–337, 2009.

[121] Y. Li, V. Patoglu, and M. K. O'Malley. Negative efficacy of fixed gain error reducing shared control for training in virtual environments. *ACM Transactions on Applied Perception*, 6:1–21, 2009.

[122] D. Liberzon and A. S. Morse. Basic problems in stability and design of switched systems. *IEEE Control Systems Magazine*, 19:59–70, 1999.

[123] F. Llewellyn. Some fundamental properties of transmission systems. In *Proceedings of IRE*, pages 271–283, 1952.

[124] W. Lorensen, H. Cline, C. Nafis, R. Kikinis, D. Altobelli, and L. Gleason. Enhancing reality in the operating room. In *IEEE Conference on Visualization*, pages 410–415, 1993.

[125] L. J. Love and W. J. Book. Force reflecting teleoperation with adaptive impedance control. *IEEE Transactions on Systems, Man, and Cybernetics Part B*, 34:159–165, 2004.

[126] J. Lunze. *Regelungstechnik 1.* Springer-Verlag Berlin Heidelberg, 1999.

[127] R. Ma and D. B. Kaber. Presence, workload and performance effects of synthetic environment design factors. *International Journal of Human-Computer Studies*, 64:541–552, 2006.

[128] T. Maeda, T. Nojima, M. Inami, and S. Tachi. Applying an 'encounter type' haptic display to telexistence. In *Proceeding of the Virtual Reality Society of Japan Annual Conference*, pages 395–398, 1999.

[129] Y. Maeda, T. Hara, and T. Arai. Human-robot cooperative manipulation with motion estimation. In *IEEE/RSJ International Conference on Intelligent Robots and Systems*, pages 2240–2245, 2001.

[130] S. Mahapatra and M. Zefran. Stable haptic interaction with switched virtual environments. In *International Conference on Robotics and Automation*, pages 1241–1246, 2003.

[131] M. K. O' Malley, A. Gupta, M. Gen, and Y. Li. Shared control in haptic systems for performance enhancement and training. *ASME Journal of Dynamic Systems, Measurement and Control*, 128:75–85, 2006.

[132] K.A. Manocha, N. Pernalete, and R.V. Dubey. Variable position mapping based assistance in teleoperation for nuclear cleanup. In *IEEE International Conference on Robotics and Automation*, pages 374–379, 2001.

[133] P. Marayong and A. M. Okamura. Speed-Accuracy Characteristics of Human-Machine Cooperative Manipulation Using Virtual Fixtures With Variable Admittance. *Human Factors: The Journal of the Human Factors and Ergonomics Society*, 46:518–532, 2004.

[134] S. Martin and N. Hillier. Characterisation of the novint falcon haptic device for application as a robot manipulator. In *Australasian Conference on Robotics and Automation*, 2009.

[135] T.H. Massie and J.K. Salisbury. The PHANTOM haptic interface: a device for probing virtual objects. In *Proceedings of the ASME Winter Annual Meeting, Symposium on Haptic Interfaces for Virtual Environment and Teleoperator Systems*, pages 295–300, 1994.

[136] M. J. Massimino. Improved force perception through sensory substitution. *Control Engineering Practice*, 3:215–222, 1995.

[137] W. A. McNeely. A new approach io force feedback for virtual reality. In *Proceeding of IEEE Virtual Reality Annual International Symposium*, pages 336–341, 1993.

[138] P. Milgram, S. Yin, and J. J. Grodski. An augmented reality based teleoperation interface for unstructured environments. In *Proc. American Nuclear Society (ANS) 7th Topical Meeting on Robotics and Remote Systems*, pages 966–973, 1997.

[139] P. Mitra and G. Niemeyer. Model-mediated Telemanipulation. *The International Journal of Robotics Research*, 27:253–262, 2008.

[140] F. Mobasser and K. Hashtrudi-Zaad. Predictive teleoperation using laser rangefinder. In *IEFE CCECE/CCGEI*, pages 1279–1282, 2006.

[141] D. Morris, C. Sewell, F. Barbagli, K. Salisbury, N. Blevins, and S. Girod. Visuohaptic simulation of bone surgery for training and evaluation. *Computer Graphics and Applications, IEEE*, 26:48–57, 2006.

[142] A. Mörtl, M. Lawitzky, A. Kucukyilmaz, M. Sezgin, C. Basdogan, and S. Hirche. The role of roles: Physical cooperation between humans and robots. *International Journal of Robotics Research*, 2012.

[143] M. Mulder. *Haptic gas pedal feedback for active car-following support.* PhD thesis, Delft University of Technology, 2007.

[144] M. Mulder, D. A. Abbink, M. M. van Paassen, and M. Mulder. Design of a haptic gas pedal for active car-following support. *IEEE Transactions on intelligent transportation systems*, 12:268–279, 2011.

[145] M. Mulder, D.A. Abbink, and E.R. Boer. The effect of haptic guidance on curve negotiation behavior of young, experienced drivers. In *IEEE International Conference on Systems, Man and Cybernetics*, pages 804–809, 2008.

[146] K. S. Narendra and A. M. Annaswamy. *Stable Adaptive Systems*. Dover Publications, Inc., USA, 2005.

[147] E. B. Nash, G. W. Edwards, J. A. Thompson, and W. Barfield. A review of presence and performance in virtual environments. *International Journal of Human-Computer Interaction*, 12:1–41, 2000.

[148] L. Ni and D. W. L. Wang. A gain-switching control scheme for position-error-based bilateral teleoperation: Contact stability analysis and controller design. *The International Journal of Robotics Research*, 23:255–274, 2004.

[149] G. Niemeyer and J.-J.E. Slotine. Stable adaptive teleoperation. *IEEE Journal of Oceanic Engineering*, 16:152–162, 1991.

[150] S. O. Oguz, A. Kucukyilmaz, T. M. Sezgin, and C. Basdogan. Haptic negotiation and role exchange for collaboration in virtual environments. In *IEEE Haptics Symposium*, pages 371–378, 2010.

[151] F. G. W. C. Paas and J. J. G. Merriënboer. The efficiency of instructional conditions: An approach to combine mental effort and performance measures. *Human Factors: The Journal of the Human Factors and Ergonomics Society*, 35:737–743, 1993.

[152] D.-J. Park and B.-E. Jun. Selfperturbing recursive least squares algorithm with fast tracking capability. *Electronics Letters*, 28:558–559, 1992.

[153] S. Park, R. D. Howe, and D. F. Torchiana. Virtual fixtures for robotic cardiac surgery. In *Proceedings of the 4th International Conference on Medical Image Computing and Computer-Assisted Intervention*, pages 1419–1420, 2001.

[154] Y. S. Park, H. Kang, T. F. Ewing, E. L. Faulring, J. E. Colgate, and M. A. Peshkin. Enhanced teleoperation for d&d. In *IEEE International Conference on Robotics and Automation*, pages 3702–3707, 2004.

[155] A. Peer. *Design and Control of Admittance-Type Telemanipulation Systems*. PhD thesis, Technische Universität München, Munich, Germany, 2008.

[156] A. Peer and M. Buss. Robust stability analysis of a bilateral teleoperation system using the parameter space approach. In *IEEE/RSJ International Conference on Intelligent Robots and Systems*, pages 2350–2356, 2008.

[157] A. Peer, Y. Komoguchi, and M. Buss. Towards a mobile haptic interface for bimanual manipulations. In *International Conference on Intelligent Robots and Systems*, pages 384–391, 2007.

[158] Z. Pezzementi, A.M. Okamura, and G.D. Hager. Dynamic guidance with pseudoadmittance virtual fixtures. In *IEEE International Conference on Robotics and Automation*, pages 1761–1767, 2007.

[159] D. J. Pierce and R. J. Plemmons. Tracking the condition number for RLS in signal processing. *Mathematics of Control, Signals, and Systems*, 5:23–29, 1992.

[160] A. Pillarisetti, M. Pekarev, A.D. Brooks, and J. P. Desai. Evaluating the role of force feedback for biomanipulation tasks. In *Proceedings of the 14th International Symposium on Haptic Interfaces for Virtual Environment and Teleoperator Systems*, pages 11–18, 2006.

[161] H. Pongrac, A. Peer, B. Färber, and M. Buss. Effects of varied human movement control on task performance and feeling of telepresence. In *EuroHaptics*, pages 755–765, 2008.

[162] D. Powell and M. K. O'Malley. Efficacy of shared-control guidance paradigms for robot-mediated training. In *WorldHaptics*, pages 427–432, 2011.

[163] M.M. Rahman, R. Ikeura, and K. Mizutani. Investigating the impedance characteristic of human arm for development of robots to co-operate with human operators. In *IEEE International Conference on Systems, Man, and Cybernetics*, pages 676–681, 1999.

[164] K. B. Reed, M. Peshkin, M. J. Hartmann, J. E. Colgate, and J. Patton. Kinesthetic interaction. In *IEEE 9th International Conference on Rehabilitation Robotics*, pages 569–574, 2005.

[165] K. B. Reed, M. Peshkin, M. J. Hartmann, J. Patton, P. M. Vishton, and M. Grabowecky. Haptic cooperation between people, and between people and machines. In *IEEE/RSJ International Conference on Intelligent Robots and Systems*, pages 2109–2114, 2006.

[166] K. B. Reed and M. A. Peshkin. Physical collaboration of human-human and human-robot teams. *IEEE Transactions on Haptics*, 1:108–120, 2008.

[167] C. E. Reiley. *Evaluation of Augmented Reality Alternatives to Direct Force Feedback in Robot-Assisted Surgery: Visual Force Feedback and Virtual Fixtures.* PhD thesis, Johns Hopkins University, 2007.

[168] D. Reintsema, K. Landzettel, and G. Hirzinger. DLR's advanced telerobotic concepts and experiments for on-orbit servicing. In *Advances in Telerobotics: Human System Interfaces, Control, and Applications*, volume 31, pages 323–345. Springer, STAR series, 2007.

[169] P. Richard and P. Coiffet. Human perceptual issues in virtual environments: Sensory substitution and information redundancy. In *IEEE international Workshop on Robot and Human Communication*, pages 301–306, 1995.

[170] P. Ridao, M. Carreras, E. Hernandez, and N. Palomeras. Underwater Telerobotics for Collaborative Research. In *Advances in Telerobotics: Human System Interfaces, Control, and Applications*, pages 347–359. Springer, STAR series, 2007.

[171] C.N. Riviere, R.S. Rader, and N.V. Thakor. Adaptive cancelling of physiological tremor for improved precision in microsurgery. *IEEE Transactions on Biomedical Engineering*, 45:839–846, 1998.

[172] L.B. Rosenberg. Virtual fixtures: Perceptual tools for telerobotic manipulation. In *IEEE Annual International Symposium on Virtual Reality*, pages 76–82, 1993.

[173] H. E. Ross and A. J. Benson. The weber fraction for the moment of inertia. In *Fechner Day 86, International Society for Psychophysics,*, pages 71–76, 1986.

[174] L. Råde, B. Westergren, and P. Vachenauer. *Mathematische Formeln*. Springer, 2000.

[175] D. Ryu, J.-B. Song, S. Kang, and M. Kim. Frequency domain stability observer and active damping control for stable haptic interaction. *IET Control Theory & Applications*, 2:261–268, 2008.

[176] J.-H. Ryu and D.-S. Kwon. A novel adaptive bilateral control scheme using similar closed-loop dynamic characteristics of master/slave manipulators. *Journal of Robotic Systems*, 18:533–543, 2001.

[177] A. Sano, H. Fujimoto, and M. Tanaka. Gain-scheduled compensation for time delay of bilateral teleoperation systems. In *IEEE International Conference on Robotics and Automation*, pages 1916 –1923, 1998.

[178] A. Schmid, R. Yechangunja, S. Thalhammer, and M.A. Srinivasan. Human-operated 3d micro-manipulator with haptic feedback. In *Proceedings of the IEEE Haptics Symposium*, pages 517–522, 2012.

[179] A. M. Schmidts, D. Lee, and A. Peer. Imitation learning of human grasping skills from motion and force data. In *IEEE/RSJ International Conference on Intelligent Robots and Systems*, pages 1002–1007, 2011.

[180] S. A. Schneider and Jr. R. H. Cannon. Object impedance control for cooperative manipulation: Theory and experimental results. *IEEE Transactions on Robotics and Automation*, 8:383–394, 1992.

[181] A. Shahdi and S. Sirouspour. Adaptive/robust control for enhanced teleoperation under communication time delay. In *IEEE/RSJ International Conference on Intelligent Robots and Systems*, pages 2667 –2672, 2007.

[182] T. B. Sheridan. *Telerobotics, Automation, and Human Supervisory Control*. MIT Press, Cambridge, MA, USA, 1992.

[183] S. Sirouspour. Robust control design for cooperative teleoperation. In *IEEE International Conference on Robotics and Automation*, pages 1133–1138, 2005.

[184] M. Sitti and H. Hashimoto. Macro to nano tele-manipulation through nanoelectromechanical systems. In *Proceedings of the 24th Annual Conference of the IEEE Industrial Electronics Society*, pages 98–103, 1998.

[185] M. Slater, V. Linakis, M. Usoh, R. Kooper, and G. Street. Immersion, presence, and performance in virtual environments: An experiment with tri-dimensional chess. In *ACM Virtual Reality Software and Technology (VRST)*, pages 163–172, 1996.

[186] J.-J. Slotine and W. Li. *Applied Nonlinear Control*. Prentice Hall, 1990.

[187] C. Smith and H. I. Christensen. A minimum jerk predictor for teleoperation with variable time delay. In *IEEE/RSJ International Conference on Intelligent Robots and Systems*, pages 5621–5627, 2009.

[188] B. Stanczyk and M. Buss. Development of a telerobotic system for exploration of hazardous environments. In *IEEE/RSJ International Conference on Intelligent Robots and System*, 2004.

[189] K. M. Stanney. *Handbook of Virtual Environments*. Lawrence Erlbaum Associates, 2002.

[190] N. Stefanov, A. Peer, and M. Buss. Role determination in human-human interaction. In *Third Joint Eurohaptics Conference and Symposium on Haptic Interfaces for Virtual Environment and Teleoperator Systems*, pages 51–56, 2009.

[191] N. Stefanov, A. Peer, and M. Buss. Online intention recognition for computer-assisted teleoperation. In *IEEE International Conference on Robotics and Automation*, pages 5334 – 5339, 2010.

[192] N. Stefanov, A. Peer, and M. Buss. Online intention recognition in computer-assisted teleoperation systems. In *Eurohaptics*, pages 233–239, 2010.

[193] M. Tadi. On the stability of second order time varying linear systems. *Transactions of the ASME*, 128:408–410, 2006.

[194] Y. Tanaka, T. Onishi, T. Tsuji, N. Yamada, Y. Takeda, and I. Masamori. Analysis and modeling of human impedance properties for designing a human-machine control system. In *IEEE International Conference on Robotics and Automation*, pages 3627 – 3632, 2007.

[195] K. S. Tang, K. F. Man, and R. S. H. Istepanian. Teleoperation controller design using hierarchical genetic algorithm. In *IEEE International Conference on Industrial Technology*, pages 707–711, 2000.

[196] K. P. Tee, D. W. Franklin, M. Kawato, T. E. Miller, and E. Burdet. Concurrent adaptation of force and impedance in the redundant muscle system. *Biological Cybernetics*, 102:31–44, 2010.

[197] J. Traub, M. Feuerstein, R. Bauernschmitt, E.U. Schirmbeck, H. Najafi, R. Bauernschmitt, and G. Klinker. Augmented reality for port placement and navigation in robotically assisted minimally invasive cardiovascular surgery. *International Congress Series*, 1268:735–740, 2004.

[198] T. Tsuji, P. G. Morasso, K. Goto, and K. Ito. Human hand impedance characteristics during maintained posture. *Biological Cybernetics*, 72:475–485, 1995.

[199] T. Tsumugiwa, R. Yokogawa, and K. Hara. Variable impedance control based on estimation of human arm stiffness for human-robot cooperative calligraphic task. In *IEEE International Conference on Robotics and Automation*, pages 644–650, 2002.

[200] C. Tzafestas, S. Velanas, and G. Fakiridis. Adaptive impedance control in haptic teleoperation to improve transparency under time-delay. In *IEEE International Conference on Robotics and Automation*, pages 212–219, 2008.

[201] M. Ueberle and M. Buss. Control of kinesthetic haptic interfaces. In *IEEE/RSJ International Conference on Intelligent Robots and Systems, Workshop on Touch and Haptics*, pages 147–151, 2004.

[202] M. Ueberle, N. Mock, and M. Buss. Vishard10, a novel hyper-redundant haptic interface. In *12th International Symposium on Haptic Interfaces for Virtual Environment and Teleoperator Systems*, pages 58 – 65, 2004.

[203] R. Ueha, H. T.T. Pham, H. Hirai, and F. Miyazaki. A simple control design for human-robot coordination based on the knowledge of dynamical role division. In *IEEE/RSJ International Conference on Intelligent Robots and Systems*, pages 3051 – 3056, 2009.

[204] U. Unterhinninghofen. *Dynamic Assist Functions in Haptic Telepresence*. PhD thesis, Technische Universität München, 2009.

[205] U. Unterhinninghofen, F. K. Freyberger, and M. Buss. Study on computer assistance for telepresent reaching movements. In *EuroHaptics*, pages 745–754, 2008.

[206] C. Urdiales, J.M. Peula, M. Fdez-Carmona, C. Barrué, E.J. Pérez, I. Sánchez-Tato, J.C. del Toro, F. Galluppi, U. Cortés, R. Annichiaricco, C. Caltagirone, and F. Sandoval. A new multi-criteria optimization strategy for shared control in wheelchair assisted navigation. *Autonomous Robots*, 30:179–197, 2011.

[207] E. H. F. van Asseldonk, M. Wessels, A. H. A. Stienen, F. C.T. van der Helm, and H. van der Kooij. Influence of haptic guidance in learning a novel visuomotor task. *Journal of Physiology-Paris*, 103:276–285, 2009.

[208] G. Vanacker. *Adaptive Steering Behavior Modelling for Power Wheelchair Control*. PhD thesis, Katholieke Universiteit Leuven, Leuven, Belgium, 2008.

[209] R. Volpe. Techniques for collision prevention, impact stability, and force control by space manipulators. In *Teleoperation and Robotics in Space*, pages 175–208, 1994.

[210] S. Wang and M. A. Srinivasan. The role of torque in haptic perception of object location in virtual environments. In *11th Symposium on Haptic Interfaces for Virtual Environment and Teleoperator Systems*, pages 302–309, 2003.

[211] Z. Wang, A. Peer, and M. Buss. Fast online impedance estimation for robot control. In *IEEE International Conterence on Mechatronics*, pages 1–6, 2009.

[212] R. B. Welch. How can we determine if the sense of presence affects task performance? *Presence: Teleoperators & Virtual Environments*, 8:574–577, 1999.

[213] D. Whitney. Historical perspective and state of the art in robot force control. In *Robotics and Automation. Proceedings. 1985 IEEE International Conference on*, pages 262–268, 1985.

[214] B. Willaert, H. van Brussel, and G. Niemeyer. Stability of model-mediated teleoperation: Discussion and experiments. In *Eurohaptics*, 2012.

[215] B. G. Witmer and M. J. Singer. Measuring presence in virtual environments: A presence questionnaire. *Presence: Teleoperators & Virtual Environments*, 7:225–240, 1998.

[216] B. Woodruff and H. Helson. Torque: A new dimension in tactile–kinesthetic sensitivity. *American Journal of Psychology*, 78:271–277, 1965.

[217] J. Yan and S.E. Salcudean. Teleoperation controller design using H_∞-optimization with application to motion-scaling. *IEEE Transactions on Control Systems Technology*, 4:244 –258, 1996.

[218] Y. Yokokohji and T. Yoshikawa. Bilateral control of master-slave manipulators for ideal kinesthetic coupling-formulation and experiment. *IEEE Transactions on Robotics and Automation*, 10:605–620, 1994.

[219] W.-K. Yoon, T. Goshozono, H. Kawabe, M. Kinami, Y. Tsumaki, M. Uchiyama, M. Oda, and T. Doi. Model-based space robot teleoperation of ETS - VII manipulator. *IEEE Transactions on Robotics and Automation*, 20:602–612, 2004.

[220] T. Yoshikawa and K. Nagai. Manipulating and grasping forces in manipulation by multifingered robot hands. *IEEE Transactions on Robotics and Automation*, 7:67–77, 1991.

[221] H. Yu, M. Spenko, and S. Dubowsky. An adaptive shared control system for an intelligent mobility aid for the elderly. *Autonomous Robots*, 15:53–66, 2003.

[222] W. Yu, R. Alqasemi, R. Dubey, and N. Pernalete. Telemanipulation assistance based on motion intention recognition. In *IEEE International Conference on Robotics and Automation*, pages 1121–1126, 2005.

[223] M. F. Zäh, S. Clarke, B. Petzold, and J. Schilp. Achieving flexible micro-assembly systems through telepresence. In *Proceedings of the Mechatronics & Robotics Conference*, pages 1473–1477, 2004.

[224] M. Zefran, F. Bullo, and M. Stein. A notion of passivity for hybrid systems. In *IEEE Conference on Decision and Control*, 2001.

[225] W.-H. Zhu and S. E. Salcudean. Teleoperation with adaptive motion/force control. In *IEEE International Conference on Robotics and Automation*, pages 231 – 237, 1999.

[226] W.-H. Zhu and S. E. Salcudean. Stability guaranteed teleoperation: an adaptive motion/force control approach. *IEEE Transactions on Automatic Control*, 45:1951–1969, 2000.

Own Publications and Supervised Student Projects

[227] A. Achhammer. Telemanipulation with impedance controlled light weight robots. Master's thesis, Technische Universität München, 2009.

[228] A. Achhammer, C. Weber (Passenberg), A. Peer, and M. Buss. Improvement of model-mediated teleoperation using a new hybrid environment estimation technique. In *IEEE International Conference on Robotics and Automation*, pages 5358–5363, 2010.

[229] S. Albrecht, C. Passenberg, M. Sobotka, A. Peer, M. Buss, and M. Ulbrich. Optimization criteria for human trajectory formation in dynamic virtual environments. In *Eurohaptics*, pages 257–262, 2010.

[230] M. Axenbeck. *Regelungen für Telepräsenzsysteme mit Zeitverzögerungen - ein Vergleich*. Bachelor Thesis, Technische Universität München, 2010.

[231] R. Engst. *Entwicklung eines online-fähigen Aadaptionsverfahrens für den Assistenzgrad*. Bachelor Thesis, Technische Universität München, 2011.

[232] P. Evrard, N. Mansard, O. Stasse, A. Kheddar, T. Schauß, C. Weber, A. Peer, and M. Buss. Intercontinental, multimodal, wide-range tele-cooperation using a humanoid robot. In *Proceedings of the 2009 IEEE/RSJ International Conference on Intelligent Robots and Systems*, pages 5635 – 5640, 2009.

[233] Y. Hao. *Online identification of inertial parameters of a rigid body for the model-mediated teleoperation approach*. Bachelor Thesis, Technische Universität München, 2011.

[234] V. Nitsch, C. Passenberg, A. Peer, M. Buss, and B. Färber. Assistance functions for collaborative haptic interaction in virtual environments and their effect on performance and user comfort. In *1st International Conference on Applied Bionics and Biomechanics*, 2010.

[235] C. Passenberg, A. Glaser, and A. Peer. Exploring the design space of haptic assistances for a maze scenario. *Transactions on Haptics: Special Issue on "Haptic Human-Robot Interaction"*, submitted, 2012.

[236] C. Passenberg, R. Groten, A. Peer, and M. Buss. Towards real-time haptic assistance adaptation optimizing task performance and human effort. In *IEEE Worldhaptics*, pages 155–160, 2011.

[237] C. Passenberg, A. Peer, and M. Buss. Model-mediated teleoperation for multi-operator multi-robot systems. In *IEEE/RSJ International Conference on Intelligent Robots and Systems*, pages 4263–4268, 2010.

[238] C. Passenberg, A. Peer, and M. Buss. A survey of environment- operator- and task-adapted controllers for teleoperation systems. *Journal of Mechatronics: Special Issue on Design and Control Methodologies in Telerobotics*, 20:787 – 801, 2010.

[239] C. Passenberg, N. Stefanov, A. Peer, and M. Buss. Enhancing task classification in human-machine collaborative teleoperation systems by real-time evaluation of an agreement criterion. In *IEEE WorldHaptics*, pages 493–498, 2011.

[240] A. Peer, S. Hirche, C. Weber, I. Krause, M. Buss, S. Miossec, P. Evrard, O. Stasse, E. S. Neo, A. Kheddar, and K. Yokoi. Intercontinental multimodal tele-cooperation using a humanoid robot. In *IEEE/RSJ International Conference on Intelligent Robots and Systems*, pages 405–411, 2008.

[241] A. Spenninger. *Selbst-adaptierende Admittanzregelung und Online-Generierung von Virtual Fixtures für Telepräsenzsysteme unter Verwendung eines iterativen Lernalgorithmus*. Bachelor Thesis, Technische Universität München, 2011.

[242] N. Stefanov, C. Passenberg, A. Peer, and M. Buss. Design and evaluation of a haptic computer-assistant for telemanipulation tasks. *Transactions on Systems, Man, and Cybernetics–Part A: Systems and Humans*, submitted, 2012.

[243] C. Weber, V. Nitsch, U. Unterhinninghofen, B. Färber, and M. Buss. Position and force augmentation in a telepresence system and their effects on perceived realism. In *WorldHaptics*, pages 226–231, 2009.

[244] M. Wintergerst. *Stabilitätsbeobachter und -regler für Telepräsenzsysteme*. Bachelor Thesis, Technische Universität München, 2011.

[245] Y. Zaripov. *Factors for determining the assistance degree*. Bachelor Thesis, Technische Universität München, 2010.